University of Zagreb

FACULTY OF SCIENCE

Maja Varga Pajtler

Nucleon transfer reactions in the ^{90}Zr+^{208}Pb system

DOCTORAL THESIS

Zagreb, 2014.

Sveučilište u Zagrebu

PRIRODOSLOVNO-MATEMATIČKI FAKULTET

Maja Varga Pajtler

Reakcije prijenosa nukleona u sustavu ^{90}Zr+^{208}Pb

DOKTORSKI RAD

Zagreb, 2014.

University of Zagreb

FACULTY OF SCIENCE

Maja Varga Pajtler

Nucleon transfer reactions in the ^{90}Zr+^{208}Pb system

DOCTORAL THESIS

Supervisors:

izv. prof. dr. sc. Matko Milin

dr. sc. Suzana Szilner

Zagreb, 2014.

PRIRODOSLOVNO-MATEMATIČKI FAKULTET

Maja Varga Pajtler

Reakcije prijenosa nukleona u sustavu ^{90}Zr+^{208}Pb

DOKTORSKI RAD

Mentori:

izv. prof. dr. sc. Matko Milin

dr. sc. Suzana Szilner

Zagreb, 2014.

Contents

Summary

Multinucleon transfer reactions have been studied in the ^{90}Zr+^{208}Pb system close to the Coulomb barrier energy in the Prisma + Clara set-up. Light binary partners have been detected in the Prisma magnetic spectrometer, while the coincident γ rays have been detected in the Clara γ-array. Trajectory reconstruction in the spectrometer provides the identification of the light fragments in their charge, mass and velocity. These allow, together with the coincidences with the Clara array, to attribute electromagnetic transitions and yields to each of the transfer channels.

In the ^{90}Zr+^{207}Pb multinucleon transfer reactions, outgoing particles with the atomic number $Z = 30 - 40$ and mass number $A = 60 - 94$ were recognized. The level schemes of the presented isotopes have been constructed and updated based on systematics with neighbouring nuclei, and data from literature. In this thesis, we focused on γ spectra of Zr (together with their heavy partner, Pb), Y and Sr isotopic chains. The γ spectrum of each isotope is presented, together with recognized γ rays. Based on these observations, level schemes are constructed. In some cases, new γ rays were observed, and if possible, γ transitions were suggested.

The Prisma + Clara spectrometers offer the possibility to measure yields of different transfer products, and to identify nuclei with good mass and charge resolution, even in this rather heavy ion collision. In addition, the semi-classical models which were thus far a good basis for the description of heavy ion collisions in somewhat lighter systems, can be tested for this heavy system.

The evidence shows that the most important degrees of freedom are surface vibrations/rotations and single particles, and their coupling. It is through the excitation of these modes that energy and angular momentum are transferred from the relative motion to the mass and

charge rearrangement and intrinsic excitations of the partners of the collision.

The experimental set-up used in the present measurement allowed us to investigate excited states, and to see if their underlying structure reflects the significance of the same degrees as in lighter nuclei.

By the study of the Pb isotopes (the heavy binary partner of Zr), the effect of evaporation which strongly affects the primary yields has been discussed. The isotopes produced after the evaporation of one or two neutrons were recognized through their γ rays, while their relative strengths allowed to quantitatively estimate the the effect of the evaporation for the first time in such a heavy system.

In our experiment, we were searching for excitation of the 0^+ states that were recognized as pairing vibration states, and that were strongly excited in the (t,p) reactions. At the level of the accumulated statistics, we could not undoubtedly confirm the excitation of those states.

However, we observed that the important part of the yield is in the excitation of the states whose underlying structure could be connected with the pairing, especially the states of the phonon-fermion coupled nature. We discussed such coupling scheme in odd Zr and Sr isotopes, taking into account the similarities in excitation energies of the odd and even isotopes, as well as the decay patterns and the decay strengths of the involved states. The analysis showed evidences of the particle-vibration coupling. In some isotopes, our conclusions about the importance of the particle-vibration coupling were partially obscured by the fact that the structure of some states of interest display a rather mixed configurations.

Keywords

Acknowledgements

I wouldn't have managed to complete this doctoral thesis without the both professional and personal support of others. From the top of the list I would like to thank:

* my menthor, dr.sc. Suzana Szilner, for all the knowledge and guidance troughout this journey, and also for her patience for my trials and errors

* my menthor, izv. prof. dr. sc. Matko Milin for the constructive recommendations in the process

* the head of the Department of Physics at the University of Osijek, iz. prof. dr. sc. Branko Vuković, as well as my colleagues, for the advices and the opportunity to complete the thesis during the limited time

* my parents, for their support and encouragement through all my education years

* my husband and son, for everything...

Sažetak

Unatoč dugogodišnjem istraživanju, atomska jezgra je još uvijek kvantni sustav pun nepoznanica. Znanje o nuklearnoj sili temelji se na istraživanjima u blizini doline stabilnosti, koja su pružila informacije o nuklearnoj sili u uvjetima ravnoteže. Kako bismo proširili postojeće znanje, nužno je proučavati nuklearnu silu u uvjetima velikih deformacija ili velikih gustoća neutrona. Poznavanju strukture jezgre doprinijele su reakcije s različitim upadnim česticama. Raspršenjima fotona, elektrona, mezona i nukleona na jezgrama dobivene su informacije o svojstvima jezgara u blizini osnovnog stanja. Ubrzavanje teških iona omogućilo je izvođenje reakcija sa složenijim sustavima, u kojima ioni mogu izmijeniti nekoliko kvantata energije i kutne količine gibanja, a može doći i do prijenosa mase i naboja. Reakcije prijenosa imaju ključnu ulogu u proučavanju strukture jezgara i korelacija među nukleonima.

U posljednje je vrijeme pojačan interes za reakcije prijenosa, uslijed saznanja da se reakcijama prijenosa više nukleona mogu stvoriti jezgre bogate neutronima. Tome ide u prilog i izgradnja nove generacije spektrometara velikog prostornog kuta koji rade na načelu rekonstrukcije putanje, a koje karakterizira visoka efikasnost, kao i visoka razlučivost u prepoznavanju produkata reakcije u masi i naboju.

U ovom radu proučavala se reakcija ^{90}Zr+^{208}Pb, izmjerena u međunarodnom akceleratorskom centru na LNL-INFN (Laboratori Nazionali di Legnaro - Instituto Nazionale di Fisica Nucleare). Reakcije prijenosa više nukleona u sustavu ^{90}Zr+^{208}Pb proučavane su na energiji bliskoj kulonskoj barijeri na eksperimentalnom postavu Prisma + Clara. Laki binarni partner detektiran je magnetskim spektrometrom Prisma, dok su γ-zrake u koincidenciji s Prismom, detektirane γ-detektorom Clara. Rekonstrukcija putanje unutar spektrometra omogućila je prepoznavanje naboja, mase i vektora brzine lakih partnera reakcije. Ovi podatci omogućili su određivanje elektromagnetskih prijelaza i udarnih presjeka svakog kanala

prijenosa, tj. svakom pojedinom izotopu jedinstveno je pridružen njegov γ-spektar. Jedan od glavnih ciljeva rada uspostavljanje je snažnije veze između mehanizma reakcije i nuklearne strukture.

Osnovni su stupnjevi slobode u modelima koji opisuju nuklearne sudare na energijama bliskim kulonskoj barijeri površinske vibracije (oko zatvorenih ljusaka), rotacije (između ljusaka) i jednočestična stanja. Pobuđenjem ovih stanja, energija i kutna količina gibanja prenose se s relativnog gibanja dvije sudarajuće jezgre na unutarnje stupnjeve slobode. Naša je hipoteza da će prijenosom nukleona dominantno pubuđena biti stanja yrasta, jednočestična stanja, kao i stanja koja se mogu opisati kao sparivanje jednočestičnih stanja i vibracija/rotacija. Cilj nam je pokazati da će mehanizam reakcije, iako se radi o dva teška sustava, očuvati selektivnost pobuđenja stanja određenih struktura - pojavu koja je već proučavana u sudarima lakih iona. Očekujemo naći koja će stanja biti najjače pobuđena i odrediti njihova zajednička svojstva vezana za strukturu jezgre. Štoviše, želimo kvantitativno pokazati do koje je mjere očuvana selektivnost pobuđenja stanja specifičnih struktura u odnosu na sudare s lakim ionima.

Teškoionski sudari

Teškoionski sudari podrazumijevaju projektile masenog broja A koji je veći ili jednak od 4, iako obično mislimo na ione puno većih masa [BW00]. U istraživanjima nuklearne strukture potrebno je poznavati puno eksperimentalnih podataka, npr. nuklearne mase, energije vezanja, energije nivoa, spinove, paritete, udarne presjeke reakcije, brzine elektromagnetskih prijelaza, električne i magnetske momente itd. [BM69]. U sudarima teških iona očekuje se mnoštvo reakcija. Iako ne postoji stroga granica između različitih tipova reakcija, možemo ih razlikovati prema parametru sudara, prenešenoj kutnoj količini gibanja, energiji itd. U perifernim su sudarima najčešći tipovi reakcija kvazielastični sudari, koji uključuju kulonska pobuđenja, elastično raspršenje, neelastično raspršenje te prijenos nukleona. Za manje parametre sudara dolazi do duboko neelastičnog raspršenja, pri čemu se veći dio kinetičke energije projektila pretvara u unutarnju energiju, tako da kinetička energija izlaznih čestica potječe većinom od kulonskog pobuđenja. Za još manje parametre sudara i pod odgovarajućim uvjetima može doći i do fuzije.

U ovom radu bavit ćemo se reakcijama prijenosa koje imaju raspon od kvazielastičnih (prijenos male energije, mase i količine gibanja) do duboko neelastičnih procesa (veliki prijenos mase i energije). One imaju značajnu ulogu u proučavanju nuklearne strukture; s lakim ionima, pružaju podatke o modelu ljusaka (prijenos jednog nukleona) i pomažu uspostavljanju korelacija između nukleona (prijenos dvaju nukleona) [Bun13]. U reakcijama prijenosa više nukleona moguće je (pravilnim odabirom sudarajućih jezgara i njihovih energija) dobiti neutronski bogate jezgre, u kojima se očekuju nova svojstva (npr. različiti magični brojevi).

Načini detekcije teškoionskih sudara

U proučavanju nuklearnih reakcija važnu ulogu imaju magnetski spektrometri, a postav spektrometra ovisi o vrsti reakcije i cilju istraživanja. Prvi spektrometri za detekciju teškoionskih sudara koristili su neka svojstva spektrometara za lake ione, npr. Q3D ili split-pole magnetski sustav [Lat04]. Split-pole spektrometar sadrži dva odvojena pola i jednu magnetsku zavojnicu te svija putanje iona u horizontalnoj ravnini. Često se koristi u području srednjih masa za određivanje udarnog presjeka izlaznih čestica u kvazielastičnom području. Q3D je kratica za spektrograf koji ima jednu kvadrupolnu leću i tri dipolna magneta. Takvi se spektrografi još uvijek koriste u laboratorijima JAERI, München, Strasbourg itd.

Za bolju efikasnost detekcije teških iona koriste se spektrometri koji rade na načelu mjerenja vremena proleta (TOF). Njihove su glavne karakteristike kvadrupolni magneti, koji fokusiraju putanje iona te time omogućuju veću efikasnost u relativno maloj fokalnoj ravnini, ali u isto vrijeme gube informaciju o putanjama iona. Primjer TOF spektrometra je PISOLO u Legnaru u Italiji.

Za veće prostorne kutove (do 100 msr), nova generacija spektrometara koristi jednostavnu magnetsku konfiguraciju u kombinaciji s rekonstrukcijom putanja iona za svaki događaj, za koju je potrebno odrediti prostorne koordinate iona u najmanje dvije točke duž putanje. Ovi se spektrometri najčešće koriste za proučavanje reakcija okrznuća, koje karakterizira veliki broj izlaznih kanala i u kojima izlazni fragmenti imaju širok raspon energija i kutnih količina gibanja, a udarni presjeci mogu varirati do nekoliko redova veličina. Trenutno su u funkciji spektrometri velikog prostornog kuta Prisma u Legnaru (Slika 2.1), MAGNEX u Cataniji i Vamos u GANIL-u.

Detekcija γ-zraka pruža informacije o nuklearnim energijskim nivoima; energija i intenzitet γ-zraka određuju položaj nivoa; vrijeme raspada određuje vrijeme poluživota nivoa; polarizacija γ-zraka određuje paritet nivoa; kutna distribucija i korelacije između γ-zraka pružaju informacije o spinovima, magnetskim momentima, kvadrupolnim momentima itd. γ-zrake emitiraju se u nuklearnim procesima tijekom radioaktivnog raspada ili u nuklearnim reakcijama, a njihove tipične energije su u rasponu od 0.1 MeV do 20 MeV. Detekcija elektromagnetskog zračenja temelji se na interakciji zračenja i tvari te razlikujemo tri glavna tipa interakcije (Slika 2.2 [LDV03]):

- fotoelektrični efekt dominira na niskim energijama ($E < 0.2$ MeV). γ-zraka apsorbira se u materijalu, a prenešena energija koristi se za izbacivanje vezanog elektrona iz atoma. Ova se šupljina popunjava, emitirane X zrake se apsorbiraju, a izbačeni elektron zaustavlja se u sudarima s drugim elektronima. Udarni presjek fotoelektričnog efekta razmjeran je Z^n/E^3

- Comptonovo raspršenje dominira na srednjim energijama (0.2 MeV $< E <$ 5 MeV), a predstavlja elastično raspršenje fotona (γ-zraka) na slobodnim elektronima. Upadni foton rasprši se uz gubitak energije, a ostatak energije odnosi elektron. Udarni presjek za Comptonovo raspršenje proporcionalan je sa Z.

- Proizvodnja para elektron-pozitron dominira na energijama $E > 5$ MeV. Razlika između energije γ-zrake i energije 1.022 MeV (dvostruka masa mirovanja elektrona), tj. suvišak energije, pretvara se u energije elektrona i pozitrona. Nakon toga pozitron se anihilira u detektoru, a proizvode se dva fotona energija 0.511 MeV. Ti se fotoni apsorbiraju u detektoru, što se očituje kao vrh u γ-spektru na koji se mora obratiti posebna pažnja, jer on nije dio γ-spektra kojeg emitira jezgra u reakciji. Udarni presjek za proizvodnju para proporcionalan je sa Z^2.

Eksperimenti za detekciju γ-zraka mogu koristiti tanke ili debele mete. U eksperimentima s debelim metama (> 30 mg/cm^2) produkti reakcije se zaustavljaju u meti. Dobra efikasnost složenih γ-detektora omogućava detekciju velikog broja γ-zraka i pruža informacije o njihovim kutnim raspodjelama i vremenskim koincidencijama, posljedica čega je mogućnost konstrukcije bogatih shema nivoa izlaznih produkata. Nedostatak ovakvih eksperimenata je nužnost

prethodnog poznavanja barem nekih od γ-zraka izlaznog sustava kako bi se izlazni produkti prepoznali po masi i atomskom broju te γ-γ koincidencije mogle pridružiti određenom izotopu. Također, u eksperimentima s debelim metama mogu se detektirati samo one γ-zrake čije je vrijeme života duže od vremena potrebnog za zaustavljanje emitiranog iona u meti.

U eksperimentima s tankim metama (< 1 mg/cm^2) produkti reakcije prolaze kroz metu i kasnije se analiziraju u masenim spektrometrima te se stoga mogu proučavati koincidencije γ-čestica. Kako su u ovom slučaju γ-zrake emitirale čestice u gibanju, γ-spektri moraju se korigirati zbog Dopplerovog efekta, što zahtijeva poznavanje vektora brzine čestica, a koji se može mjeriti novom generacijom spektrometara. Nedostatak je ove metode slabija statistika (manji broj detektiranih γ-zraka) u usporedbi s eksperimentima s debelim metama, zbog ograničenog mogućeg prostornog kuta γ-detektora i male debljine mete, kojom je onemogućen veliki broj reakcija.

Eksperimentalni postav

Eksperiment ^{90}Zr+^{208}Pb izveden je u Laboratori Nazionali di Legnaro u Italiji. Snop ^{90}Zr ubrzavan je akceleratorskim sustavom Tandem-ALPI. Tandem XTU je elektrostatski Van de Graaffov akcelerator koji može raditi samostalno ili kao injektor za supervodljivi linearni akcelerator ALPI. Može ubrzavati ione od ^{1}H do ^{197}Au [www3]. ALPI je linearni supervodljivi akcelerator za teške ione do energija 20 MeV/nukleon prilagođen ionima masa $30 < A < 238$ [For87].

Prisma (Slika 3.1) je magnetski spektrometar za ione s masama $A = 50 - 200$, energija $E = 5 - 10$ MeV/A. Njezina su osnovna svojstva [Ste02]:

- Veliki prostorni kut od 80 msr ($\pm 6°$ za ϑ i $\pm 11°$ za ϕ)

- Visoka prihvatljivost momenta $\pm 10°$

- Razlučivost mase: $\Delta M/M \approx 1/300$ i atomskog broja: $\Delta Z/Z \approx 1/90$

- Energijska rezolucija do 1/1000 (preko vremena proleta)

- Rotacija u kutnom rasponu od $-20°$ do $+130°$,

iako mogu varirati u ovisnosti o reakciji, kinetičkoj energiji iona, njihovim masama itd. [Mij12].

Optički sustav Prisme sastoji se od magnetskog kvadrupola i magnetskog dipola. Prisma ne koristi druge optičke elemente za korekcije aberacija, nego se putanje iona rekonstruiraju događaj po događaj koristeći informacije o položaju iona u ulaznom detektoru i u fokalnoj ravnini te o vremenu proleta. Upravo zbog velikih dimenzija magnetskih elemenata, utjecaj rubnih polja je zanemariv. Svojstva magnetskog kvadrupola dana su u Tablici 3.1, a svojstva magnetskog dipola u Tablici 3.2.

Detektorski sustav Prisme sastoji se od ulaznog detektora (MCP - ploča s mikrokanalićima velike površine; Slika 3.3) i detektora u fokalnoj ravnini: višežičanog lavinskog brojača s paralelnim pločama (MWPPAC - Slika 3.4) i ionizacijske komore (IC - Slika 3.5). Ulazni detektor daje informacije o položaju (u x i y smjeru) i vremenu. Vremenska rezolucija mu je 400 ps, a prostorna rezolucija 1 mm u oba smjera, dok mu je efikasnost u eksperimentima s teškim ionima gotovo 100%. MWPPAC pruža informacije o x i y položaju iona u fokalnoj ravnini, kao i vremenski signal potreban za mjerenje vremena proleta (u koincidenciji s MCP). Vremenska rezolucija mu je 200-300 ns, a prostorna rezolucija 1 mm u x smjeru i 2 mm u y smjeru. Ionizacijska komora bilježi podatke o ukupnoj kinetičkoj energiji iona te o gubitku kinetičke energije u svakoj od četiri jednake sekcije, kojima je podijeljena u dubinu.

Clara je polukugla koja se sastoji od 25 četverodijelnih Ge detektora visoke čistoće u zajedničkom štitu od Comptonovog zračenja, postavljena u blizini mete, ali na suprotnu stranu od spektometra Prisma (Slika 3.6), točnije, na kutove između 104° i 180°, s obzirom na smjer ulaza u spektrometar [Gad04] te rotira zajedno s Prismom. Karakteristike Clara detektora za γ-zraku energije $E_\gamma = 1.3$ MeV su:

- Efikasnost fotovrha: 3%

- Omjer događaja u vrhu i ukupnog broja događaja: $P/T \sim 45\%$

- Energijska rezolucija za $v/c \approx 10\%$: 0.6%.

Vezanje Clara detektora s Prisma spektrometrom omogućava mjerenje koincidencija čestica-γ, tj. svakoj čestici prepoznatoj spektrometrom Prisma pridružen je njezin karakteristični γ-spektar.

Kolaboracija Prisma + Clara razvila je posebne programe za analizu podataka. Podatci se zapisuju na magnetske vrpce i tvrdi disk, a čitaju se programom GSORT, koji je dio paketa GASPWARE. Koristeći ovaj program, podatci se sortiraju u 1D (spektre), 2D (matrice) i 3D histograme (kubuse). Ovi se histogrami dalje analiziraju koristeći programe CMAT i XTRACKN, koji služe za bolju vizualizaciju podataka. Svi detektori u sustavu Prisma+Clara moraju se kalibrirati. Za kalibraciju Clara detektora korišteni su radioaktivni izvori ^{152}Eu i ^{56}Co. Kako efikasnost Ge detektora ovisi o energiji upadnog fotona, potrebno je odrediti i efikasnost Clara detektora, koja se određuje prema izrazu

$$\text{efikasnost} = \frac{\text{površina koju zatvara } \gamma\text{-vrh}}{\text{intenzitet } \gamma\text{-zrake}}.$$

Ta ovisnost efikasnosti detektora o energiji γ-zrake prikazana je na Slici 4.10 i opisana funkcijom

$$eff = e^{a+b\cdot\ln E + c\cdot(\ln E)^2 + d\cdot(\ln E)^3 + e\cdot(\ln E)^4 + f\cdot(\ln E)^5},$$

pri čemu je eff oznaka za efikasnost detektora, E energiju γ-zrake, a parametri a, b, c, d i e navedeni su u Tablici 4.2.

Kako je kalibracija detektora Clara provedena koristeći izvor koji miruje, a γ-spektri analizirani u eksperimentu potječu od iona koji se kreću velikim brzinama (do $0.1c$ za ione cirkonija, pri čemu većina iona ima brzine oko $0.09c$, Slika 4.11), mora se provesti korekcija uslijed Dopplerovog efekta. Odnos između emitirane ($E_{\gamma 0}$) i detektirane (E_γ) energije γ-zrake je

$$E_\gamma = E_{\gamma 0} \frac{\sqrt{1 - \frac{v_b^2}{c}}}{1 - \frac{v_b}{c}\cos\vartheta_b},$$

gdje je v_b brzina lakog izlaznog partnera, a ϑ_b kut koji $\overrightarrow{v_b}$ čini s Ge kristalom koji detektira γ-zraku (Slika 4.12). Uz pretpostavku da se radi o binarnim reakcijama $a + A \longrightarrow b + B$, gdje je a projektil, A meta u mirovanju, a b i B izlazne čestice nalik projektilu i meti, moguće je odrediti i parametre v_B i ϑ_B, na temelju čega se može napraviti i Doppler korekcija γ-spektara teških partnera reakcije.

Kao što je već spomenuto, Clara sadrži 25 četverodijelnih detektora u zajedničkom štitu od Comptonovog zračenja, koji se sastoji od BGO (bizmut germanat) scintilatora. Štit radi na načelu antikoincidencije s kristalima Ge, odbacujući događaje koji istovremeno emitiraju

γ-zraku u kristalu Ge i BGO materijalu. Svrha ovog postupka je odbacivanje svih γ-zraka koje nisu u potpunosti detektirane, i na taj način smanjivanje pozadinskog dijela spektra koji potječe od Comptonovog raspršenja. Sam postupak provodi se posebno konstruiranim naredbama u programu GSORT.

Rekonstrukcija putanje i identifikacija iona

Rekonstrukcija putanje iona te njihovo prepoznavanje provodi se upotrebom programa GSORT i posebno razvijenih rutina, koje su dijelovi programa. Prisma bilježi sljedeće podatke:

- Prostorne koordinate u ulaznom detektoru (MCP)

- Prostorne koordinate u fokalnoj ravnini (MWPPAC)

- Vrijeme proleta (TOF) između MCP i MWPPAC

- Energiju oslobođenu u svakoj sekciji ionizacijske komore, ΔE

- Ukupnu energiju, E, oslobođenu u ionizacijskoj komori, u kojoj se ioni zaustavljaju.

Poznavajući koordinate iona u ulaznom detektoru, udaljenost između elemenata spektrometra te sile koje djeluju na ione unutar magneta, moguće je izračunati jednadžbe gibanja iona kroz spektrometar [Mon11]. Važna je pretpostavka da se ioni gibaju planarno nakon izlaska iz kvadrupolnog magneta, a koja se temelji na činjenici da je uzdužna dimenzija Prisme (6.5 m) mnogo veća od poprečne (0.2 m) te da je moguće zanemariti rubna polja magneta. Iz gore navedenih podataka, pomoću programa GSORT, računaju se sljedeći podatci:

- Duljina puta iona, D

- Polumjer zakrivljenosti putanje unutar dipolnog magneta, R

- Ukupna energija oslobođena u ionizacijskoj komori, E

- Domet iona u ionizacijskoj komori, r.

Prema Betheovoj formuli, gubitak energije nabijene čestice pri interakciji s materijom može se svesti na izraz

$$\frac{dE}{dx} \propto \frac{mZ^2}{E},$$

gdje je E energija čestice, x udaljenost koju čestica prijeđe, m masa čestice, Z atomski broj čestice. Prema prethodnom izrazu (gdje su dx, E i dE veličine ekvivalentne veličinama r, E i ΔE), u matrici E vs. r uočavaju se različita područja, koja pripadaju različitim elementima, kao na Slici 5.1. Najintenzivnije područje odgovara raspršenom snopu Zr, a ostala područja pridružuju se ostalim elementima, poštivajući činjenicu da za danu energiju E atomski broj Z opada s porastom r. Postavljajući dvodimenzionalne uvjete na željeno područje (tj. događaje koji odgovaraju željenom elementu), nastavlja se postupak prepoznavanja različitih izotopa odabranog elementa.

Unutar dipolnog magneta Lorentzova sila svija putanje iona te vrijedi $\frac{mv^2}{R} = qvB$, gdje je m masa, a q naboj iona. Brzina iona v računa se kao omjer puta koji ion prijeđe, D, i vremena proleta, TOF: $v = \frac{D}{TOF}$. Uzimajući u obzir relativističke popravke zbog velikih brzina iona te poznavajući kinetičku energiju iona oslobođenu u ionizacijskoj komori, slijedi

$$\frac{A}{Q} = \frac{BR}{\frac{D}{TOF\sqrt{1-\beta^2}}}$$

te

$$E \propto QBRv.$$

Prema tome, u matrici koja prikazuje ukupnu oslobođenu energiju u ionizacijskoj komori, E, i umnožak brzine iona i polumjera zakrivljenosti unutar dipolnog magneta, vR, uočavaju se različita područja, od kojih svako predstavlja različito nabojno stanje iona, kao na Slici 5.3. Moguće je izračunati najvjerojatnije nabojno stanje za svaki element, kojemu ujedno pripada i najintenzivnije područje u matrici E vs. Rv. S obzirom na nagib ostaih područja u matrici, svakom se od njih pridružuje pripadno nabojno stanje. Poznavajući omjer mase i nabojnog broja, svakom se području u matrici može tada pridružiti i maseni broj. Ovaj se postupak primjenjuje na sve ostale izotope, a masena raspodjela svih izotopa opaženih u eksperimentu, za koje je zabilježena barem jedna γ zraka, prikazana je na Slici 5.5.

Rezultati

Interakcijom jezgara ^{90}Zr i ^{208}Pb proizveden je velik broj različitih izlaznih jezgara. Zahvaljujući koincidenciji γ-čestica, svakoj se jezgri detektiranoj u spektrometru Prisma jedinstveno pridružuje njezin γ-spektar. U ovom smo se radu fokusirali na proučavanje spektara

izotopa Zr, Pb, Y i Sr. Za svaki smo proučavani izotop prikazali njegov γ-spektar, naveli prepoznate γ-zrake te konstuirali sheme nivoa koji su opaženi u našem mjerenju. Energije, spinovi i pariteti nivoa, njihovi omjeri grananja i energije prijelaza navedeni su kao u prihvaćenim nivoima za svaki izotop (National Nuclear Data Center at Brookehaven National Laboratory - http://www.nndc.bnl.gov [www4]). U slučajevima u kojima je to moguće, vrijednosti preuzete iz [www4] zaokružene su na prvu decimalu. Broj događaja u eksperimentu, kao što je i očekivano u γ-čestičnim mjerenjima, premali je za uspostavljanje koincidencija između γ-zraka pojedinog izotopa, tj. γ-γ-čestica koincidencija. Imajući to u vidu, naš cilj usmjerili smo prema razumijevanju strukture najjačih pobuđenih stanja, u kontekstu selektivnosti reakcije prijenosa nukleona u teškoionskim sudarima.

Temeljem prethodnih mjerenja na eksperimentalnom postavu Prisma + Clara, a koja se tiču reakcija prijenosa više nukleona, očekivano je pobuđenje stanja određenih struktura. Točnije, zbog činjenice da ove reakcije na niskim energijama (blizu kulonske barijere) maksimiziraju prenešenu kutnu količinu gibanja, očekivano je pobuđenje stanja visokih spinova. Također, kako se reakcije prijenosa s lakim ionima koriste između ostalog za pobuđenje jednočestičnih stanja, u ovoj je reakciji očekivano pobuđenje stanja jednočestičnog karaktera. Nadalje, nedavna istraživanja pokazala su da reakcije prijenosa više nukleona pobuđuju i stanja koja se opisuju vezanjem fonona i fermiona, što je pojava koju smo potražili i u našoj reakciji.

Prije same analize spektara, bilo je potrebno iz svakog pojedinog spektra izdvojiti γ-zrake koje su, zbog nesavršenog razdvajanja nabojnih stanja i masa za ove vrlo teške jezgre prilikom analize, preslikane iz spektara susjednih jezgara. Ova korekcija spektara sastojala se od oduzimanja skaliranog γ-spektra onog izotopa kojemu pripada neželjena γ-zraka od spektra koji promatramo, i to u cijelom rasponu energija. Taj postupak nije značajno promijenio broj događaja u očišćenom spektru za one γ-zrake koje pripadaju promatranom izotopu, osim u posebnim slučajevima, kada promatrani spektar i spektar koji se oduzima imaju γ-zraku slične energije. Spektri korišteni za korekcije, kao i pripadajući koeficijenti, navedeni su u Tablicama 6.1, 6.25 i 6.35. U cijelom su radu proučavani samo spektri korigirani na ovaj način.

U spektrima se tako mogu primijetiti složene pozadine širokih vrhova, koje potječu od

loše Doppler korekcije γ-zraka binarnog partnera.

U slabijim kanalima reakcije, za stanja koja imaju složen obrazac raspada, opazili smo samo najsnažije grane raspada. U tim smo slučajevima provjerili da je očekivani broj događaja za slabije prijelaze u skladu s opaženim brojem događaja i pozadinskim zračenjem za promatrani energijski nivo. γ-zrake koje iz gore navedenih razloga nisu opažene, navedene su u Tablicama 1, 2, 3 i 4 u Appendixu.

Izotopi cirkonija

U ovom su eksperimentu proučavani izotopi cirkonija $^{89-94}$Zr. Njihovi γ-spektri prikazani su na Slikama 6.7, 6.9, 6.12, 6.17, 6.22 i 6.28, a opažene γ-zrake navedene su u Tablicama 6.2, 6.3, 6.4, 6.6, 6.1.5 i 6.1.6. Na temelju opaženih γ-zraka konstruirane su sheme nivoa, prikazane na slikama 6.8, 6.10, 6.13, 6.18, 6.23 i 6.29.

Kanal izotopa ^{89}Zr je prilično slab u ovom eksperimentu (zabilježeno je oko 43000 događaja). U vrpci pozitivnog pariteta opazili smo selektivno pobuđenje stanja visokog spina (do $25/2^+$). Tri najniža stanja u vrpci negativnog pariteta ($1/2^-$, $5/2^-$ i $3/2^-$) mogu se u jednostavnom modelu ljusaka prepoznati kao jednočestiča stanja povezana s neutronskom šupljinom u orbitalama $p_{1/2}$, $f_{5/2}$ i $p_{3/2}$.

U izotopu ^{90}Zr, najsnažnije su pobuđena stanja 2_1^+ (E_{ex} = 2186.3 keV), 4_1^+ (E_{ex} = 3076.9 keV) i 3_1^- (E_{ex} = 2747.9 keV), a primjećuje se i pobuđenje ostalih stanja yrasta do 10^+. Opažene su dvije nove γ-zrake; E_γ = 213.7 keV and 1872 keV (označene * u Tablici 6.3). Za γ-zraku E_γ = 1872 keV predlažemo da pripada jednom od dva moguća prijelaza (na temelju razlike energija poznatih energijskih nivoa): E_i = 4062(5) keV ($J^\pi = 4_2^+$) $\longrightarrow$ E_f = 2186.3(15) keV ($J^\pi = 2_1^+$) ili E_i = 4946(6) keV ($J^\pi = 4_6^+$) $\longrightarrow$ E_f = 3076.9(15) keV ($J^\pi = 4_1^+$), iako prednost dajemo prvom navedenom prijelazu, posebice jer sličan raspad vidimo u shemi raspada teškog binarnog partnera, ^{208}Pb.

Najjače pobuđena stanja u izotopu ^{91}Zr su energijski niskoleže ća stanja pozitivnog pariteta, štoviše, pobuđena su sva poznata stanja do energije E_{ex} = 2170.2 keV ($J^\pi = (11/2)^-$). Prva četiri stanja, koja su ujedno i najsnažnije pobuđena ($1/2^+$, $5/2^+$, $7/2^+$ i $3/2^+$), mogu se shvatiti kao jednočestična stanja ljuske $4\hbar\omega$. Kako bismo bolje proučili karakter najsnažnije pobuđenih stanja, usporedili smo jačine pobuđenja dobivene našim eksperimentom s on-

ima dobivenim u (d, p) eksperimentima [Sha13, BH70, BHK76], u kojima se očekuje jako pobuđenje jednočestičnih stanja. Ova je usporedba prikazana na Slici 6.14, gdje su plavom bojom prikazani podatci iz reakcije ^{90}Zr+^{208}Pb, a crvenom, žutom i zelenom bojom podaci iz [Sha13], [BH70] i [BHK76], redom. U slučaju ^{90}Zr+^{208}Pb, visine stupaca na slici dobivene su oduzimanjem zbroja intenziteta γ-zraka koje popunjavaju određeni energijski nivo od zbroja intenziteta γ-zraka koje se raspadaju s istog nivoa te normiranjem dobivenih iznosa. Slika jasno pokazuje da su i u reakcijama induciranim lakim ionima, kao i u našoj reakciji, slične jačine pobuđenja opažene za stanja $J^\pi = 1/2^+$ ($E_{ex} = 1204.8$ keV) i $J^\pi = 3/2^+$ ($E_{ex} = 2042.4$ keV), što sugerira njihov jednočestični karakter. Dodatnu potvrdu tome nalazimo u [DBI11], gdje su teorijskim računom temeljenom na modelu ljusaka dobiveni brojevi zauzeća prikazani u Tablici 6.5.

U jezgri ^{91}Zr posebno je zanimljiva usporedba dvaju stanja spina $9/2^+$ (E_{ex}=2131.5 i 2914.2 keV), od kojih jedno može biti jednočestično stanje (uslijed neutronske šupljine u orbitali $g_{9/2}$), dok drugo može biti posljedica vezanja osnovnog stanja $5/2^+$ na kvant vibracija 2^+ u rastegnutoj konfiguraciji. Slična se situacija ponavlja za dva stanja spina $(11/2)^-$ ($E_{ex} = 2170.2$ i 2320.5 keV), od kojih jedno može imati dominantno jednočestični karakter, a drugo potjecati od vezanja osnovnog stanja i fonona 3^- u rastegnutoj konfiguraciji. Za ova stanja različiti teorijski modeli predviđaju miješanu konfiguraciju, o čemu će više riječi biti u nastavku teksta.

U ^{91}Zr opažena je i jedna nova γ-zraka (E_γ =3466 keV), za koju predlažemo da pripada raspadu stanja $E_i = 3469$ keV ($J_i^\pi = 7/2^+$) na osnovno stanje.

U spektru izotopa ^{92}Zr opaženo je snažno pobuđenje stanja yrasta (do 16^+), s naglaskom na najniža stanja 2^+ ($E_{ex} = 934.5$ keV), 4^+ ($E_{ex} = 149.5$ keV) i 6^+ ($E_{ex} = 2957.4$ keV), kao i 3^- ($E_{ex} = 2339.7$ keV). Slika 6.20 prikazuje usporedbu jačine pobuđenja najsnažnije pobuđenih stanja u našem eksperimentu s onima opaženima u (t, p) mjerenjima opisanima u [IMB75] i [Fly74]. Visine stupaca na slici dobivene su kao i u primjeru ^{91}Zr. Uočavamo da se naši rezultati slažu s navedenim citiranim rezultatima za stanja niskih spinova, s izuzetkom stanja 2_1^+ ($E_{ex} = 934.5$ keV) i 4_1^+ ($E_{ex} = 1495.5$ keV).

U vrpci pozitivnog pariteta izotopa ^{93}Zr, pobuđena su sva poznata stanja do energije $E_{ex} \sim 1425$ keV (Slika 6.23). U višem energijskom dijelu spektra, selektivno su pobuđena

stanja yrasta do $J^\pi = (25/2^+)$ ($E_{\mathrm{ex}} = 4716.3$ keV). U nižem energijskom dijelu spektra, opažena su slična stanja kao u ^{91}Zr, koja su pobuđena približno jednakom jakošću. Točnije, opazili smo jako pobuđenje stanja $1/2^+$ i $3/2^+$, koja mogu imati dominantan jednočestični karakter. Također, opazili smo i pobuđenje stanja $9/2_1^+$ ($E_{\mathrm{ex}} = 949.8$ keV), koje se može objasniti vezanjem osnovnog stanja i kvanta vibracija 2^+ u rastegnutoj konfiguraciji. U vrpci negativnog pariteta, pobuđena su samo dva poznata stanja : $11/2^-$ i $(15/2^-)$. Opažene su i tri nove γ-zrake te predloženi elektromagnetski prijelazi kojima bi one mogle odgovarati, što je navedeno u Tablici 6.8 i prikazano na Slici 6.25.

U spektru izotopa ^{94}Zr, sva opažena stanja pripadaju liniji yrasta, i to do spina 14 u pozitivnoj te do spina 7 u negativnoj vrpci. Također, opažena je i jedna nova γ-zraka.

Slike 6.31 i 6.32 pokazuju usporedbu γ-spektara izotopa Zr dobivenih u reakciji ^{90}Zr+^{208}Pb, i reakciji ^{40}Ca+^{96}Zr. Ove usporedbe pokazuju snažno pobuđenje istih nivoa u obje reakcije. Usporedba najsnažnije pobuđenih stanja u svim opaženim izotopima Zr prikazana je na Slikama 6.33 i 6.35. U parnim izotopima, opažene su energije pobuđenja do ~ 8 MeV, s naglaskom na stanja yrasta u vrpcama pozitivnog pariteta. U vrpcama negativnog pariteta, pobuđena su stanja 3^-, 5^- i 7^-. Bitno je napomenuti da u parnim izotopima Zr nismo opazili pobuđenje viših 0^+ stanja.

Najjače pobuđena stanja pozitivnog pariteta u ^{91}Zr i ^{93}Zr su stanja yrasta. Niskoenergijski dio spektra neparnih izotopa Zr obilježava pobuđenje stanja jednočestičnog karaktera. U jednostavnom modelu ljusaka (Slika 6.3), očekivana jednočestična stanja u ^{89}Zr uzrokovana neutronskom šupljinom u ljusci $3\hbar\omega$ bila bi $J^\pi = 9/2^+, 1/2^-,\ 5/2^-,\ 3/2^-$ i $7/2^-$, od kojih smo opazili sve osim $7/2^-$. U ^{91,93}Zr, nespareni neutron u ljusci $4\hbar\omega$ (točnije, u orbitalama $g_{7/2}$, $d_{3/2}$, $s_{1/2}$ ili $h_{11/2}$) rezultirao bi jednočestičnim stanjem spina $J^\pi = 9/2^+, 7/2^+,\ 3/2^+$, $1/2^+$ i $11/2^-$.

Osnovno stanje analiziranih izotopa Zr slijedi jednostavni model ljusaka, tj. nakon popunjavanja ljuske $3\hbar\omega$, neutroni popunjavaju orbitalu $2d_{5/2}$, zbog čega izotopi ^{91,93,95}Zr imaju spin osnovnog stanja $5/2^+$. ^{97,99}Zr imaju spin osnovnog stanja $1/2^+$, pri čmu neutroni popunjavaju orbitalu $3s_{1/2}$. Prvih nekoliko niskoenergijskih stanja mogu se promatrati kao stanja jednočestičnog karaktera. U našem eksperimentu opazili smo stanja $7/2^+$, $1/2^+$, $3/2^+$ i $11/2^-$. Slika 6.34 prikazuje energije tih stanja (t.j. prvih $7/2_1^+$, $1/2_1^+$, $3/2_1^+$ i $11/2_1^-$ stanja)

u izotopima ^{91,93,95,97}Zr. Primjećujemo da sva stanja istog spina imaju približno jednake energije za različite izotope Zr, osim u slučaju $3/2^+$, što upućuje na miješanu konfiguraciju tog stanja. Također, ovo daje naslutiti da redoslijed i energije orbitala $1g_{7/2}$, $3s_{1/2}$ i $1h_{11/2}$ ne variraju mnogo u ovom području, u kojem izotopi Zr popunjavaju orbitalu $d_{5/2}$.

Ponašanje jednočestičniih energija orbitala $p_{1/2}$, $p_{3/2}$, $f_{5/2}$ i $g_{9/2}$ prikazano je na Slici 6.3, gdje se može primijetiti da osim stanja $3/2^+$ u ^{93}Zr, ostala stanja sa Slike 6.34 slijede ona sa Slike 6.3. Za izotope Zr s masenim brojem $A > 97$, spinovi osnovnog stanja su $(1/2^+)$, $(3/2^+)$ i $(5/2^-)$ za ^{99}Zr, ^{101}Zr i ^{103}Zr, redom. Očekivana jednočestična stanja su $5/2^+$, $1/2^+$, $11/2^-$, $1/2^+$ i $3/2^+$, uslijed nesparenog neutrona u ljusci $4\hbar\omega$.

Osim snažnog pobuđenja jednočestičnih stanja, reakcije prijenosa nukleona selektivno popunjavaju stanja visokog spina pozitivnog i negativnog pariteta u ^{89}Zr, ^{91}Zr i ^{93}Zr, stoga u tim izotopima primjećujemo spinove do 17/2 i 25/2.

Osim jednočestičnih stanja i stanja visokih spinova, opazili smo i pobuđenje stanja čija se struktura može objasniti vezanjem jednočestičnih stanja i fonona. Izotopi ^{91}Zr i ^{93}Zr imaju spin osnovnog stanja $5/2^+$, koji potječe od jednog nesparenog neutrona u orbitali $d_{5/2}$. Sparivanjem tog neutrona na stanje 2^+, dobio bi se multiplet stanja $9/2^+$, $7/2^+$, ... $1/2^+$, za koja se u slučaju slabog vezanja očekuje energija bliska energiji stanja 2^+ u susjednom izotopu Zr. Slično, sparivanjem osnovnog stanja sa stanjem 3^-, očekujemo multiplet $11/2^-$, $9/2^-$, ... $1/2^-$. Mehanizam reakcije ne popunjava sve komponente multipleta jednako, nego prednost daje rastegnutoj konfiguraciji ($9/2^+$ i $11/2^-$) zbog toga što je vjerojatnost prijenosa najveća za najveći prijenos kutne količine gibanja [BW00]. Ova činjenica potvrđena je dosad provedenim mjerenjima na spektrometru Prisma [Szi07, Szi11, Lun07, Rec12].

U nastavku teksta obratit ćemo pozornost na moguća vezanja fonona (u rastegnutoj konfiguraciji) i osnovnog stanja za izotope cirkonija s masenim brojevima od $A = 89$ do $A = 97$, kao što je prikazano u Tablici 6.10. Ponašanje stanja 2^+ u parno-parnim izotopima Zr prikazano je u Tablici 6.11, dok je za stanja 3^- prikazano u Tablici 6.12. Slike 6.36 i 6.37 prikazuju usporedbu energija prvih 2^+ (i 3^-) stanja u parnim izotopima Zr te stanja koja bi se mogla opisati vezanjem fonona 2^+ (tj. 3^-) u rastegnutoj konfiguraciji na osnovno stanje u neparnim izotopima (kao što je prikazano u Tablici 6.10).

Kako bismo dobili jasniju sliku o ponašanju kvadrupolnih i oktupolnih stanja u parno-

parnim izotopima Zr te o njihovom vezanju na osnovno stanje, saželi smo postojeće podatke u Tablice 6.11, 6.12 i 6.13. Također, spektre razmatranih izotopa prikazali smo na Slikama 6.31 i 6.32, dobivenim u reakcijama ^{90}Zr+^{208}Pb i ^{40}Ca+^{96}Zr [Szi07].

Iz Tablice 6.11, vidi se da je u svim promatranim parno-parnim izotopima Zr najjači prijelaz $2^+ \rightarrow 0^+$ (ovo vrijedi i za ^{96}Zr iako taj izotop ne razmatramo detaljno). B(E2) za sva 2^+ stanja kreće se od 0.055 b^2e^2 u ^{96}Zr do 0.008 b^2e^2 u ^{92}Zr. U slučaju oktupolnih stanja, treba spomenuti jezgru ^{208}Pb, koja čini idealan laboratorij za proučavanje fononskih stanja, budući da joj je prvo pobuđeno stanje kolektivno 3^- stanje na energiji 2.62 MeV. Kolektivnost ovog stanja (B(E3; $3^- \rightarrow 0^+$) = 34 W.u.) potječe od različitih konfiguracija.

"Zatvorena jezgra" Zr predstavlja kompliciraniju situaciju. Niskoenergijskim dijelom spektra dominiraju stanja 2^+ te nešto više energijsko stanje 3^-. Stanje 3^- u ^{96}Zr je vrlo kolektivno [B(E3; $3^- \rightarrow 0^+$) = 51 W.u.]. Ako promotrimo Tablicu 6.12, vidimo kako se obrazac raspada za stanje 3^- mijenja od $A = 90$ do $A = 96$. U ^{90}Zr, dominantan je raspad preko prijelaza E1 na stanje 2^+, a samo oko 4% pripada prijelazu E3 na osnovno stanje. U ^{96}Zr, prijelaz E1 je najjači, dok oko 20% pripada prijelazu E3 na osnovno stanje. Kako se približavamo sredini ljuske, situacija postaje složenija, što se posebno očituje kod ^{92}Zr, gdje je obrazac raspada stanja 3^- vrlo složen. Još uvijek je prijelaz E1 najjači, slijedi ga raspad na stanja 4_1^+ ($\sim 30\%$) i 2_2^+ ($\sim 11\%$), dok prijelaz E3 ima zanemariv utjecaj ($\sim 0,1\%$). U slučaju ^{94}Zr, obrazac raspada je sličan kao u ^{90}Zr.

Situacija se ponavlja i u parno-neparnim izotopima. To je posebno očito u slučaju ^{95}Zr [Szi07, BF73, Pan05], gdje je raspodjela jakosti prijelaza E1 i E3 slična onoj opaženoj u ^{96}Zr. U ^{89}Zr, prvo stanje $15/2^-$ (koje je kandidat za vezanje osnovnog stanja $9/2^+$ i kvanta vibracija 3^-) na energiji 2150.6 keV raspada se preko E_γ = 29.3 keV (I_γ = 100%) i E_γ = 206.9 keV (I_γ = 42%). Prva od navedenih γ-zraka ima premalu energiju da bi bila opažena detektorom Clara, dok druga ima permali intenzitet te ih stoga nismo opazili u našem eksperimentu. U slučaju ^{93}Zr, obrazac raspada stanja $11/2^-$ nije u potpunosti poznat. Od poznatih prijelaza, opazili smo E1 prijelaz stanja ($11/2^-$) na energiji 2374.6 keV, a moguće je da smo opazili i raspad E3 (E_γ = 2375 keV). Međutim, omjer broja događaja za te raspade (E3/E1) nije sukladan očekivanom.

Također, potražili smo i moguće prijelaze E1 i E3 sa stanja označenih s $9/2^-$, $11/2^-$ na

energijama 2025(10) keV i 2363(10) keV u ^{93}Zr. U ovom slučaju, E1 prijelazima odgovarale bi γ-zrake energija 1075 i 1413 keV, dok bi prijelazima E3 odgovarale γ-zrake energija 2025 i 2363 keV. Kako bismo povećali statistiku, ove smo γ-zrake potražili u nekorigiranom spektru izotopa ^{93}Zr (kojeg smo korigirali oduzimajući skalirani spektar ^{92}Zr, u kojem nema značajnih γ-zraka na energijama oko $2-3$ MeV). Opazili smo vrh na energiji oko 2367 keV, iako u ovom području spektra viskoa pozadina (background) te smanjena efikasnost detektora otežavaju prepoznavanje γ-zraka. Očekivani prijelaz E1 (1413 keV) preklapa se s relativno snažnim γ-zrakama u ^{93}Zr, $E_\gamma = 1334.6$ keV (intenziteta $\sim 30\%$) i $E_\gamma = 1425.2$ keV ($\sim 40\%$). Prema tome, ne možemo jednoznačno tvrditi da smo opazili raspad stanja 2363 keV (uz pretpostavku da je spin tog stanja $11/2^-$) preko očekivanih prijelaza E1 i E3. U slučaju stanja $9/2^-$, $11/2^-$ na energiji 2025 keV, nismo opazili očekivani E3 prijelaz.

Slična situacija ponovila se i u jezgri ^{91}Zr, gdje smo opazili dva stanja $11/2^-$ sličnh energija. Štoviše, gledajući Sliku 6.37, uočavamo da energije oba $11/2^-$ stanja odudaraju od prikazanih energija susjednih izotopa.

Ova situacija je podrobnije opisana u Ref. [BHK76], gdje su autori tražili stanja koja potječu od sparivanja pedeset prvog neutrona i stanja 2^+ i 3^-. U ovom eksperimentu, kutne raspodjele izlaznih čestica u reakcijama (d, p), (p, p') i (p, d) analizirane su split-pole spektrografom i detektirane nizom tvrdih položajno osjetljivih detektora. Zaključeno je da se stanja istog spina i pariteta, ali različito vezana na osnovno stanje snažno miješaju jedno s drugim i s jednočestičnim stanjima te da se model jednostavnog slabog vezanja ne može primijeniti u slučaju ^{91}Zr i vezanja na fonon 3^-. Također je zaključeno da je najveći dio jednočestičnih stanja vezanih uz orbitalu $h_{11/2}$ sadržan u stanju na energiji 2.170 MeV (stanje koje je snažno pobuđeno u reakciji (p, p')).

Ovaj se zaključak ne slaže s raspravom prikazanom u Ref. [SNL09]. Ovdje se detaljno raspravlja o evoluciji stanja $11/2^-$ u izotopima Zr, temeljeno na modelu ljusaka, koji je proveden u proširenom prostoru modela ljudaka ($1f_{5/2}$, $2p_{1/2}$, $2p_{3/2}$, $1g_{9/2}$) za protone i ($2d_{5/2}$, $3s_{1/2}$, $2d_{3/2}$, $1g_{7/2}$, $1h_{11/2}$) za neutrone. Efektivna interakcija proton-proton nađena je usrednjenjem matričnog elementa za dva tijela za izotope $^{57-78}$Ni i izotone s brojem neutrona $N = 50$ (^{70}Cu-^{100}Sn). Interakcija neutron-neutron temeljena je na izračunima u području kositra, a interakcija proton-neutron temelji se na razvoju jednočestičnih stanja između ^{79}Ni i ^{101}Sn.

Rezultati ovog računa u usporedbi s eksperimentalnim nivoima opaženima u našem mjerenju (do stanja $(11/2^-)$ na energiji 2.2 MeV) prikazani su na Slici 6.16. Račun modela ljusaka pokazao je da stanje $11/2^-$ (na energiji 2.2 MeV) nije potpuno jednočestično stanje vezano uz $h_{11/2}$, nego da ima dominantnu komponentu $\pi(p_{1/2}^1 g_{9/2}^1)\ \nu(d_{5/2}^1)$ (55%). Štovše, ukupan broj neutrona u orbitali $h_{11/2}$ dobiven ovim računom je samo 0.16. Također, ovim računom dobio se dobar opis eksperimentalno opaženih stanja yrasta, s iznimkom stanja 3^-, koje odudara od eksperimentalnih podataka (pogotovo za ^{94}Zr). Kao što je već rečeno, kolektivno stanje 3^- dolazi od složene superpozicije pobuđenja među ljuskama, izvan valentnog prostora obuhvaćenog modelom ljusaka. Stoga je moguće da odudaranje stanja 3^- na slici 6.37 potječe od miješanja različitih konfiguracija (jače nego u ostalim izotopima Zr) ili da je stanje koje ima dominantnu strukturu fermion-fonon u zasad još nepoznatom stanju $11/2^-$. Usporedba sa susjednim izotopima sugerira da će takvo stanje imati energiju u području oko 2.7 MeV, u kojem još nije pronađeno stanje ovog spina.

Budući da teškoionski sudari omogućuju proučavanje odnosa između jednočestičnih modova i modova prijenosa parova (zbog mogućnosti prijenosa više nukleona), u ovoj smo reakciji potražili stanja koja bi se mogla opisati kao sparivanje vibracija, točnije pobuđena stanja 0^+, jer se pobuđenjem ovih stanja u reakcijama prijenosa više nukleona mogu dobiti informacije o efektu rezidualne interakcije, a time i sparivanju.

U reakciji ^{90}Zr$+^{208}$Pb posebno je zanimljivo potražiti modove sparivanja vibracija u sferičnim jezgrama ^{92,94}Zr. Zatvorena podljuska i ljuska za $Z = 40$ i $N = 50$ u ^{90}Zr dobro su polazište za sparivanja vibracija i protona i neutrona. Pobuđenje stanja 0^+ na energijama 5441, 4424 i 4126 keV već je opaženo u jezgri ^{90}Zr te protumačeno u okviru modela sparivanja vibracija [Bro73], međutim, s još uvijek nepoznatim obrascem raspada. Mi smo potražili moguće raspade tih stanja na stanja 2^+ opažena u našem mjerenju (na energijama 2186.3, 3308.8, 3842.2 keV). Moguće γ-zrake i pripadajući prijelazi prikazani su u Tablici 6.15. Iako smo u ovom području, gdje se očekuje sparivanje vibracija, opazili stanja 2^+, nismo uočili raspade poznatih stanja 0^+ na niskoleže ća stanja 2^+.

Isti smo postupak ponovili i s izotopoma ^{92}Zr i ^{94}Zr. Mogući raspadi stanja 0^+ na stanja 2^+ prikazani su u Tablicama 6.15 (za ^{92}Zr) i 6.16 (za ^{94}Zr). U ^{92}Zr, prijelaz sa stanja 0^+ na energiji $E_{\text{ex}} = 3992$ keV na opaženo stanje 2^+ energije $E_{\text{ex}} = 3057.4$ keV (označeno kosim

brojkama u Tablici 6.15) preklapa se s najjačim prijelazom u izotopu ^{92}Zr, što je prijelaz sa stanja 2_1^+ na osnovno stanje.

U ^{94}Zr, ukupan broj događaja manji je nego u ^{90}Zr i ^{92}Zr te je opažen samo raspad s prvog 2^+ stanja ($E_{\mathrm{ex}} = 918.8$ keV). Mogući raspadi s pobuđenih 0^+ stanja ($E_{\mathrm{ex}} = 1300.2(12)$ i $3776(7)$ keV) na ovo 2^+ stanje (prikazani u Tablici 6.16) nisu opaženi.

Spomenimo i usporedbu spektara Zr dobivenim u našem eksperimentu s onima dobivenim mjerenjem ^{40}Ca+^{96}Zr [Szi07]. Slike 6.21, 6.24 i 6.30 prikazuju spektre ^{92,93,94}Zr opažene ovim dvama eksperimetima. Primjećujemo da su u reakciji ^{90}Zr+^{208}Pb jače pobuđeni prijelazi sa stanja viših spinova nego što je to u reakciji ^{40}Ca+^{96}Zr. Slična je situacija sa stanjima visokog spina i u ostatku spektra (na nižim energijama). Ako ovu spoznaju primijenimo na nove γ-zrake uočene u našem eksperimentu (^{90}Zr+^{208}Pb), zaključit ćemo da izostanak promatrane γ-zrake u spektru dobivenom u reakciji ^{40}Ca+^{96}Zr (osim u slučaju slabe statistike, tj. malog broja događaja) vjerojatno znači da promatrana zraka odgovara raspadu stanja visokog spina.

Izotopi olova

Spektri olova, s naznačenim najjačim γ-prijelazima prikazani su na Slikama 6.7, 6.9, 6.12, 6.17, 6.22 i 6.28, a opažene γ-zrake navedene su u Tablicama 6.17, 6.19, 6.20, 6.21 i 6.22. Sheme nivoa, konstruirane na temelju promatranih spektara, prikazane su na Slikama 6.45, 6.46, 6.47, 6.48 i 6.49.

Jezgra ^{208}Pb je dvostruko magična jezgra s popunjenom protonskom ljuskom $4\hbar\omega$ i popunjenom neutronskom ljuskom $5\hbar\omega$ (Slika 6.44). Lakši opaženi izotopi (^{205,207}Pb) imaju neutronsku šupljinu u ljusci $5\hbar\omega$, dok ^{209}Pb ima jedan nespareni neutron u ljusci $6\hbar\omega$ (Slika 6.44). Kako su osnovna stanja izotopa ^{205,207}Pb $5/2^-$ i $1/2^-$, očekujemo da su neutronske šupljine u orbitalama $2f_{5/2}$ i $3p_{1/2}$. Za neutronsku šupljinu u istoj ljusci (točnije, orbitali $1i_{13/2}$, $3p_{1/2}$, $3p_{3/2}$, $2f_{5/2}$, $2f_{7/2}$ ili $1g_{9/2}$) očekuju se jednočestična stanja $13/2^+$, $1/2^-$, $3/2^-$, $5/2^-$, $7/2^-$ ili $9/2^-$. S druge strane, ^{209}Pb ima jedan nespareni neutron u orbitali $2g_{9/2}$, zbog čega je spin njegovog osnovnog stanja $9/2^+$. Pobuđenjem tog nesparenog neutrona u više orbitale iste ljuske, očekuju se jednočestična stanja $5/2^+$, $11/2^+$, $7/2^+$, $1/2^+$, $3/2^+$ or $15/2^-$.

^{205}Pb ima gotovo degenerirano osnovno stanje (Slika 6.45), sa spinovima $J^\pi = 5/2^-$ i $J^\pi = 1/2^-$ koji se razlikuju samo za ~ 3 keV. U njegovom spektru pobuđena su tri stanja

negativnog pariteta, koja se raspadaju prijelazom na osnovno stanje. Pretpostavljamo da su to jednočestična stanja, uzrokovana neutronskom šupljinom u orbitalama $3p_{1/2}$ i $2f_{5/2}$.

U spektru ^{206}Pb, najsnažnije pobuđena stanja su $2^+, 3^+, 4^+$, dok je opaženo još i stanje 6^+ (Slika 6.46). U vrpci pozitivnog pariteta, pobuđena su sva stanja do energije $E_{ex} = 1704.5$ keV ($J^\pi = 1^+$) osim $J^\pi = 0^+$ ($E_{ex} = 1166.4$ keV). U vrpci negativnog pariteta opažena su sva stanja do energije ~ 3300 keV.

U vrpci negativnog pariteta izotopa ^{207}Pb (Slika 6.47), opažena su samo prva tri pobuđena stanja, i to s vrlo visokim intenzitetom (Slika 6.12). U vrpci pozitivnog pariteta, prisutna su stanja $9/2_1^+$, $9/2_2^+$ i $13/2_1^+$. Sva navedena stanja mogu imati jednočestični karakter; kako ^{207}Pb ima jednu neutronsku šupljinu u ljusci $5\hbar\omega$, jednočestična stanja određena su položajem te šupljine, tj. stanja $5/2^-$, $3/2^-$, $7/2^-$ i $13/2^+$ mogu biti posljedica neutronske šupljine u orbitalama $2f_{5/2}, 3p_{3/2}, 2f_{7/2}$ ili $1i_{13/2}$. Također, stanje $9/2^+$ može nastati pobuđenjem jednog neutrona u orbitalu $2g_{9/2}$.

Snažne γ-zrake u spektru ^{208}Pb raspadaju se sa stanja negativnog pariteta, a u našem eksperimentu, pobudili smo prva četiri takva stanja (Slika 6.48). U vrpci pozitivnog pariteta, opažena su prva tri pobuđena stanja (do energije $E_{ex} = 4423.9$ keV), koja ujedno pripadaju liniji yrasta. Iznenađujuće, najjači prijelaz u vrpci pozitivnog pariteta pripada raspadu stanja 4_2^+ energije $E_{ex} = 5216.2$ keV.

U spektru ^{209}Pb (Slika 6.7), koji je slab izlazni kanal ove reakcije, opazili smo dva najniža γ-prijelaza (s nivoa $J^\pi = 11/2^+$ i $15/2^-$), što je prikazano na Slici 6.49.

U izotopima $^{206-209}$Pb opažen je efekt sekundranih procesa, evaporacije neutrona, stoga smo na njega obratili posebnu pozornost. Eksperimentalni postav Prisma + Clara omogućava kvantitativno određivanje efekta evaporacije, koji se može javiti nakon prijenosa nukleona. Kao što je već rečeno, γ-spektri jezgara Pb konstruiraju se koristeći binarni karakter reakcije. Postavljajući uvjete na određene atomske (Z) i masene (A) brojeve lakog partnera, može se izračunati vektor brzine teškog partnera reakcije te izvršiti odgovarajuća Doppler korekcija. U tim su spektrima opažene γ-zrake primarnog binarnog partnera, kao i γ-zrake jezgara koje nastaju nakon evaporacije jednog ili više neutrona (Slika 6.50 prikazuje γ-spektre izotopa Pb prije korekcije). O ovim se procesima raspravlja u [Szi07], gdje je zaključeno da za kanal $-2p + 2n$ (u reakciji ^{40}Ca+^{96}Zr), oko 60% ukupnih događaja pripada pravom binarnom

partneru, dok je ostatak raspoređen izotopima koji nastaju nakon evaporacije jednog ili dvaju neutrona. Za još slabije kanale, kao što je $-4p$, γ-zrake koje potječu od pravog binarnog partnera imaju zanemariv utjecaj. U kanalima prijenosa neutrona, većina događaja pripada pravim binarnim partnerima. Ova je pojava blisko povezana s opaženim ukupnim gubitkom kinetičke energije (TKEL - total kinetic energy loss). Za kanale pobiranja neutrona, najveći doprinos TKEL-u događa se pri optimalnoj Q-vrijednosti ($Q_{opt} \sim 0$), dok su za kanale ogoljavanja protona opaženi veći TKEL; stoga evaporacija neutrona ima jači učinak na konačnu raspodjelu masa. U Tablici 6.23, navedene su γ-zrake nastale nakon evaporacije neutrona u opaženim izotopima Pb.

Slike 6.51 i 6.52 prikazuju najjače pobuđena stanja parnih i neparnih izotopa Pb. Kako je ^{208}Pb dvostruko magična jezgra, najniža stanja nalaze se na energijama pobuđenja mnogo većim nego u susjednim izotopima te su opažene energije do ~ 5000 keV. U vrpcama pozitivnih pariteta ^{206}Pb i ^{208}Pb pobuđena su stanja yrasta do 6^+, iako su prisutna i druga 2_2^+ i 4_2^+ stanja . U vrpcama negativnog pariteta, jake γ-zrake pripadaju raspadima stanja yrasta 3^- i 5^- u oba iztotopa. U ^{206}Pb, opažena su također i stanja 7^-, 6^- i 9^-, dok su u ^{208}Pb opažena i stanja 4^- i 5_2^-.

U neparnim izotopima Pb opaženo je samo nekoliko najnižih energijskih nivoa, osim u spektru ^{207}Pb, gdje su pobuđena i dva stanja spina $9/2^+$. Za ove niskoenergijske nivoe pretpostavljamo jednočestični karakter, kao posljedicu neutronske šupljine u orbitalama $1i_{13/2}$, $3p_{1/2}$, $3p_{3/2}$, $2f_{5/2}$, $2f_{7/2}$, $1g_{9/2}$ (za ^{205,207}Pb), tj. nesparenog neutrona u orbitali $1i_{11/2}$ za ^{209}Pb (Slika 6.44).

Slika 6.53 prikazuje usporedbu pobuđenih nivoa ^{90}Zr i njegovog binarnog partnera ^{208}Pb, što je zanimljivo jer se radi o polumagičnoj i magičnoj jezgri. U obje jezgre opazili smo yrast stanja pozitivnih i negativnih pariteta. U ^{90}Zr opazili smo i drugo i treće stanje $2_2^+, 3_2^-$, a u ^{208}Pb, drugo 4_2^+ stanje te stanje 5^-. Gledajući oba spektra, uočavamo pobuđenja do energija oko 5 MeV, što upućuje na to da je energija nakon reakcije podjednako raspodijeljena u oba partnera.

Izotopi itrija

Spektri opaženih izotopa itrija prikazani su na Slikama 6.55, 6.57, 6.60, 6.62, 6.64, 6.66, 6.68 i 6.70, a opažene γ-zrake navedene su u Tablicama 6.26, 6.27, 6.28, 6.29, 6.30, 6.31, 6.32 i 6.33. Na Slikama 6.56, 6.58, 6.61, 6.63, 6.65, 6.67 i 6.69 prikazane su sheme nivoa, konstruirane na temelju opaženih spektara.

Reakcija ^{90}Zr+^{208}Pb pobudila je izotope itrija s masama $87 \leq A \leq< 94$, t.j. kanale od $(-1p - 2n)$ do $(-1p + 5n)$. Jezgra itrija ima 39 protona, tako da je jedna protonska šupljina smještena u orbitali $2p_{1/2}$ (Slika 6.54). Primjećujemo da svi neparni izotopi itrija imaju spin osnovnog stanja $1/2^-$, koji je određen jednim nesparenim protonom. U proučavanim spektrima izotopa Y opažena su stanja visokog spina, a koja su do sada bila opažena samo u različitim fuzijsko-evaporacijskim procesima.

Slike 6.72 i 6.73 prikazuju usporedbu najsnažnije pobuđenih stanja u parnim i neparnim izotopima itrija. U parnim izotopima opažena su pobuđena stanja visokih spinova. U spektru ^{90}Y, opažena su stanja yrasta pozitivnog pariteta do spina (12^+), dok je u vrpci negativnog pariteta pobuđeno samo prvo energijsko stanje. To objašnjavamo na sljedeći način: ako usporedimo spektre svih promatranih izotopa itrija, primjećujemo da su svuda selektivno opažena stanja visokih spinova. Kako su trenutno u ^{90}Y poznata samo stanja niskih spinova u vrpci negativnog pariteta, to ostavlja mogućnost da se neke od opaženih γ-zraka mogu raspadati sa stanja visokog spina negativnog pariteta.

Kako jezgra ^{88}Y ima jednu neutronsku šupljinu u ljusci $N = 50$ i jednu protonsku šupljinu u podljusci $Z = 40$, očekuje se da se niskoležeća pobuđena stanja mogu opisati jednočestičnom konfiguracijom, što pokazuje i izračun temeljen na modelu ljusaka [Bun13], prikazan na Slici 6.59. Prema ovom računu, valne funkcije stanja 4^-, 5^-, 8^+ i 9^+ imaju jednočestičnu konfiguraciju više od 80%.

U spektru ^{92}Y opažene su γ-zrake koje pripadaju raspadima energijskih nivoa čije točne energije i spinovi nisu poznati, nego su poznati samo njihovi relativni odnosi. Unatoč tome, vidljivo je da opažene γ-zrake čine kaskadu, koja završava na izomernom stanju, što je obrazac kakav smo opazili i kod drugih itrijevih, ali i cirkonijevih izotopa, u kojima je istaknuto pobuđenje stanja yrasta. Stoga pretpostavljamo da i pobuđena stanja u ^{92}Y pripadaju liniji yrasta.

U spektru ^{94}Y većina opaženih γ-zraka pripada jačim kanalima reakcije s istog atomskog broja Z (^{90}Y i ^{92}Y) ili masenog broja A (^{94}Zr). Osim tih γ-zraka, opazili smo i tri dosad nepoznate γ-zrake. Na temelju usporedbe s opaženim spektrima ^{90}Y i ^{92}Y, zaključujemo da opažene γ-zrake u ^{94}Y čine kaskadu te predlažemo shemu raspada kao na Slici 6.69. Redoslijed predloženih energijskih nivoa određen je intenzitetom opaženih γ-zraka, a predloženi elektromagnetski prijelazi navedeni su u Tablici 6.34.

U svim je neparnim izotopima itrija opaženo niskoležeće stanje $9/2^+$, koje može biti jednočestičnog karaktera, s protonom u orbitali $1g_{9/2}$. Zajedničko svojstvo svim ovim stanjima $9/2^+$ je da imaju dugo vrijeme života (nekoliko sekundi) i raspadaju se uglavnom izomernim prijelazom. U Tablici 6.24 prikazane su energije ovih stanja te njihovi raspadi i vremena života.

U promatranim izotopima itrija (s neutronskim brojem $48 \leq N \leq 55$) neutroni popunjavaju orbitalu $1g_{9/2}$ za izotope ^{87,88}Y, a za izotope $^{90-94}$Y, neutronska ljuska $3\hbar\omega$ je zatvorena, tako da neutroni popunjavaju orbitale ljuske $4\hbar\omega$ (Slika 6.54).

Nespareni proton u orbitali $2p_{1/2}$ doprinosi osnovnom stanju neparnih itotopa itrija, stoga je spin osnovnog stanja $1/2^-$. Jednočestična protonska stanja koja se očekuju u neparnim izotopima Y su $5/2^-$, $3/2^-$ i $7/2^-$, a potječu od nesparenog protona u orbitalama $1f_{5/2}$, $2p_{3/2}$ or $1f_{7/2}$. Slika 6.73 pokazuje da smo neka od tih stanja opazili u našem eksperimentu.

U spektrima neparnih izotopa itrija također vidimo selektivno pobuđenje stanja visokih spinova, (do $(29/2^+)$ u ^{89}Y) te visoke energije pobuđenja. U spektrima ^{91}Y i ^{93}Y opazili smo samo prvih nekoliko stanja negativnog spina, što također objašnjavamo činjenicom da do sada nisu opažena stanja negativnog pariteta u području visokih spinova te da neke od opaženih γ-zraka mogu pripadati raspadima za sada nepoznatih nivoa visokih spinova.

Izotopi stroncija

Spektri izotopa Sr prikazani su na Slikama 6.77, 6.79, 6.81, 6.83, 6.85, 6.87 i 6.89. Opažene γ-zrake navedene su u Tablicama 6.36, 6.37, 6.38, 6.40, 6.41, 6.42 i 6.44, a konstruirane sheme nivoa prikazane su na Slikama 6.78, 6.80, 6.82, 6.84, 6.86, 6.88 i 6.90.

U spektru ^{86}Sr (Slika 6.80) opažena su stanja yrasta do (10^+) u vrpci pozitivnog pariteta, dok su u vrpci negativnog pariteta pobuđena stanja 3^- i 5^- te visokoenergijska ($E_{\mathrm{ex}} \sim 6$

MeV) stanja (11^-) i (12^-) .

U spektru ^{87}Sr opaženo je samo jedno pobuđeno stanje pozitivnog pariteta ($E_{\mathrm{ex}} = 1740.0$ keV, $J^\pi = 13/2^+$). Razlog za to vjerojatno leži u činjenici da se stanja viših energija raspadaju γ-zrakama energija ~ 2000 keV, za koje je efikasnost detektora Clara bitno smanjena. Raspad visokoenergijskih stanja negativnog pariteta završava na stanju $13/2^+$, koje se raspada na osnovno stanje. Uzevši u obzir ovakav obrazac raspada, zaključujemo da je direktno popunjavanje stanja $13/2^+$ oko 27%. Kako neutronski stupnjevi slobode imaju bitnu ulogu u selekciji pobuđenih stanja, pretpostavljamo da stanje $13/2^+$ može nastati sparivanjem kvanta vibracija 2^+ i osnovnog stanja $9/2^+$ (određenog nesparenim neutronom u orbitali $1g_{9/2}$), u rastegnutoj konfiguraciji. Spomenimo i tri nove γ-zrake, energija $300-500$ keV, koje su slične energijama opaženih prijelaza $(220-830$ keV$)$ između stanja negativnog pariteta u rasponu energija $2.5-4.5$ MeV. Za ove γ-zrake predložili smo elektromagnetske prijelaze navedene u Tablici 6.39.

Najjače pobuđena stanja u ^{88}Sr su 2^+, 3^- i 5^-. U području viših energija ($E > 5$ MeV, Slika 6.84), većina opaženih stanja nema poznat paritet [www4]. Unatoč tome, primjećujemo da γ-zrake čine kaskade koje počinju na nivoma s energijama $E_{\mathrm{ex}} \sim 7.5-8$ MeV i spinovima ($J \sim 10-11$).

U vrpci pozitivnog pariteta izotopa ^{89}Sr, opažena su samo prva dva pobuđena stanja ($J^\pi = 1/2^+$ i $J^\pi = (7/2)^+$, Slike 6.85 i 6.86), što su ujedno i dva najniža energijska stanja, a mogu se objasniti jednočestičnom konfiguracijom koja potječe od nesparenog neutrona u orbitalama $3s_{1/2}$ ili $1g_{7/2}$. U jednostavnom modelu ljusaka možemo očekivati i sljedeća jednočestična stanja: $1/2^+$, $7/2^+$, $5/2^+$, $3/2^+$ i $11/2^-$, koja potječu od nesparenog neutrona u orbitalama $3s_{1/2}$, $1g_{7/2}$, $2d_{5/2}$, $2d_{3/2}$ ili $1h_{11/2}$. S druge strane, ako promatramo moguće vezanje kvanta vibracija 2^+ na osnovno stanje $5/2^+$, u rastegnutoj konfiguraciji očekujemo spin $9/2^+$. Opaženo stanje $9/2_1^+$ (energije $E_{\mathrm{ex}} = 2061.5$ keV) raspada s γ-zrakom $E_\gamma = 2061.6$ keV, koja se preklapa sa širokim vrhom na energiji 2079 keV, a koju smo pridružili raspadu sa stanja $11/2^-$. Štoviše, γ-spektar ^{89}Sr obilježava jako pobuđenje stanja negativnog pariteta visokog spina, a selektivno su opažena stanja do čak $(25/2)$. Uzimajući u obzir ovu selektivnost reakcije, te slijedeći raspad tih stanja na stanje $(19/2)^-$ state, zaključujemo da bi stanja $(21/2)$ and $(25/2)$ mogla pripadati vrpci negativnog pariteta.

U spektru ^{89}Sr opažena je jedna nova γ-zraka, energije $E_\gamma = 1237.9$ keV. Na temelju razlike energija pobuđenih nivoa, možemo je pridružiti jednom od sljedećih prijelaza: $E_i = 4626$ keV (J_i^π nepoznat) $\longrightarrow E_f = 3388.1$ keV ($J_f^\pi = 15/2^-$) ili $E_i = 5442$ keV (J_i^π nepoznat) $\longrightarrow E_f = 4208.8$ keV ($J_f^\pi = (19/2)^-$). Oba ova početna nivoa nepoznatog spina do sada su opažena samo u reakcijama (p, d), u kojima je prijenos kutne količine gibanja ograničen. Kako smo opazili većinom stanja visokih spinova, pretpostavljamo da se ova γ-zraka također raspada sa stanja visokog spina u području energija iznad 5 MeV. Ovome ide u prilog i intenzitet ove γ-zrake, koji je sličan intenzitetu γ-zrake energije 1534.7 keV.

U γ-spektru ^{90}Sr najjača γ-zraka odgovara rapadu stanja 2^+ ($E_{\text{ex}} = 831.7$ keV) i 4^+ ($E_{\text{ex}} = 1655.9$ keV). Osim toga, opazili smo raspad stanja (0_2^+) na energiji 2674 keV ($E_\gamma = 1842.3$ keV), koje je pobuđeno u reakcijama (t, p). Zanimljivo je da je to jedini od proučavanih izotopa u kojemu je opaženo pobuđenje 0^+ stanja na višim energijama. Ovakvo snažno pobuđenje drugog 0_2^+ stanja objašnjeno je u Ref. [FHS76] činjenicom da za prijenose $N = 50 \longrightarrow N = 52$ orbitale $2d_{3/2}$ i $3s_{1/2}$ doprinose amplitudi prijenosa sličnim iznosima, tako da veliki dio udarnog presjeka za stanje 0^+ može proizići iz interakcija sparivanja.

Novouočenu γ-zraku $E_\gamma = 1489.0$ pridružili smo raspadu stanja 3144.9 keV. Za stanje slične energije (3146(10) keV) pobuđeno reakcijom (t,p), predloženi spin (temeljen na usporedbi s DWBA kalkulacijama) je 5^-. Ovdje skrećemo pozornost na činjenicu da je u ^{88}Sr također bilo snažno pobuđeno stanje 5^-.

Većina opaženih γ-zraka u spektru ^{90}Sr je trenutno nepoznata, ali usporedbom sa spektrima susjednih jezgara, zaključujemo da ove γ-zrake zbilja pripadaju izotopu ^{90}Sr. Ako usporedimo pobuđena stanja jezgara ^{88}Sr i ^{90}Sr, primjećujemo da su u ^{88}Sr pobuđeni spinovi do $\sim$10 te stoga pretpostavljamo da i nepoznate γ zrake u ^{90}Sr (navedene u Tablici 6.43) pripadaju raspadima stanja visokih spinova. Također, intenziteti ovih γ-zraka slični su intenzitetima γ-zraka koje se u ^{88}Sr raspadaju sa stanja viših spinova ($J \sim 7$ or 8), a koji iznose oko 20 do 30% najjačeg stanja 2_1^+. Napomenimo da se takva stanja ne mogu lako pobuditi (t, p) reakcijama i β raspadom, u kojima je ovaj izotop ranije proučavan.

Mali broj događaja (oko $\sim$ 29000) u kanalu ^{91}Sr uzrok je da je njegovom spektru prepoznato samo nekoliko γ-zraka (Slike 6.89 i 6.90). Najsnažniji prijelazi pripadaju raspadima stanja $(9/2^+)$, $(11/2^-)$ i $(15/2^-)$. Osim stanja visokih spinova, u ^{91}Sr opažena su sva poznata

niskoležeća stanja do spina $9/2^+$ ($E_{\text{ex}} = 993.5$ keV).

Slike 6.91 i 6.92 prikazuju najsnažnije pobuđena stanja parnih i neparnih izotopa Sr. U najjačim kanalima reakcije ($^{86-89}$Sr) opažena su pobuđenja visokih energija, do 8000 keV (u ^{88}Sr), s visokim spinovima. Najjače pobuđena stanja u parnim izotopima su prva 2_1^+ i 4_1^+ stanja, ali su prisutna i stanja yrasta do spina (10^+). Za razliku od izotopa Zr, snažno su pobuđena i stanja negativnog pariteta, s opaženim spinovima do $(11)^-$ u ^{88}Sr. Iznimka je ^{90}Sr, koji je do sada proučavan samo u β^- i (t,p) reakcijama.

Zbog malog broja događaja za ^{85}Sr, u ovom je izotopu opaženo samo prvih nekoliko pobuđenih nivoa. U shemama izotopa ^{87}Sr, ^{89}Sr i ^{91}Sr, opaženi su relativno visoki spinovi u vrpci negativnog pariteta. Kod ^{87}Sr i ^{89}Sr, opažena su stanja viokog spina s nepoznatim paritetima ($J^\pi = (21/2)$ i $(23/2)$ u ^{87}Sr te $J^\pi = (21/2)$ i $(25/2)$ u ^{89}Sr), koja smo ucrtali u vrpcu negativnog pariteta zbog kaskade γ-zraka koja slijedi. Svim proučavanim izotopima Sr zajedničko je to što su stanja visokih spinova dosad opažena samo u fuzijsko-evaporacijskim procesima.

38 protona u jezgri Sr ostavljaju 2 protonske šupljine u ljusci $3\hbar\omega$. S druge strane, neutronska je podljuska $3\hbar\omega$ zatvorena za proučavane izotope Sr, a kako se krećemo od ^{85}Sr do ^{91}Sr, neutroni popunjavaju orbitalu $1g_{9/2}$, a zatim $2d_{5/2}$ (Slika 6.75). Nespareni neutron u neparnim izotopima Sr određuje spin i paritet osnovnog stanja; nespareni neutron u orbitali $1g_{9/2}$ uzrokje spin osnovnog stanja $9/2^+$ u ^{85}Sr i ^{87}Sr, a nespareni neutron $2d_{5/2}$ spin osnovnog stanja $5/2^+$ u ^{89}Sr i ^{91}Sr.

Kako neutronski stupnjevi slobode imaju velik utjecaj u odabiru pobuđenih stanja u izotopima Zr, razmotrit ćemo moguća jednočestična stanja u neparnim izotopima Sr. U slučaju ^{85}Sr i ^{87}Sr, u jednostavnom modelu ljusaka, očekujemo stanja $1/2^-$, $5/2^-$, $3/2^-$ i $7/2^-$, uslijed nesparenog neutrona u orbitalama $1p_{1/2}$, $1f_{5/2}$, $2p_{3/2}$ ili $1f_{7/2}$. Za ^{89}Sr i ^{91}Sr, stanja jednočestičnog karaktera $7/2^+$, $3/2^+$, $1/2^+$ i $11/2^+$ očekuju se zbog nesparenog neutrona u orbitalama $1g_{7/2}$, $2d_{3/2}$, $3s_{1/2}$ ili $1h_{11/2}$. Kao što se vidi na Slici 6.92, u našem su eksperimentu opažena stanja čija se konfiguracija može opisati jednočestičnim karakterom.

U raspavi o pobuđenim stanjima izotopa Zr, zaključili smo da se većina snažno pobuđenih stanja u neparnim izotopima može opisati kao jednočestična stanja ili kao vezanje osnovnog stanja i kvanta vibracija. Kako bismo provjerili događa li se takvo vezanje i u neparnim

izotopima Sr, prikazujemo Slike 6.93 i 6.94, na kojima su uspoređene energije prvih stanja 2^+ i 3^- u parnim izotopima Sr, kao i energije stanja u neparnim izotopima, a koja očekujemo kao stanja vezanja osnovnog stanja i stanja 2^+ ili 3^- u rastegnutoj kofiguraciji, prikazana u Tablici 6.45. Analogno kao kod izotopa Zr, uočavamo da neki od susjednih izotopa Sr imaju slične energije prikazanih stanja, a ova je sličnost još i više izražena nego u izotopima Zr, posebno za vezanje osnovnog stanja na stanje 3^-, što ide u prilog pretpostavci o čestično-vibracijskom karakteru ovih stanja.

Zaključak

Reakcije prijenosa nukleona proučavane su u sustavu ^{90}Zr$+^{208}$Pb na energiji bliskoj kulonskoj barijeri na eksperimentalnom postavu Prisma + Clara, u akceleratorskom centru *Laboratori Nazionali di Legnaro-INFN*. Eksperimentalni postav sastojao se od magnetskog spektrometra Prisma velikog prostornog kuta te γ-detektora Clara. Snop ^{90}Zr, ubrzan Tandem-ALPI akceleratorima, upadao je na izotopno čistu metu ^{208}Pb.

U reakciji prijenosa nukleona ^{90}Zr$+^{208}$Pb pobuđeni su kanali atomskih brojeva $Z = 30 - 40$ i masenih brojeva $A = 60 - 94$. U ovom smo se radu fokusirali na spektre izotopnih lanaca Zr (i njegovog teškog partnera, Pb), Y i Sr. Naglasak smo stavili na izotope Zr $^{89-94}$Zr, koji su ujedno najjači izlazni kanali reakcije. U neparnim jezgrama Zr i Sr (kanal $-2p$), nespareni neutron određuje spin osnovnog stanja izotopa, koji je $9/2^+$ u ^{89}Zr i ^{85,87}Sr (zbog neutronske šupljine u orbitali $1g_{9/2}$) te $5/2^+$ u ^{91,93}Zr i ^{89,91}Sr (uslijed nesparenog neutrona u orbitali $2d_{5/2}$). Očekuje se da aktivne jednočestične orbitale u opaženim izotopima Zr i Sr potječu od nesparenog neutrona u orbitalama $2p_{1/2}$, $1f_{5/2}$ ili $2p_{3/2}$. To bi se u ^{89}Zr i ^{85,87}Sr očitovalo kroz jednočestična stanja $1/2^-$, $5/2^-$ i $3/2^-$, dok bi u slučaju ^{91,93}Zr i ^{89,91}Sr nespareni neutron u $1g_7/2$, $2d_{5/2}$, $2d_{3/2}$, $3s_{1/2}$ ili $1h_{11/2}$ uzrokovao stanja $7/2^+$, $5/2^+$, $3/2^+$, $1/2^+$ ili $11/2^-$. U prikazanim shemama nivoa opažamo ova stanja, štoviše, ona prevladavaju u niskoenergijskom dijelu spektra izotopa Zr i Sr.

Prirodu jednočestičnih stanja izotopa ^{91}Zr i ^{93}Zr raspravili smo detaljnije uspoređujući jačine pobuđenja ovih stanja u našem eksperimentu s onima dobivenima u različitm (d,p) mjerenjima (Slike 6.14, 6.26), u kojima se očekuje jače pobuđenje jednočestičnih stanja. Također, usporedili smo naše rezultate s računom modela ljusaka opisanim u [SNL09] i

[DBI11] (Slike 6.16 i 6.27), gdje se račun za izotope Zr proveo u proširenom ([SNL09]) i potpunom ([DBI11]) prostoru modela ljusaka ($1f_{5/2}$, $2p_{1/2}$, $2p_{3/2}$, $1g_{9/2}$) za protone i ($2d_{5/2}$, $3s_{1/2}$, $2d_{3/2}$, $1g_{7/2}$, $1h_{11/2}$) za neutrone. Ove usporedbe podupiru našu pretpostavku o jednočestičnom karakteru ovih niskoležećih stanja.

Posebnu pozornost posvetili smo proučavanju stanja čija se priroda može opisati sparivanjem fonona i fermiona, s obzirom na to da se taj stupanj slobode pokazao značajnim u modelima reakcija. U proučavanju strukture snažno pobuđenih stanja istražili smo mogućnost sparivanja osnovnog stanja u neparnim izotopima Zr i Sr na 2^+ ili 3^- fonone u rastegnutoj konfiguraciji (Tablice 6.45 i 6.10). Rastegnuta konfiguracija ima prednost kod mehanizma prijenosa jer je vjerojatnost prijenosa najveća pri najvećem prijenosu kutne količine gibanja [BW00]. Rezultati prikazani na Slikama 6.36, 6.37, 6.93 i 6.94 pokazuju da su u većini proučavanih izotopa modovi raspada i energije stanja 2^+ and 3^- u parnim izotopima slični onima u neparnim izotopima za očekivana stanja konfiguracije čestica-vibracija.

Posebno su nas zanimala stanja $9/2_1^+$, $9/2_2^+$, $11/2_1^-$ i $11/2_2^-$ u ^{91}Zr, jer ova stanja mogu imati i jednočestični, ali i čestično-vibracijski karakter. Kako bismo istražili katakter ovih stanja, uzeli smo u obzir obrasce raspada i pripadajuće jačine raspada stanja 2^+ i 3^- u parnim izotopima i očekivanih čestično-vibracijskih stanja u neparnim izotopima. Također, usporedili smo svoje rezultate s teorijskim modelima iz [BHK76] i [SNL09], koji pokazuju snažno miješanje različitih konfiguracija, posebno za stanja spina $11/2^-$.

U našem smo eksperimentu potražili i pobuđenja stanja 0^+ koja su prepoznata kao stanja sparivanja vibracija, a bila su snažno pobuđena u reakcijama prijenosa dvaju neutrona (t, p). Na temelju prikupljenih podataka nismo mogli sa sigurnošću utvrditi pobuđenje ovih stanja.

U svim proučavanim jezgrama (s izuzetkom slabijih kanala reakcije, kao što su ^{89}Zr, ^{85}Sr ili ^{94}Y), vidljivo je da većina pobuđenih stanja pripada liniji yrasta (tj. to su stanja koja imaju najveći spin za danu energiju). U brojnim jezgrama, selektivno su pobuđena stanja visokog spina (do 16^+ u ^{92}Zr ili $29/2^+$ u ^{89}Y), što pokazuje da su reakcije prijenosa više nukleona dobar alat za pobuđivanje stanja visokih spinova i energija (čak do ~ 8 MeV u ^{89}Y).

Proučavajući izotope Pb (teški binarni partner Zr), raspravili smo o efektu evaporacije, koji snažno utječe na broj događaja pridružen primarnom binarnom partneru. Temeljem

uočenih γ-zraka, prepoznali smo izotope koji nastaju nakon evaporacije jednog ili dvaju neutrona. Pri tome, relativni intenziteti γ-zraka po prvi puta omogućuju kvantitativno određivanje efekta evaporacije u ovako teškom sustavu.

U pažljivom proučavanju γ-spektara, prepoznali smo i nove γ-prijelaze (koji nisu do sada zabilježeni u National Nuclear Data Center at Brookehaven National Laboratory - http://www.nndc.bnl.gov) te ih pridijelili odgovarajućem izotopu. Za izotope Zr, opažene γ-spektre usporedili smo s onima dobivenima ranije u reakciji ^{40}Ca+^{96}Zr [Szi07]. U slučajevima u kojima je to bilo moguće, raspravili smo i o mogućem raspadu ovih γ-zraka temeljem usporedbe sa susjednim jezgrama. Predložili smo da se neke od ovih novih γ-zraka raspadaju sa stanja viših spinova, dok neke potječu od stanja dominantnog jednočestičnog karaktera ili karaktera sparivanja čestica-vibracija.

Prikazani rezultati značajno doprinose razumijevanju selektivnosti mehanizma reakcija prijelaza više nukleona u smislu odabira stanja specifičnih struktura. Točnije, opazili smo jako pobuđenje stanja koja se mogu povezati sa sparivanjem jednočestičnih stupnjeva slobode i kvanta vibracija. Budući da je određivanje efekta sparivanja fermion-bozon teško izvedivo samo na osnovu proučavanja energija, dodatno razumijevanje važnih stupnjeva slobode u ovom području masa i naboja zahtijeva i dodatna mjerenja ostalih važnih svojstava, kao što je jačina elektromagnetskih prijelaza.

Introduction

Despite nearly half a century of intensive study, the nucleus remains a fascinating quantum-laboratory, still full of surprises. Our knowledge about the nuclear force is still based on studies close to the valley of stability. Those studies give information about the nuclear force in the equilibrium. In order to learn more, it is necessary to study the properties of nuclear force in extreme conditions (such as large deformations or large neutron densities). Nuclear structure properties strongly influence the diverse mechanisms associated with nuclear reactions, thus it is also important to study the reaction mechanism.

Our understanding of the structure of nuclei greatly benefited from reactions induced by a very large variety of probes. With photons, electrons, mesons and nucleons we learned about the properties of nuclei in the vicinity of their ground states. The acceleration of heavy ions offered the possibility to bring together two complex systems. In the collision process they might exchange several quanta of energy and angular momentum and of mass and charge. Transfer reactions play an essential role in the study of the structure of nuclei and in establishing the properties of particle-particle correlations in the nuclear medium.

In the last decade, the renewed interest in transfer reactions has been mainly due to the realization that multinucleon transfer reactions could be used to populate nuclei moderately rich in neutrons. It is in this region of the nuclear chart where the most challenging aspects in the behavior of the nuclear structure have been foreseen. This renewed interest benefited from the construction of the new generation large solid angle spectrometers based on trajectory reconstruction, with which one could gain more than an order of magnitude in overall efficiency, still keeping a good identification of reaction products.

In this work, the reaction ^{90}Zr+^{208}Pb, performed at LNL (Laboratori Nazionali di Legnaro) -INFN (Instituto Nazionale di Fisica Nucleare), the international accelerator center will

be investigated. Multinucleon transfer reactions in the ^{90}Zr+^{208}Pb system have been studied close to the Coulomb barrier energy in the Prisma + Clara setup. Light binary partners have been detected in the Prisma magnetic spectrometer, while the coincident γ rays have been detected in the Clara γ -array. Trajectory reconstruction in the spectrometer provides the identification of the light fragments in their charge, mass and velocity. These allow to attribute electromagnetic transitions and their strengths to each of the transfer channels, i.e. each γ spectrum is uniquely assigned to a specific isotope. Finally, new states can be identified and compared to theoretical models. Those for the nucleon transfer channels will be studied in detail in this thesis. One of the primary goals of this work is to establish a stronger relation between reaction mechanism and nuclear structure.

In the reaction ^{90}Zr+^{208}Pb, the nuclei with magic and semi-magic number of protons and neutrons have been involved. The comparison between measurement and theory, being the determination of nuclear model parameters better known, could lead to deeper understanding of the underlying mechanism.

The main degrees of freedom included in models that describe nuclear collisions at energies close to the Coulomb barrier are surface vibrations (around closed shells), rotations (between shells) and single particle states. Through excitement of these states, energy and angular momentum are transferred from the relative motion of two colliding nuclei to internal degrees of freedom. Our hypothesis is that states whose structure can be explained as the coupling of single particle states and vibration-rotation (same states that are important in describing reaction dynamics) will be strongly excited through nucleon transfer. Our goal is to show that reaction mechanism, although we are dealing with two heavy systems, preserves selectivity in excitation of the states of certain structures, a phenomenon already studied in light ion collisions. We expect to find out which states will be the most strongly excited ones and determine if there are some common characteristics in the structure of those states. Moreover, we want to quantitatively show to which extent the selectivity in the excitation of states of specific structures is preserved in comparison with collisions of light ions.

Chapter 1

Heavy ion reactions

Heavy ion reactions imply reactions involving projectiles with a mass number A equal or greater than 4, but when speaking of the case of heavy ion reactons, ions are of much greater mass [BW00]. Interesting phenomena occur when dealing with heavy ion reactions because of a strong electric field between ions, their large masses and compositeness. When dealing with nuclear reactions involving heavy ions, many different reaction modes may be expected. Although there is not a strong limit between different types of reactions, they can still be distinguished, depending on the reaction impact parameter, transferred angular momentum or energy, etc.

In peripheral collisions, the most frequent types of reactions are quasielastic reactions, which include Coulomb excitations, elastic scattering, nuclear inelastic scattering and transfer of nucleons. For lower impact parameters, deep inelastic scattering occurs, where most of the kinetic energy of the projectile is converted into internal energy. For even lower impact parameters and under appropriate conditions fusion may occur.

In experiments probing nuclear structure, many experimental data are needed, e.g. nuclear masses and binding energies, level energies and J^π values, reaction cross sections, γ-ray transition rates, electric and magnetic moments, β decay rates and so on [BM69].

1.1 Quasielastic reacions

The term quasielastic scattering first occured in the 1970s to distinguish peripheral collisions with minor kinetic energy losses from sudden deep inelastic reactions, with major energy losses and mass transfers. Quasielastic reactions include Coulomb excitations, elastic and nuclear inelastic scattering, and transfers of few nucleons. There is no clear limit between quasielastic and deep inelastic reactions, considering mass or energy transfer, although quasielastic reactions are sometimes referred to as reactions in which the projectile after reaction emerges more or less intact, only with slightly different mass, charge and energy. More central collisions lead to deep inelastic scattering and fusion, in which the outgoing channels have considerably different mass, energy and charge than ingoing ones. Domination of quasielastic reactions is especially emphasized near energies close to the Coulomb barrier, and it makes dominant mode of reactions in low energy region.

1.1.1 Coulomb excitations

If the interacting ions have energy lower than the Coulomb barrier, the main interaction between them will be point Coulomb interaction, and their relative trajectory will be hyperbolic. Coulomb interaction has been a powerful tool for studying electromagnetic properties of nuclei. Because of its simplicity, it was studied in detail, therefore it played a key role in determining low-lying collective states of the most nuclei of the periodic system.

1.1.2 Elastic and nuclear inelastic scatterings

Elastic scattering is a type of reaction in which only trajectories of ions and their spin orientations are altered, without energy or mass transfer. Both ions remain in their ground states. Interaction between ions consists of two parts: Coulomb potential and nuclear ion-ion potential. Elastic scattering provides the study of the ion-ion part of the potential.

In the classical description of elastic scattering, the deflection function is evaluated, which gives the functional dependence of the scattering angle on the reaction impact parameter. Knowing the deflection function, the differential cross section of the reaction can be evaluated. The deflection function for heavy ion reactions has some characteristic features, namely,

maximum value at the rainbow angle, Coulomb dominated region for large impact parameters and negative scattering angles for small impact parameters (Fig. 1.1 [BW00]).
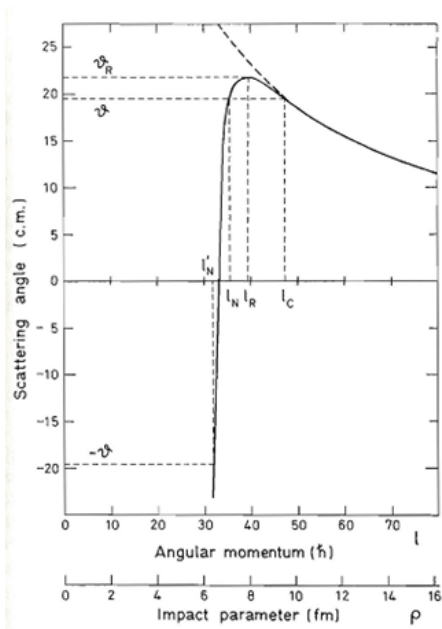
Figure 1.1: Deflection function for elastic scattering of ions in the reaction ^{13}C on ^{40}Ca at $E_{lab} = 68$ MeV [BW00].

The differential cross sections for relatively light ions is dominated by ion-ion potential (because Coulomb excitations and nuclear surface reactions are weak), so it can easily be studied by means of these reactions. The situation is different when dealing with heavy ions because of the prolific nature of reactions. Nevertheless, with coupling the new generation of heavy ion spectrometers and large γ arrays, it has become feasible to extract an elastic differential cross section. Several such experiments have been conducted with the experimental setup that uses coincidence between reaction fragments and detected γ spectra (γ-particle coincidence). Total kinetic energy loss (TKEL) spectrum has been measured with the spectrometer and then compared with the TKEL spectrum in coincidence with the γ array. The difference between the two spectra for the experiment ^{90}Zr+^{208}Pb at $E_{lab} = 560$ MeV is shown in Fig. 1.2 [Szi07], and represents events belonging to elastic scattering. By subtracting these two spectra for every possible laboratory angle (in steps of one degrre) ϑ_{LAB}, one obtains a differential cross-section for the elastic scattering (Fig. 1.3, [Szi07]), which shows

the appearance of absorption for larger scattering angles.
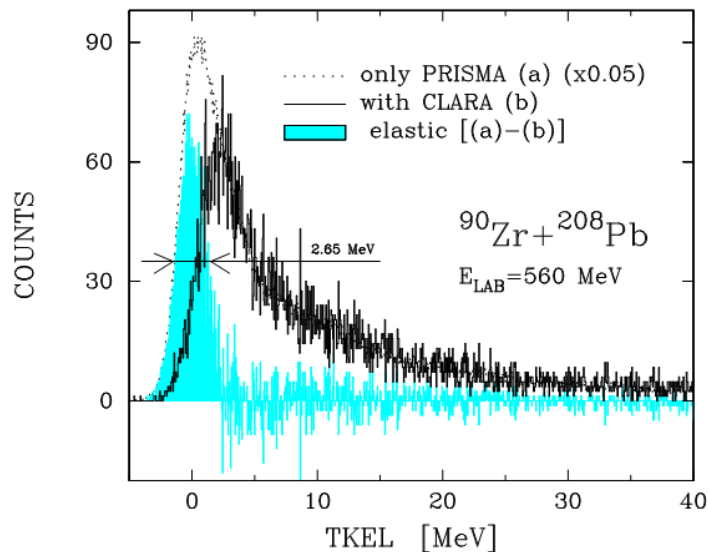
Figure 1.2: Total kinetic energy loss (TKEL) spectra of ^{90}Zr ions in the reaction ^{90}Zr+^{208}Pb at $E_{lab} = 560$ MeV observed by Prisma spectrometer (a) and in coincidence with the Clara detector (b). The blue area refers to the difference between (a) and (b) and indicates TKEL spectrum for elastic scattering. Figure is taken from [Szi07].
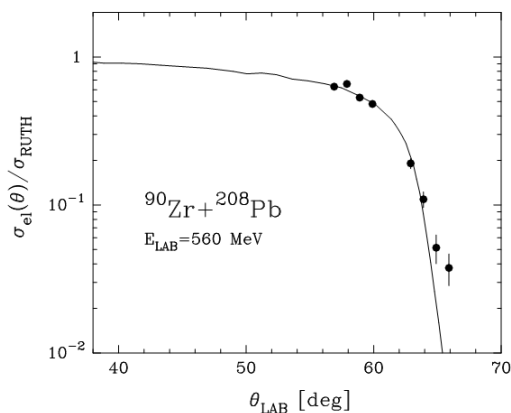
Figure 1.3: Differential cross section for the reaction ^{90}Zr+^{208}Pb at $E_{lab} = 560$ MeV normalized to the Rutherford scattering [Szi07].

Nuclear inelastic scattering includes exciting one or both ions involved in the reaction,

and besides rotational and vibrational states of low frequency, vibrational states of high frequency can be reached as well, because of shorter interaction time [BW00].

As an example, Fig. 1.4 [Reh91], shows differential cross section for the reaction ^{28}Si+^{208}Pb at bombarding energy of 255 MeV (the Coulomb barrier for this reaction is ∼154 MeV), for elastic and the strongest inelastic channels. Interference between different partial waves for nuclear inelastic channels is noticeable.
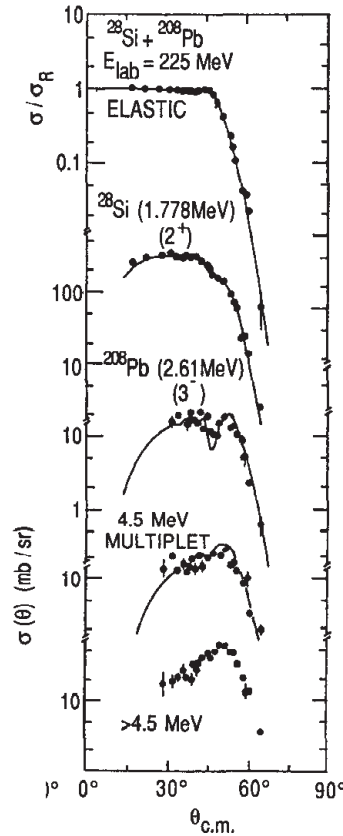
Figure 1.4: Angular distributions for elastic scattering and nuclear inelastic excitations for the system ^{28}Si+^{208}Pb for bombarding energy of 255 MeV; The Coulomb barrier for this system is 154 MeV [Reh91].

1.1.3 Transfer reactions

Transfer reactions imply transfer of one or more nucleons between colliding ions. In fact, transfer reactions spread from quasielastic (small energy, mass and a momentum transfer) to deep inelastic processes (larger mass and energy transfer) [Reh91, Cor99]. They play a key role in nuclear structure studies; with light ions, they provide information on shell model (transfer of one nucleon) and help establishing correlations between nucleons (transfer of two nucleons) [CMN05]. Single nucleon transfer reactions were the first reactions used to gain some information about nuclear structure.

Regarding multinucleon transfer reactions, it is possible (with proper choice of colliding nuclei and energy) to obtain neutron rich nuclei, in which new features are expected (e.g. new shell gaps), and special interest is put on the structure of neutron rich nuclei (namely, shape coexistence, large variations of the quadrupole collectivity, low-lying intruder states and octupole correlations) [Mar09]. For the production of neutron-rich nuclei, the interacting nuclei (i.e. their isotopes), as well as the bombarding energy should be carefully chosen.

Figure 1.5 [CPS09], shows contours of differential cross-sections as a function of a change in projectile neutron number ΔN_p and charge number ΔZ_p for the reaction ^{A}Ca+^{120}Sn at bombarding energy of 150 MeV, calculated with the GRAZING model [Win94, Win95, www5]. It is clearly seen how the choice of Ca isotope affects the favor of neutron pick-up or proton stripping, which are reactions that are allowed (from optimum Q-value) for stable nuclei. Similar results (contours) are obtained for a large variety of combinations of light projectile and a heavy target. For example, in Fig. 1.5 the shifting character of the reaction is shown; from the reactions that favor neutron pick-up and proton stripping for the heavier Ca isotopes to ones that favor neutron stripping and proton pick-up for lighter Ca isotopes is observed.

Figure 1.6 [CPS09], shows a 2-dimensional spectrum obtained for the light partner of the reaction ^{40}Ca+^{208}Pb at $E_{lab} = 235$ MeV. The full line represents the location of the N/Z ratio for the compound nucleus, while the dashed lines represent pure neutron and proton stripping channels. Final nuclei are all on the left side of the full line, indicating the direct character of the reaction. Angle and energy integrated cross sections of this reaction are plotted in Fig. 1.7 [Szi05]).
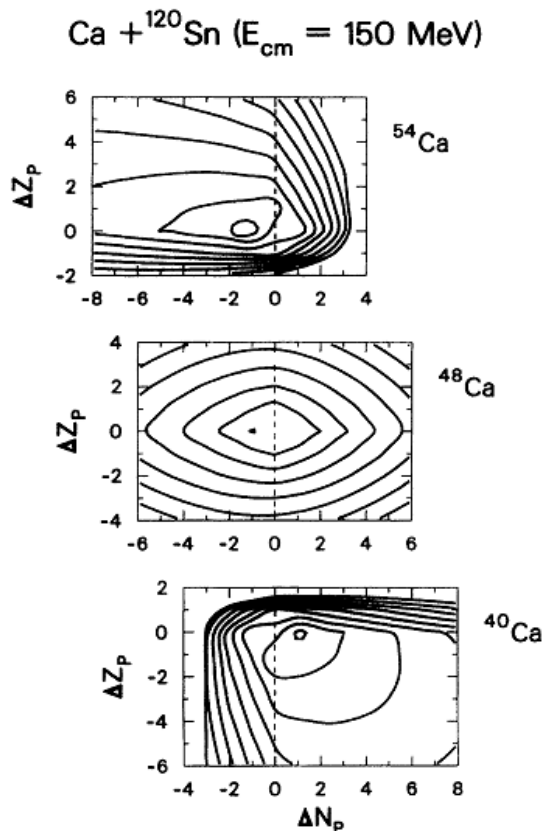
Figure 1.5: Differential cross-sections as a function of the change in projectile neutron number ΔN_p and charge number ΔZ_p for the reaction ^{A}Ca+^{120}Sn at $E_{lab} = 150$ MeV [CPS09]. The calculations are based on the GRAZING model.

Deep inelastic scattering

Deep inelastic scattering is characterized by a large amount of energy and mass transfer. Outgoing fragments emerge with energies less than the Coulomb barrier, and angular distributions that grow toward smaller angles [Reh88]. While this last feature points to very fast processes, large energy losses suggest that two ions are very deformed before they exit the interaction. In general, large energy and mass transfers can excite high spin states with complex structure, which consists of several holes and particles.

As previously mentioned, transfer reactions can spread from quasielastic (with low total kinetic energy loss-TKEL) to deep inelastic regime (large TKEL). Figures 1.8 and 1.9 [Cor13] show the evolution (from quasielastic to deep-inelastic region) of the TKEL spectra
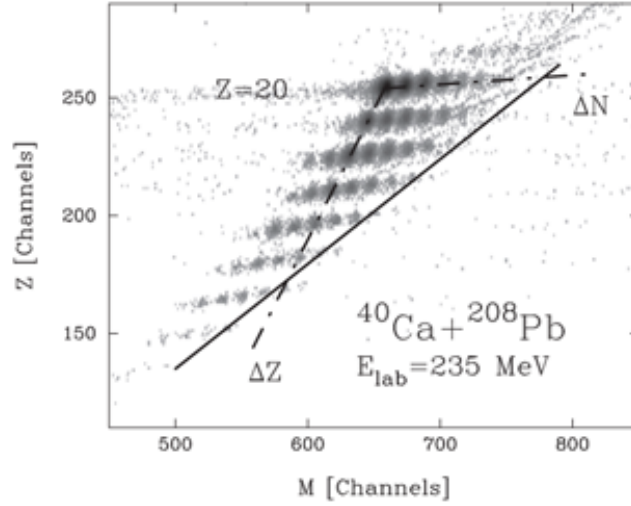
Figure 1.6: Mass-charge distribution of transfer products in the ^{40}Ca+^{208}Pb reaction at $E_{lab} = 235$ MeV [CPS09].
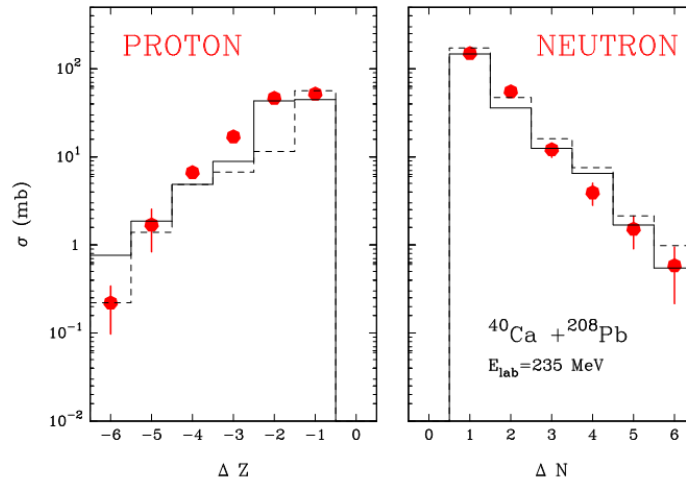
Figure 1.7: Total (angle and Q-value integrated) cross-sections for pure proton stripping and pure neutron pick-up channels for the ^{40}Ca+^{208}Pb reaction at $E_{lab} = 235$ MeV [Szi05].

for different number of transferred protons and neutrons for the light partner of the reaction ^{90}Zr+^{208}Pb at $E_{lab} = 560$ MeV. It is noticeable how the shape of the TKEL (or Q-value) spectra changes with the number of transferred nucleons; for the pure neutron transfer, one observes quasi-elastic peak and increased energy loss related to larger neutron transfers.

TKEL spectra of the reaction channels that are not directly populated differ considerably from one another, but this distinction vanishes with the increasing number of transferred nucleons.

Figure 1.10 [Cor09] shows Q-value and mass distributions for the reaction ^{48}Ca+^{238}U at $E_{lab} = 330$ MeV (almost 50% higher than the $E_{Coul} = 233$ MeV) and at $\theta = 52°$ (grazing angle for the reaction is $\theta_g = 55°$) for quasielastic and deep-inelastic regime. It is apparent that mass distributions for deep inelastic reaction are bell (Gaussian) shaped, while for quasielastic reaction they follow the shape defined by the optimum Q values.
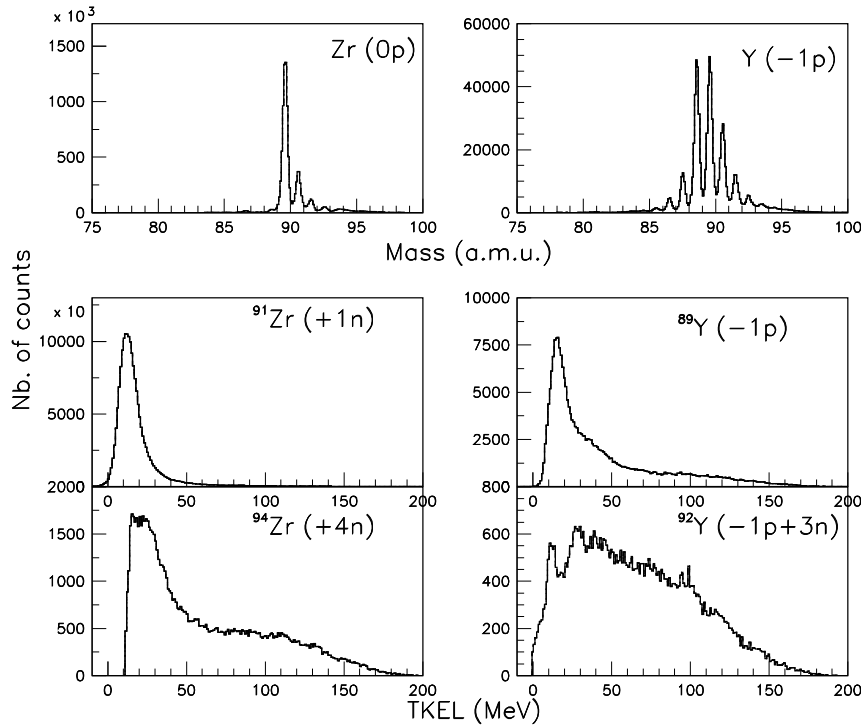
Figure 1.8: Mass (top panels) and TKEL (middle and bottom panels) spectra obtained in the reaction ^{90}Zr+^{208}Pb for the indicated transfer channels. $0p$ and $-1p$ in the mass spectra refer to Zr and Y isotopes, respectively [Cor13].
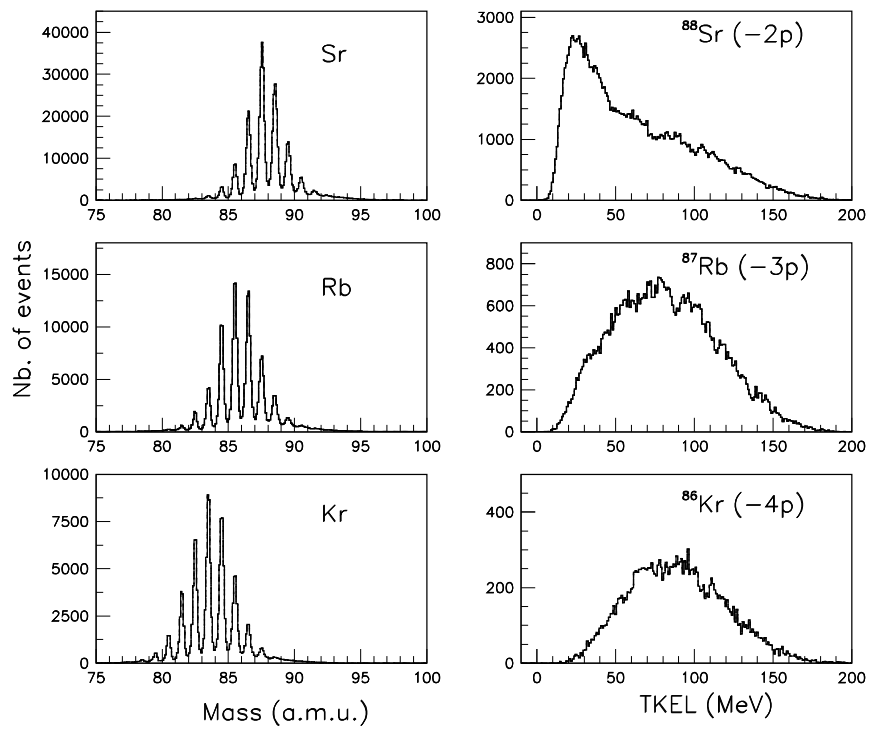
Figure 1.9: Mass and TKEL spectra obtained in the reaction ^{90}Zr+^{208}Pb for the indicated proton stripping transfer channels [Cor13].
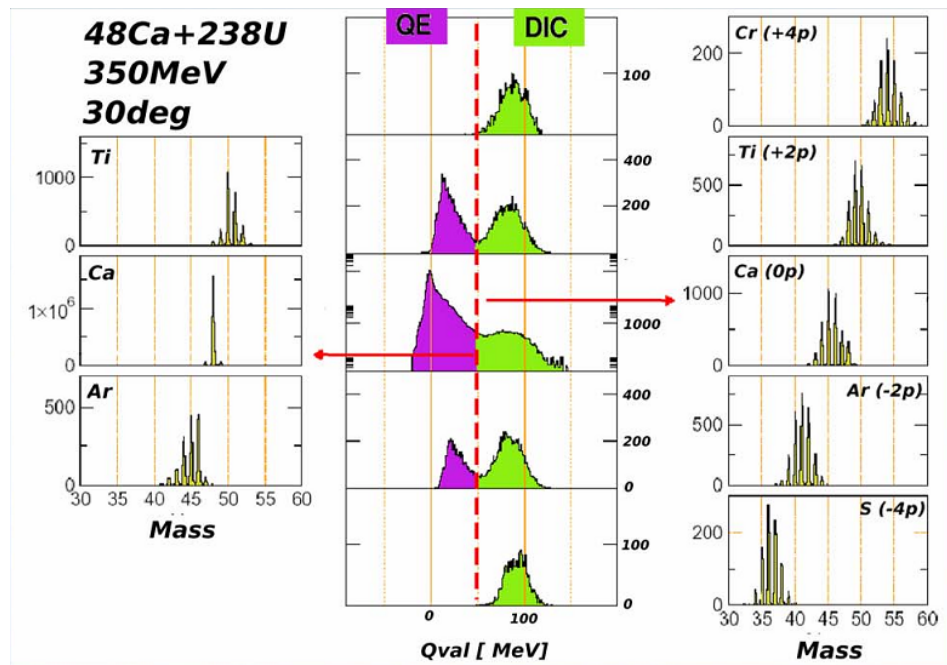
Figure 1.10: Q-value and mass distributions for the reaction ^{48}Ca+^{238}U at $E_{lab} = 330$ MeV for quasielastic and deep-inelastic regime (the Coulomb barrier for this system is 245 MeV) [Cor09].

Chapter 2

Detection techniques for heavy ion reactions

2.1 Magnetic spectrometers for heavy ions

In nuclear reaction studies, magnetic spectrometers play an important role. Setup of the spectrometer depends on reaction type and on the goal of the research. Some of the main characteristics of spectrometers used in heavy ion reaction studies will be described in this section.

The first spectrometers for heavy ion reactions were developed on the basis of the light ion spectrometers, e.g. Q3D or split-pole magnetic systems [Lat04]. A split pole spectrometer is often used in the medium mass region for determining angular distribution cross sections of outgoing fragments in quasi-elastic regime [www1]. Q3D is the abbreviation for the spectrograph that has one quadrupole lens and three dipole magnets. The quadrupole lens focuses ions to the focal plane and magnetic fields of dipole magnets separate ion trajectories depending on their magnetic rigidity (ratio of the momentum and charge of the ion, $\frac{mv}{q}$), which results in the unique position of ions in the focal plane for each ion and energy [www2]. Q3D spectrographs are still used in laboratories in JAERI, Munich, Strasbourg, etc.

For getting better detection efficiency, time-of-flight (TOF) spectrometers were developed. Their main characteristics are quadrupole magnets, used to focuse ion trajectories at the relatively small focal plane. An example of the TOF spectrometer is PISOLO in the Legnaro

laboratory [Mon00], which was extensively used in the multinucloen transfer reaction studies.

To obtain larger solid angles (up to 100 msr), a new generation of spectrometers use a simple magnetic configuration combined with an event-by-event reconstruction of ion trajectories, for which space coordinates of ions for at least two points along the trajectory have to be determined. These spectrometers are mainly designed for studies of grazing reactions, which result in many different outgoing channels, in which outgoing fragments have a wide range of energies and angular momenta and their cross section may vary by several orders of magnitude. Large acceptance magnetic spectrometers operating at the moment are Prisma in Legnaro (Fig. 2.1), MAGNEX in Catania and Vamos in Caen, Ganil. More details about Prisma can be found in following chapters.
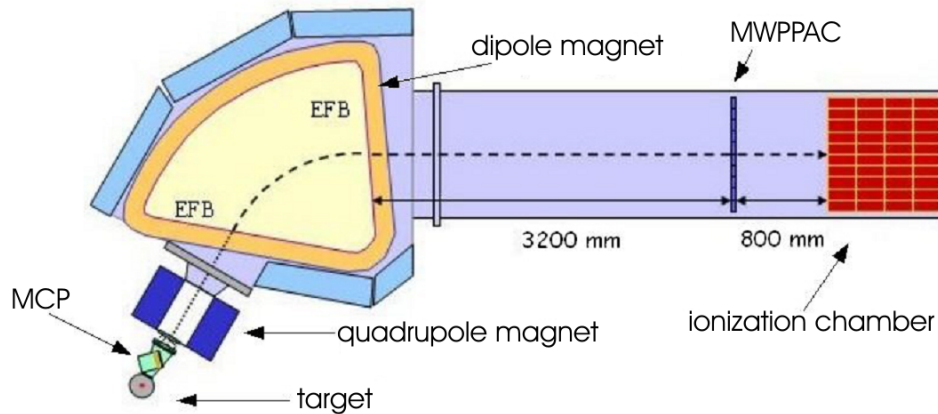
Figure 2.1: Scheme of the Prisma spectrometer [Mer06].

2.2 γ-ray detectors

γ rays are emitted in nuclear processes during radioactive decay or in nuclear reactions and their typical energies range from 0.1 MeV to 20 MeV. The detection of γ rays gives information about nuclear energy levels; energy and intensity of γ rays determine the position of the level; decay time determines the lifetime of the level; polarization of γ rays determines parity of the level; angular distribution and correlation between γ rays ensure information about spins, magnetic moments, static quadrupole moments, etc.

2.2.1 Interaction of electromagnetic radiation with matter

The detection of electromagnetic radiation is based on the interaction of radiation with matter. There are three main types of interaction (Fig.2.2) [LDV03]:

1. Photoelectric effect which dominates the low energies ($E < 0.2$ MeV), and whose cross section is is proportional to Z^n/E^3.

2. Compton scattering which dominates the intermediate energy range (0.2 MeV$< E < 5$ MeV), with the cross sections proportional to the Z. Scattered γ ray can:

   a. interact with the same detector (i.e. with electrons inside the same detector) via photoelectric effect or another Compton scattering, and this process continues until total energy of γ ray is stored in the detector

   b. escape the detector, and in this way, a part of γ energy is lost.

3. Production of electron-positron pair which dominates the higher energies $E > 5$ MeV, with the cross sections which is proportional to Z^2. The difference between γ ray energy and 1.022 MeV (twice the electron rest mass), i.e. the energy excess, is converted into energies of electron and positron. Afterwards, positron is annihilated in the detector and two photons with energies of 0.511 MeV are created, which is seen as a peak in the γ spectrum.

2.2.2 γ ray expertiments

Large γ-ray arrays have been successfuly used in the nuclear structure studies for nuclei produced in the transfer reactions, especially for heavy nuclei with poorer energy resolution via particle detection. Two methods, co called "thick-" and "thin-target" experiments, have been employed in the stuydies of transfer reactions induced by heavy ions at energies close to the Coulomb barrier.

In thick target experiments all the reaction products are stopped and the transfer cross sections are automatically integrated over total angular range. The complementary, thin-target approach assumes γ-particle coincidences, thus detecting fragments in the restricted
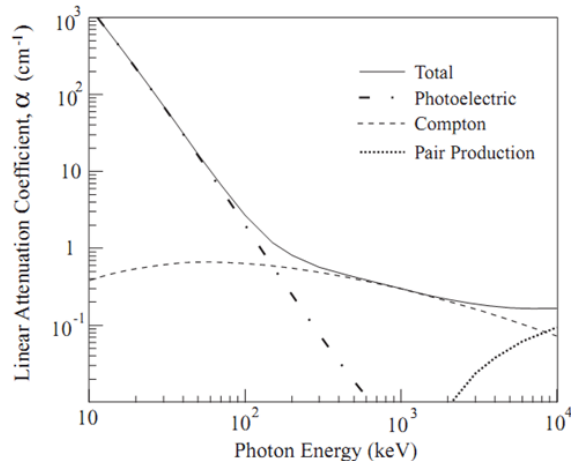
Figure 2.2: Linear γ attenuation coefficient for photoelectric, Compton and pair-production interactions as a function of γ ray energy [LDV03].

angular range. In this way, even efficient γ arrays are often lacking double or triple γ coincidences, commonly present in the thick-target measurements.

Thick target experiments imply target thickness ≥ 30 mg/cm^2, inside which the transfer products are stopped. Target is located in the center of a large γ array, whose good efficiency allows detection of multiple γ rays, and can provide the information about angular distributions and correlations. Consequently, it is possible to construct a very rich level schemes. This method can be applied only if at least one of the γ rays of the outgoing fragments is known, i.e. the reaction products can be recognized only through their previously attributed γ transitions. In addition, in the thick target experiments the short lived states can not be studied. This problem is overcome in the thin target experiments, with a target of thickness ≤ 1 mg/cm^2. The γ rays are emited in-flight, and the reaction products are later analyzed in spectrometers, hence, γ-particle coincidences can be studied. Since γ rays are in this case emitted by a moving particle, one has to correct γ spectra for Doppler effect, which requires the knowledge of the velocity vector of the fragment, measured in the spectrometers. Experimental setup Prisma + Clara (more of which can be read in following chapters) is a typical setup for a thin target experiment. One of the disadvantages of this method is somehow lower γ statistics when compared with thick target. Concerning the life-time, this method is not very well suited for the study of the isomeric states, or the states whose life-time is longer

than the time of flight of the fragment in the spectrometer. At the end, we thus can conclude that the best approach for the studies of the transfer products would be the combination of the results of the two methods.

Chapter 3

Experimental setup

The experiment ^{90}Zr+^{208}Pb was performed at Tandem-ALPI accelerator center at Laboratori Nazionali di Legnaro of INFN using the Clara + Prisma experimental setup. The ^{90}Zr beam impinging on a 280 μg/cm^2 ^{208}Pb target was provided by the Tandem-ALPI accelerators at 560 MeV, with an average current of 3 pnA. High efficiency of magnetic spectrometer Prisma ensured identification of up to 20-30 transferred particles.

Prisma has been designed for the heavy ion reaction studies, with special emphasis on transfer reactions and transition from quasielastic to deep-inelastic processes. The possibility of coupling Prisma with a large γ array, such as Clara, allows performing experiments in which a unique γ spectrum is assigned to every ion detected in the spectrometer. Furthermore, Prisma and Clara provide complementary information about ions, which helps in data analysis; e.g. high energy resolution of Clara can be accomplished only by knowing velocities of ions (because of the need for Doppler correction of γ spectra), a data that is provided by Prisma, via event-by-event reconstruction of ion trajectories. In this chapter, the main characteristics of the elements of Prisma and Clara detectors will be presented.

3.1   Tandem-ALPI accelerator complex

In order to study multinucleon transfer reactions, ion beams need to be accelerated to requested energies and intensities (above the Coulomb barrier), which is enabled by the use of accelerators. In this experiment, Tandem-ALPI accelerators were used. They can accelerate

ion beams up to ^{197}Au, with energies up to 20 MeV/nucleon.

Tandem-XTU is electrostatic Van de Graaff accelerator [Lat04], which can operate in stand alone mode or as an injector for the superconductiong linac ALPI. Its maximum working voltage is 15 MV, and possible ions for acceleration range from ^{1}H to ^{197}Au [www3].

For the heavy ^{90}Zr+^{208}Pb system the beam energy gained in the Tandem accelerator was not enough to overcome the Coulomb barrier, the ions were additionally accelerated in the ALPI accelerator. ALPI is a linear superconductiong accelerator for heavy ions up to energies of 20 MeV/nucleon.

3.2 Prisma spectrometer

Prisma (Fig. 3.1) is a magnetic spectrometer designed for the $A = 50 - 200$, $E = 5 - 10$ MeV/A heavy ion beams of the LNL accelerator complex. Its main features are [Ste02, Szi07, Mij12]:

- large solid angle of 80 msr ($\pm 6°$ for θ and $\pm 11°$ for ϕ)

- wide momentum acceptance $\pm 10\%$

- mass M and Z resolutions of $\Delta M/M \approx 1/230$ and $\Delta Z/Z \approx 1/90$

- energy resolution up to 1/1000

- rotation in a large angular range from -20° to +130°.

Prisma consists of a magnetic qudrupole singlet followed by a magnetic dipole. Detector system of Prisma consists of position-sensitive entrance (MCP), and focal plane detectors, namely multiwire parallel plate avalanche counter (MWPPAC) and ionization chamber (IC); Fig 2.1. The abovementioned parts of Prisma will be described in the following sections.

3.2.1 Optical elements

Optical elements of Prisma are magnetic quadrupole and magnetic dipole. Prisma does not use other optical elements for aberration corrections; rather the trajectories of ions are reconstructed event-by-event by use of position and time of flight information from the entrance
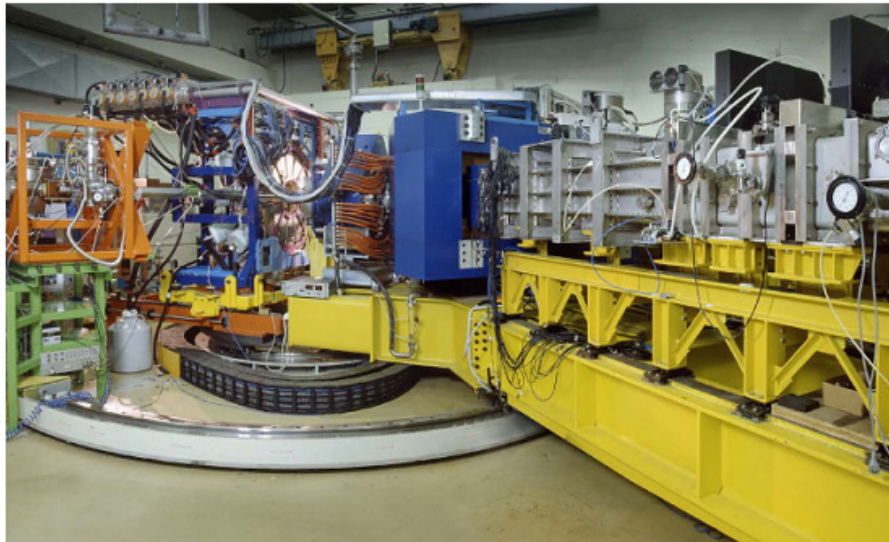
Figure 3.1: Photo of the magnetic spectrometer Prisma [Ste02]

and focal plane detectors. Also, because of the large dimensions of the elements, the influence of the fringing fields is negligible.

Magnetic quadrupole

Magnetic quadrupole is located 50 cm from the target and 60 cm before the dipole magnet. If the frame of reference is set as in Fig. 3.2, with the velocity of ions in the z direction, then the magnetic field of an ideal quadrupole has two components [Got07]:

$$B_x = -by; B_y = -bx,$$

where $b > 0$ is the quadrupole gradient. The resultant magnetic force on the charge q moving in a quadrupole has components:

$$F_x = qv_zbx; F_y = -qv_zby. \tag{3.1}$$

These forces focus ions on the vertical axis (y-axis) down to a dispersion plane (xy plane), achieving the main purpose of the quadrupole: collection efficiency. Characteristics of the quadrupole magnet are listed in Table 3.1.
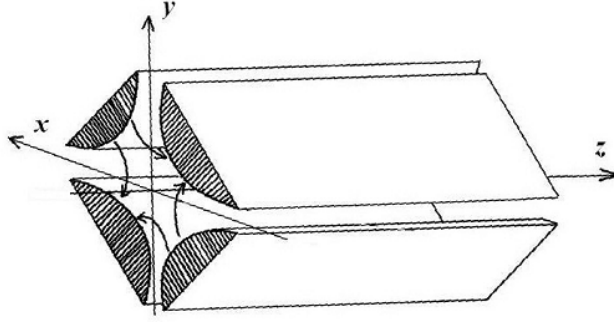
Figure 3.2: Frame of reference for the quadrupole magnet [Got07]

Table 3.1: Characteristics of the quadrupole magnet

Max field gradient	5.3	T/m
Max pole tip field	0.848	T
Effective length	510	mm
Entrance diameter	320	mm

Magnetic dipole

The main function of the dipole magnet is the separation of ions with different magnetic rigidities. The bending angle of the magnet is 60°, maximum bending radius of ions inside the dipole is 1.2 m, and the maximum magnetic field is 1 T, which yields maximum magnetic rigidity of 1.2 Tm. Mass-energy product of the dipole is 70 MeV amu, making the dispersion of 4 cm/%. Characteristics of the dipole magnet are listed in Table 3.2.

Table 3.2: Characteristics of the dipole magnet

Max field	1	T/m
Bending radius	1200	mm
Bending angle	60	°
Entrance angle	-20	°
Exit angle	5	°
Pole gap	200	mm

While traversing the dipole magnet, Lorentz force is exerted on ions, bending their trajectiories according to an equation:

$$\frac{mv^2}{R} = qvB, \tag{3.2}$$

where q is the charge of the ion, m its mass, B magnetic field of the dipole and R the curvature radius of the ion trajectory.

3.2.2 Entrance MCP detector

The entrance detector of Prisma provides time and position (both, in X and Y direction) information. It is based on a pair of large - area ($80 \times 100 \text{ mm}^2$) Micro-Channel Plates (MCP) and placed 25 cm from the target [Mon05].

Walls of the detector are made of stainless steel, biased at 2000 V. Inner parts of the detector are an entrance and inner grid (made of 20 μm gold-plated tungsten wires spaced 1 mm), placed symmetrically around the carbon foil ($\approx 20 \ \mu$g/cm^2), and spaced 4 mm from it (Fig. 3.3). The inner grid accelerates secondary electrons produced in the foil after the passage of ions, while the outer grid balances forces on the foil. Electrons spiral towards MCP under the influence of a magnetic field (produced by an external coil) applied to preserve the position information, where they are being multiplied. A position sensitive anode consists of two mutually orthogonal Cu-Be 70 μm delay lines, wrapped around rounded plastic frames, which share the charge coming from the MCP. Time resolution of the MCP detector is 400 ps, and spatial resolution is 1 mm in both X and Y directions, with efficiency of nearly 100%, in typical experiments with heavy-ion beams.

Possible problems that may occur in MCP detectors (especcialy large area detectors) are the background of δ-electrons, X-rays and unwanted light charged particles. No such problems are noticed in the entrance detector of Prisma because of its design and placement within the spectrometer:

- the detector is placed in a box separated from the scattering chamber

- secondary electrons emitted backwards are detected

- inner grid of the detector is biased to a large negative voltage

- magnetic field deflects unwanted electrons.

Characteristics of the detector and its position between the target and the quadrupole magnet are carefully chosen and have an influence on the overall characteristics of Prisma. Good counting rate of the detector allows placing it close to the target, and its position with regard to the quadrupole matches the solid angle of Prisma.
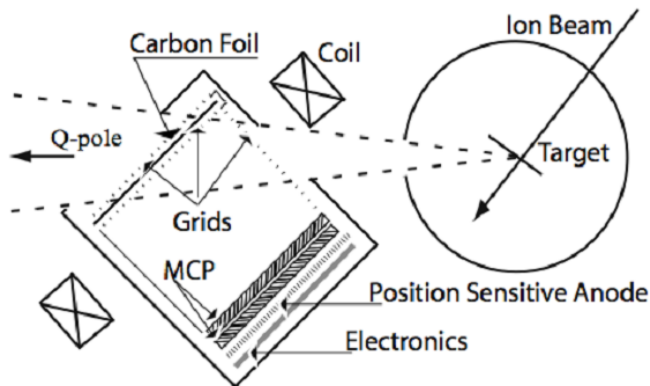
Figure 3.3: Shematic view of the MCP detector [Mon05]

3.2.3 Focal plane detector

The focal plane detector consists of a multiwire parallel plate avalanche counter (MWPPAC) and ionization chamber (IC), which has been designed to match large acceptance of Prisma and provides identification of nuclei produced in binary reactions [Beg05]. This combination of focal plane detectors and their characteristics fulfill the following Prisma requirements:

- good nuclear charge resolution for ions up to $Z \leq 60$ and at energies of 2-10 MeV/amu

- energy resolution of $\sim 1\%$, which, together with the time of flight information, allows identification of the ion charge state

- timing signal with resolution 300-500 ns

- counting rates up to 100 kHz

- position information with resolution of 1 mm and 2 mm, in X and Y direction, respectively.

Multiwire parallel plate avalanche counter

A MWPPAC provides X and Y positions of the ions at the focal plane of Prisma, as well as a timing signal needed for time of flight measurements (in coincidence with the MCP detector).

The detector has a three electrode structure: a central cathode, which provides the timing signal, and two wire planes (anodes, providing X and Y signals), orthogonally oriented with respect to each other (Fig. 3.4), and symmetrically placed, at ground potential, with respect to the cathode (biased to 500-600 V) and at a distance of 2.4 mm from it.

The X-anode is divided into 10 equal and independent sections, each of them having 100 gold-plated tungsten wires extended over an area of 10×13 cm^2. The Y-anode consists of 130 wires (each 100 cm long) and is common to all anode sections. The wires have a diameter of 20 μm and the spacing between them is 0.1 mm for the X-anode and 0.2 mm for the Y-anode (alowing position revolution of 1 and 2 mm, as already mentioned). The anode consists od 3300 tungsten wires distributed over 10 sections, the same as the X-anode, and spaced 0.3 mm from each other.

Because of the narrow spacing between the X and Y anodes (each wire acts as an independent cell), the avalanche caused by the impinging particle is well localized in space, providing good spatial resolution. The timing signal obtained by the cathode has a resolution of 200-300 ns.

Ionization chamber

After leaving the MWPPAC detector, ions enter the ionization chamber (IC), which gives the information about total kinetic energy of ions and the loss of kinetic energy inside the chamber.

The active volume of the ionization chamber is $120 \times 17.6 \times 110$ cm^3 (width, height and depth, respectively), to match the large acceptance of Prisma. Such a long depth of the detector is chosen in order to stop ions of wide kinetic energy range produced in a nuclear reaction and entering into Prisma and to have a long enough ionization range for heavy ions.
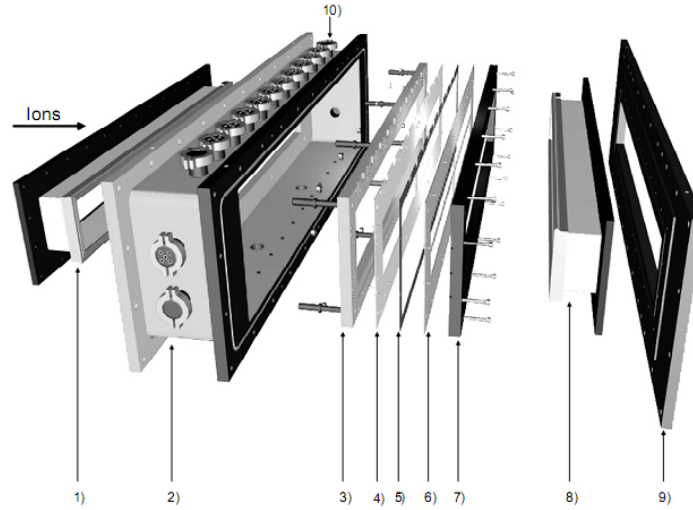
Figure 2. Exploded view of the MWPPAC.
1) Input window; 2)Vacuum vessel; 3) Aluminum X frame; 4) X PCB; 5) Vetronit spacer; 6) Cathode-Y PCB;
7) Aluminum Cathode-Y frame; 8) Exit window; 9) Matching connection flange;
10) Individual electrical connections for each section.

Figure 3.4: Schematic view of the MWPPAC [Beg05]

It is divided into 12 equal sections along the horizontal axis (10, to mach the 10 sections of the MWPPAC and two additional sections on each side, left and right, that are used as vetoes for the ions going partially outside active volume of the ionization chamber) and 4 equal sections in depth, in order to allow measuring kinetic energy loss in each of the sections, ΔE and total energy, E (Fig. 3.5).

Between the electrodes, there is a Frisch grid, distanced 20 mm from the anode and 170 mm from the cathode. It is made of 12000 tungsten wires (each 1 m long and having a diameter of 100 μm) spaced 1 mm apart.

The gases mostly used in the ionization chamber are CH_4 and CF_4; CF_4 having lower ion mobility than CH_4, but a higher stopping power, so it is used for more energetic heavy ions.
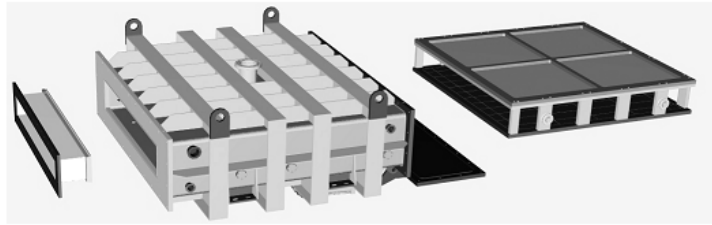
Figure 3.5: Schematic view of the ionization chamber; entrance window (left), vacuum vessel (center) and the electron package (right) [Beg05]

3.3   γ-array Clara

Clara is a γ-array that consists of 25 clover detectors placed on a hemisphere (covering a solid angle of 2π) at the target position of Prisma, but at the opposite side of the spectrometer (Fig. 3.6), namely, at backward angles between $\vartheta = 104°$ and $\vartheta = 180°$ with respect to the entrance direction of the spectrometer [Gad04]. This configuration is chosen because a large acceptance of Prisma does not allow a solid angle greater than 3π, and large velocities of reaction products prevent the placement of the detectors close to $\vartheta = 90°$. The array rotates with the Prisma spectrometer.

Figure 3.6:   Photo of the Clara detector

Each clover detector is composed of 4 HP-Ge crystals (of a diameter 50 mm and length 70 mm) from the Euroball array in a common Compton shield made of BGO scintillators. The purpose of scintillators is to reject events that simultaneously trigger both the Ge and the BGO detectors as a consequence of a Compton scattering interaction, that way improving peak-to-background ratio. The performance of Clara for $E_\gamma = 1.3$ MeV are the following:

- photopeak efficiency $\approx 3\%$

- peak to total ratio $\approx 45\%$

- energy resolution $\approx 0.6\%$ for $v/c = 10\%$.

Coupling the Clara array with the Prisma spectrometer allows studying fragment-γ coincidence, i.e. characteristic γ spectrum is attributed to each particle identified with Prisma.

Due to large velocities of outgoing particles ($\approx 10\%c$ in a typical Prisma + Clara experiment), Doppler correction of γ spectra is needed, which is enabled by the velocity vector provided by Prisma. The final Doppler broadening is thus due only to the angular apertue of the crystals. A detailed description of the Doppler correction will be given in the following chapter.

3.4   Sorting program

For the purpose of data analysis, Prisma + Clara collaboration had developed special analyzing programs. Data are written to a magnetic tape and a hard disk, and are read by using of the program GSORT, a part of the GASPWARE package. By use of this program, data can be sorted in 1D, 2D or 3D histograms, called spectra, matrices and cubes, respectively. These histograms are then analyzed using the programs CMAT and XTRACKN, which are designed for a better visualization of data. Examples of histograms can be found in following chapters.

Chapter 4

Calibration of the detectors

Calibration of all the detector parts of the Prisma + Clara setup is done after every experiment. The calibration procedure is described in the following sections.

4.1   Calibration of the MCP

There is a great difference between the number of data (i.e. all events) recorded in the MCP and the events recorded in the MCP in coincidence with the focal plane detector [Mon09]. This difference is due to unwanted particles detected in the MCP (like electrons, scattered beam etc.), but since they do not pass through the spectrometer, they can easily be rejected from the analysis.

Coincidence of the entrance detector with the focal plane detector is needed to recognize the referent lines and points decisive for calibration, which are visible (Fig. 4.1) because of the metal elements (wires and nails) which stop the ions. Precisely, raw data need to be aligned, so that referent shapes (lines and points) are placed at the beforehand known places. Subsequently, it is possible to convert the x and y signals from the MCP into mm.
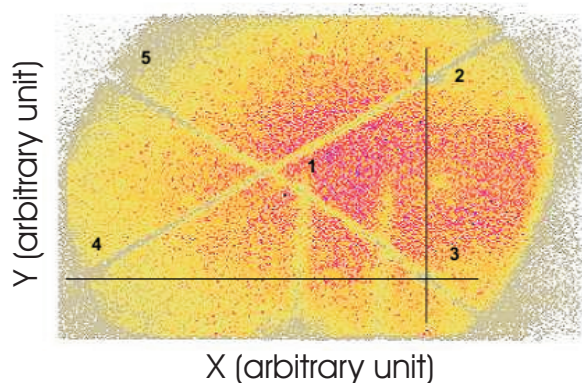
Figure 4.1: Data collected at the entrance detector in the coincidence with the focal plane detector before aligning (namely, rotating and translating) the data according to reference points and lines [Mon09]

4.2 Calibration of the MWPPAC

4.2.1 The x coordinate

The MWPPAC provides the following information:

- up position (y_{up})

- down position (y_{down})

- left (x_{left})

- right (x_{right})

- cathode $(cath)$

- time of flight (TOF)

The first two parameters $(y_{up}$ and $y_{down})$ are common to all 10 sections of the MWPPAC and are used to obtain the y coordinate. It is used for the on-line monitoring of the beam, and to assure the planarity of the trajectories.

Since the MWPPAC is divided into 10 sections in the x direction, the remaining four parameters are recorded for each of the 10 sections. By subtracting $(x_{right} - x_{left})/2$, i.e. the

signals coming from the two ends of the delay line, the x_{fp} coordinate is obtained ($x_{fp} = (x_{right} - x_{left})/2$), which can then be, through the calibration, transferred into milimeters.

As the amplitudes of the cathod signal are higher, in the case when one of the signals, x_{right} or x_{left} is missing, this cathode signal can be used ($cath$) to partially replace the missing signal and to obtain x_{fp} coordinate. This procedure includes calibration of the cathode signal by means of extracting the slope and the offset of the lines in the histogram describing the relation between x_{fp} and $(x_{left} - cath)/2$ in case of missing x_{right} (Fig. 4.2) for each section of the MWPPAC. x_{fp} is then obtained as $x_{fp} = (x_{left} - cath)/2$.
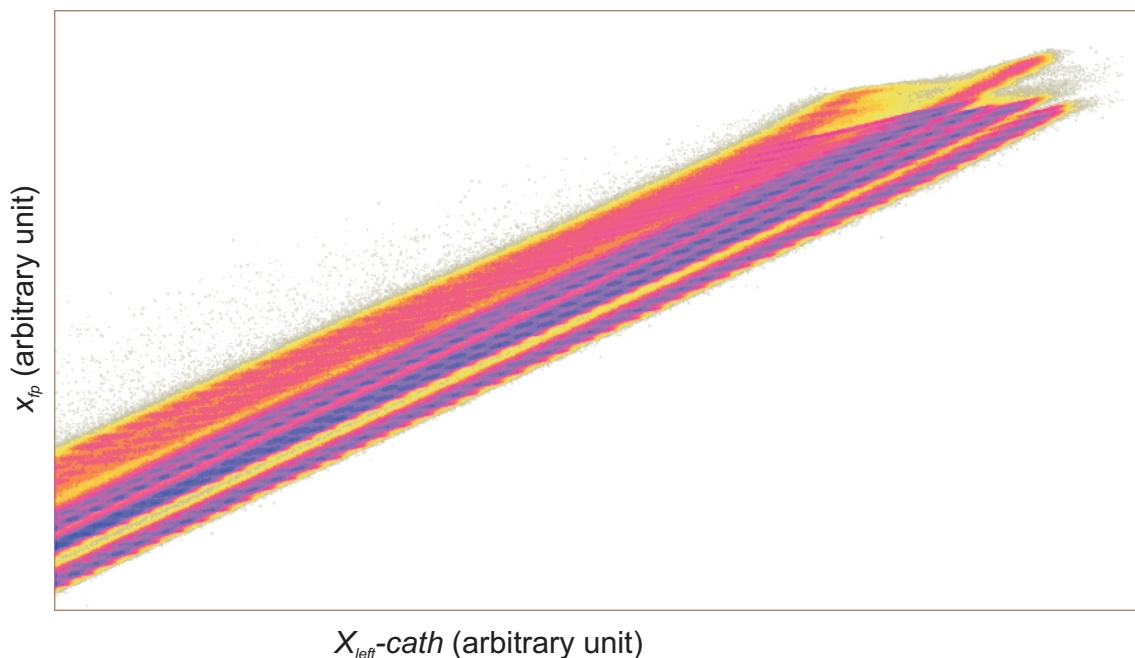
Figure 4.2: Matrix showing x_{fp} vs. $(x_{left} - cath)/2$, for all sections of the MWPPAC

The GSORT code for the analysis has already built in subroutines that combine the three signals (x_{left}, x_{right} and $cath$) to determine x_{fp}.

4.2.2 Time of flight

The time of flight (TOF) signal is defined by the time difference between the timing signal from the MCP and from the cathode of the MWPPAC. The first step is the transformation of the TOF signal into ns. Further on, ten different TOF signals (from 10 sections of the

MWPPAC) need to be aligned, to obatain the unique TOF over the whole focal plane. Figure 4.3 shows the matrix TOF vs. x_{fp} before (A) and after (B) the alignment.

The TOF signal has an absolute offset that needs to be properly evaluated. This is made by looking for a common y-intercept of the lines visible in the TOF vs. D/R matrix (where D is the total length of the ion path and R is the curvature radius of the path), Fig. 4.4. Assuming that $D = 6$ m and knowing the kinetic energy of the ions (which yields the velocity of the ions $v \approx 0.1c$), the time of flight is estimated:

$$TOF = \Delta t = \frac{D}{v} \approx \frac{6m}{0.1c} \approx 2 \cdot 10^{-7} s = 200ns.$$
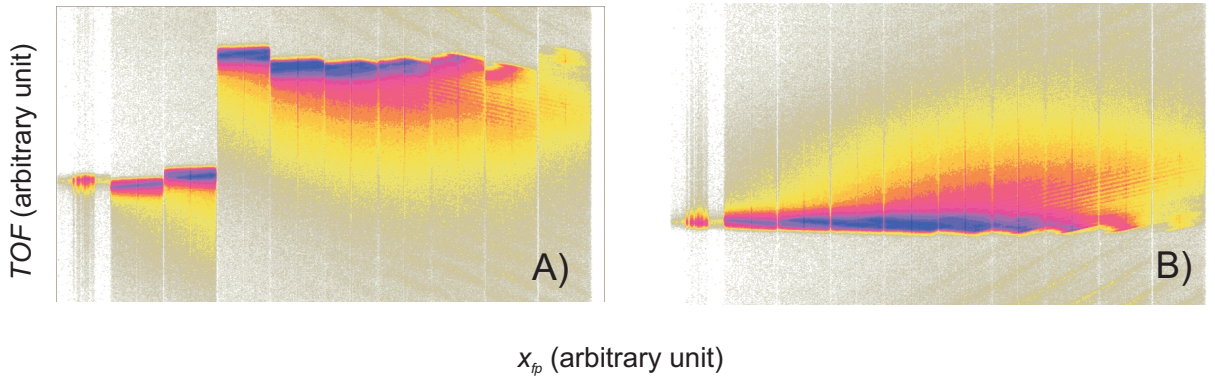
Figure 4.3: Time of flight signal in ten different sections of the MWPPAC before (A) and after (B) the alignment of the signals in the ten sections of the MWPPAC

In addition, the check and fine tuning of this procedure concerning the TOF offset is made by use of the Ge γ spectra measured in Clara. By setting gates on the most intense γ lines after applying Doppler correction, the energy and width of the γ line can be checked. This is an iterative procedure that includes correction of the TOF offset and ends when the user becomes satisfied with the peak energy and width.

4.3 Calibration of the IC

The ionization chamber is divided into 40 sections: 10 pads in the X direction (matching the 10 sections of the MWPPAC detector), and 4 equal sections in depth, as shown in Fig. 3.5. In the data analysis, only trajectories which end inside the IC ("veto" sections), i.e. whose
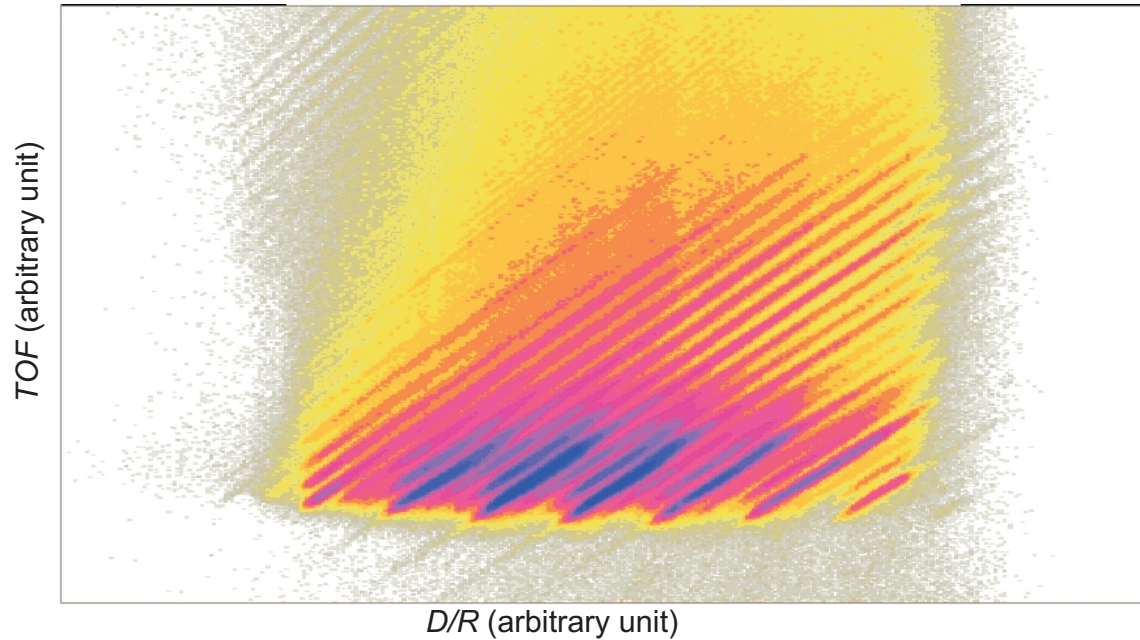
Figure 4.4: Matrix showing TOF vs D/R

total energy has been measured, are considered. The alignment of the signals in each IC section is done through the off-line calibration by using a charge integration device.

4.4 Clara calibration

Clara consists of 25 clover detectors (which sums up to 100 single detectors, numbered from 00 to 99), each of them surrounded by the BGO scintillator, which are used as Compton shields.

Parameters assigned to each Ge detector are:

- Q0 (energy)

- Q1 (time)

- Q2 (20 MeV ADC - analog-to-digital converter - channel)

- Q3 (4 MeV ADC channel)

- Q4 (TDC - time to digital converter)

An individual calibration file was made for each of the parameters, Q2, Q3 and Q4. Radioactive sources used for calibration were ^{152}Eu and ^{56}Co (with the ^{152}Eu source we covered the energy range up to 1400 keV, and with ^{56}Co energy range from 1200 to 3200 keV).

Table 4.1: Energies of the γ rays of the sources ^{152}Eu and ^{56}Co used for the calibration of the Clara array

^{152}Eu		^{56}Co
energy (keV)	intensity%	energy (keV)
121.7817	35.67	1238.282
244.6975	7.64	1360.215
344.2785	29.00	1771.351
411.1165	2.24	2015.181
443.9650	3.18	2034.755
778.9040	12.96	2598.459
964.0790	14.65	3201.962
1085.869	10.24	3253.416
1089.737	1.73	3272.990
1112.069	13.69	
1299.140	1.63	
1408.006	21.07	

Spectra of the aforementioned sources recorded in one of the detectors from the Clara array for the parameter Q2 are shown in Fig 4.5 and 4.6, in the reduced energy range. The most important peaks used in calibration are labeled in Table 4.1.

The same radioactive sources have been used for the calibration of the timing signal (Q4) of the Clara detector. The recorded timing signal are shifted to different channels with respect to each other (as shown in Fig. 4.7, where the two visible peaks belong to the two different Clara detectors). The calibration procedure allignes all signals by finding an offset for each detector.
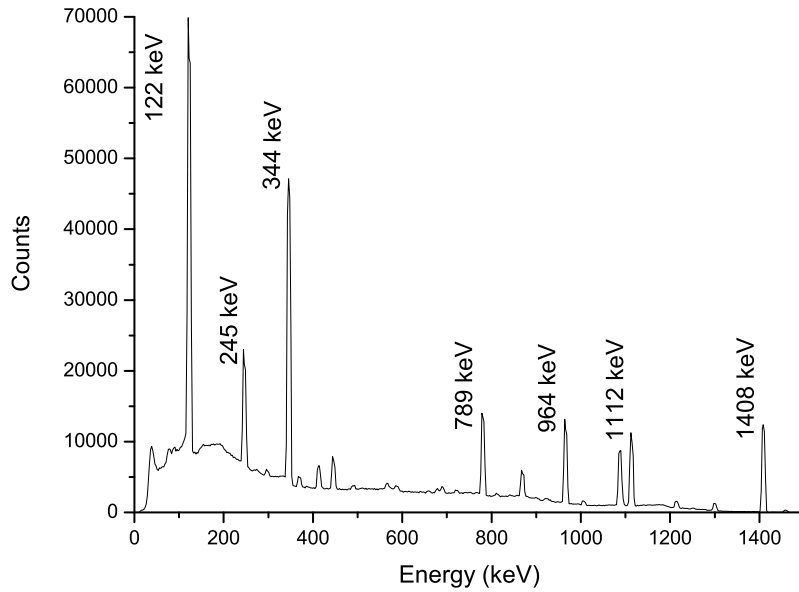
Figure 4.5: ^{152}Eu spectrum recorded in one of the detectors from the Clara array
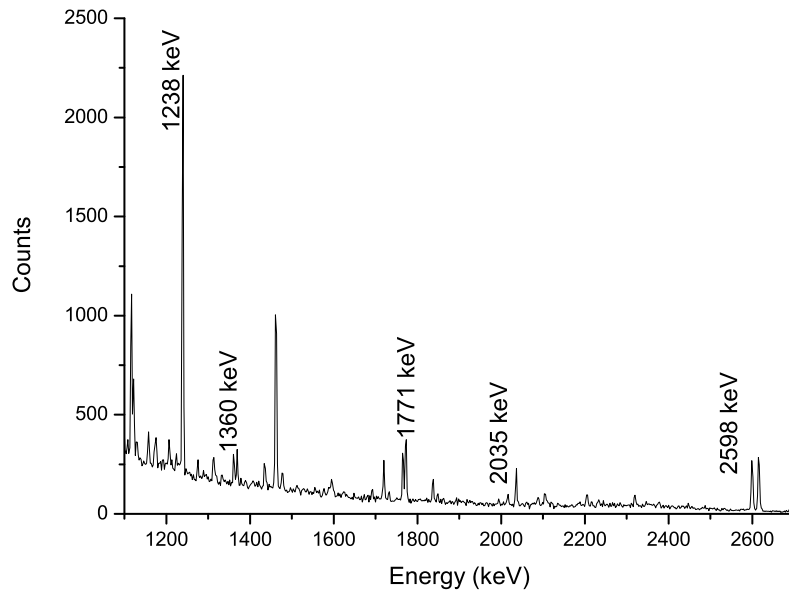
Figure 4.6: ^{56}Co spectrum recorded in one of the detectors from the Clara array
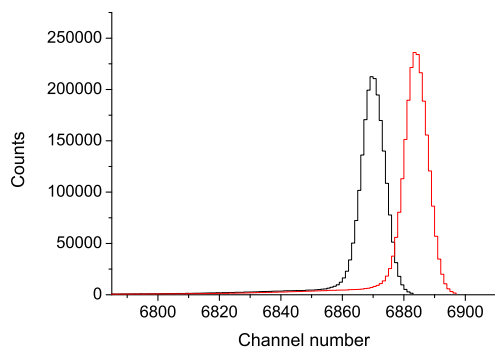
Figure 4.7: The timing signal (Q4 parameter) recorded in two different Ge detectors of the Clara array.
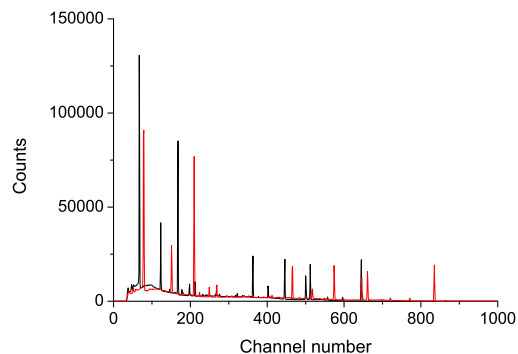
Figure 4.8: Sum of the signals recorded from the radioactive sources ^{152}Eu and ^{56}Co for the Q2 parameter in two different Ge detectors of the Clara array

In addition, the energy signals, parameters Q2 and Q3 (energy on the scale up to 20 MeV and 4 MeV, respectively) need to be alligned. This has been done by comparing signals of all 100 detector, for both calibration sources (^{152}Eu and ^{56}Co). Figure 4.8 shows a one-dimensional spectrum of the Q2 parameter, before aligment precedure, for two different Ge detectors made with the superimposed radioactive sources.

Further on, for Q2 and Q3 parameters, it was necessary to perform a fine tuning of the Ge detectors in order to correct possible shifts that could have showed up during different runs of the experiment. It is important to emphasize that signals used for the recalibration procedure contain data collected during the experiment. Namely, one has to compare different runs and follow with the alignemnt procedure when any shifts in the signal occurs (example of such shift for two detectors is shown in Fig. 4.9, for the parameter Q2).

It is well known that the efficiency of the Ge detector depends strongly on the the energy of the incident photon, in the 0-4 MeV energy range. Thus, the efficiency corrections have been extracted by the means of the the ^{152}Eu radioactive source (spectrum of ^{152}Eu is shown in Fig. 4.5). The ^{152}Eu source γ-ray intensities are known and the efficiency for each γ ray (i.e. energy) is obtained by:

$$\text{efficiency} = \frac{\text{area enclosed by } \gamma \text{ peak}}{\text{intensity of the } \gamma \text{ ray}}.$$
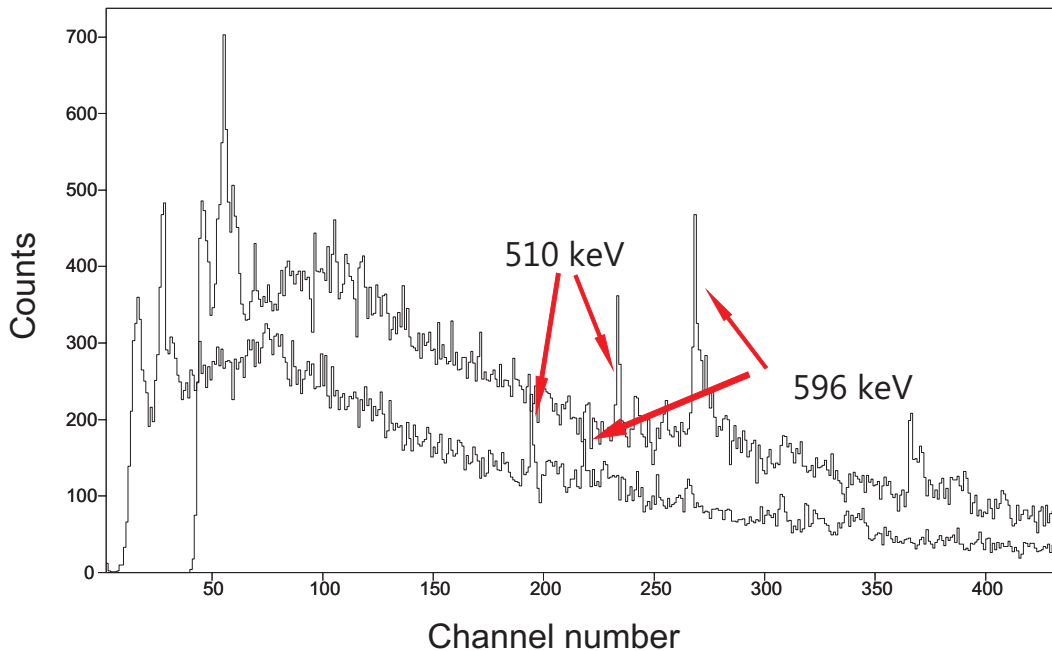
Figure 4.9: Signals recorded in two Ge detectors for the first five runs of the experiment

Table 4.2: Coefficients of the efficiency function of the Clara γ array

a	7.5586
b	1,7049
c	0.11384
d	-0.027086
e	$-0.76394 \cdot 10^{-2}$
f	$0.87936 \cdot 10^{-3}$

The function that describes the detector efficiency dependence on γ-ray energy (see Fig. 4.10) is given by:

$$eff = e^{a+b\cdot\ln E+c\cdot(\ln E)^2+d\cdot(\ln E)^3+e\cdot(\ln E)^4+f\cdot(\ln E)^5},$$

where the parameters a, b, c, d and e are found by the data fit and they are presented in Table 4.2. Here, eff stands for detector efficiency and E γ ray energy. Due to the X-ray shield that was put in front of detectors, there is a deviation of the data from the curve (for energies ≤ 300 keV). For higher energies (> 1600 keV), the above function has been used for
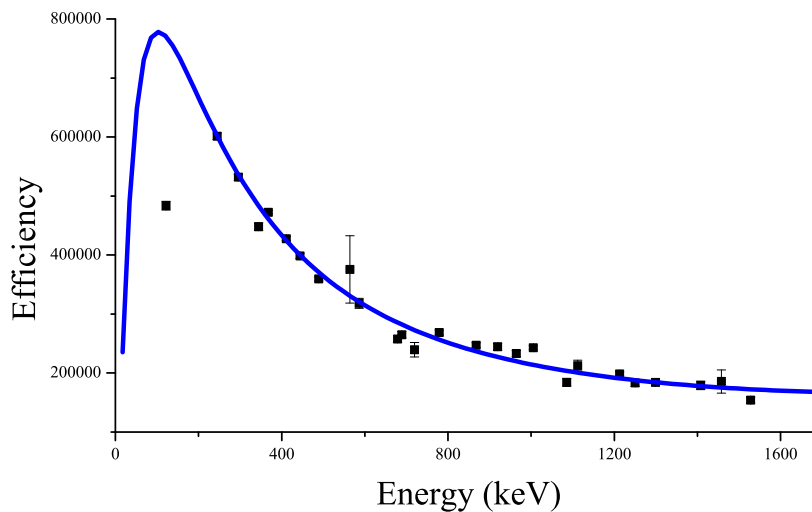
Figure 4.10: Efficiency dependence of Ge detectors on γ energy

the extrapolation of the detector efficiency.

4.5 Doppler correction of the γ spectra

Since the calibration of the Clara array is done using the sources that are at rest, and the γ spectra analyzed in the experiment are collected from the ions traveling with large velocities (up to $0.1c$ for Zr ions, with the majority of the Zr ions around 0.09 c, Fig. 4.11), the spectra need to be corrected for the Doppler effect.

The relation between the emitted ($E_{\gamma 0}$) and detected (E_γ) γ ray energy is:

$$E_\gamma = E_{\gamma 0} \frac{\sqrt{1 - \frac{v_b^2}{c}}}{1 - \frac{v_b}{c} \cos \vartheta_b},$$

where v_b is the velocity of the light (projectile-like) outgoing partner of the reaction, and ϑ_b the angle that v_b forms with the Ge crystal that detects the γ ray (Fig. 4.12).

Under the assumption of a pure binary reaction $a + A \longrightarrow b + B$, where a is the projectile, A is the target at rest, and b and B projectile-like and target-like reaction products, it is possible, by knowing v_b and ϑ_b (parameters that are provided by the Prisma spectrometer after trajectory reconstructions), to obtain also the parameters v_B and ϑ_B. From the conservation
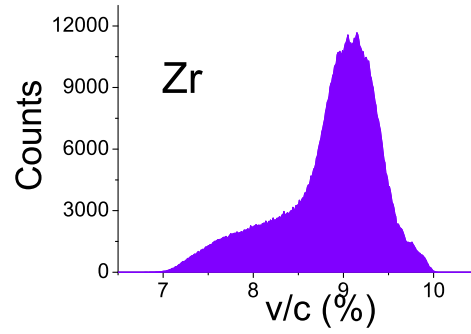
Figure 4.11: Distribution of the velocity of Zr ions
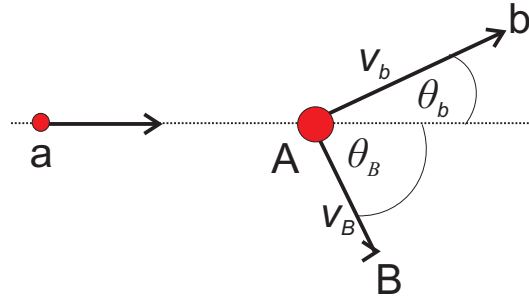
Figure 4.12: Scheme of a collision $a + A \longrightarrow b + B$

law of the total momentum $\overrightarrow{p} = m_a \overrightarrow{v_a}$:

$$m_a \overrightarrow{v}_a = m_b \overrightarrow{v_b} + m_B \overrightarrow{v_B},$$

where m_a, m_b and m_B are the masses of the corresponding nuclei, two equations can be obtained, one for each axis, x and y:

$$m_a v_a = m_b v_b \cos \vartheta_b + m_B v_B \cos \vartheta_B$$

$$m_b v_b \sin \vartheta_b = m_B v_B \sin \vartheta_B.$$

Since the energy, and thus the velocity v_a of the projectile a is known, from these two equations, parameters v_B and ϑ_B can be obtained:

$$\tan \vartheta_B = \frac{\sin \vartheta_b}{\frac{m_a v_a}{m_b v_b} - \cos \vartheta_b}$$

$$v_B = \frac{m_b v_b}{m_B} \frac{\sin \vartheta_b}{\sin \vartheta_B}.$$

39

Calculating the velocity vector (i.e. v_B and ϑ_B) of the target-like particle, it is possible to make a Doppler correction of its γ spectrum, even though the ion is not detected in Prisma. Figure 4.13 shows γ spectra measured in coincidence with ^{90}Zr ions: without Doppler correction (panel A); Doppler corrected for the light partner, i.e. spectrum of ^{90}Zr after Doppler correction (panel B); and Doppler corrected for the heavy partner, i.e. ^{208}Pb the binary partner of ^{90}Zr after Doppler correction (panel C). Red arrows show how the "wrong" Doppler correction, or no correction at all, contribute to the complex bacground (wide peak-like structure) in the binary partner spectrum.
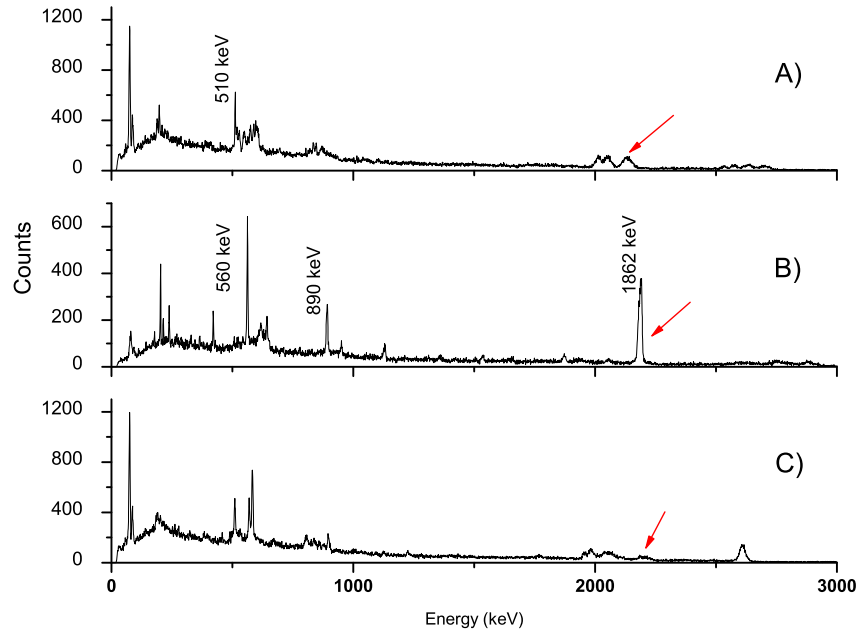
Figure 4.13: γ spectra measured in coincidence with ^{90}Zr ions: without Doppler correction (A); spectrum of ^{90}Zr after Doppler correction (B); and ^{208}Pb after Doppler correction (C). Red arrows show how Doppler correction of the γ spectrum for the ^{90}Zr reflects its heavy partner ^{208}Pb by showing a "bump" in the ^{208}Pb spectrum.

Another consequence of the Doppler effect is the broadening of a γ line due to a finite opening angle $\Delta\vartheta$ of the detector. This broadening results in deteriorating energy resolution, given by:

$$\Delta E_\gamma = E_{\gamma 0} \frac{v_b}{c} \sin \vartheta_b \Delta \vartheta_b,$$

where $E_{\gamma 0}$, v_b and ϑ_b are defined as before. Reducing the opening angle for the detection, $\Delta\vartheta$, by increasing the distance between the target and the detector, would reduce Doppler broadening, but with the same number of detectors, it would also reduce the detection efficiency, so compromise must be made between those two parameters.

4.6   Add-back procedure

Clara consists of 25 clover detectors, each of them containing 4 HP-Ge crystals, surrounded by a BGO scintillator that acts as a Compton shield. The BGO shield works in anti-coincidence with the Ge crystal, rejecting all the events that simultaneously released γ rays in the Ge crystal and the BGO material. The purpose of this procedure is to reject all the γ rays that were Compton scattered in the Ge crystal, this way reducing the Compton background of the spectrum. Consequently, the procedure also lowers the statistics of the experiment.

Since each clover detector contains four HP-Ge crystals, it can work in the add-back mode, which uses the configuration of the clover detector to improve the statistic and to recover some of the rejected γ rays. The method assumes that simultaneous triggering of two adjacent Ge crystals in one clover detector implies that Compton scattered γ ray in one of them entered in the other and adds up the energies of the γ rays in both crystals to recover the original energy of the incoming γ ray (Fig. 4.14, left panel). Simultaneous signals in non-adjacent crystals are ignored in the add-back mode (Fig. 4.14, right panel), since they mostly contribute to the background.

Figure 4.15 shows γ spectrum of ^{90}Zr with (black line) and without (red line) the add-back procedure. It is clearly seen how add-back procedure improves peak to valley ratios.
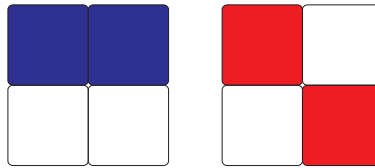
Figure 4.14: Scheme of a clover detector; simultaneous signals in two adjacent crystals (left) add up in the add-back procedure, while signals in non-adjacent crystals (right) are rejected, since they are found to contribute mostly to the background.
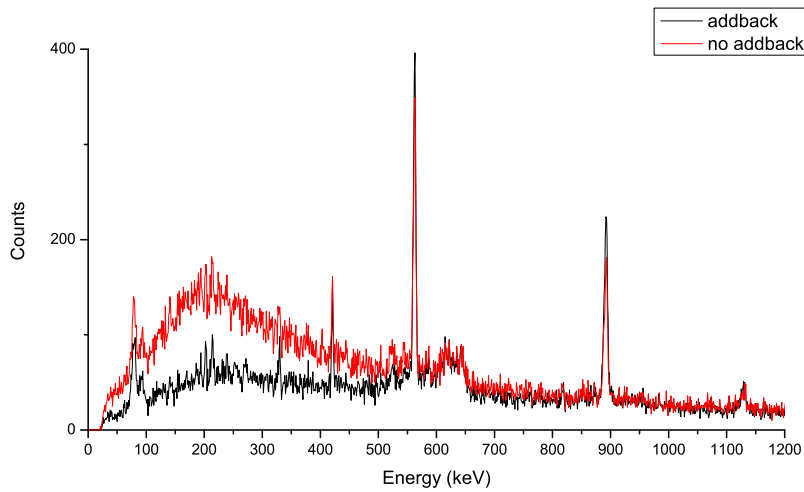
Figure 4.15: γ spectrum of ^{90}Zr with (black line) and without (red line) the add-back procedure

Chapter 5

Trajectory reconstruction and ions identification

Trajectory reconstruction and identification of ions are made by using the GSORT programm and specially developed routines as a part of the programm. After calibration of every part of the Prisma + Clara setup, parameters necessary for identification of reaction products and coincident γ rays were obtained [Val09].

5.1 Motion of the ions inside the Prisma spectrometer

Prisma records the following data:

- spatial coordinates in the entrance detector (MCP)

- spatial coordinates in the focal plane detector (MWPPAC)

- time of flight (TOF) between MCP and MWPPAC

- energy released in each section of the ionization chamber, ΔE

- total energy released in the ionization chamber, E

Knowing the coordinates in the entrance detector, the distances between the elements of the spectrometer and forces acting on ions inside the magnets (Section 3.2.1), it is possible to calculate the equations of motions of the ions through the spectrometer [Mon11]. Of

great importance is the assumption of the planarity of the ion trajectories after leaving the quadrupole magnet, which lies on two facts: longitudinal dimension of the Prisma spectrometer (6.5 m) being much larger then the transversal one (0.2 m) and the possibility to ignore the fringing fields of the magnets. These two facts have been confirmed with the calculation based on the Monte Carlo method.

By solving the equation (3.1, page 21), hyperbolic motion of the ions inside the quadrupole magnet is obtained. In the region between the magnets, no forces act on the ions, so the trajectory is linear, and the dipole magnet curves the trajectories according to the equation (3.2, page 23). After leaving the dipole, trajectory becomes linear again and remains this way until the ions are stopped in the ionization chamber. From the data collected by Prisma, the XFP Prisma routine of the GSORT code calculates x_{fp} coordinates of ions (in mm), in the focal plane, as explained in Subsection 4.2.1. The TRACK Prisma routine from the same package calculates:

- length of the path of the ions, D

- curvature radius of the trajectory inside the dipole magnet, R

- total energy released in the ionization chamber, E

- range of ions inside the ionization chamber, r.

Once the data are obtained, it is possible to continue with the identification of ions.

5.2   Bethe formula and Z identification

Energy loss of charged particles in interaction with matter is decribed by the Bethe formula, which in a relativistic case has a form:

$$-\frac{dE}{dx} = \frac{4\pi}{m_e c^2} \cdot \frac{nZ^2}{\beta^2} \cdot \left(\frac{e^2}{4\pi\varepsilon_0}\right) \cdot \left[\ln\left(\frac{2m_e c^2 \beta^2}{I \cdot (1-\beta^2)}\right) - \beta^2\right],$$

where $\beta = \frac{v}{c}$, v is particle velocity, c is the speed of light, E is particle energy, x is the distance traveled by the particle, Ze is the charge of the particle, m_e is the rest mass of the electron, n electron density in the detector material (i.e. the gas in the ionization chamber),

I potential of the gas and ε_0 permittivity of vacuum. In a nonrelativistic case, the formula simplifies to:

$$-\frac{dE}{dx} = \frac{4\pi n Z^2}{m_e v^2} \cdot \left(\frac{e^2}{4\pi\varepsilon_0}\right)^2 \cdot \left[\ln\left(\frac{2m_e v^2}{I}\right)\right],$$

so, for the energy loss follows:

$$\frac{dE}{dx} \propto \frac{mZ^2}{E},$$

where m is mass of the ion.

According to the previous expression (where dx, E and dE from the expression are equivalent to r, E and ΔE used in the program code), in the matrix E vs. r (r being the range of ions in the ionization chamber), different distributions are noticed, which denote different elements, as in Fig. 5.1. The most intense region belongs to the scattered Zr beam, and other regions are then associated with other elements, respecting the fact that for a fixed energy E, atomic number Z decreases with growing r. By putting a two-dimensional gate on a region of interest, (i.e. events that belong to a certain element of interest), the identification of different isotopes of a chosen element can be continued.
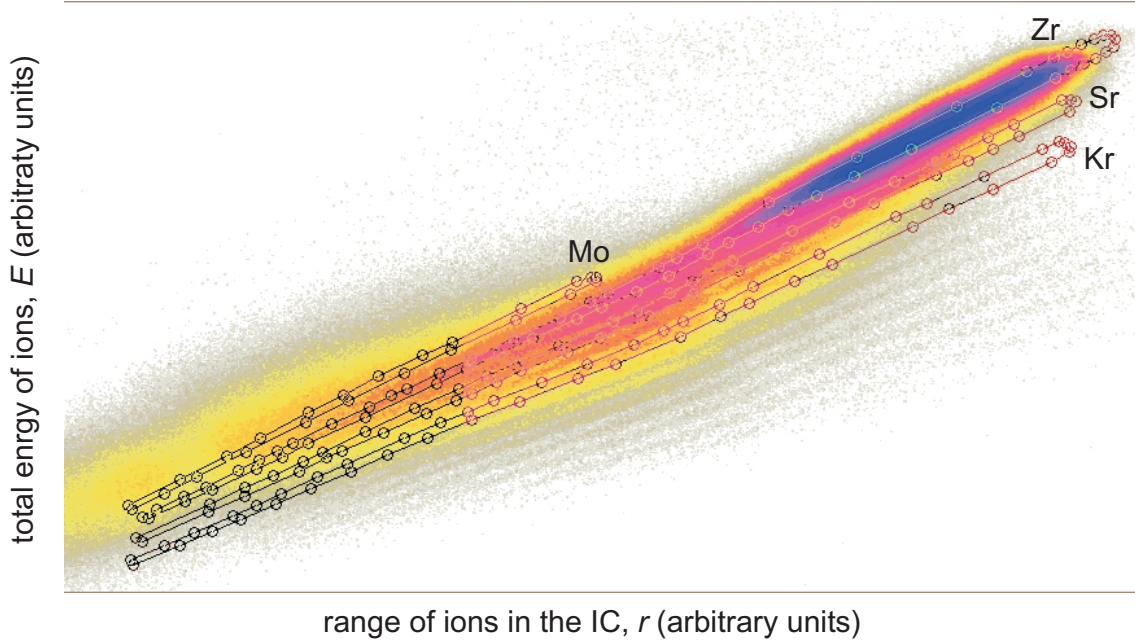
Figure 5.1: Matrix showing energy of ions, E versus their range in the ionization chamber, r. Distinct distributions belong to ions of different elements

5.3   Mass identification

The Lorentz force that acts on the ions inside the dipole magnet curves their trajectories according to equation (3.2, page 23): $\frac{mv^2}{R} = qvB$. It follows:

$$\frac{A}{Q} \simeq \frac{m}{q} = \frac{BR}{v},$$

where A and Q are the mass and charge number of the ion, respectively. Velocity of ions, v is calculated as the ratio between the path that is traversed by the ion, D, and the time of flight, TOF: $v = \frac{D}{TOF}$. Then,

$$\frac{A}{Q} = \frac{BR}{\frac{D}{TOF}}.$$

Velocities of ions are often greater than 10% of the speed of light, so for the time of flight, TOF, one has to consider relativistic corrections:

$$TOF = TOF\sqrt{1 - \beta^2},$$

which finally leads to:

$$\frac{A}{Q} = \frac{BR}{\frac{D}{TOF\sqrt{1-\beta^2}}}. \tag{5.1}$$

Fig. 5.2 shows how Zr ions with different ratios A/Q are distributed over the entire focal plane.

The kinetic energy of ions, i.e. energy released in the ionization chamber is:

$$E = \frac{1}{2}mv^2.$$

Since the mass of the ion, m is proportional to the mass number of the ion, A, we have:

$$E \propto QBRv.$$

Thus, in the matrix that shows energy released in the ionization chamber, E, versus the product of velocity of the ion and curvature radius inside the dipole magnet, $v \cdot R$, different distributions are visible, each of them representing a different charge state of ions, as in Fig. 5.3, which shows E vs. Rv matrix for the Zr ions.
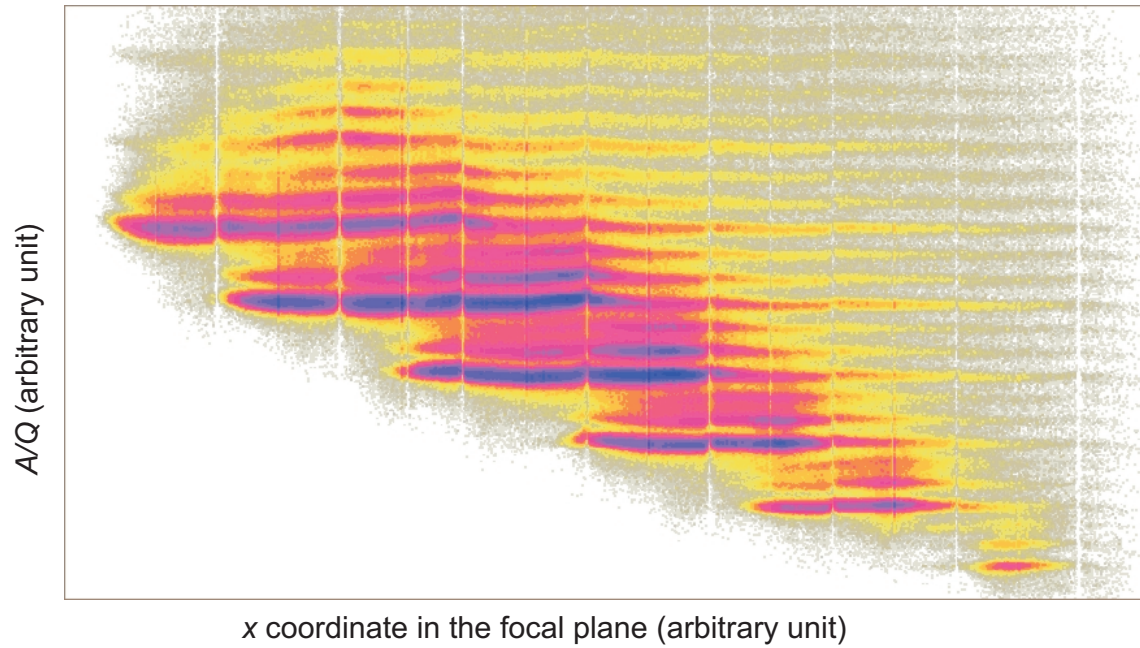
Figure 5.2: Matrix showing the ratio of mass over the charge (A/Q) vs. x_{fp} coordinate in the focal plane for Zr ions
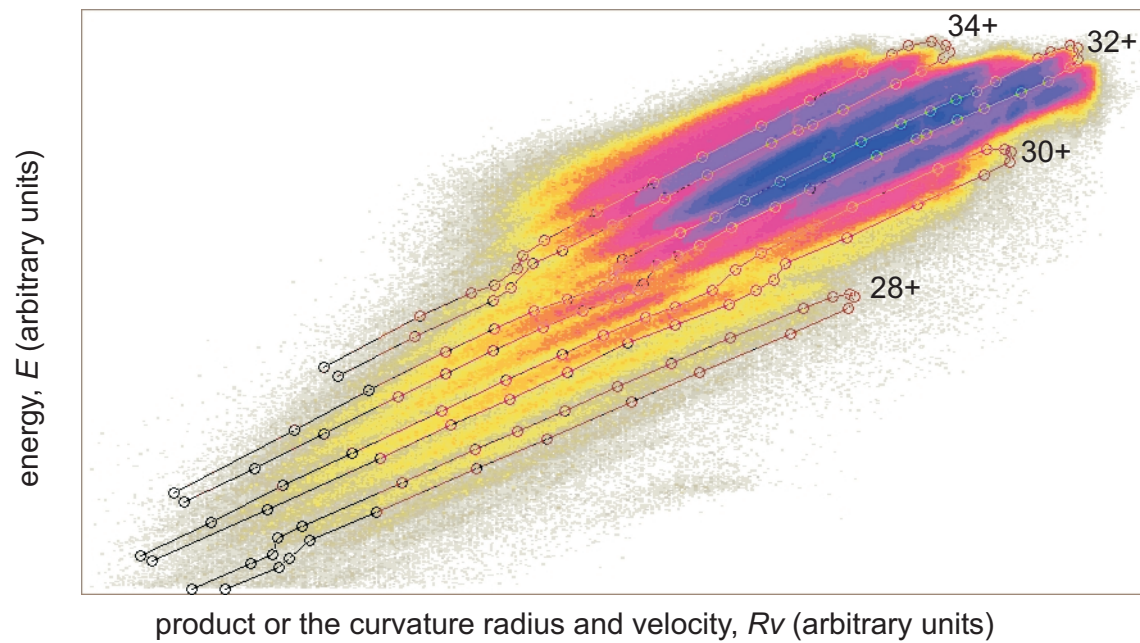
Figure 5.3: Matrix showing E vs. Rv for Zr ions

It is possible to calculate the most probable charge state for every element, to which the most intense area in the matrix E vs. Rv belongs. An empirical formula [SIM82] for the average equilibrium charge-state is:

$$Q = [1 - e^{-1.25X + 0.32X^2 - 0.11X^3}][1 - 0.0019(Z_2 - 6)\sqrt{X} + 0.00001(Z_1 - 6)^2 X],$$

where Z_1 and Z_2 are the ion and target foil atomic numbers respectively, and X is the reduced ion velocity. Fig. 5.4 shows the atomic charge state distributions for three Zr isotopes [CPS09]. The other charge states are assigned to other regions with respect to their slope in the matrix.
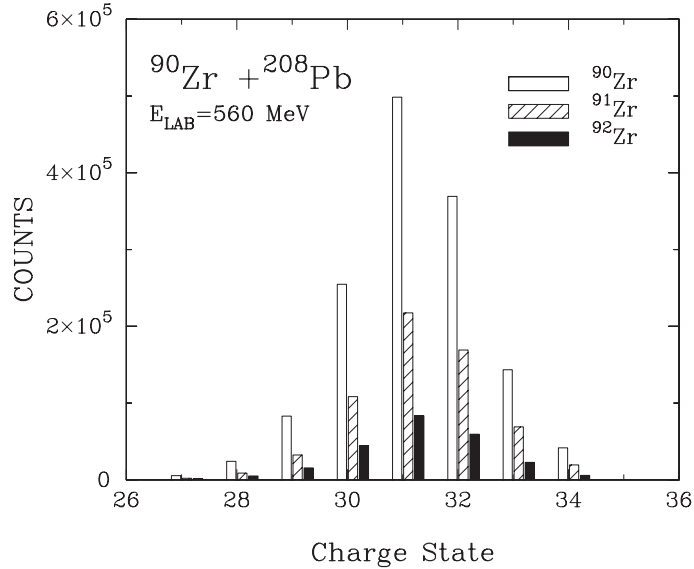
Figure 5.4: Atomic charge state distributions for three Zr isotopes [CPS09]

Knowing the ratio of mass over the charge number from the equation (5.1), the mass number is associated with each region.

The same procedure is then applied to all the other isotopes. Mass distribution of all the isotopes observed in this experiment, in coincidence with the Clara array, is shown in Fig. 5.5.
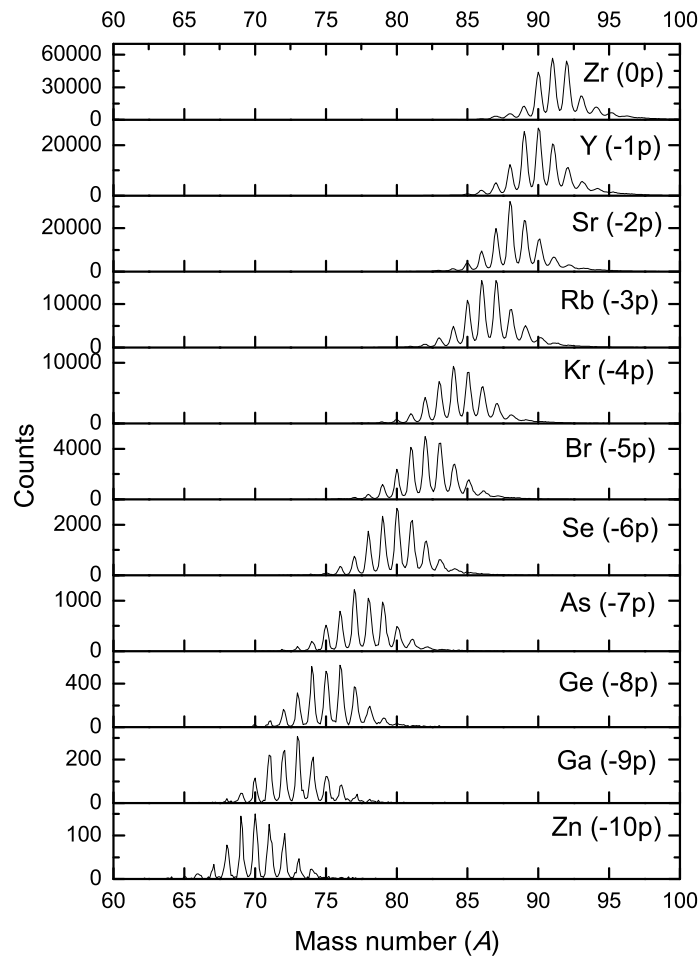
Figure 5.5: Mass distribution of all the observed isotopes in the Prisma spectrometer, in coincidence with the Clara array.

Chapter 6

Experimental results and discussion

Interaction of ^{90}Zr beam on ^{208}Pb target resulted in a population of a wide range of nuclei. Due to γ-fragment coincidences, γ rays detected in the Clara γ array are uniquely assigned to each light fragment detected in the Prisma spectrometer. In this chapter, γ-ray spectra of the strongest populated channels, namely Zr, Y and Sr isotopic chains will be presented. Fig. 6.1 shows a schematic view of the placement of these nuclei in the chart of nuclides. The interacting nuclei in this experiment were ^{90}Zr, with a magic number of neutrons, and doubly magic ^{208}Pb (not shown in Fig. 6.1).

Level schemes, as well as possible assignments of new transitions presented and discussed in this chapter are based on systematics with neighbouring nuclei, and on the main properties of MNT reactions. Energies, spins and parities of levels, their branching ratios and energies of transitions, if not differently stated, are the ones accepted in the Nuclear Data Sheets or listed at the National Nuclear Data Center [www4]. Energy values taken from [www4] are rounded to one decimal place where possible (i.e. where decimal places of the value are known). Statistics of collected data, as usual in γ-fragment coincidence measurements, were generally insufficient to establish coincidence relationships between γ rays assigned to each isotope. The aim was oriented towards understanding the structure of the strongest populated states in view of the selectivity of heavy-ion transfer reactions.

Previous Prisma + Clara measurements have shown that multinucleon transfer reactions can be rather selective in the population of states of specific structure, thus here we point out important characteristics of multinucleon transfer reactions and their manifestation in our
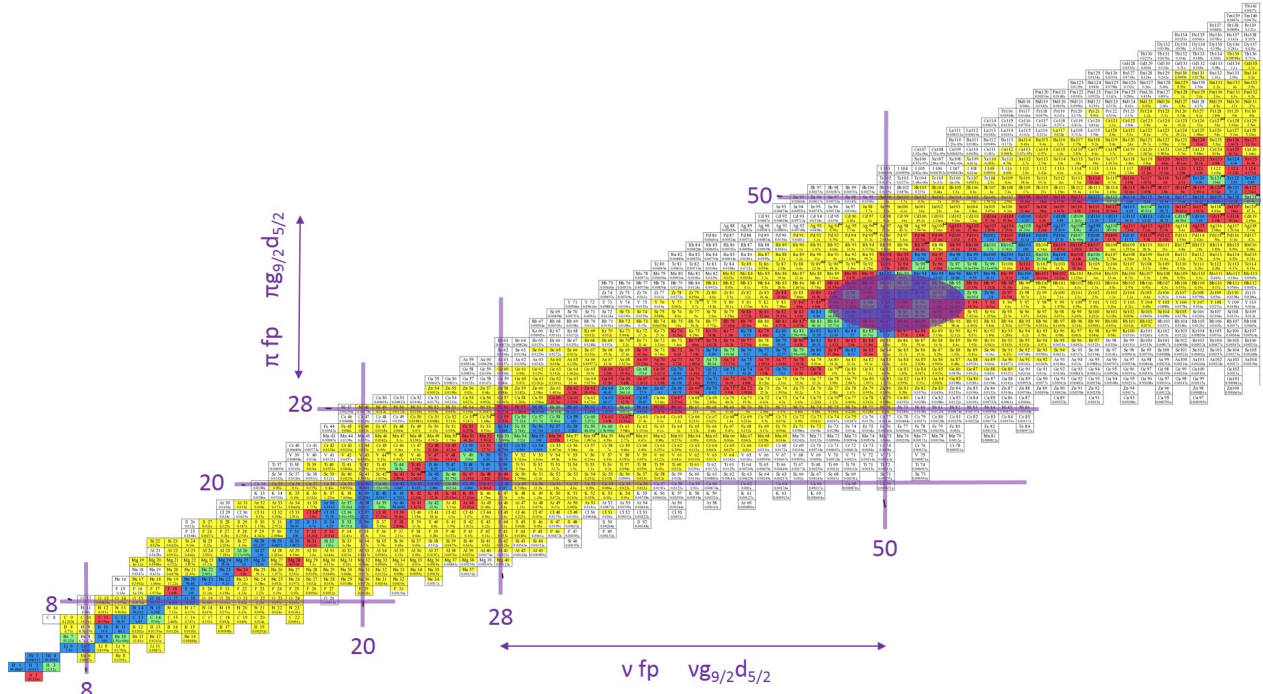
Figure 6.1: Schematic view of the placement of the observed nuclei (Zr, Y and Sr isotopes) in the chart of nuclides. The studied nuclei are placed in the rounded area.

data. One of the recognized characteristics of heavy-ion induced reactions is their possibility to transfer large angular momenta. At these rather low energies (close to the Coulomb barrier), the transfer process maximizes transferred angular momentum to allow a good matching between orbital angular momenta of the involved states [Szi11]. In our spectra this is reflected as a strong population of yrast states.

Traditionally, transfer reactions with light ions were recognized as a good tool to study single-particle states, and they have been extensively used in construction of the shell model. Furthermore, we also expect to see a strong population of states of single-particle character. In our case, the transfer of nucleons is induced by the collision of two heavy nuclei, where multiple nucleons can be transferred. Recently, it has been shown that MNT also provide a significant population of phonon-fermion states. Thus, in our spectra, besides the strong population of states of single-particle character, we expect to observe states which can be described through phonon-fermion coupling [Mon11, MLG12].

Magic nuclei provide a unique laboratory for testing the applicability of various nuclear-structure models. In the $^{90}_{40}\text{Zr}^{50}$ nucleus, the filling of the neutron sub-shells from $1s_{1/2}$ to $1g_{9/2}$ corresponds to the magic neutron number $N = 50$ (see Fig. 6.2). In accordance with the extreme shell model (where the occupation probabilities for single-particle orbits are 0 or 1), the proton sub-shells from $1s_{1/2}$ to $2p_{1/2}$ must be filled in ^{90}Zr. According to this classical shell model, the $2d_{5/2}$ neutron subshell is filled in the ^{96}Zr nucleus.
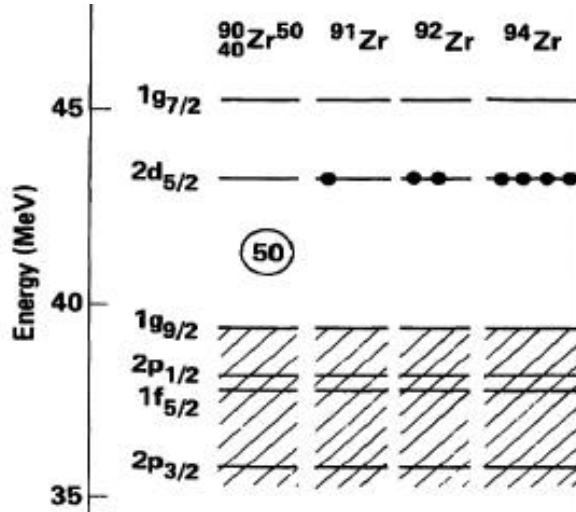
Figure 6.2: Active neutron orbitals in even-even Zr isotopes.

To illustrate the important orbitals in the region of interest, we plotted in Fig. 6.3 the approximate energies of proton and neutron levels in the ^{90}Zr nucleus according to the shell model calculations presented in Ref. [FBA68]. A more recent shell model calculation in the extended shell model space has been studied by the Strasbourg shell-model group [Sim10]. We will refer to these calculations for the various Zr isotopes studied in this thesis. Proton effective single-particle energies for Zr isotopes as a function of neutron number, according to shell model calculations [SNL09], are depicted in Figure 6.4. Here, a shell model study of Zr isotopes was performed in an extended shell model space ($1f_{5/2}$, $2p_{1/2}$, $2p_{3/2}$, $1g_{9/2}$) for protons and ($2d_{5/2}$, $3s_{1/2}$, $2d_{3/2}$, $1g_{7/2}$, $1h_{11/2}$) for neutrons. The effective proton-proton interaction was found by fitting the two-body matrix elements for Ni isotopes with $A = 57-78$ and $N = 50$ isotones (^{70}Cu-^{100}Sn), neutron-neutron interaction was based on calculation in the tin region, and proton neutron interaction used the propagation of single-particle states

between ^{79}Ni and ^{101}Sn.

Fig. 6.4 shows how the proton shells for $Z = 40$ evolve when filing the neutron orbitals. It is noticed that in the region of N explored in this work ($N = 49 - 56$), the $f_{5/2}$ and $p_{1/2}$ orbital become degenerate, and cross each other at $N = 56$, and then again at very neutron rich $N = 82$ shell closure. For less neutron rich Zr isotopes, the $p_{3/2}$ orbital has a rather close effective single-particle energy.

In odd Zr isotopes (^{91,93,95}Zr), based on a simple shell model picture, and by considering only the last uncoupled nucleon, it is expected that one unpaired neutron is in the $d_{5/2}$ orbital, causing the $5/2^+$ ground states. In the case of ^{89}Zr, which has a hole in the $g_{9/2}$ orbital, its ground state is $9/2^+$. When exploring one-particle states, one deals with $3\hbar\omega$ (full, except for ^{89}Zr) and $4\hbar\omega$ shells, thus an unpaired neutron in $g_{7/2}$, $d_{5/2}$, $d_{3/2}$, $s_{1/2}$ or $h_{11/2}$ orbitals, would provide $J^\pi = 7/2^+, 5/2^+, 3/2^+, 1/2^+$ and $11/2^-$ states. These *single-particle* character states are expected to dominate low energy spectra of even-odd Zr isotopes. In addition, states with a hole in the $3\hbar\omega$ shell, with the $g_{9/2}$, $p_{1/2}$, $f_{5/2}$, $p_{3/2}$ or $f_{7/2}$ orbitals, will contribute to $J^\pi = 9/2^+, 1/2^-, 5/2^-, 3/2^-, 7/2^-$ states. As will be shown later, such states are strongly excited in zirconium isotopes.

It has been discovered that ground states of Sr, Zr and Mo isotopes with neutron ranging from the magic number $N = 50$ up to $N \sim 60$ are weakly deformed, but they undergo a shape transition from nearly spherical to well deformed prolate (or oblate) deformations as $N = 60$ is approached and crossed. This region was intensively studied within the the framework of different relativistic mean-field calculations.

The main features of the shape evolution in the axial case can be summarized as follows: isotopes with $N = 50 - 54$ show a sharp potential energy curve around the spherical minimum, that becomes rather shallow at $N = 56 - 58$. Isotopes with $N = 60$ are already deformed with oblate and prolate minima very close in energy. Regarding Zr isotopes, both oblate and prolate minima are found at about the same energy. The shape change at $N \sim 60$ has been predicted to a different extent by various theoretical models. It is also expected that prolate quadrupole deformations would increase smoothly from $N = 50$ up to $N = 56$, the region we are exploring in this work, and then jump suddenly to large deformations between $N = 58$ and $N = 60$.
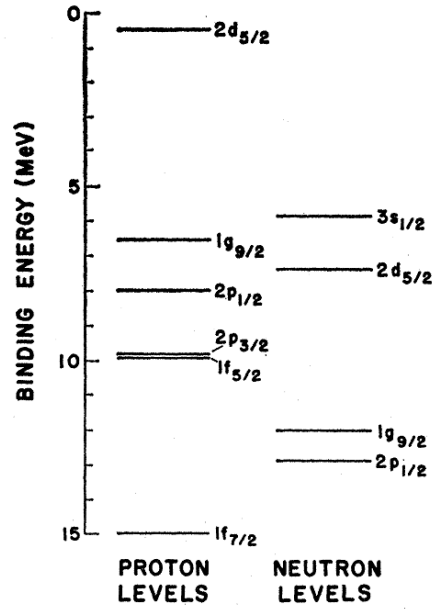
Figure 6.3: Approximate energies of proton and neutron levels in the ^{90}Zr nucleus according to shell model calculations in [FBA68]
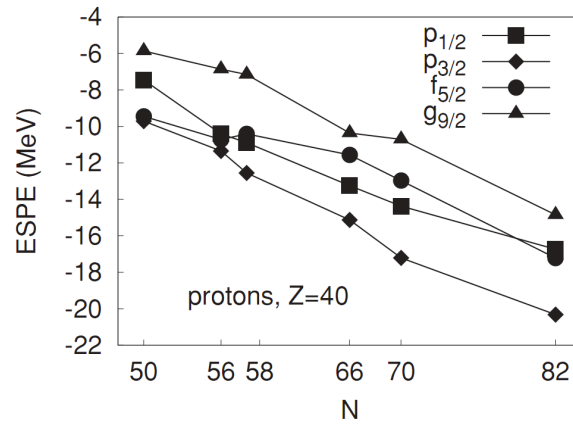
Figure 6.4: Proton effective single-particle energies for Zr isotopes taken from [SNL09], where a shell model study of Zr isotopes was performed in an extended shell model space ($1f_{5/2}$, $2p_{1/2}$, $2p_{3/2}$, $1g_{9/2}$) for protons and ($2d_{5/2}$, $3s_{1/2}$, $2d_{3/2}$, $1g_{7/2}$, $1h_{11/2}$) for neutrons.

To illustrate this behaviour, Fig. 6.5 shows the evolution of nuclear structure in even Zr isotopes from [Elh08], where it has been shown that structure evolves from spherical (^{90}Zr) to strongly deformed (^{102}Zr) nucleus, with a subshell closure at $N = 56$ (^{96}Zr).
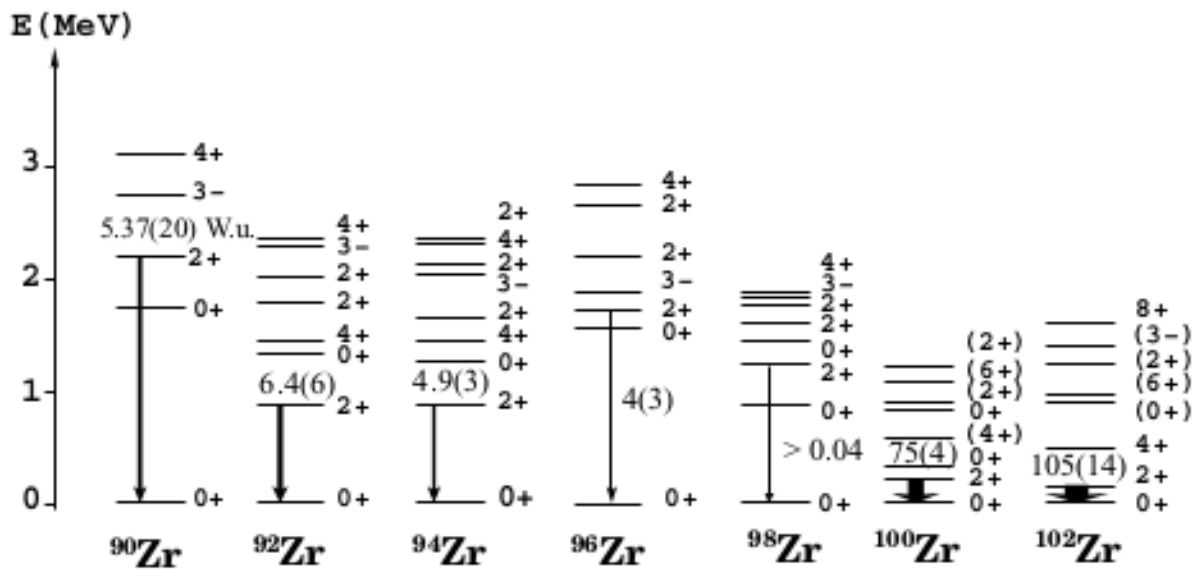
Figure 6.5: Evolution of nuclear structure in even Zr isotopes taken from [Elh08]

6.1 γ-ray spectroscopy and structure of zirconium nuclei

Direct detection of heavy ions is notoriously very difficult. It is worth noticing that bombarding energy must be kept close to the Coulomb barrier as a compromise between having high primary cross sections and reasonable final yield. Due to low ion kinetic energies ($E/A \approx 6$ MeV/amu), and large A and Z, the separation between the different elements and isotopes is more difficult than with the light ions (see for example [Szi07]). When looking for example, the Zr γ spectra, some γ rays that do not necessarily belong to a given isotope can be noticed. By comparing spectra of different zirconium isotopes (A separation), and by comparing them with spectra of yttrium (-1p channels, Z separation) isotopes, some γ spectra may have some contamination. An example is shown in Fig. 6.6, where some γ rays of ^{90}Y appear in the ^{90}Zr γ-spectrum.

To clean spectra in a safe way, we scaled the spectrum of interest that contains some γ rays which have been attributed to the close by isotope and subtracted (in the whole energy scale) the scaled spectrum from the one we want to clean. Figure 6.6 shows how some γ rays which we recognized as transitions in ^{90}Y are cleaned from ^{90}Zr spectrum. These contaminations have been checked by selecting gates of different widths for Z (Fig. 5.1) and ionic charge state (Fig. 5.3). The final widths of the gates have been selected as a compromise between the reduced contamination and the sufficient number of events in the weaker γ lines which were important to our discussion (new γ, or γ decaying from the specific configuration).

Scaling factors used in this procedure are listed in Table 6.1. The same scaling factors are used to correct γ spectra of heavy-binary partners, i.e. lead isotopes. Here, we have to emphasize that the cleaning procedure does not significantly affect the number of counts for γ peaks that actually belong to the observed isotope, except in some cases where the observed and the subtracted spectra contain γ ray with the same energy (as for expample, $E_\gamma \sim 140$ keV in ^{90}Zr and ^{90}Y). In the following sections, only these corrected γ spectra will be discussed.

In some spectra, there are wide areas and peaks which originate from wrongly Doppler corrected γ rays of the associated binary partner. This phenomenon occurs both with a
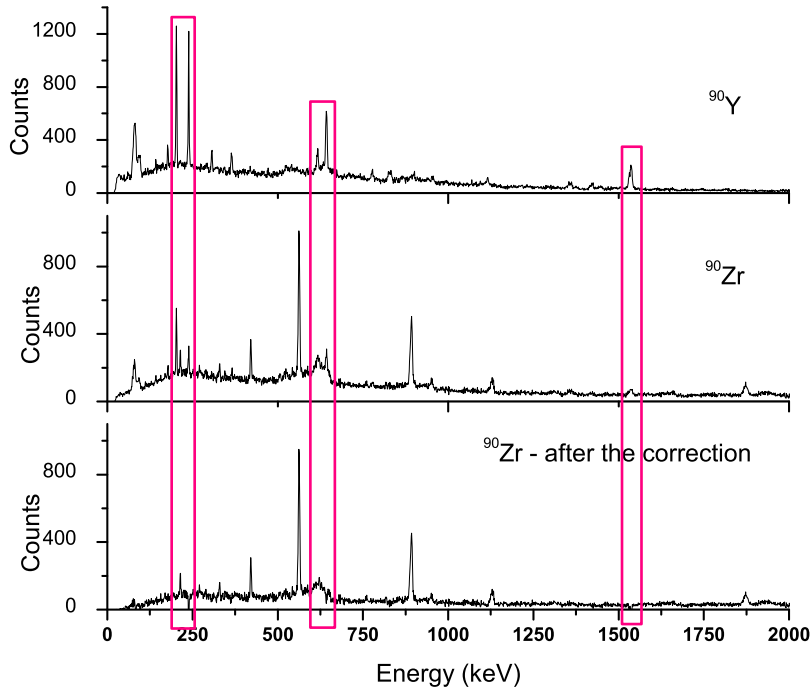
Figure 6.6: γ spectrum of ^{90}Y (top panel), ^{90}Zr before (middle panel) and after correction (bottom panel). Ordinate axis is expressed in number of events. Red rectangles mark γ transitions of interest.

Table 6.1: Scaling factors and expressions used for correction of Zr γ spectra. For example, corrected γ spectrum for ^{89}Zr, with the name ^{89}Zr$_{corr}$, has been obtained by subtraction of scaled ^{89}Y and ^{92}Zr spectra.

corrected γ spectrum	mathematical expression used for the correction
^{89}Zr$_{corr}$	^{89}Zr-0.150*^{92}Zr
^{90}Zr$_{corr}$	^{90}Zr-0.367*^{90}Y
^{91}Zr$_{corr}$	^{91}Zr-0.227*^{91}Y
^{92}Zr$_{corr}$	^{92}Zr-0.256*^{92}Y
^{93}Zr$_{corr}$	^{93}Zr-0.890*^{93}Y-0.104*^{92}Zr
^{94}Zr$_{corr}$	^{94}Zr-0.202*^{93}Zr

light and heavy partner, depending on the velocity used in Doppler corrections, as will be seen in later sections. In some cases, when excited states have a complex decay pattern, with transitions of different intensities, in weaker Zr channels we mostly observed only the strongest decay branch. In such cases, we have checked that the expected number of events in weaker transitions is consistent with the observed yield and background level of this channel. For consistency, these γ rays are listed separately in Table 1 in the Appendix and the intensity limit (for example $I_\gamma < 5\%$) is clearly denoted for each isotope. Also, if any γ rays are missing in the cascades, their absence is explained in the text.

In this chapter, we will discuss the structure of $^{89-94}$Zr. When needed, we will also consider spectra of their respective heavy binary partners ($^{209-204}$Pb). Observed transitions, their γ energies (E_γ), their intensities (I_γ) and energies of associated initial (E_i) and final (E_f) states are listed in Tabs. 6.2, 6.3, 6.4, 6.6, 6.1.5, 6.1.6, 6.17, 6.19, 6.20, 6.21 and 6.22. Level schemes of Zr and Pb isotopes (with adopted spins and parities of energy levels) built on observed transitions in our measurement are also shown (Figs. 6.8, 6.10, 6.13, 6.18, 6.23, 6.29, 6.45, 6.46, 6.47, 6.48 and 6.49). Some previously unknown γ rays have been observed and they will be discussed in more detail.

6.1.1 ^{89}Zr
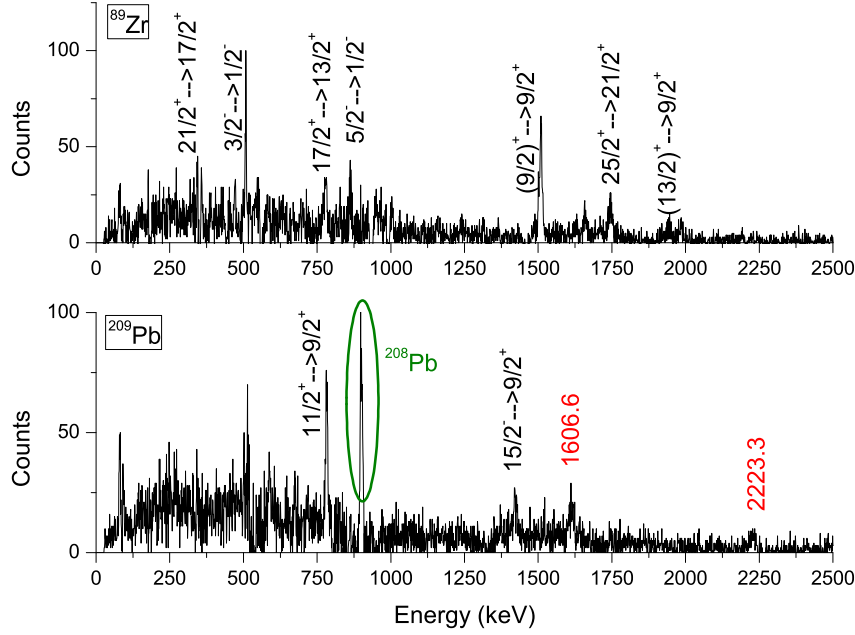
Figure 6.7: Doppler corrected γ ray spectrum for ^{89}Zr (top panel) and Doppler corrected spectrum for associated heavy binary partner, ^{209}Pb (bottom panel). Notice the peak in the ^{209}Pb spectrum which belongs to one-neutron evaporated channel, i.e. ^{208}Pb (marked green). The strongest transitions are labeled in the figure, with spins and parities of initial and final states, as listed in Ref. [www4]. Energies (in keV) of yet unknown γ rays (i.e. γ rays which could not be placed in the level scheme) are written in red.

The ^{89}Zr nucleus was weakly populated in our measurement, and in the fragment-γ coincidence spectra about ~ 43000 events were collected over the whole energy range (up to 4 MeV). In ^{89}Zr $(-1n)$, although a rather weak transfer channel, high excitation energies have been observed (see Figs. 6.7 and 6.8 and Table 6.2). Transition from $E_{\mathrm{ex}} = 587.8$ keV ($J^\pi = 1/2^-$), where E_{ex} denotes the energy of the excited state, to the ground state has not been observed (denoted by a dashed line in Fig. 6.8) due to the long half-life of $T_{1/2} = 4.161$ min, which is longer than the time needed for ions to pass the whole Prisma spectrometer, and consequently no coincidence between a fragment in the focal plane and prompt γ ray has been detected. Some other γ rays havent been observed due to their low intensity and

they are listed in Table 1 in the Appendix.

This nucleus has been studied in fusion-evaporation reactions (induced by ^{18}O,^{13}C and α), as well as in light-ion induced transfer reactions (using p, ^{3}He, d) (see Ref. [www4] and referneces therein).

The first three lowest states ($1/2^-$, $5/2^-$ and $3/2^-$) in the negative parity band could be explained in a classical shell model picture as one neutron hole in the $p_{1/2}$, $f_{5/2}$ or $p_{3/2}$ orbital. The calculation in Ref. [SSS92] shows that the wavefunctions of the negative-parity states ($1/2^-$, $5/2^-$ and $3/2^-$) have large components in which a neutron hole in the $p_{1/2}$ and $p_{3/2}$ orbitals is coupled to a proton state which is mainly composed of $g_{9/2}$ configuration.

In the positive parity band we observed a selective population of high spin states at high energies. The state $13/2^+$ ($E_{\mathrm{ex}} = 1943.7$ keV) can be obtained by a (stretched) coupling of a 2^+ quanta to the ground state spin ($9/2^+$), which we further discuss in Section 6.2.

Table 6.2: γ transitions observed in the present work for the ^{89}Zr isotope. The first column lists energies of γ rays (E_γ) in keV, the second and third columns show energies (E_i), spins and parities (J_i^π) of initial states, while energies (E_f), spins and parities (J^π) of final states are listed in the fourth and fifth columns. In the last column, transition intensities after taking into account the Clara efficiency, are listed (normalized to the strongest transition).

| E_γ (keV)	E_i (keV)	J_i^π	E_f (keV)	J_f^π (number)	I_γ (%)
271.2	2995.3	21/2+	2724.1	17/2+	3.47
507.4	1094.9	3/2-	587.8	1/2-	32.20
780.4	2274.1	17/2+	1943.7	13/2+	29.52
863.3	1451.2	5/2-	587.8	1/2-	22.13
1511.7	1511.8	(9/2)+	0.0	9/2+	100.00
1657.5		transferred from ^{89}Y			
1742.2	4735.4	25/2+	2995.3	21/2+	42.35
1943.7	1943.7	13/2+	0.0	9/2+	24.65
1984.1		transferred from ^{89}Y			
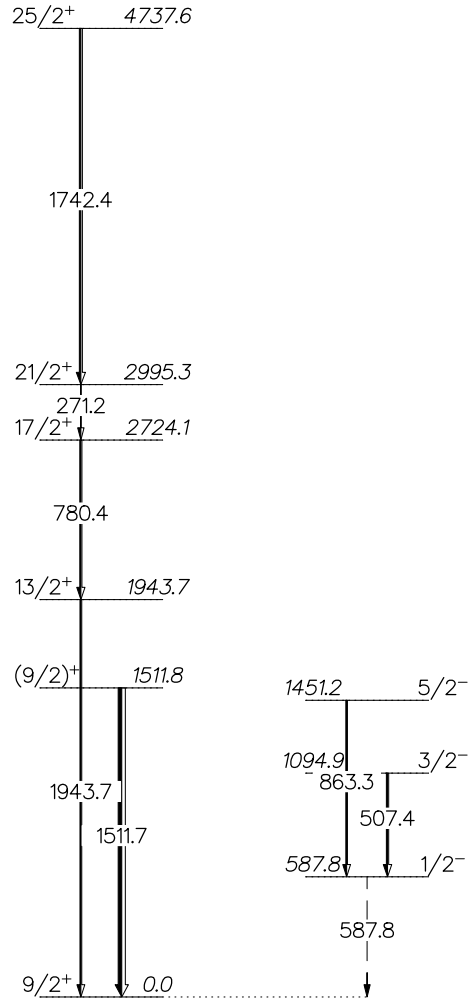
Figure 6.8: Experimental positive (left) and negative (right) parity states observed in our measurement for ^{89}Zr. Relative γ ray intensities are indicated by widths of arrows. Energies, spins and parities of levels, their branching ratios (all their tabulated γ intensities are $I_\gamma = 100\%$), and energies of transitions are as in Ref. [www4]. All energy levels up to $\sim$1500 keV have been observed, with the exception of $E_{\mathrm{ex}} = 587.7$ keV ($J^\pi = 1/2^-$), with a long lifetime as discussed in the text. Above $\sim$1500 keV, only high spin states have been selectively observed.

6.1.2 ^{90}Zr
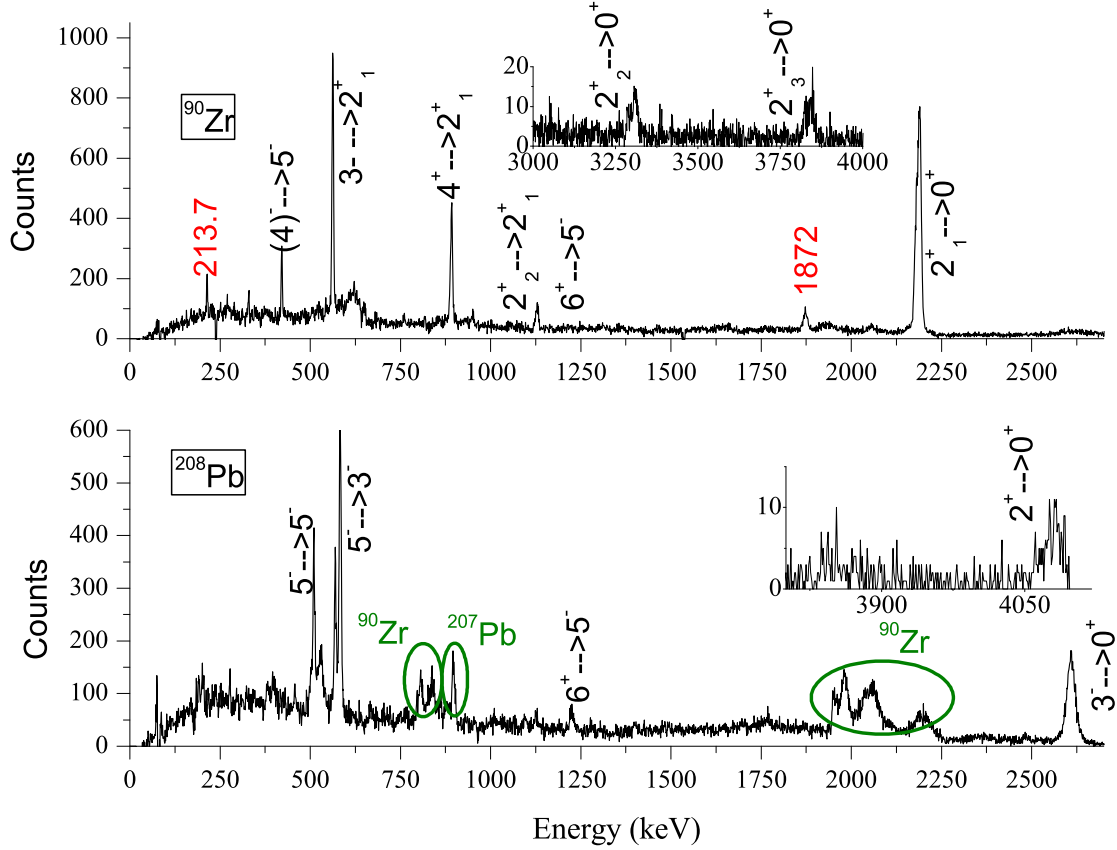
Figure 6.9: Doppler corrected γ spectra of ^{90}Zr (top panel) and associated heavy binary partner ^{208}Pb (bottom panel). Spins and parities (as in [www4]) of initial and final states of the strongest transitions are tagged. Energies (in keV) of yet unknown γ rays (i.e. γ rays which could not be placed in the level scheme) are written in red. Area around 800 keV and around 2000 keV in the spectrum of ^{208}Pb (denoted green) contain wrongly corrected γ rays from ^{90}Zr. $E_\gamma = 897.8$ keV (middle green area in the spectrum of ^{208}Pb) belongs to ^{207}Pb (one neutron evaporated channel).

Figure 6.9 shows that strongly excited in ^{90}Zr are 2_1^+ ($E_{ex} = 2186.3$ keV), 4_1^+ ($E_{ex} = 3076.9$ keV) and 3_1^- ($E_{ex} = 2747.9$ keV) states. We also observed the excitation of the second and third 2^+ states; 2_2^+ ($E_{ex} = 3308.8$ keV) and 2_3^+ ($E_{ex} = 3842.2$ keV). Figure 6.10 shows that

yrast states up to 10^+ have been observed. It is important to note that $E_\gamma = 141.2$ keV ($E_i = 3589.4$ keV, $J_i^\pi = 8^+ \longrightarrow E_f = 3448.2$ keV, $J_f^\pi = 6^+$) is not present in the spectrum in Fig. 6.9. The identification of this line, after cleaning of the spectrum, was not unique due to the subtraction of the γ ray with similar energy in the ^{90}Y spectrum, thus it is denoted by the dashed line in the level scheme.

Table 6.3: γ transitions observed in the present work for the ^{90}Zr isotope. The first column lists energies of γ rays (E_γ) in keV, the second and third columns show energies (E_i), spins and parities (J_i^π) of initial states, while energies (E_f), spins and parities (J_f^π) of final states are listed in the fourth and fifth columns. In the last column, transition intensities after taking into account the Clara efficiency, are listed (normalized to the strongest transition).

E_γ (keV)	E_i (keV)	J_i^π	E_f (keV)	J_f^π (number)	I_γ (%)
213.7(4)*					1.42
329.1	3076.9	4+	2747.9	3-	1.53
420.3	2739.3	(4)-	2319.0	5-	3.50
561.6	2747.9	3-	2186.3	2+	18.39
890.6	3076.9	4+	2186.3	2+	18.73
948.7		transferred from ^{90}Y			
1122.0	3308.8	2+	2186.3	2+	1.94
1129.2	3448.2	6+	2319.0	5-	2.63
1872(1)*					10.41
2054.6	5644.0	10+	3589.4	8+	0.46
2056.1	4375.1	7-	2319.0	5-	0.46
2186.2	2186.3	2+	0.0	0+	100.00
3309.1	3308.8	2+	0.0	0+	1.16
3844.9	3842.2	2+	0.0	0+	1.24

Besides the 3^- state, some higher spin negative parity states have also been excited, namely $(4)^-$ ($E_{\mathrm{ex}} = 2739.3$ keV), and 7^- ($E_{\mathrm{ex}} = 4375.1$ keV) states. The decay of the band-head ($J^\pi = 5^-$) of the negative parity band, $E_\gamma = 2319.0$ keV, ($E_i = 2319.0$ keV $I_i^\pi = 5^-$

$\longrightarrow 0^+_{\text{g.s.}}$) has not been observed because it decays through isomeric transition (lifetime of this state is 809.2 s). γ rays belonging to a weaker decay branch have not been observed (with tabulated γ intensities $I_\gamma < 5\%$). Those γ rays are listed in Table 1 in the Appendix.

Figure 6.11 shows the comparison of our results with the shell model calculations from [SNL09]. The shell model space and the effective two-nucleon interaction was described in the beginning of this chapter. We see rather good matching, except for the 0^+ state at $E_{\text{ex}} = 1.790$ MeV.

Two unknown γ rays have been observed; $E_\gamma = 213.7$ keV and 1872 keV (denoted by * in Table 6.3). $E_\gamma{=}213.9$ keV has been observed in the fusion evaporation studies, via the $^{76}\text{Ge}(^{18}\text{O}, 4n\gamma)^{90}\text{Zr}$ reaction, as a decay of a high-spin, high-excitation-energy state $(13)^+$ at 7437.8 keV. The highest spin and excitation energy state observed in our measurement for ^{90}Zr, for which we were able to follow the cascade towards the ground state is the 10^+ state at 5644.0 keV. The states between the $(13)^+$ at 7437.8 keV and 10^+ at 5644.0 keV, decay either via a complex patterns where the total flux spreads over several γ transitions or via high energy γ transitions, for which the CLARA array is not very efficient. Thus it is very plausible, that the 213.7 keV transitions belongs to this high-spin, high-excitation-energy state, $(13)^+$ at 7437.8 keV, even if the complete cascade towards ground state has not been observed.

$E_\gamma = 1872$ keV could be assigned to two possible transitions (based on the energy difference between known energy levels) $E_i = 4062(5)$ keV ($J^\pi = 4^+_2$) $\longrightarrow E_f = 2186.274(15)$ keV ($J^\pi = 2^+_1$) or $E_i = 4946(6)$ keV ($J^\pi = 4^+_6$) $\longrightarrow E_f = 3076.927(15)$ keV ($J^\pi = 4^+_1$), although we favour the first one, especially because we found a similar pattern in the ^{208}Pb decay scheme (see Figs. 6.48 and 6.53), where both, first and second 4^+ states have been excited.
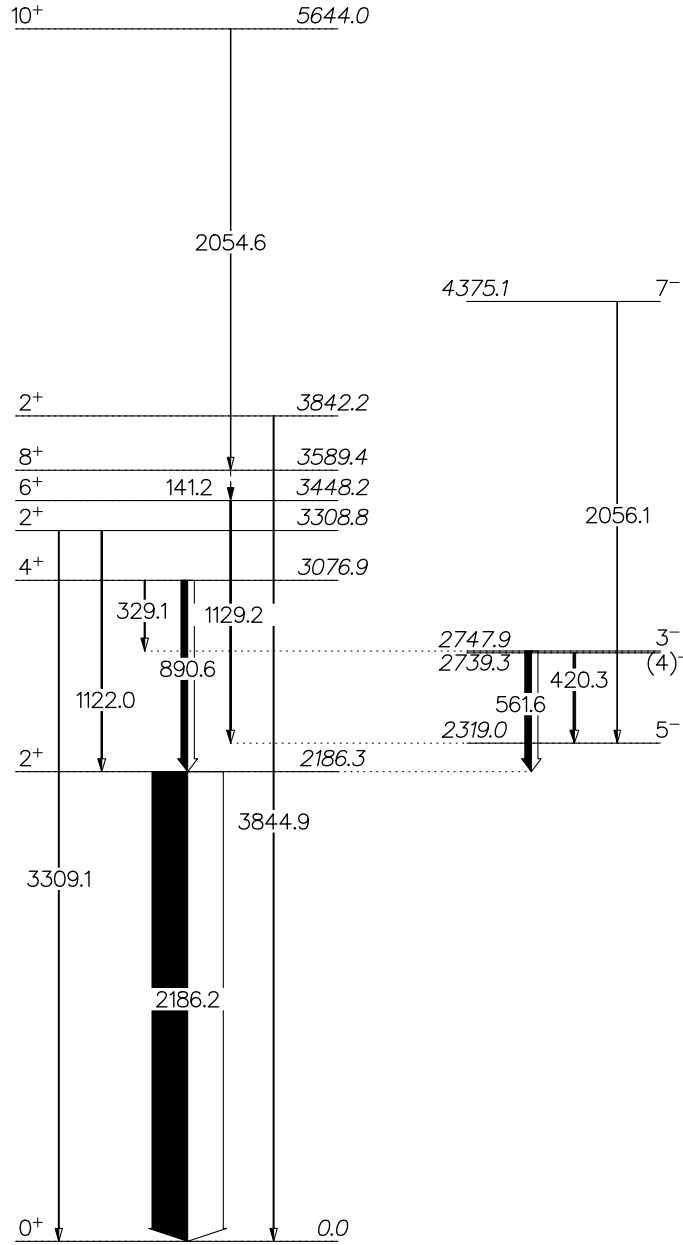
Figure 6.10: Experimental positive (left) and negative (right) parity states observed in our measurement for ^{90}Zr. Relative γ ray intensities are indicated by widths of arrows. Energies, spins and parities of levels, their branching ratios and energies of transitions are as in Ref. [www4]. All known states with energies up to the ∼ 3800 keV energy have been observed, with the exception of the first 0^+ state at 1760.7 keV. Weaker decay branches, with tabulated γ intensities $I_γ < 5\%$, have not been observed.
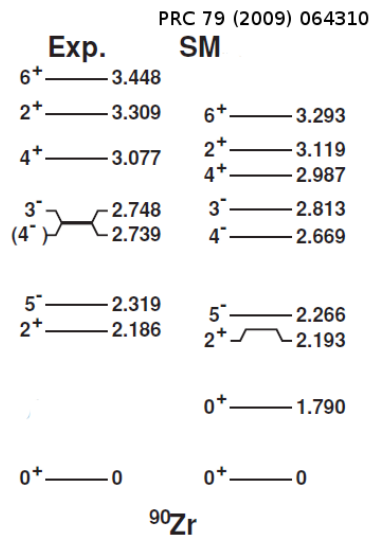
Figure 6.11: Experimental low-lying spectra of ^{90}Zr (observed in this work-left) compared with the SM calculations obtained in [SNL09] (right).

6.1.3 ^{91}Zr
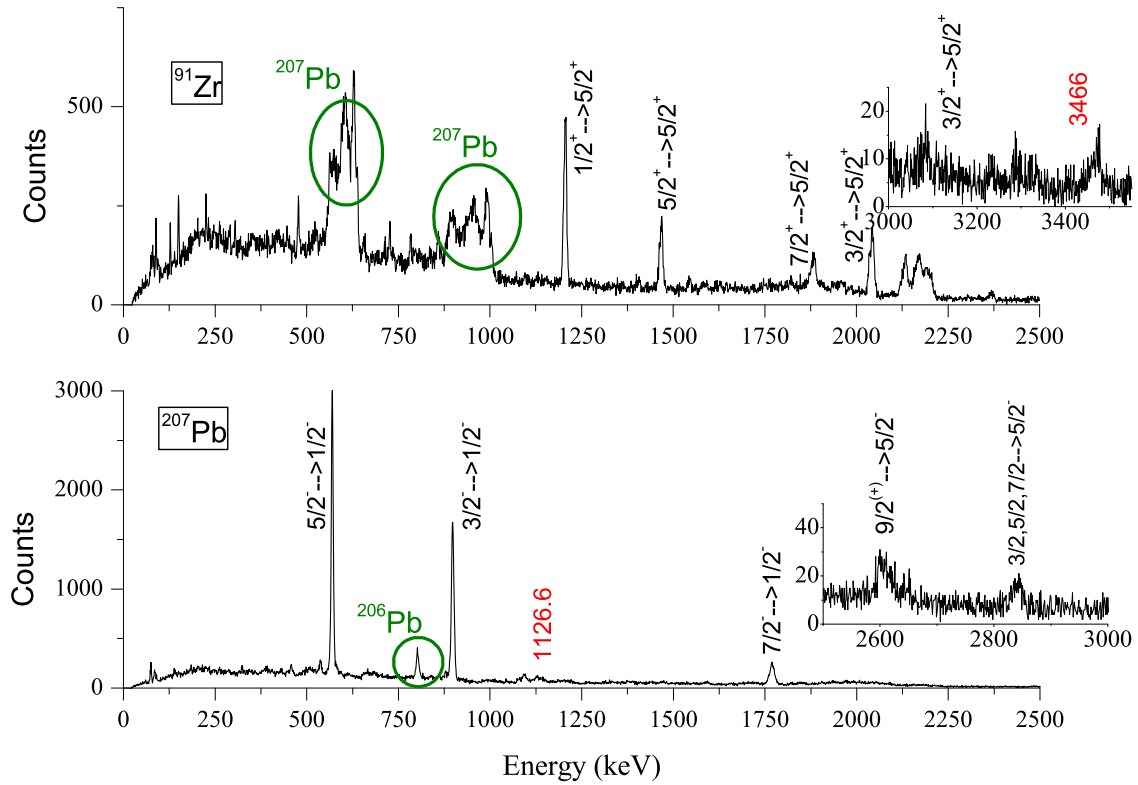
Figure 6.12: Doppler corrected γ spectra of ^{91}Zr (top panel) and associated heavy binary partner ^{207}Pb (bottom panel). Spins and parities (as in [www4]) of initial and final states of the strongest transitions are tagged. Energies (in keV) of unknown γ rays (i.e. γ rays which could not be placed in the level scheme) are written in red. Areas around 600 keV and 900 keV in the spectrum of ^{91}Zr (marked green) contain wrongly corrected γ rays from ^{207}Pb. $E_\gamma = 881$ keV in the spectrum of ^{207}Pb (marked green) belongs to ^{206}Pb, i.e. one neutron evaporated channel.

The top panel of Fig. 6.12 represents the γ spectrum of ^{91}Zr. Note that the green area around 580 keV corresponds to γ rays of ^{91}Zr (namely, $E_\gamma = 573$, 570, 596.9 keV, decaying from $E_i = 2857.1$ keV, $J_i^\pi = (13/2)^+$), which are superimposed on a complex background arriving from wrongly corrected γ rays of the ^{207}Pb, thus precise energies and intensities of

these γ lines are less certain.

Table 6.4: γ transitions observed in the present work of the ^{91}Zr isotope. The first column lists energies of γ rays (E_γ) in keV, the second and third columns show energies (E_i), spins and parities (J_i^π) of initial states, while energies (E_f), spins and parities (J_f^π) of final states are listed in the fourth and fifth columns. In the last column, transition intensities after taking into account the Clara efficiency, are listed (normalized to the strongest transition).

E_γ (keV)	E_i (keV)	J_i^π	E_f (keV)	J_f^π	I_γ (%)
89.6	2259.9	(13/2)-	2170.2	(11/2)-	3.99
126.7	5741		5613		2.77
151.1	2320.5	(11/2)-	2170.2	(11/2)-	5.39
224.8	2394.9	(9/2)-	2170.2	(11/2)-	6.23
443.8	2764.6	(13/2-, 15/2-)	2320.5	(11/2)-	3.41
477.2	2764.6	(13/2-, 15/2-)	2287.8	(15/2)-	9.67
725.7	2857.1	(13/2)+	2131.5	(9/2)+	14.71
782.7	2914.2	(9/2)+	2131.5	(9/2)+	13.14
859.0	3146.9	(17/2)+	2287.8	(15/2)-	21.58
1204.8	1204.8	1/2+	0.0	5/2+	100.00
1466.3	1466.4	5/2+	0.0	5/2+	58.17
1545	4712.1		3167.3		14.30
1882.2	1882.2	7/2+	0.0	5/2+	53.21
2042.3	2042.4	3/2+	0.0	5/2+	72.23
2131.5	2131.5	(9/2)+	0.0	5/2+	47.99
2170.0	2170.2	(11/2)-	0.0	5/2+	25.66
2366.5	2366.6		0.0	5/2+	6.84
3083.3	3083.3	3/2+	0.0	5/2+	4.76
3466(3)*					3.50

Again, some γ rays from plotted levels are not visible in the spectrum due to a weak branch of the decay (tabulated γ intensities $I_\gamma < 14\%$), and they are listed in Table 1 in

the Appendix. There are some other γ rays not seen in the spectrum, which are denoted by dashed lines in Fig. 6.90, and we will briefly discuss them here. $E_\gamma = 901$ keV decaying from $E_{\mathrm{ex}} = 5613.1$ keV could not be precisely extracted because it is placed in the area where wrongly Doppler corrected γ rays from ^{207}Pb contaminate the spectrum. Also, the level $E_{\mathrm{ex}} = 3167.3$ keV decays through isomeric transition so the two γ rays decaying from this level could not be observed.

Strongly excited states of ^{91}Zr are positive parity low spin states. Indeed, all known states up to $E_{\mathrm{ex}} = 2170.2$ keV ($J^\pi = (11/2)^-$) are excited. The first four ($1/2^+$, $5/2^+$, $7/2^+$ and $3/2^+$) could be seen as single-particle states exploring the $4\hbar\omega$ shell, as explained previously. Note that these are the strongest excited states, together with the $3/2^+$ state at $E_{\mathrm{ex}} = 2042.4$ keV.

It is important to note that although levels $E_{\mathrm{ex}} = 5741$ keV and $E_{\mathrm{ex}} = 4712.1$ keV do not have definite spin and parities according to [www4], [Tho08] reports that their spins are likely to be $27/2^-$ and $23/2^+$, respectively, based on polarization measurements and DCO (directional correlation of oriented states) on the experiment ^{13}C(^{82}Se, $xn\gamma$)$^{95-n}$Zr at 50 MeV with both, thick and thin targets.

To better explore the character of strongly populated states, we compared strengths obtained in our measurement with strengths obtained in light-ion induced transfer reactions, (d, p) [Sha13, BH70, BHK76]. This comparison is shown in Fig. 6.14. In light ion-induced reactions, a strong population of the states of single-particle character is expected. Since in both cases, light- and heavy-ion induced reaction, one neutron has been transferred, we felt it interesting to compare these two cases. The references [Sha13, BH70, BHK76] include ^{90}Zr(d, p)^{91}Zr reactions, with deuteron energy of $E_d = 15$ MeV (Fig. 6.14, panel (b)), $E_d = 33.3$ MeV (Fig. 6.14, panel (c)) and $E_d = 15.89$ MeV (Fig. 6.14, panel (d)). In the case of [Sha13] (Fig. 6.14, panel (b)), angular distribution was measured, while in [BH70] (Fig. 6.14, panel (c)) and [BHK76] (Fig. 6.14, panel (d)) spectroscopic factors were extracted. Here, we compared only levels which have been excited in our measurement ($J^\pi = 1/2^+, 5/2^+, 7/2^+, 3/2^+, (9/2)_1^+, (9/2)_2^+, (11/2)_1^-, (11/2)_2^-$). Besides these levels (drawn in Fig. 6.14), other energy levels have been also relatively strongly excited in the (d, p) reactions, namely second $7/2^+$ and $1/2^+$ states ($J^\pi = 1/2_2^+$ at $E_{\mathrm{ex}} = 2557.8$ and $J^\pi = 7/2_2^+$ at
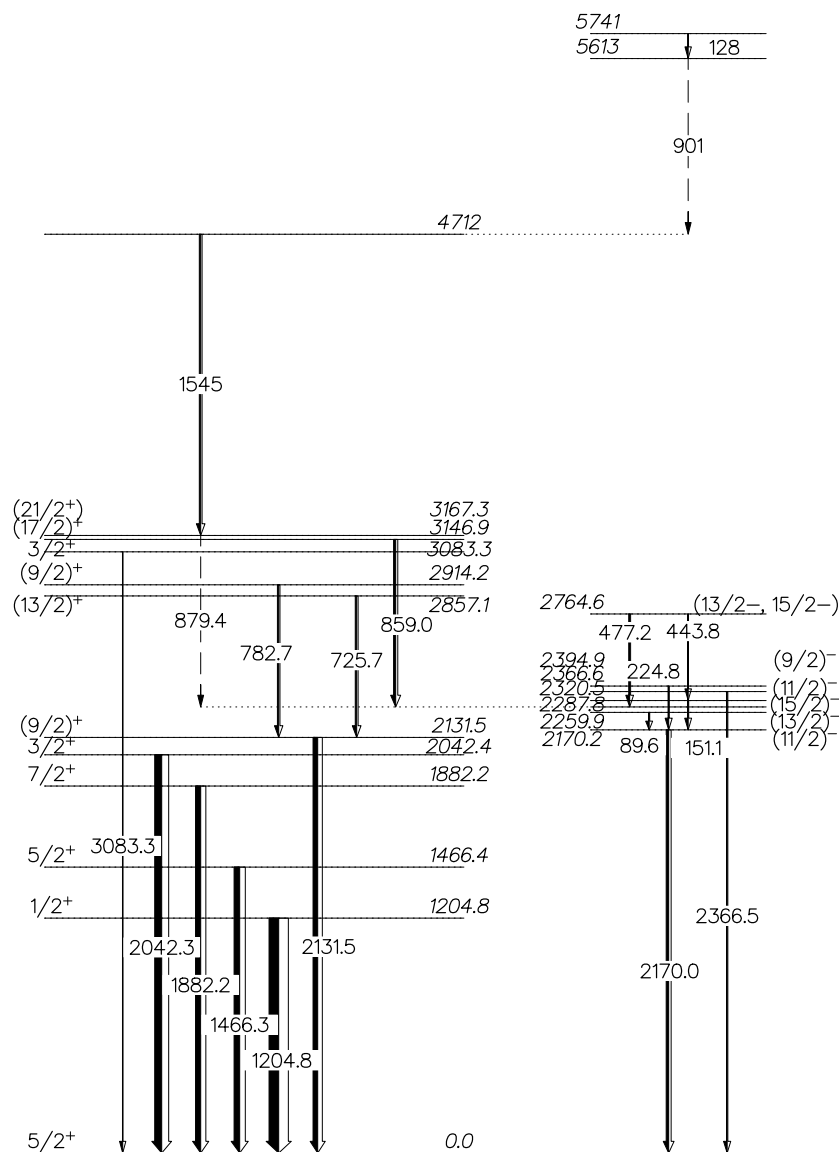
Figure 6.13: Experimental positive (left) and negative (right) parity states for ^{91}Zr. Relative γ ray intensities of the observed transitions are indicated by widths of arrows. Energies, spins and parities of levels, their branching ratios and energies of transitions are as in Ref. [www4]. All known states up to $E_{ex} \sim 2170$ keV have been observed. In the higher energy part of the scheme, only higher spin states have been observed. γ rays belonging to a weaker decay branch ($I_\gamma < 14\%$) or very low energy ($E_\gamma < 70$ keV) have not been observed.

$E_{ex} = 2200.5$ keV), whose excitations we did not observe.

Blue bars in Fig. 6.14 (a) signify reported intensities for different ^{91}Zr states obtained in
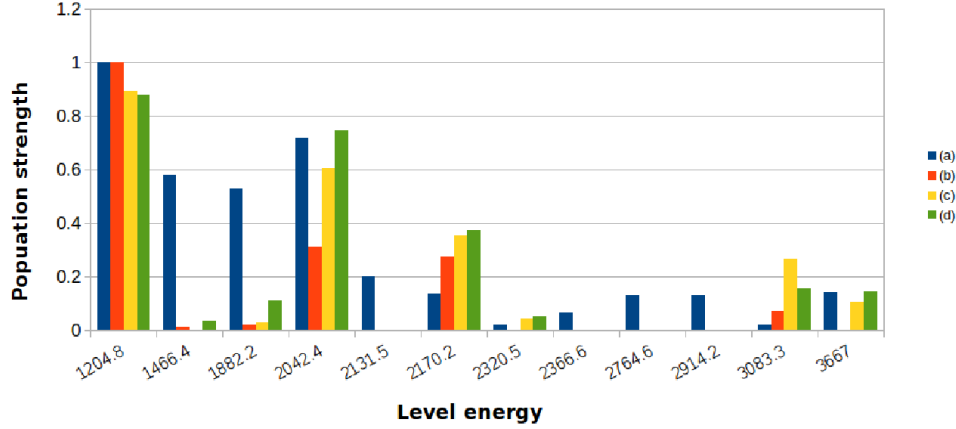
Figure 6.14: Population strengths of the observed levels of ^{91}Zr, normalized to the strongest transition for each case. Blue bars (data set labeled with (a)) contain current data; data from (b) contain cross sections of the observed sates from [Sha13], while (c) and (d) contain extracted spectroscopic factors for the same states from [BH70] and [BHK76], respectively. Data from (b), (c) and (d) are all obtained in ^{90}Zr$(d, p)^{91}$Zr reactions.

the present work in the following way: first, intensity of each transition was corrected for the efficiency of the γ array (as listed in the last column of Table 6.4 and depicted by arrow widths in Fig. 6.13). Then, to obtain population strengths of each energy level, intensities of all γ rays that feed each level were subtracted from the sum of intensities of γ rays decaying from the same level. Finally, these intensities were then normalized to the strongest transition, i.e. transition from $1/2^+ \longrightarrow 5/2^+$. Red bars in Fig. 6.14 (b) were obtained by normalizing cross sections taken from [Sha13] to the largest cross section (in this case, the largest cross section was for $E_{\text{ex}} = 1204.8$ keV), for each energy level. Yellow and green bars in the same figure (labels (c) and (d), respectively) were obtained by evaluating the spectroscopic factors reported in [BH70] and [BHK76]. In both cases, the strongest spectroscopic factor was for the ground state.

Figure 6.14 shows that in both, light- and heavy-ion induced one neutron transfer reactions, similar strengths have been observed for $J^\pi = 1/2^+$ ($E_{\text{ex}} = 1204.8$ keV) and $J^\pi = 3/2^+$ ($E_{\text{ex}} = 2042.4$ keV) states, indicating their strong single-particle character. At the same time, intensities of higher spin states, $5/2^+$, $7/2^+$ and $9/2^+$ are much stronger in our case than in

light ion reactions.

In contrast, our heavy ion induced reaction excited also many negative parity states (as seen in Fig. 6.13, and then again in Fig. 6.14), while in cited light ion reactions (Fig. 6.14 -red [Sha13], yellow [BH70] and green [BHK76]), the only negative parity state that was strongly populated was $E_{ex} = 2170.0$ keV ($J^\pi = (11/2)^-$).

Single particle energies of the lowest states of ^{91}Zr were reported in [Tho08], where they were obtained by taking differences in binding energies of nuclei which differ in mass by one nucleon. Fig. 6.15 shows those calculated single-particle energies (in MeV), where nuclei used in calculations were ^{88}Sr, ^{89}Sr, ^{87}Sr, ^{89}Y and ^{87}Rb.
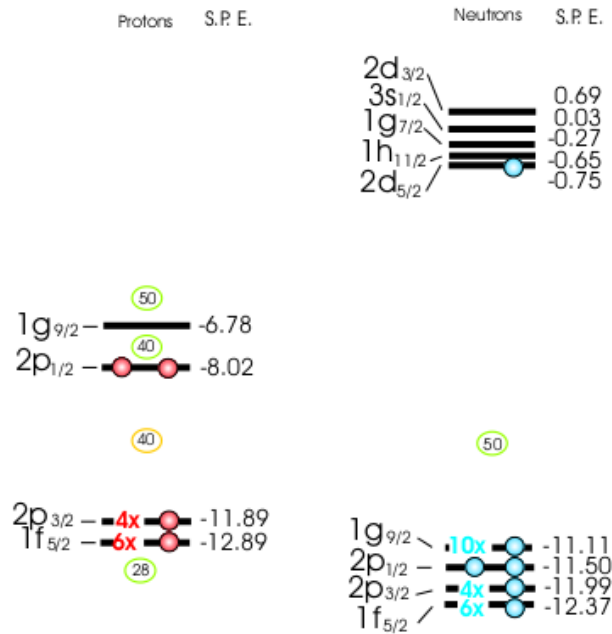
Figure 6.15: Proton and neutron single-particle energies (in MeV) of ^{91}Zr, taken from [Tho08]. Single particle energies were obtained by taking the differences in binding energies of nuclei which differ in mass by one nucleon (in this case, nuclei used in calculations were ^{88}Sr, ^{89}Sr, ^{87}Sr, ^{89}Y and ^{87}Rb).

Regarding single-particle states, it is worth mentioning results from [DBI11], where shell-model calculations for ^{91}Zr were reported. The calculations were carried out within the full model space ($1f_{5/2}$, $1p_{1/2}$, $2p_{3/2}$, $1g_{9/2}$) for protons and ($2d_{5/2}$, $3s_{1/2}$, $2d_{3/2}$, $1g_{7/2}$, $1h_{11/2}$) for

neutrons. The results of the calculation are shown in Table 6.5, which shows occupation numbers of single-particle levels of the ground state and the first excited states. Fig. 6.16, shows a comparison of the result of calculations from [SNL09] and experimental results from [www4]. Table 6.5 shows that the unpaired neutron occupies predominately a single shell (with occupation numbers > 0.88), which confirms a single-particle character of excited states $1/2^+$, $5/2^+$ and $7/2^+$.

Table 6.5: Occupation numbers of the single-particle levels of the ground state and the first excited states in ^{91}Zr, taken from [DBI11], where shell model calculations were carried out within the full model space ($1f_{5/2}$, $1p_{1/2}$, $2p_{3/2}$, $1g_{9/2}$) for protons and ($2d_{5/2}$, $3s_{1/2}$, $2d_{3/2}$, $1g_{7/2}$, $1h_{11/2}$) for neutrons.

	Protons				Neutrons				
J^π	$5/2^+_{\text{g.s.}}$	$1/2^+$	$5/2^+$	$7/2^+$	J^π	$5/2^+_{\text{g.s.}}$	$1/2^+$	$5/2^+$	$7/2^+$
$1f_{5/2}$	5.207	5.428	5.611	5.488	$2d_{5/2}$	0.989	0.015	0.988	0.885
$2p_{3/2}$	3.819	3.890	3.642	3.581	$1g_{7/2}$	0.001	0.001	0.004	0.106
$2p_{1/2}$	1.645	1.737	0.822	0.758	$2d_{3/2}$	0.002	0.003	0.003	0.004
$1g_{9/2}$	1.329	0.943	1.924	2.181	$3s_{1/2}$	0.003	0.976	0.002	0.001
					$1h_{11/2}$	0.004	0.005	0.001	0.001

In our measurement, we populated two $9/2^+$ states (E_{ex}=2131.5 and 2914.2 keV), which could be formed in different ways. Since we expect the reaction to excite states of a single-particle, as well as phonon-fermion coupling characters, we will discuss these two $9/2^+$ states in this view. The $9/2^+$ state may be a single-particle state (due to a hole in the $g_{9/2}$ orbital) or it could arise from a coupling of the ground $5/2^+$ state to a 2^+ vibration quanta. For the state $9/2^+_1$ with energy $E_{\text{ex}} = 2131.5$ keV, which is similar to the energy of the 2^+_1 state in ^{90}Zr, the particle-vibrational scheme has been assumed, as will be explained in Section 6.2. This leaves a possibility for the $9/2^+_2$ state ($E_{\text{ex}} = 2914.2$ keV) to be of single-particle character, although, since it has not been populated in measurements cited in Refs. [Sha13, BHK76], we cannot discuss it based solely on this measurement.

A similar situation occurs with two $(11/2)^-$ states ($E_{\text{ex}} = 2170.2$ and 2320.5 keV), where
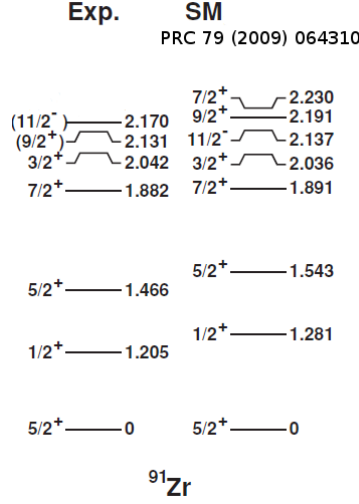
Figure 6.16: Experimental low-lying spectra of ^{91}Zr (observed in this work-left) compared with the SM calculations obtained in [SNL09] (right).

one of them could have a dominant single-particle character (due to one unpaired neutron in the $1h_{11/2}$ orbital), while the other one could arise from a dominant coupling of the ground state to the 3^- quanta in the stretched configuration. Although the state at $E_{\text{ex}} = 2170.2$ keV is strongly populated in (d,p) measurements (as seen in Fig. 6.14), shell model calculations from [SNL09] show that it is not a pure single-particle level $h_{11/2}$. At the same time, based solely on the comparison of the energies presented in Figure 6.37, we cannot deduce anything about the particle-vibration coupling. Both of these $11/2^-$ states will be further discussed in Section 6.2.1.

Beyond $E_{\text{ex}} \sim 2000$ keV, we have observed a selective population of higher spin states (both in positive and negative parity bands). The exception is $E_{\text{ex}} = 3083.3$ with $J^{\pi} = 3/2^+$, a rather low spin state, which decays directly to the ground state. The level $E_{\text{ex}} = 2366.6$ keV, with unknown spin and parity is drawn as a part of the negative parity band because of the higher level density in the negative parity band. However, it is also possible that it is a level of positive parity.

One unknown γ ray has been observed ($E_{\gamma} = 3466$ keV), denoted by * in Table 6.4, for which we propose (based on the energy difference between known energy levels) the transition from $E_i = 3469(5)$ keV ($J_i^{\pi} = 7/2^+$) to the ground state.

6.1.4 ^{92}Zr
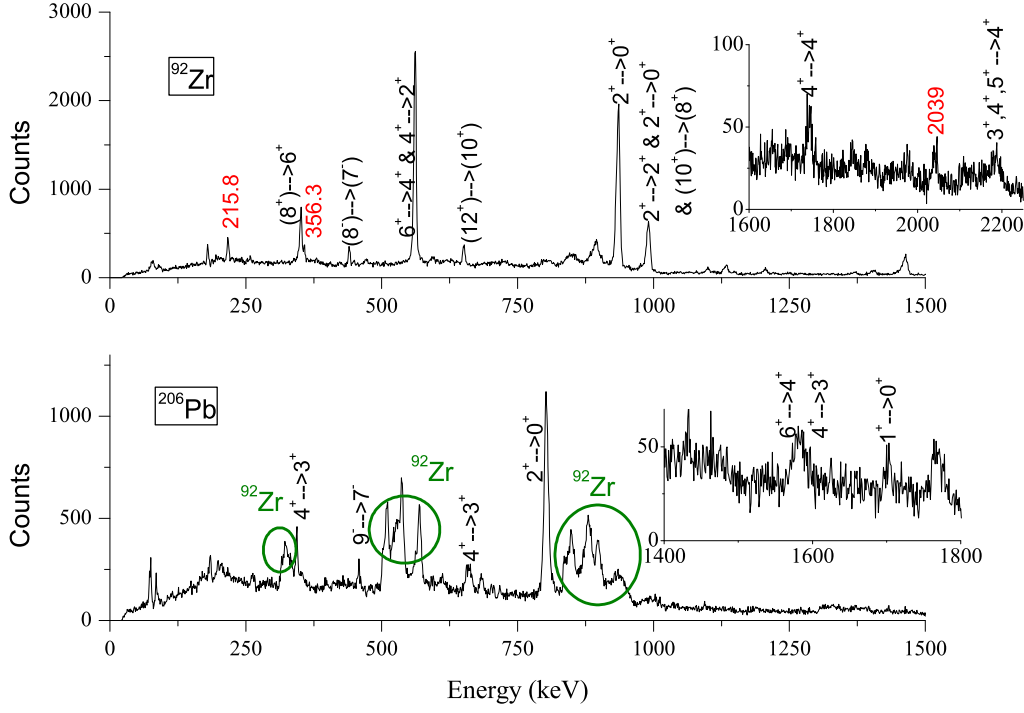
Figure 6.17: Doppler corrected γ spectra of ^{92}Zr (top panel) and associated heavy binary partner ^{206}Pb (bottom panel). Spins and parities (as in [www4]) of initial and final states of the strongest transitions are tagged. Energies (in keV) of yet unknown γ rays are written in red. Areas marked green in the spectrum of ^{206}Pb contain wrongly Doppler corrected γ rays from ^{92}Zr.

In the ^{92}Zr spectrum (Fig. 6.17), strong excitation of yrast states is visible (up to 16^+), with the emphasis on the lowest 2^+ ($E_{\mathrm{ex}} = 934.5$ keV), 4^+ ($E_{\mathrm{ex}} = 1495.5$ keV) and 6^+ ($E_{\mathrm{ex}} = 2957.4$ keV) states (Fig. 6.18). In addition, the excitation of negative parity band (with strong excitation of the 3^- ($E_{\mathrm{ex}} = 2339.7$ keV), 5^- ($E_{\mathrm{ex}} = 2486.0$ keV) and 7^- ($E_{\mathrm{ex}} = 3379.8$ keV)) states has been observed. Some weaker branches ($I_\gamma < 11\%$) have not been observed, in agreement with expected number of counts, as listed in Table 1 in the Appendix. $E_\gamma = 902.9$ keV ($E_i = 2398.4$ keV, $J_i = 4^+ \longrightarrow E_f = 1495.5$ keV, $J_f = 4^+$) with tabulated

intensity $I_\gamma = 100\%$ has not been observed because it could not be accommodated within the strong peak at 879.9 keV. New γ rays are denoted by * in Table 6.6.

Table 6.6: γ transitions observed in the present work of the ^{92}Zr isotope. The first column lists energies of γ rays (E_γ) in keV, the second and third columns show energies (E_i), spins and parities (J_i^π) of initial states, while energies (E_f), spins and parities (J_f^π) of final states are listed in the fourth and fifth columns. In the last column, transition intensities after taking into account the Clara efficiency, are listed (normalized to the strongest transition).

E_γ (keV)	E_i (keV)	J_i^π	E_f (keV)	J_f^π	I_γ (%)
178.6	3998.7	(9-)	3819.4	(8-)	3.29
215.8(4)*					4.95
351.3	3308.7	(8+)	2957.4	6+	14.28
356.3(5)*					4.56
439.6	3819.4	(8-)	3379.8	(7-)	3.71
471.3	2957.4	6+	2486.0	5-	3.31
559.6	2957.4	6+	2398.36	4+	11.68
560.9	1495.5	4+	934.5	2+	69.91
650.6	4947.2	(12+)	4296.6	(10+)	17.99
893.8	3379.8	7-	2486.0	5-	28.38
934.5	934.5	2+	0.0	0+	100.00
987.9	4296.6	(10+)	3308.7	(8+)	4.92
990.5	2486.0	5-	1495.5	4+	30.29
990.5	3057.4	2+	2066.7	2+	3.01
1098.3	6045.5	(14+)	4947.2	(12+)	5.20
1132.1	2066.7	2+	934.5	2+	8.95
1209.2	3275.8	2+,3+	2066.7	2+	6.84
1369.3	2864.7	4+	1495.5	4+	6.39
1400.3	7445.8	(16+)	6045.5	(14+)	0.41
1405.1	2339.7	3-	934.5	2+	8.19
1461.9	2957.4	6+	1495.5	4+	17.99

1463.8	2398.4	4+	934.5	2+	9.01
1741.8	3236.9	4+	1495.5	4+	7.34
2039(2)*					6.70
2180.3	3675.8	3+, 4+, 5+	1495.5	4+	13.31

Figure 6.19 (from [SNL09]) shows comparison of our results with the shell model calculations. The shell model space and the effective two-nucleon interaction was described in the beginning of this chapter. As with ^{91}Zr, we see fairly good agreement with the calculations.

Figure 6.20 shows a comparison of population strengths of the strongest excited states of current measurement with (t, p) measurements reported in [IMB75] (label (b) in Fig. 6.20) and [Fly74] (label (c) in Fig. 6.20). Tritium energies in the aforementioned ^{90}Zr$(t, p)^{92}$Zr reactions were $E_t = 20$ MeV and $E_t = 12$ MeV in [IMB75] and [Fly74], respectively.

Red bars in Fig. 6.20 represent population strengths extracted from the measured cross sections, and yellow bars in the same figure represent population strengths extracted from the yields (number of counts) for each excited level, normalized to the strongest state in each data set. Blue bars represent current data obtained in the same way as described in Section 6.1.3.

Moreover, except for the levels drawn in Fig. 6.20, additional levels have been strongly excited in the cited measurements ([IMB75] and [Fly74]) (namely $E_{ex} = 2904.1$ kev ($J^\pi = 0^+$) and $E_{ex} = 3992$ kev ($J^\pi = 0^+$) in (b); and $E_{ex} = 3057.4$ kev ($J^\pi = 2^+$) and $E_{ex} = 3471.9$ kev ($J^\pi = 1^+$) in (c)), but since we did not observe those levels, we do not have enough information for comparison.

Our results roughly follow those from Refs. [IMB75] and [Fly74] for low spin states, with the exception of 2_1^+ ($E_{ex} = 934.5$ keV) and 4_1^+ ($E_{ex} = 1495.5$ keV). It should be emphasized that for the excitation of the 6_1^+ state ($E_{ex} = 2957.4$ keV) we observed a much stronger population when compared with the (t, p) reaction. In addition, while no higher spin states were reported in Refs. [IMB75] and [Fly74], we have observed states up to 16^+.

The new γ lines that were identified: 215.8, 356.3, and 2039 keV, are to be considered.
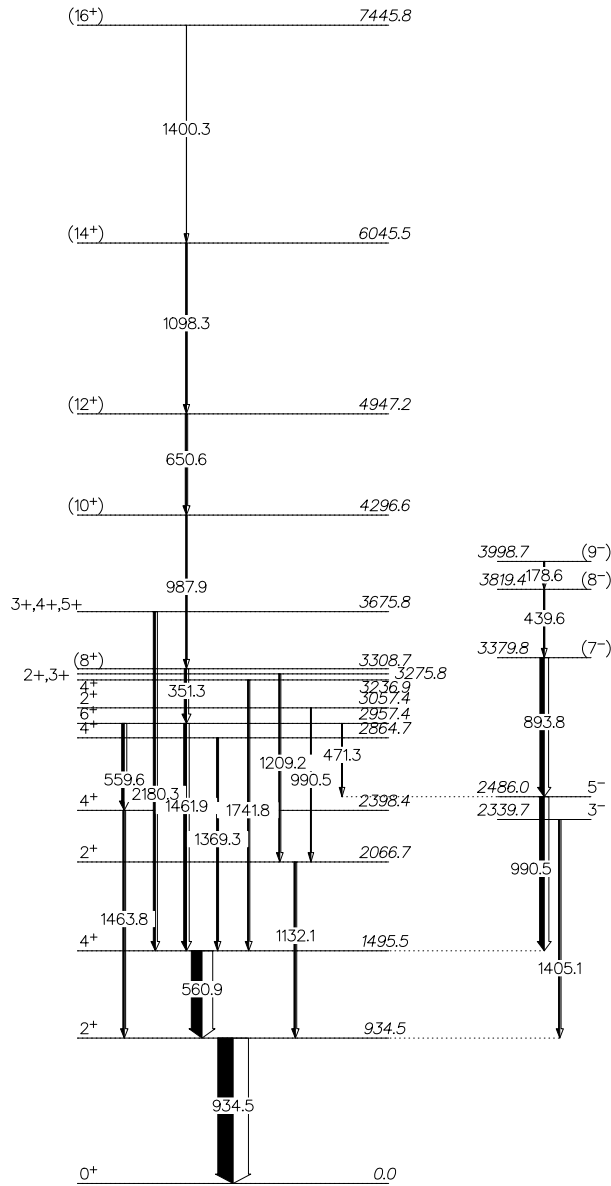
Figure 6.18: Experimental positive (left) and negative (right) parity states observed in our measurement for ^{92}Zr. Relative γ ray intensities are indicated by widths of arrows. Energies, spins and parities of levels, their branching ratios and energies of transitions are as in Ref. [www4]. Yrast states up to (16^+) in the positive parity band have been observed. γ rays from plotted levels with a decay branch with tabulated intensities lower than 40% have not been observed.

For additional indication about these γ lines we compared the γ spectra of the ^{92}Zr ($+2n$ channel) obtained in the ^{90}Zr+^{208}Pb reaction, with the spectra from the reaction^{40}Ca+^{96}Zr.
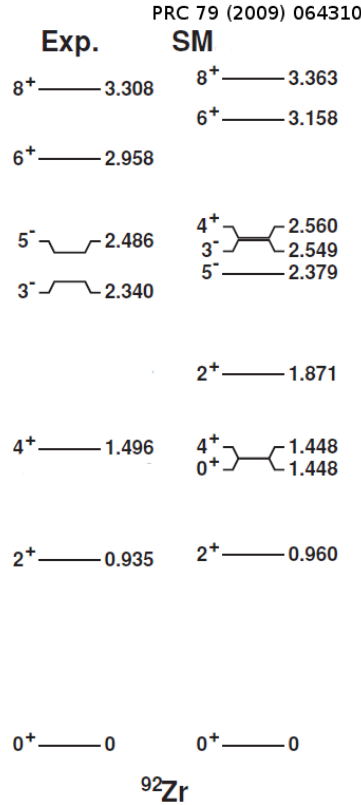
Figure 6.19: Experimental low-lying spectra of ^{92}Zr (observed in this work-left) compared with the SM calculations obtained in [SNL09] (right), for yrast states up to 8^+ and for the lowest observed negative parity states (3^- and 5^-).

The reaction ^{40}Ca+^{96}Zr was measured by accelerating a ^{40}Ca beam on ^{96}Zr target by the Tandem and ALPI booster of LNL at bombarding energies of 152 MeV [Szi07]. Projectile-like fragments (i.e. Ca-like) have been selected with the magnetic spectrometer Prisma placed at $\theta_{\rm lab} = 68°$, in the vicinity of the grazing angle. Thus, it is important to remember that spectra of Zr isotopes are the target-like spectra, where the velocity vector of these undetected heavy partners have been evaluated taking into account the binary character of the reaction, and measured velocity vector of the projectile-like fragment. Hence, in the corresponding γ spectra, γ rays belonging to the primary binary partner, as well as the ones of the nuclei produced after evaporation takes place, are present. The ^{92}Zr isotope has been reached via the removal of 4 neutrons from the ^{96}Zr target, thus, the two ^{92}Zr spectra arriving from two
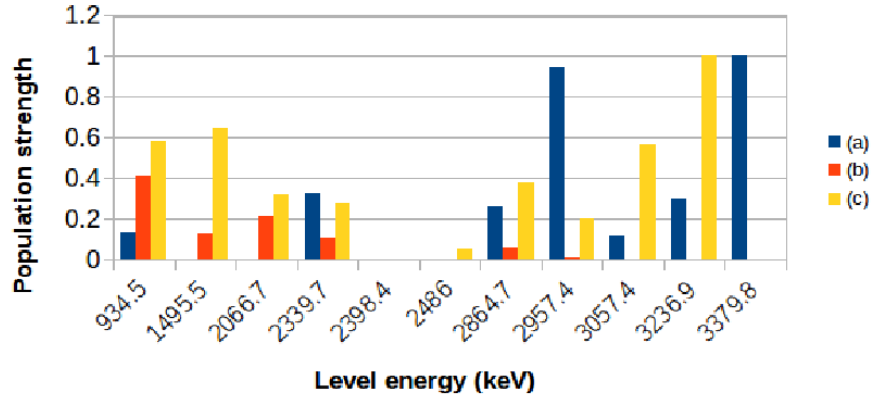
Figure 6.20: Population strengths of the observed levels of ^{92}Zr, normalized to the strongest transition for each case. Blue bars (data set labeled with (a)) contain current data; data from (b) are extracted from the measured cross sections of observed sates from [IMB75], while (c) contains number of counts for each level from [Fly74]. Data from (b) and (c) are obtained in ^{90}Zr$(t,p)^{92}$Zr reactions.

different reactions, have different statistics, and are not necessarily the same.

Comparison of these ^{92}Zr spectra for the expanded energy region around 2 MeV (see Fig. 6.21) clearly demonstrates that the 2180.3 keV transition is present in both of them, which is not so clear for the 2039 keV transition. The low-lying transitions (215.8, 356.3 keV) are not present in the ^{92}Zr spectrum from the ^{40}Ca+^{96}Zr reaction.

Later on, it will be shown that in cases of ^{93}Zr and ^{94}Zr, transitions from higher spin states appear much stronger in the ^{90}Zr+^{208}Pb system than in the ^{40}Ca+^{96}Zr, so the absence of the $E_\gamma = 215.8, 356.3$ in ^{92}Zr suggests they decay from some high spin state .
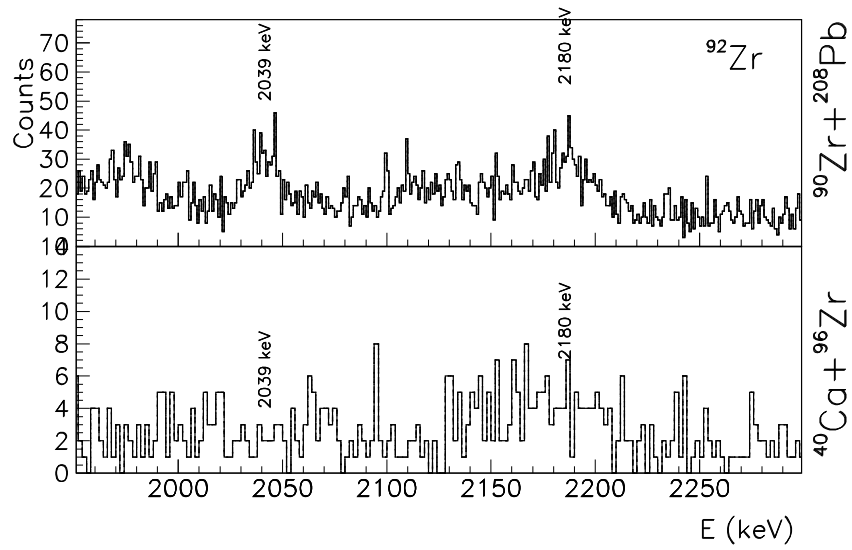
Figure 6.21: γ spectra of ^{92}Zr observed in our experiment (top panel) and in the experiment ^{40}Ca+^{96}Zr (bottom panel) [Szi07], for the energy region around 2 MeV.

6.1.5 ^{93}Zr
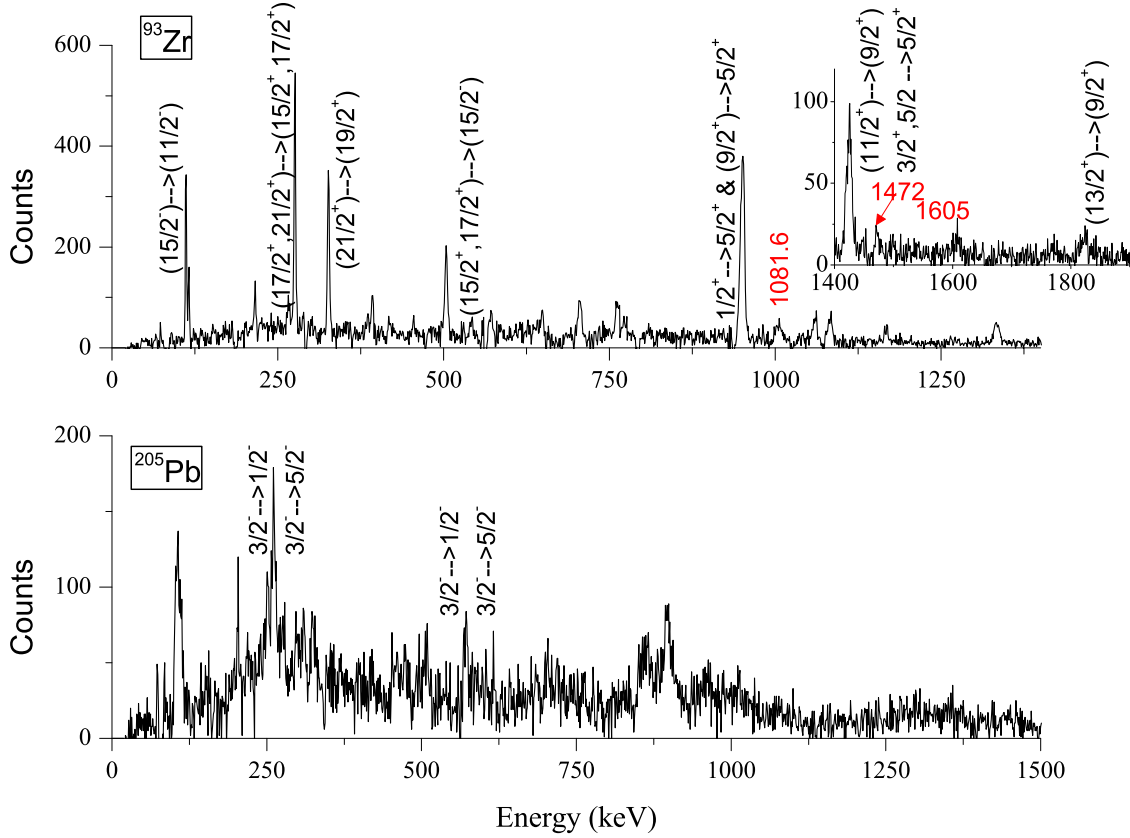
Figure 6.22: Doppler corrected γ spectra of ^{93}Zr (top panel) and associated heavy binary partner ^{205}Pb (bottom panel). Spins and parities (as in [www4]) of initial and final states of the strongest transitions are tagged. Energies (in keV) of yet unknown γ rays (i.e. γ rays which could not be placed in the level scheme) are written in red.

In the positive parity band of the ^{93}Zr, all known states up to $E_{\text{ex}} \sim 1425$ keV are present (see Fig. 6.23). In the higher energy part, yrast states up to $J^{\pi} = (25/2^{+})$ ($E_{\text{ex}} = 4716.3$ keV) have been rather selectively observed. In the low energy part of the spectrum, similar states as in ^{91}Zr have been observed, and populated with similar strength. Namely, we observed a strong population of $1/2^{+}$ and $3/2^{+}$ states, which can be understood as states with strong single-particle character. We also observed the excitation of $9/2_{1}^{+}$ ($E_{\text{ex}} = 949.8$

keV) state, which can be explained as coupling of the ground state to a 2^+ vibration quanta in the stretched configuration (more in Section 6.2). In the negative parity band, only two states with known decay schemes ($11/2^-$ and ($15/2^-$)) have been observed.

Table 6.7: γ transitions observed in the present work of the ^{93}Zr isotope. The first column lists energies of γ rays (E_γ) in keV, the second and third columns show energies (E_i), spins and parities (J_i^π) of initial states, while energies (E_f), spins and parities (J_f^π) of final states are listed in the fourth and fifth columns. In the last column, transition intensities after taking into account the Clara efficiency, are listed (normalized to the strongest transition).

E_γ (keV)	E_i (keV)	J_i^π	E_f (keV)	J_f^π	I_γ (%)
111.1	2485.7	(15/2-)	2374.6	(11/-)	14.11
115.1	2600.8		2485.7	(15/2-)	6.72
215.2	2989.6	(15/2+,17/2+)	2744.3	(13/2+)	16.78
265.8	266.8	3/2+	0.0	5/2+	10.93
275.2	3264.8	(17/2+,21/2+)	2989.6	(15/2+,17/2+)	34.74
326.0	3656.6	(21/2+)	3330.5	(19/2+)	29.68
391.9	3656.6	(21/2+)	3264.8	(17/2+,21/2+)	5.04
503.8	2989.6	(15/2+,17/2+)	2485.7	(15/2-)	34.74
705.5	2989.6	(15/2+,17/2+)	2284.3	(13/2+)	29.90
762.5	5478.8		4716.3	(25/2+)	32.45
946.9	947.1	1/2+	0.0	5/2+	100.00
949.8	949.8	(9/2+)	0.0	5/2+	47.22
1057.7	4716.3	(25/2+)	3656.6	(21/2+)	34.85
1081.6(7)*					35.70
1168.6	1168.6	1/2+	0.0	5/2+	10.32
1167.8	6646.6		5478.8		10.32
1334.6	2284.3	(13/2+)	949.8	(9/2+)	29.46
1425.2	1425.3	3/2+,5/2	0.0	5/2+	40.80
1424.7	2374.6	(11/2-)	949.8	(9/2+)	21.10
1472(1)*					23.40

1605(1)*					10.94
1824.4	2744.3	(13/2+)	949.8	(9/2+)	9.89

γ rays which have not been observed due to their weak decay branch ($I_\gamma < 32\%$) are listed in Table 1 in the Appendix. The $E_\gamma = 65.6$ keV has not been observed because of its low energy and it is denoted by a dashed line in Fig. 6.23.

Three unknown γ rays have been observed (denoted by * in Table 6.1.5). $E_\gamma =$1081.6, 1472 and 1605 keV, which could be attributed to transitions as stated in Table 6.8, are shown in Fig. 6.25 (based on the energy difference between known energy levels). γ ray with energy $E_\gamma = 1472$ keV could belong to the transition from $E_i = 1470.1$ keV ($J_i^\pi = (1/2^+, 3/2, 5/2^+)$) to the ground state ($J_f^\pi = 5/2^+$), but since we have not observed another γ ray from the same energy level which decays with stronger intensity, we propose it decays from $E_{\text{ex}} = 1463(5)$ keV ($J^\pi = 7/2^+, 9/2^+$), as listed in Table 6.8.

Looking at neighbouring odd Zr isotopes, ^{91}Zr and ^{95}Zr, where the $7/2^+$ state decays to the ground state, we suggest that $E_\gamma = 1605$ keV decays from $7/2^+, 9/2^+$ ($E_{\text{ex}} = 1598$ keV) in ^{93}Zr, where our preference is for $7/2^+$. The state $7/2^+, 9/2^+$ at 1598 keV was populated in the one neutron pick-up (^{92}Zr($\alpha,^3$He), ^{92}Zr(d,p)) and stripping (^{94}Zr(d,t)) reactions. The neutron pick-up reaction also (even with the large spectroscopic factor) populated the same spin-parity state at 1463(5) keV. The energy of our 1472 keV γ ray is close to the possible transition to the ground state, although outside of the quoted error. It should be noticed that the line 1463 keV is more intense than the 1605 keV line, in agreement with stronger excitation of the first $7/2^+, 9/2^+$ state. Taking into account the energy difference of adopted levels, the same transition, 1472 keV, may also be attributed to the decays of higher lying $7/2^+, 9/2^+$ states observed in the light-ion induced reaction (1735(?), or 2638(10) keV) but as a large multipolarity decays. Thus, our preference is the attribution to the lowest known $7/2^+, 9/2^+$ state.

In addition, we attributed $E_\gamma = 1081.6$ keV to the decay from the lowest negative parity state $E_{\text{ex}} = 2025$ keV ($J^\pi = 9/2^-, 11/2^-$), based on similarity with the level scheme of ^{91}Zr, where we observed high density of negative parity states with rather high spins.
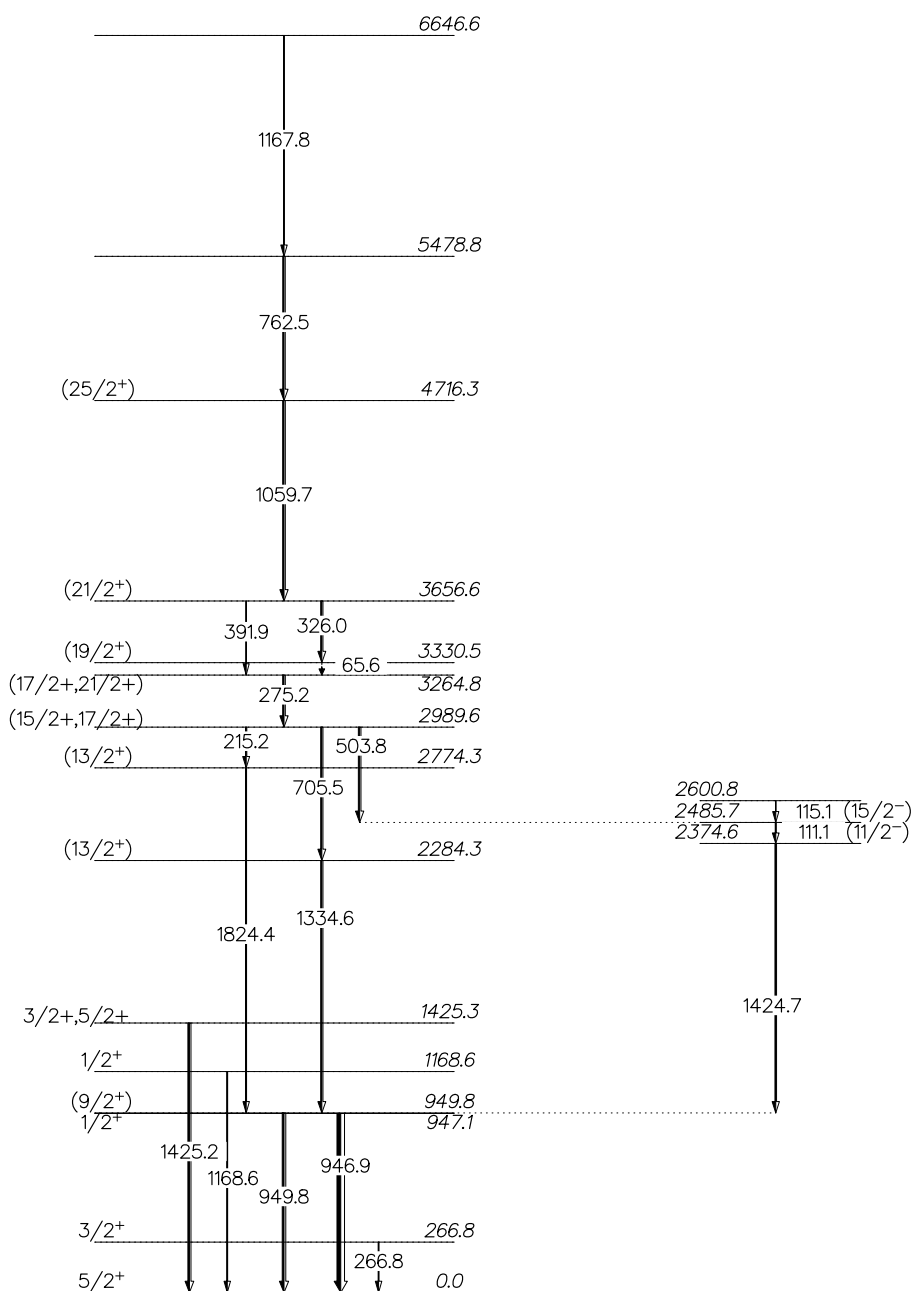
Figure 6.23: Experimental positive (left) and negative (right) parity states observed in our measurement for ^{93}Zr. Relative γ ray intensities are indicated by widths of arrows. Energies, spins and parities of levels, their branching ratios and energies of transitions are as in Ref. [www4]. All known states up to $E_{\rm ex} \sim 1400$ keV have been observed, while in the higher energy excitation region, higher spin states have been selectively observed. All decay branches up to the $I_\gamma > 32\%$ are plotted.

Since we noticed a resemblance between level schemes of ^{91}Zr and ^{93}Zr (i.e. excitation of single-particle states in the lower energy part and selective population of higher spin levels), we expect to see the decay of $11/2^-$ to the ground state in ^{93}Zr, as it was the case in ^{91}Zr. This is another reason why we suggested that $E_{\text{ex}} = 2025$ keV ($J^\pi = 9/2^-, 11/2^-$) decays through $E_{\text{ex}} = 949.8$ keV ($J^\pi = (9/2^+)$) and to the ground level.

Table 6.8: Possible new transitions for yet unknown γ rays of ^{93}Zr, based on the energy difference of known energy levels. The first column lists energies of γ rays (E_γ) in keV, the second and third columns show energies (E_i), spins and parities (J_i^π) of suggested initial states, while energies (E_f), spins and parities (J_f^π) of suggested final states are listed in the fourth and fifth columns. In the last column, transition intensities after taking into account the Clara efficiency, are listed (normalized to the strongest transition, as in Table 6.1.5)

E_γ (keV)	E_i (keV)	J_i^π	E_f (keV)	J_f^π	I_γ (%)
1081.6(7)	2025(10)	9/2-, 11/2-	947.09(8)	1/2+	35.70
1605(1)	1598(5)	7/2+, 9/2+	0.0	5/2+	10.94
1472(1)	1463(5)	7/2+, 9/2+	0.0	5/2+	23.40

Similar to ^{92}Zr, we would like to compare present results with ones obtained in the experiment ^{40}Ca+^{96}Zr [Szi07], explained in Section 6.1.4. Regarding the ^{93}Zr isotope, we choose to present the expanded region between 1 and 1.7 MeV, because of new transitions observed in our experiment, i.e. 1081.6, 1472 and 1605 keV. This energy region for the ^{93}Zr isotope populated in the ^{90}Zr+^{208}Pb (top) and ^{40}Ca+^{96}Zr (bottom) reactions is plotted in Fig. 6.24. According to this comparison, it is our conclusion that 1081.6, 1472 and 1605 keV transitions are present in both spectra, although with different relative intensities.

We will now look more closely at $J^\pi = 11/2^-$ and $J^\pi = 9/2^-, 11/2^-$ states at 2374.6 keV and 2025 keV, respectively. Beforehand, we drew attention to Fig. 6.26, which shows population strengths of $3/2^+$, $1/2^+$, $3/2^+$, $5/2^+$ and $11/2^-$ states. Heights of blue and red bars are obtained the same way as in the cases of ^{91}Zr and ^{92}Zr, where blue bars represent data from current measurement and red bars data from [BF73]. Spectroscopic factors have been measured in one neutron ^{92}Zr$(d,p)^{93}$Zr transfer reaction [BF73], with deuterons of energy
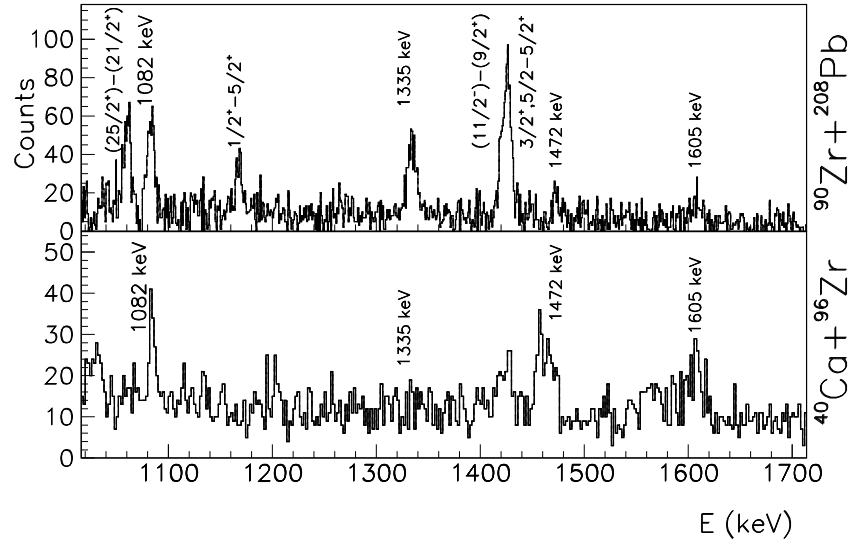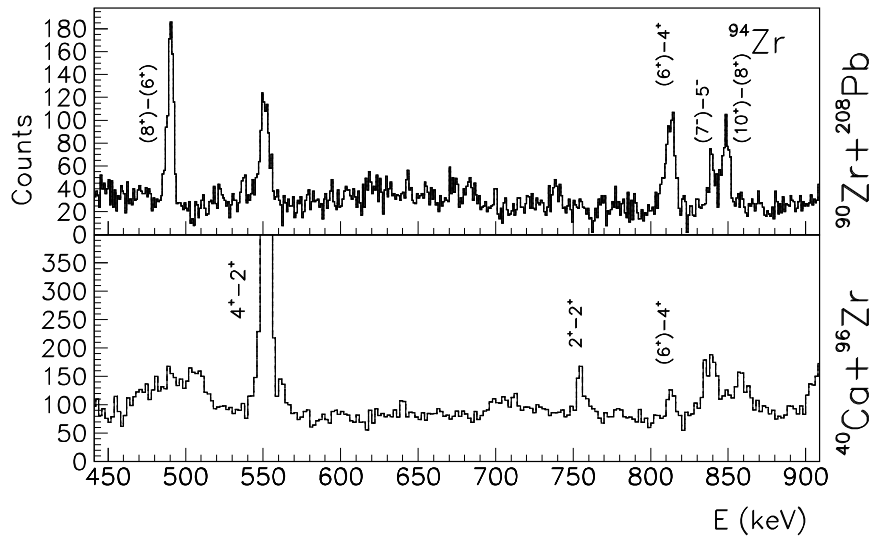
Figure 6.24: γ spectra of ^{93}Zr observed in our experiment (top panel) and in the experiment ^{40}Ca+^{96}Zr (bottom panel) [Szi07], for the energy region around 1500 keV.

$E_d = 15$ MeV. In this reaction ([BF73]), a strong population of $9/2^-,11/2^-$ state at 2025 keV has been observed. Since we suggested that γ ray $E_\gamma = 1081.6$ keV (as stated in Table 6.8 and depicted in Fig. 6.25) decays from the same level, it is interesting to compare population strengths of this state obtained from [BF73] to our measurement if we assume the aforesaid decay.
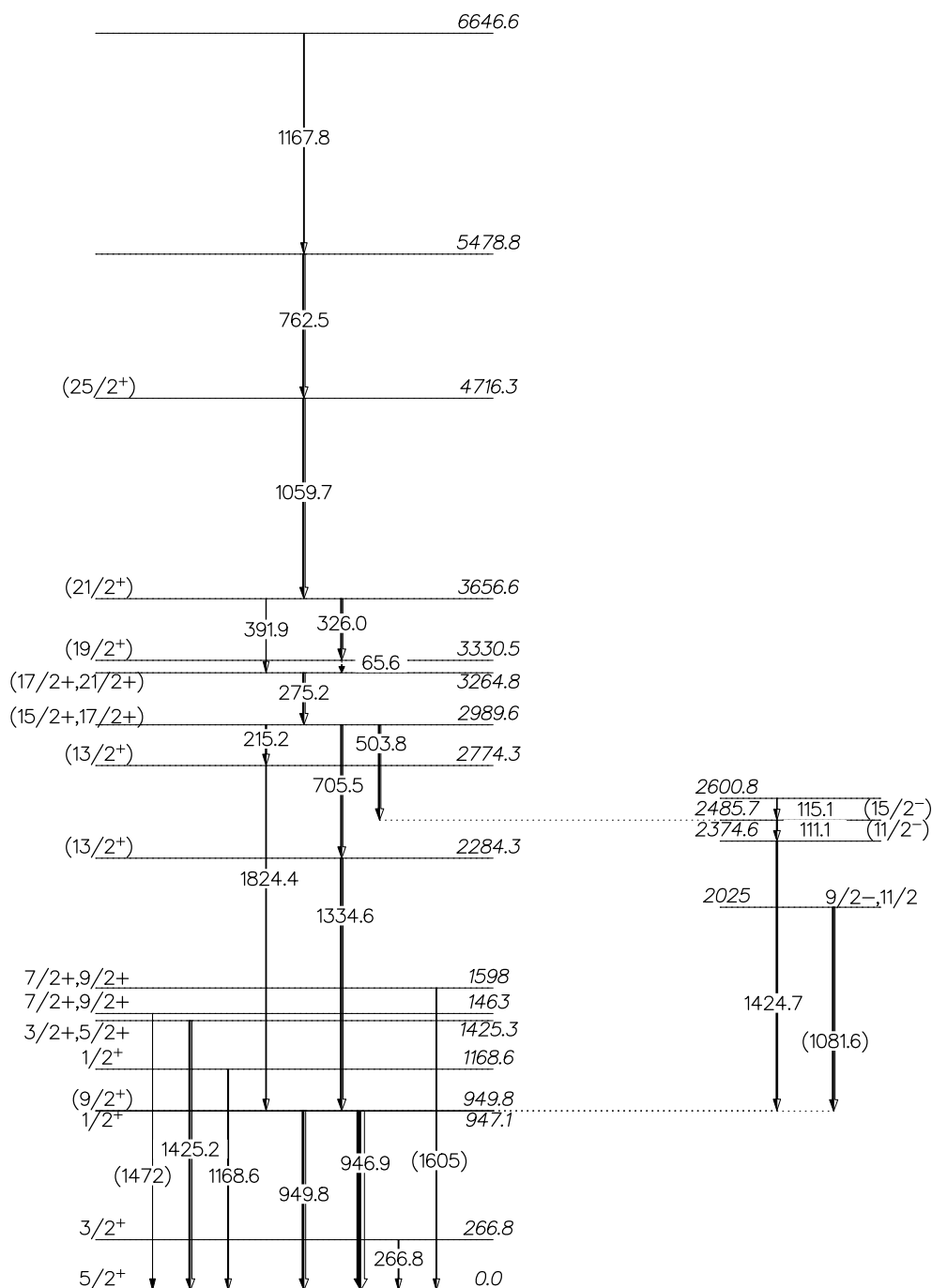
Figure 6.25: Experimental positive (left) and negative (right) parity states of ^{93}Zr, together with proposed new γ transitions ($E_\gamma = 1081.6, 1472, 1605$ keV) from $E_{\mathrm{ex}} = 2025$ keV ($J^\pi = 9/2^-, 11/2^-$), $E_{\mathrm{ex}} = 1463$ keV ($J^\pi = 7/2^+, 9/2^+$) and $E_{\mathrm{ex}} = 1598$ keV ($J^\pi = 7/2^+, 9/2^+$). Energies of the newly observed γ rays are written in parentheses. Relative γ ray intensities are indicated by widths of arrows. Energies, spins and parities of levels, their branching ratios and energies of transitions are as in Ref. [www4].
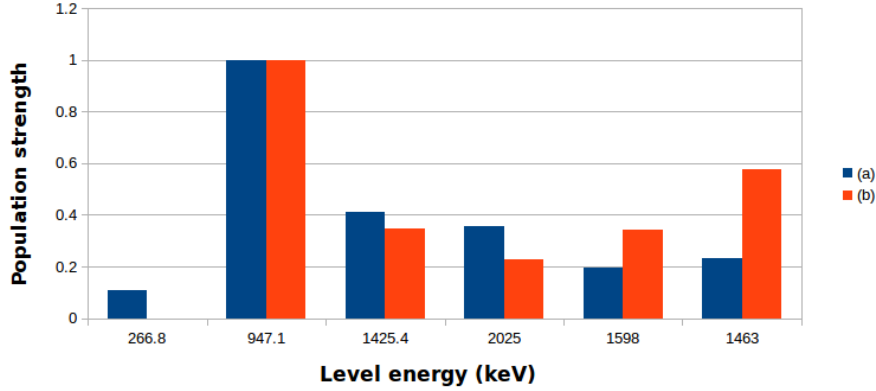
Figure 6.26: Population strengths of observed levels of ^{93}Zr, normalized to the strongest transition for each case. Blue bars (data set labeled with (a)) represent current data and data from (b) contain spectroscopic factors of observed sates from [BF73] obtained in the reaction ^{92}Zr$(d,p)^{93}$Zr. The decay of energy levels $E_{\mathrm{ex}} = 1463$, 1598 and 2025 keV are not known at the moment, but they are suggested levels for the decay of newly observed γ rays.

The $11/2^-$ state could arrive from the neutron in the $h_{11/2}$ orbital, or it can be due to the $5/2^+ \otimes 3^-$ coupling. As seen in Fig. 6.26, the level $E_{\mathrm{ex}} = 2025$ keV was strongly populated in the ^{92}Zr$(d,p)^{93}$Zr reaction, as well as in our measurement (again, if we assume that it decays through $E_\gamma = 1081.6$ keV), which suggests its single-particle character. The level at $E_{\mathrm{ex}} = 2374.6$ keV has energy close to the energy of the 3^- state in ^{92}Zr (see Fig. 6.37), thus we propose that its underlying structure is due to particle-vibartion coupling. In Section 6.2.1 we discuss these two states in more detail.

Besides the states shown in Fig. 6.26, $E_{\mathrm{ex}} = 2770$ ($J^\pi = (3/2)^+$) and $E_{\mathrm{ex}} = 2991$ ($J^\pi = 7/2^+, 9/2^+$) were strongly populated in the cited measurement ([BF73]). These states were measured using only particle identification (i.e. protons were recorded with emulsion placed in the focal plane of the broad-range spectrograph) with the resolution for the proton spectra of ~ 25 keV with unknown decay.

Figure 6.27 shows comparison of our results with shell model calculations from [SNL09].
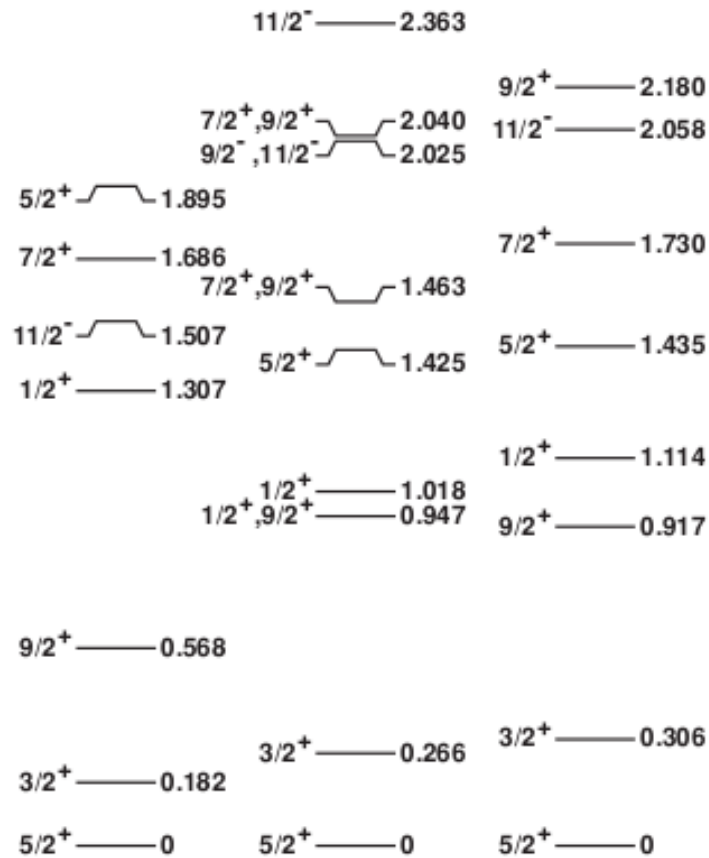
Figure 6.27: Experimental level scheme of the low-lying energy spectrum of ^{93}Zr taken from [www4] (middle), compared with the results from [SNL09] (right) and Nucl. Phys. A443, 39 (1985) (left)

6.1.6 ^{94}Zr
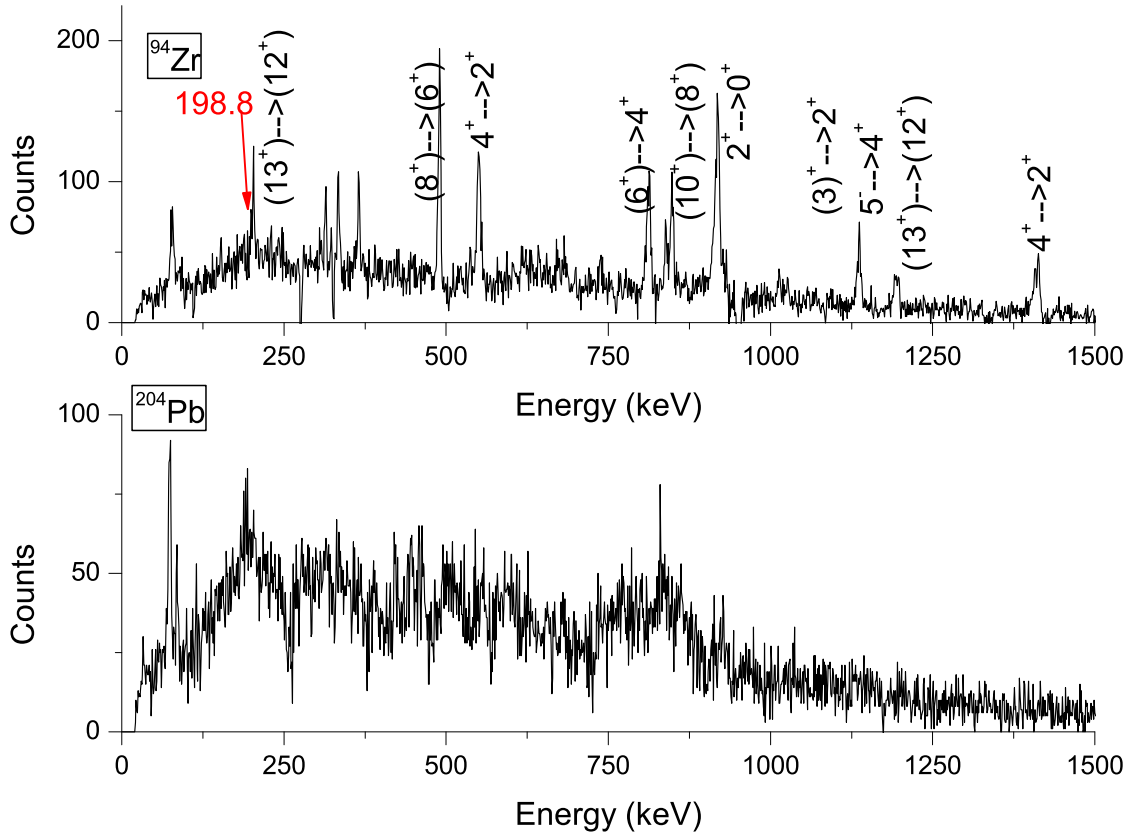
Figure 6.28: Doppler corrected γ spectra of ^{94}Zr (top panel) and associated heavy binary partner ^{204}Pb (bottom panel). Spins and parities (as in [www4]) of initial and final states of the strongest transitions are tagged. Energy (in keV) of yet unknown γ ray is written in red.

All observed transitions in the ^{94}Zr isotope can be accommodated within the yrast state cascade. We observed the excitation up to spin 14 in the positive parity band and up to spin 7 in the negative parity band, as seen in Fig. 6.29. One unknown γ transition has been observed in this isotope, $E_\gamma = 198.8$ keV, which is denoted by * in Table 6.1.6.

Table 6.9: γ transitions observed in the present work of the ^{94}Zr isotope. The first column lists energies of γ rays (E_γ) in keV, the second and third columns show energies (E_i), spins and parities (J_i^π) of initial states, while energies (E_f), spins and parities (J_f^π) of final states are listed in the fourth and fifth columns. In the last column, transition intensities after taking into account the Clara efficiency, are listed (normalized to the strongest transition).

E_γ (keV)	E_i (keV)	J_i^π	E_f (keV)	J_f^π	I_γ (%)
198.8(4)*					9.24
202.3	6006.8	(13+)	5804.5	(12+)	6.14
313.6	5804.5	(12+)	5490.9	(11+)	9.31
333.1	4812.4	(12+)	4479.3	(10+)	13.11
364.9	6371.7	(14)	6606.8	(13+)	11.84
489.2	3631.6	(8+)	3142.4	(6+)	36.88
550.9	1469.6	4+	914.8	2+	33.40
812.5	3142.4	(6+)	2329.9	4+	36.02
837.4	3442.5	(7-)	2605.0	5-	19.14
847.7	4479.3	(10+)	3631.6	(8+)	29.09
918.7	918.8	2+	0.0	0+	100.00
1011.6	5490.9	(11+)	4479.3	(10+)	13.69
1134.9	2605.0	5-	1469.6	4+	8.31
1138.9	2057.6	3-	918.8	2+	26.14
1194.4	6606.8	(13+)	4812.4	(12+)	29.11
1411.4	2329.9	4+	1411.4	2+	51.35
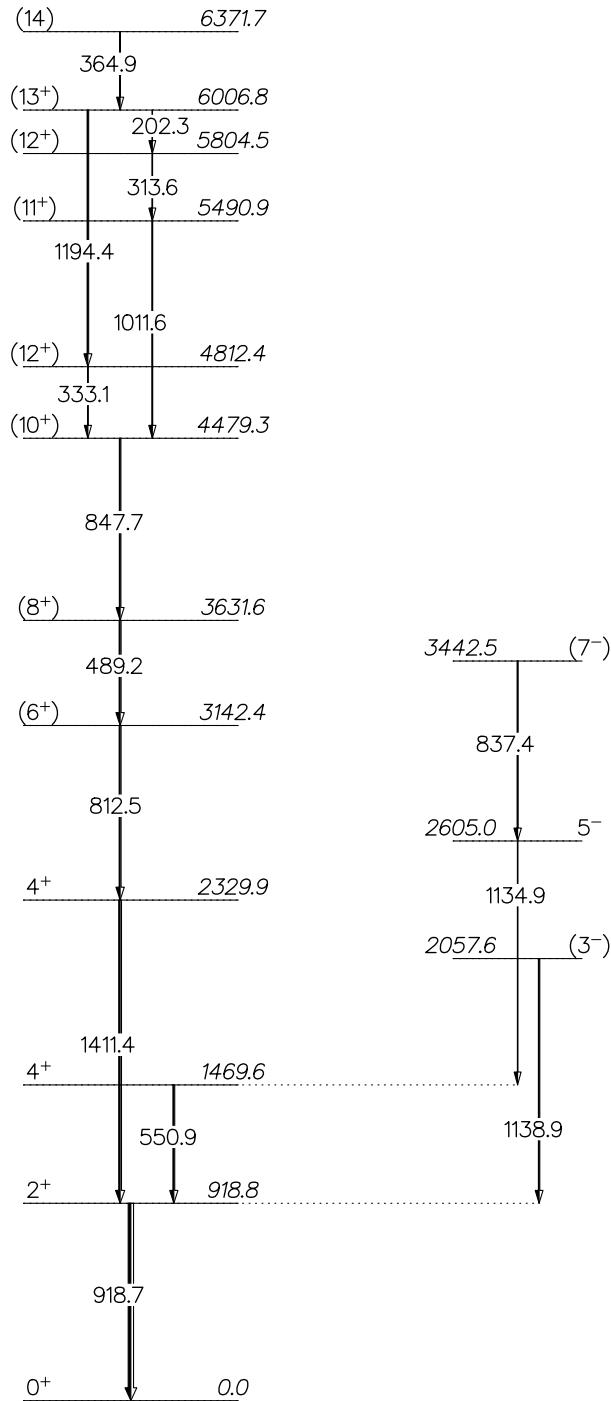
Figure 6.29: Experimental positive (left) and negative (right) parity states observed in our measurement for ^{94}Zr. Relative γ ray intensities are indicated by widths of arrows. Energies, spins and parities of levels, their branching ratios and energies of transitions are as in Ref. [www4]. Yrast states up to (14) in the positive and (7^-) in the negative parity band have been observed.

We again compare results from our measurement with those from the reaction ^{40}Ca+^{96}Zr [Szi07] (explained in Section 6.1.4). To have a clearer view on the population pattern of the states in these two transfer reactions, ^{90}Zr+^{208}Pb (top) and ^{40}Ca+^{96}Zr (bottom), we present the energy region between 500 and 1000 keV in the ^{94}Zr (see Fig. 6.30). This region has been selected for better illustration of different population of the high-spin states. This figure clearly shows that in the case of the heavier system, i.e. ^{90}Zr+^{208}Pb (top) transitions from higher spin states are much stronger (see for example $(8^+) \rightarrow (6^+)$ and $(10^+) \rightarrow (8^+)$ transitions), the situation which we already encountered in ^{92}Zr and ^{93}Zr.

Figure 6.30: γ spectra of ^{94}Zr observed in our experiment (top panel) and in the experiment ^{40}Ca+^{96}Zr (bottom panel), for the energy region around 700 keV.

6.2 General remarks about the Zr spectra
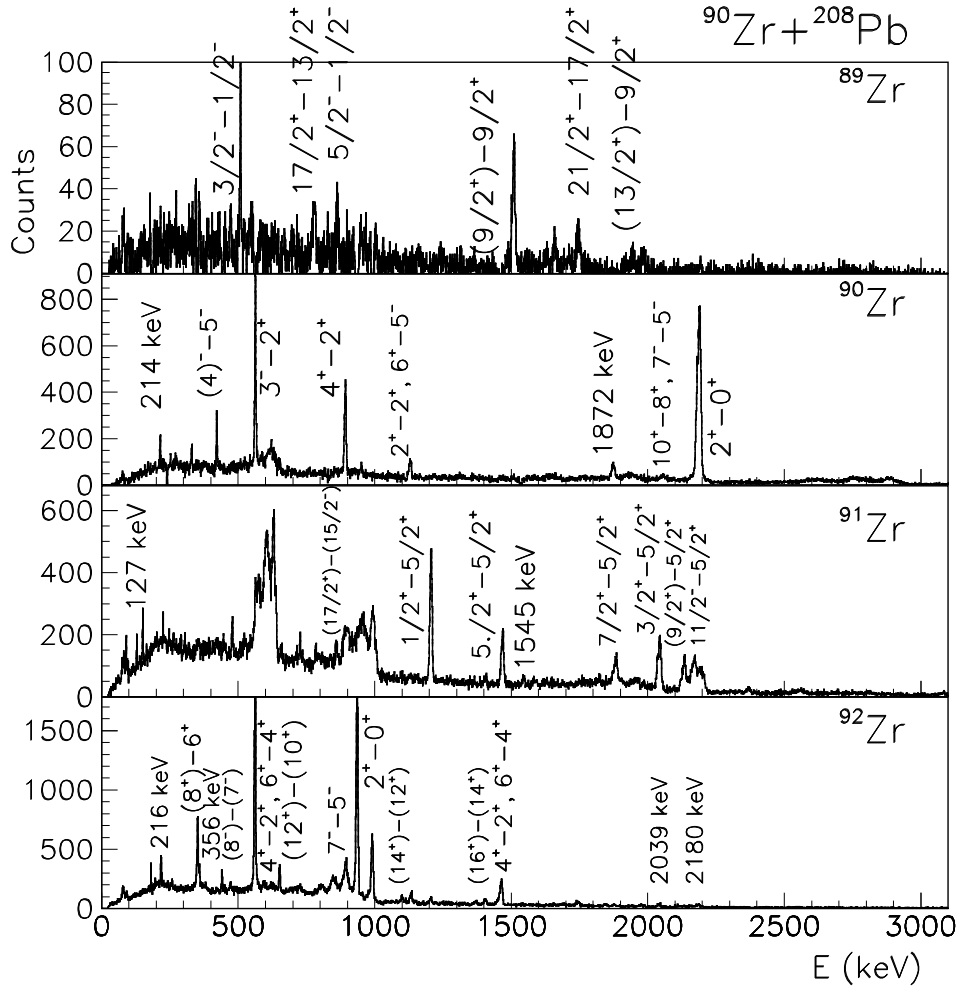
Figure 6.31: γ spectra of $^{89-92}$Zr isotopes observed in the experiment ^{90}Zr+^{208}Pb. Spins and parities (as in [www4]) of initial and final states of the strongest transitions are tagged.

In this section we will look more closely at the strongest populated states in the Zr isotopic chain. Figures 6.31 and 6.32 show the observed γ spectra of Zr isotopes in the ^{90}Zr+^{208}Pb reaction (for isotopes $^{89-94}$Zr) and in the ^{40}Ca+^{96}Zr reaction (for ^{95,96}Zr), taken from [Szi07]. Figures 6.33 and 6.35 show a comparison between populated energy states of even and odd Zr isotopes, respectively. In even Zr isotopes (Fig. 6.33), excitation energies up to ~ 8 MeV have been observed, with the emphasis on yrast states in positive parity bands. Negative
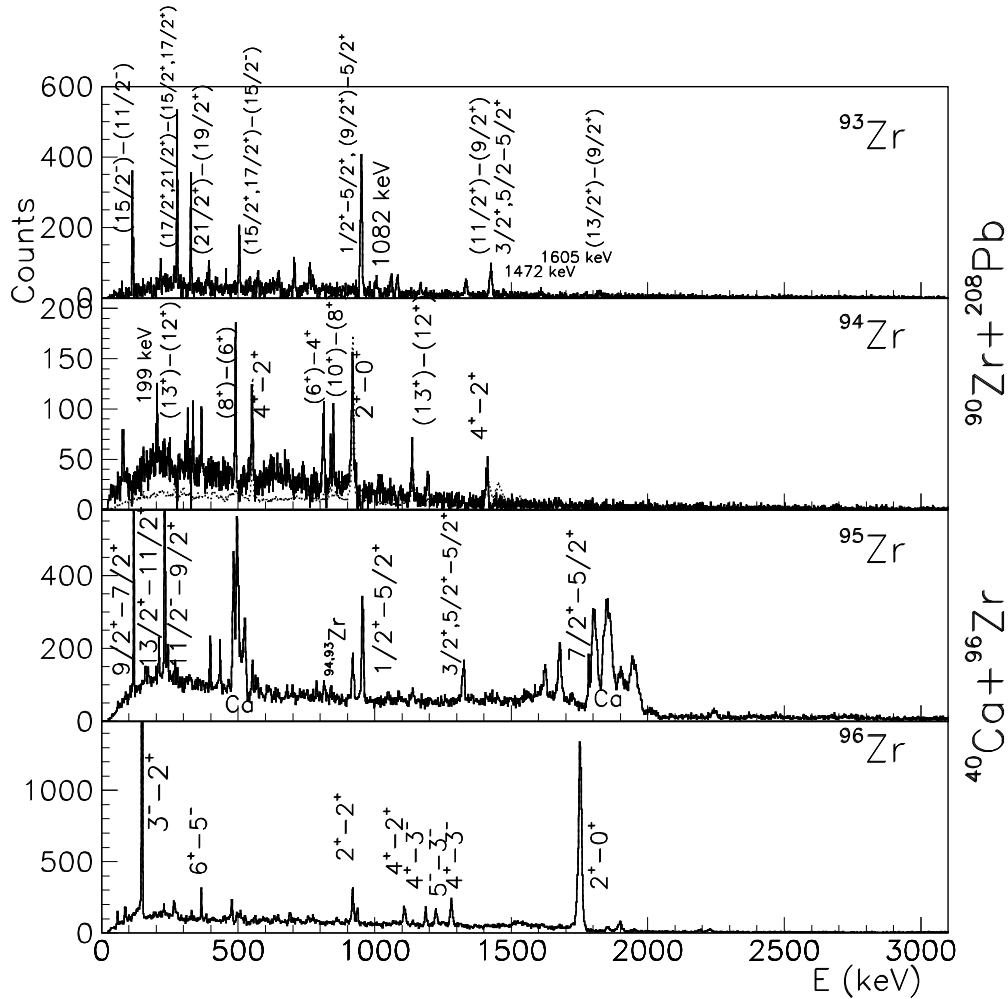
Figure 6.32: γ spectra of ^{93,94}Zr isotopes observed in the experiment ^{90}Zr+^{208}Pb and γ spectra of ^{95,96}Zr isotopes observed in the experiment ^{40}Ca+^{96}Zr (from [Szi07]). Spins and parities (as in [www4]) of initial and final states of the strongest transitions are tagged.

parity states have also been excited, with strong excitation of 3^-, 5^- and 7^- states. In schemes of even Zr isotopes, besides yrast states, only a higher order of 2^+ and 4^+ states have been observed, although with lower intensities. Also, it is worth noticing that for even Zr isotopes we did not observe excitation of exited 0^+ states, as will be discussed in Section 6.2.2.

In the level scheme of ^{89}Zr, a rather weak transfer channel, high spin states have been observed in the positive parity band, and only the lowest three negative parity states, which, as
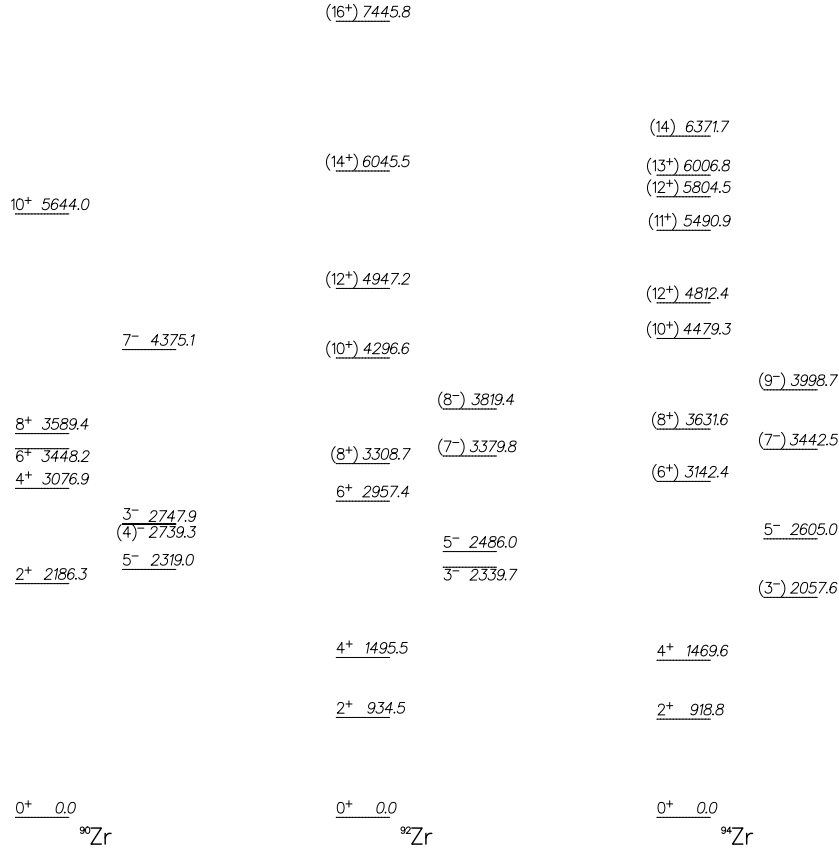
Figure 6.33: Simplified level schemes (only strongly excited states are plotted) of ^{90}Zr (left), ^{92}Zr (middle) and ^{94}Zr (right) isotopes. For each isotope positive (left) and negative (right) parity states are plotted separately.

already stated in Section 6.1.1, most probably are of single-particle character. The strongest populated positive parity states in ^{91}Zr and ^{93}Zr isotopes are yrast states. Low energy spectra of odd Zr isotopes is characterized by population of states of single-particle character. In the classical shell model picture (see Fig. 6.3), expected single-particle states of ^{89}Zr caused by a neutron hole in the $3\hbar\omega$ shell would provide spins $J^\pi = 9/2^+, 1/2^-, 5/2^-, 3/2^-$ and $7/2^-$, which all except $7/2^-$ have been observed in our measurement. In the case of ^{91,93}Zr, one unpaired neutron in the $4\hbar\omega$ shell (more precisely, $g_{7/2}$, $d_{3/2}$, $s_{1/2}$ or $h_{11/2}$ orbitals) provides single-particle states with spins $J^\pi = 9/2^+, 7/2^+, 3/2^+, 1/2^+$ and $11/2^-$.

Ground states of analysed odd Zr isotopes follow the classical shell model, i.e. after closing $3\hbar\omega$ shell, neutrons fill the $2d_{5/2}$ orbital, which results in ^{91,93,95}Zr having a ground state spin $5/2^+$. ^{97,99}Zr have ground state spin $1/2^+$, filling the $3s_{1/2}$ orbital. Nevertheless, the first

97

few low energy states can be seen as states of single-particle character. We thus expect to observe $7/2^+$, $1/2^+$, $3/2^+$ and $11/2^-$ states, as stated in Section 6.1. Figure 6.34 shows a comparison in energy of these states (i.e. first $7/2_1^+$, $1/2_1^+$ and $3/2_1^+$) for ^{91,93,95,97}Zr. Except for $3/2^+$ states, other states have similar energies for different Zr isotopes. This suggests that order and energies of $1g_{7/2}$ and $3s_{1/2}$ orbitals do not change drastically in this region where Zr isotopes are filling $d_{5/2}$ shell. The behaviour of the $3/2^+$ states suggests their mixed configuration, rather than pure single-particle character.

The behaviour of single-particle energies of $p_{1/2}$, $p_{3/2}$, $f_{5/2}$ and $g_{9/2}$ orbitals is shown in Fig. 6.3 and, except the $3/2^+$ state in ^{93}Zr, other data from Fig. 6.34 roughly follow those from Fig. 6.3. For Zr isotopes with $A > 97$, ground state spins are $(1/2^+)$, $(3/2^+)$ and $(5/2^-)$ for ^{99}Zr, ^{101}Zr and ^{103}Zr, respectively. Expected single-particle states are again $5/2^+$, $1/2^+$, $11/2^-$, $1/2^+$ and $3/2^+$, due to an unpaired neutron in the $4\hbar\omega$ shell. Ref. [SNL09] reports about $9/2^+$ isomer states in ^{99}Zr and ^{101}Zr , interpreted as one neutron hole excitations. Shell model calculation from the same reference shows one-quasiparticle character of the ground state $1/2^+$, as well as of excited states $3/2^+$, $7/2^+$ and $11/2^-$ in ^{97}Zr, built on the closed ^{96}Zr core and also predicts the $5/2^+$ as one-hole state in the ^{98}Zr core.
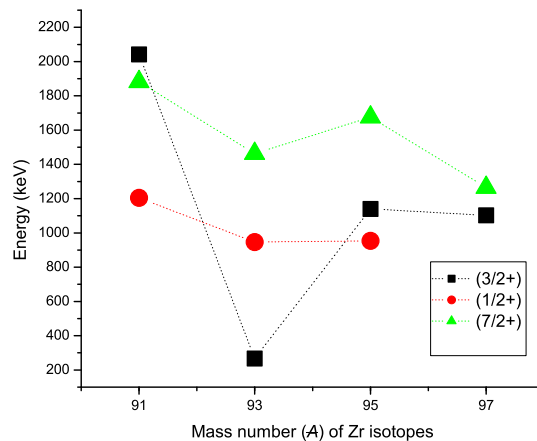
Figure 6.34: Energies of the first $7/2_1^+$, $1/2_1^+$ and $3/2_1^+$ of odd Zr isotopes taken from [www4], which are expected to have single-particle character. Except for $3/2^+$ states, other states have similar energies for different Zr isotopes.

Besides a strong population of single-particle states, it turned out that transfer reactions selectively populate high spin states in both positive and negative parity bands of ^{89}Zr, ^{91}Zr and ^{93}Zr, thus we observed a population up to spin 25/2+, 17/2 and 25/2, respectively. The state 3/2$^+$ at 3083 keV in ^{91}Zr stands out from this rule with its much lower spin than its surrounding.
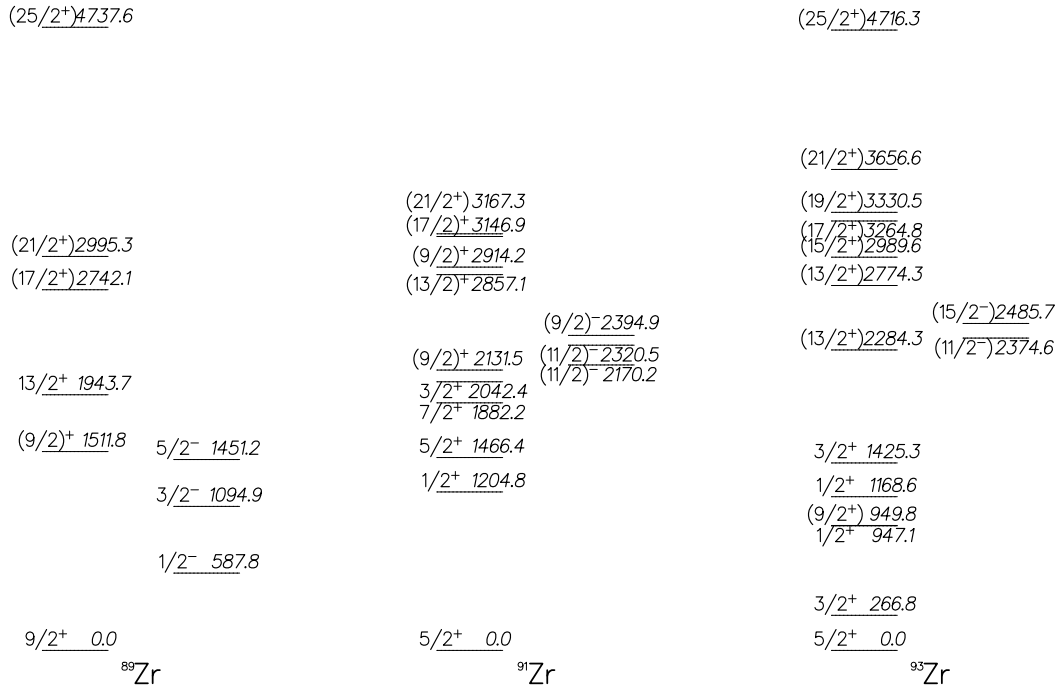
Figure 6.35: Simplified level schemes (only strongly excited states are plotted) of ^{89}Zr (left), ^{91}Zr (middle) and ^{93}Zr (right) isotopes. Positive and negative parities are plotted separately.

In addition to strong excitation of states of single-particle character, and high spin states, we also observed a population of states whose underlying structure could be explained by coupling of single-particle states and phonons. Both, ^{91}Zr and ^{93}Zr have a 5/2$^+$ ground state, which can be described by one valence neutron in the $d_{5/2}$ orbital. In fact, all odd Zr isotopes, from ^{91}Zr to ^{95}Zr have 5/2$^+$ as a ground state. When coupling this neutron to a 2$^+$ state, multiplet of states 9/2$^+$, 7/2$^+$, ... 1/2$^+$ at energy close to the one of 2$^+$ in neighbouring Zr isotope is expected. Similarly, by coupling the same state with a 3$^-$, one expects a 11/2$^-$, 9/2$^-$, ... 1/2$^-$ multiplet. The reaction mechanism does not populate components of two multiplets uniformly but favours stretched configurations (11/2$^-$ and 9/2$^+$), since transfer probability has its maximum at the largest angular momentum transfer

[BW00]. This fact has been shown so far in experiments performed at Prisma spectrometer [Szi07, Szi11, Lun07, Rec12].

Before taking a closer look at a possible coupling scheme, once again we consider the comparison of Zr spectra observed in our measurement with those from the ^{40}Ca+^{96}Zr reaction [Szi07], mentioned earlier in Sections 6.1.4, 6.1.5 and 6.1.6. As Figures 6.21, 6.24 and 6.30 show, in the ^{90}Zr+^{208}Pb case, the transitions from the the higher spin states are much stronger than in ^{40}Ca+^{96}Zr. A similar situation is also present for other high-spin states in different energy regions. If we apply this conclusion to new transitions found in the analysis of the ^{90}Zr+^{208}Pb reaction, the fact that one specific transition does not appear in the Zr spectra obtained in the ^{40}Ca+^{96}Zr reaction, if not affected by statistic, probably implies that this transition belongs to the decay of the high-spin state.

6.2.1   Some considerations about fermion-phonon coupling

In this section we would like to discuss in more detail the possible coupling of phonon in the Zr isotopes (the stretched configuration only) to the ground state of different Zr isotopes from $A = 89$ to $A = 97$, as listed in Table 6.10. Systematics of the behaviour of the 2^+ states in the even-even Zr isotopes is illustrated in Table 6.11, while the similar systematic of the 3^- states is presented in Table 6.12.

Table 6.10: Expected states of possible couplings of the ground state (second column) in Zr isotopes (first column) to a 2^+ (third column) and 3^- (fourth column) vibration quanta, considering the stretched configuration only.

isotope	$J^\pi_{g.s.}$	$J^\pi_{g.s.} \otimes 2^+$	$J^\pi_{g.s.} \otimes 3^-$
^{89}Zr	$9/2^+$	$13/2^+$	$15/2^-$
^{91,93,95}Zr	$5/2^+$	$9/2^+$	$11/2^-$
^{97}Zr	$1/2^+$	$5/2^+$	$7/2^-$

Figures 6.36 and 6.37 show the comparison of energies of the first 2^+ (and 3^-) states in even Zr isotopes with states that could correspond to coupling of 2^+ (i.e. 3^-) phonon to the ground state in the stretched configuration (as listed in Table 6.10).
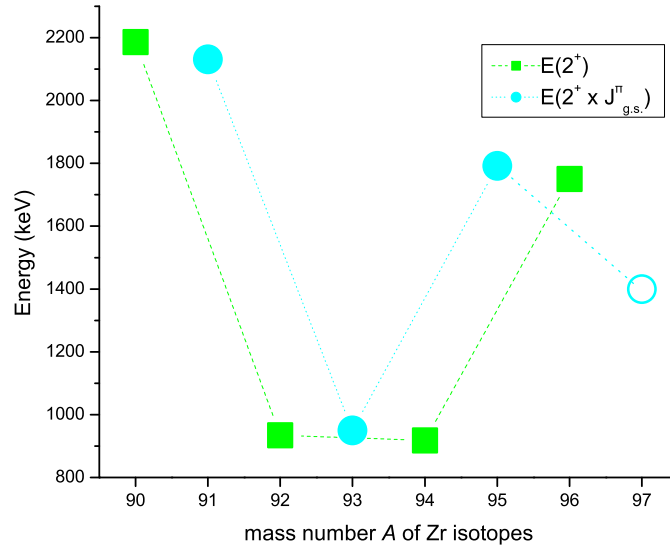
Figure 6.36: Energies of the first 2^+ states (green squares) in even Zr isotopes, together with energies of $9/2^+_1$ states in ^{91,93,95}Zr (solid blue circles) and $5/2^+$ in ^{97}Zr (open blue circle). Dashed lines are here only to guide the eyes.

Table 6.11: Decay patterns and the strengths of the (electromagnetic) EM transitions (in b^2e^2) of the first 2^+ states in different Zr isotopes. The first column lists Zr isotopes of interest, the second and third columns list spins and parities and energies of initial states, the fourth column shows strengths of EM transitions. The fifth and sixth columns contain energies and tabulated intensities of EM transitions. The seventh column shows the multipolarity of the transition, while the last two columns contain spins and parities and energies of final states.

isotope	J^π_i	E_i (keV)	B(E2) (b^2e^2)	E_γ (keV)	I_γ (%)	E/M	J^π_f	E_f (keV)
^{90}Zr	2^+	2186.3	0.065	2186.2	100	E2	0^+	0.0
				425.5	0.3	E2	0^+	1760.7
^{92}Zr	2^+	934.5	0.083	934.5	100	E2	0^+	0.0
^{94}Zr	2^+	918.8	0.066	918.8	100	E2	0^+	0.0
^{96}Zr	2^+	1750.5	0.055	1750.4	100	E2	0^+	0.0
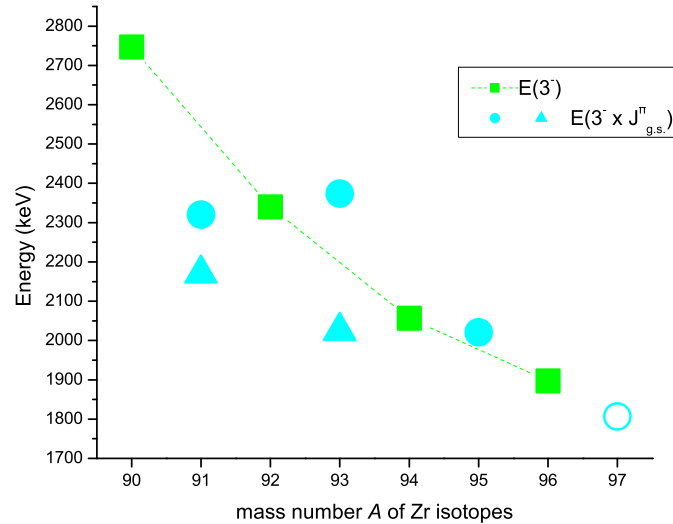
Figure 6.37: Energies of the first 3^- states in even Zr isotopes (solid green squares), and energies of the first $11/2_1^-$ in ^{91,95}Zr and second $11/2_2^-$ in ^{93}Zr (solid blue circles) and first $7/2_1^-$ in ^{97}Zr (open blue circle). The state denoted by a filled blue triangle represents the first $11/2_1^-$ states in ^{91,93}Zr. Dashed lines are here only to guide the eyes.

To better understand the behaviour of different quadrupole and octupole states in even-even Zr isotopes, and about their couplings to the ground states, we summarized existing data in Tables 6.11, 6.12 and 6.13. To better comprehend the populated isotopes in the two reactions (^{90}Zr+^{208}Pb and ^{40}Ca+^{96}Zr [Szi07], as explained in previous sections), we plotted all of them in Figs. 6.31 and 6.32. In short, the Zr isotopes from $A = 89$ to $A = 96$ have been populated.

Table 6.12: Decay patterns and the strengths of the EM transitions of the first 3^- states in different Zr isotopes. The first column lists Zr isotopes of interest, the second and third columns list spins and parities and energies of initial states, the fourth column shows strengths of EM transitions. The fifth and sixth columns contain energies and tabulated intensities of EM transitions. The seventh column shows the multipolarity of the transition, while the last two columns contain spins and parities and energies of final states.

isotope	J_i^π	E_i (keV)	B(E3) (b^3e^3)	E_γ (keV)	I_γ (%)	E/M	J_f^π	E_f (keV)
^{90}Zr	3^-	2747.9	0.027/0.108	561.6	100		2^+	2186.3
				2747.8	4		0^+	0.0
^{92}Zr	3^-	2339.7	0.067	1405.1	100	(E1)	2_1^+	934.5
				844.1	30	(E1+M2)	4_1^+	1495.5
				492.4	11	(E1+(M2))	2_2^+	1847.3
				2339.9	0.1	E3	0^+	0.0
				272.9	?		2_3^+	2066.7
^{94}Zr	3^-	2057.6	0.087	1138.9	100		2_1^+	918.8
				588.0	2.8		4_1^+	1469.6
^{96}Zr	3^-	1897.2	0.186	146.7	100	(E1)	2_1^+	1750.5
				1897.2	19	[E3]	0^+	0.0

Table 6.13: Decay patterns and the strengths of the EM transitions of the possible $J_{g.s.}^\pi \otimes 2^+$ and $J_{g.s.}^\pi \otimes 3^-$ states in different Zr isotopes. The first column lists Zr isotopes of interest, the second and third columns list spins and parities of excited states. The fourth and fifth columns contain energies and tabulated intensities of EM transitions, while the sixth column displays the multipolarity of the transition. The last two columns contain spins and parities and energies of final states. Note that in ^{93}Zr several states labelled as $7/2^+, 9/2^+$ exist at 1463, 1598, 2040, 2078, 2638, 2991, 3044, 3230, 3322 keV (all with errors of $5-12$ keV), while in ^{93}Zr states labelled as $9/2^-, 11/2^-$ (decay is not known) at 2662, 2716, 2873 keV (with error of 10 keV) are found. Note that, in ^{95}Zr we included new data from [Szi07]. In a more complicated decay pattern, the decay of additional intermediate states was also included.

isotope	J_i^π	E_i (keV)	E_γ(keV)	I_γ (%)	E/M	J_f^π	E_f (keV)
^{89}Zr	$13/2^+$	1943.7	1943.7	100	E2	$9/2^+$	0.0
	$15/2^-$	2150.6	29.3	100	(M1+(E2))	$13/2^-$	2121.3

			206.9	42	(E1)	13/2$^+$	1943.7
	13/2$^-$	2121.3	177.6	100		13/2$^+$	1943.7
			2121.3	46		9/2$^+$	0.0
^{91}Zr	(9/2)$^+$	2131.5	2131.5	100	(E2)	5/2$^+$	0.0
	(9/2)$_2^+$	2914.2	782.7	100		(9/2)$^+$	2131.5
	(11/2)$^-$	2170.2	2170.0	100	(E3)	5/2$^+$	0.0
			38.7	25	[E1]	(9/2)$^+$	2131.5
	(11/2)$_2^-$	2320.5	151.1			(11/2)$^-$	2170.2
			60.3			(13/2)$^-$	2259.9
	(13/2)$^-$	2259.9	89.6	100		(11/2)$^-$	2170.2
^{93}Zr	(9/2$^+$)	949.8	949.8	100	E2	5/2$^+$	0.0
	9/2$^-$,11/2$^-$	2025					
	9/2$^-$,11/2$^-$	2363					
	(11/2$^-$)	2374.6	1424.7	100		(9/2$^+$)	949.8
^{95}Zr	(9/2$^+$)	1792.2	115.9	100		(7/2$^+$)	1676.3
			1792.3	12		5/2$^+$	0.0
	(11/2$^-$)	2021.6	229.4	100		(9/2$^+$)	1792.2
			2022	$\sim$20		5/2$^+$	0.0
^{97}Zr	(3/2$^+$,5/2$^+$)	1400.0	1400	100		1/2$^+$	0.0
			296.9	25		3/2$^+$	1103.1
			136.4	0.8		7/2$^+$	1264.4
	(7/2$^-$)	1806.9	407.1	100		(3/2$^+$,5/2$^+$)	1400.0
			542.5	17		7/2$^+$	1264.4
	7/2$^+$	1264.4	161.2	100	[E2]	3/2$^+$	1103.1
			1264.2	4	[M3]	1/2$^+$	0.0
	3/2$^+$	1103.1	1103.0	100		1/2$^+$	0.0

Table 6.11 shows that in ^{90,92,94}Zr (also in ^{96}Zr not discussed here in detail), all the 2_1^+

states decay predominantly to the ground state, with B(E2) of all 2^+ ranging from 0.055 b^2e^2 in ^{96}Zr to 0.008 b^2e^2 in ^{92}Zr. Regarding octupole states, we would like to mention the ^{208}Pb nucleus, which constitutes an ideal laboratory for the study of phonon states, since its first excited state is the collective 3^- at 2.62 MeV. The collectivity of the 3^- state (B(E3; $3^- \rightarrow 0^+$) = 34 W.u.) is not dominated by a few particle-hole components but derives from the cooperative action of many configurations. The "closed-shell" Zr nucleus represents a more complicated situation. The low-energy part of the spectrum is dominated by a 2^+ state and a higher lying 3^-. The 3^- state in ^{96}Zr is very collective [B(E3; $3^- \rightarrow 0^+$) = 51 W.u.]. Table 6.12 shows how the decay pattern of the 3^- states changes from $A = 90$ to $A = 96$. In ^{90}Zr, the dominant decay is via E1 transition to the 2^+ state, and only about 4% goes via E3 decay to the ground state. In ^{96}Zr, the E1 transition is still the strongest decay branch, but about 20% goes through E3 transition to the ground state. Going toward the middle of the shell, the situation becomes more complicated. This is especially indicative in the case of ^{92}Zr, where the decay pattern of the 3^- state is very complicated. The E1 transition is still the strongest one, followed by a transition to the 4_1^+ (~ 30%) and 2_2^+ (~ 11%) states, being the E3 transition of a negligible strength (~ 0.1%). In the case of ^{94}Zr, the decay pattern is similar to the one observed in ^{90}Zr.

This situation is repeated in odd-even isotopes. Is it especially obvious in the case of ^{95}Zr [Szi07, BF73, Pan05], where distribution of strengths over E1 and E3 transitions is very similar to the one observed in ^{96}Zr. In ^{89}Zr, the first $15/2^-$ state at 2150.6 keV decays through $E_\gamma = 29.3$ keV ($I_\gamma = 100$%) and $E_\gamma = 206.9$ keV ($I_\gamma = 42$%). The energy of the first γ ray is too low to be well recognized by the Clara detector, while the intensity of the other one is too low, thus these γ rays have not been observed in our spectrum. Regarding the ^{93}Zr nucleus, the decay pattern of the tabulated $11/2^-$ states is not well known. From the known decays, we observed the E1 transition of the $(11/2^-)$ state at 2374.6 keV, and possibly its E3 decay ($E_\gamma = 2375$ keV). However, the ratio of the number of events in the E3/E1 transitions is not as expected. From the other possible $11/2^-$ states, we looked for the possible E1 and E3 transitions of the states labeled as $9/2^-$,$11/2^-$ at 2025(10) keV and 2363(10) keV. In this case, we expect γ rays of E1 transitions with energies 1075 and 1413 keV, respectively. The expected E3 transitions would provide γ rays of 2025 and 2363 keV,

respectively. In the search for these E3 transitions with rather high γ ray energies, we looked in the uncorrected spectrum of ^{93}Zr, in order to increase statistics. Notice that the spectrum of ^{93}Zr was corrected by taking into account spectra of ^{93}Y and ^{92}Zr, which do not have any significant γ rays in the energy region around $2-3$ MeV. We observed a peak at around 2367 keV, over a complex background. The expected E1 transition (1413 keV), overlaps with two relatively strong transitions in ^{93}Zr, $E_\gamma = 1334.6$ keV (with the intensity of $\sim 30\%$) and $E_\gamma = 1425.2$ keV ($\sim 40\%$). Thus, we cannot without a significant doubt demonstrate the decay of 2363 keV state (assumed to be $11/2^-$), via expected E1 and E3 transitions. (In the case of the state $9/2^-,11/2^-$ at 2025 keV, we did not observe expected E3 transition.) A very similar situation has been reached in the ^{91}Zr nuclei, where two $11/2^-$ states with similar energy can be found. In fact, looking at the behaviour of both in Fig. 6.37, the first and the second $11/2^-$ states are outside of the systematics.

This situation was extensively discussed in Ref. [BHK76], where the authors were searching for states which originate from coupling of the 51st neutron to 2^+ and 3^- states. In this experiment, angular distributions of the outgoing particles of (d, p), (p, p') and (p, d) reactions were analysed with a split-pole spectrograph and detected using an array of four position sensitive solid state detectors. They concluded that states with the same spin and parity, but based on different core states, mix strongly with each other and with single-particle states, and that the simple weak coupling model cannot be applied in the case of ^{91}Zr and coupling to the 3^- phonon. They also concluded that a major fraction of single-particle states available in connection with the $h_{11/2}$ is contained in the 2.170 MeV state (a state strongly excited in the (p, p') reaction).

This conclusion is not in agreement with the discussion presented in Ref. [SNL09]. The evolution of the $11/2^-$ state in Zr isotopes is discussed in more detail, as based on the SM calculations, which was performed in an extended shell model space $(1f_{5/2}, 2p_{1/2}, 2p_{3/2}, 1g_{9/2})$ for protons and $(2d_{5/2}, 3s_{1/2}, 2d_{3/2}, 1g_{7/2}, 1h_{11/2})$ for neutrons. The effective proton-proton interaction was found by fitting the two-body matrix elements for Ni isotopes with $A = 57-78$ and $N = 50$ isotones (^{70}Cu-^{100}Sn), neutron-neutron interaction was based on calculation in the tin region, and proton neutron interaction used propagation of the single-particle states between ^{79}Ni and ^{101}Sn. The results of this calculation in comparison with the experimental

levels observed in our measurements (up to the $(11/2^-)$ state at 2.2 MeV) are shown in Fig. 6.16. The SM calculation showed that the $11/2^-$ (at 2.1 MeV) level is not a pure single-particle $h_{11/2}$ level, but it is calculated to have a dominant $\pi(p^1_{1/2}g^1_{9/2})\ \nu(d^1_{5/2})$ component (55%). In fact, the total number of neutrons in the $h_{11/2}$ is calculated to be only 0.16. Also, the same SM calculation showed a nice description of measured data for the yrast bands, but their description for 3^- states deviates considerably from experimental data (especially for ^{94}Zr). The 3^- collective states may correspond to a more complex superposition of cross shell excitations out of the valence space of the discussed SM calculations. Thus, it is possible, that the deviation of the systematics presented in Fig. 6.37 is due to the strong mixing of different configurations (stronger than in other Zr isotopes) or that true particle-vibration strength is in a yet unknown $11/2^-$ state. The systematics suggests that such states should be around 2.7 MeV, where no states of such spin have been found. Thus, we can conclude that the deviation from the systematic for the ^{91}Zr is probably due to the very strong mixing.

6.2.2 Some considerations about pairing-vibration states in the Zr isotopes

Heavy ion reactions offer an excellent opportunity to study the interplay between single particle and pair transfer modes since large amount of nucleons can be transferred in the reaction. Specific interest is coming from the study of the population strength of 0^+ in even-even isotopes, since the population of these states via multinucleon transfer carry information on the effect of the residual interaction and therefore also on the pairing.

In the ^{90}Zr$+^{208}$Pb reaction particularly attractive is the possibility to identify pair vibrational modes in the spherical ^{92,94}Zr nuclei. Figure 6.38 shows spectra of ^{88}Sr (bottom panel), ^{90}Zr (middle panel) and ^{92}Zr (upper panel) observed in our measurement. A subshell and shell closure at $Z = 40$ and $N = 50$ in ^{90}Zr provide a good vacuum for both proton and neutron pairing vibrations. The population of 0^+ states at 5441, 4424 and 4126 keV excitation energy was indeed observed in ^{90}Zr nuclei and interpreted within the pair vibrational model [Bro73].

Zr nuclei have been populated in two-neutron pick-up channels with (p, t) reactions

[BAR71, IMB75] (Figs. 6.41 and 6.40) and in two-proton pick-up channels with $(^{14}C, ^{16}O)$ reactions [May82] (Fig. 6.2.2). The work has also been done on ^{90}Zr via (n, n') scattering [Gar03], where a large number of final states have been reached.
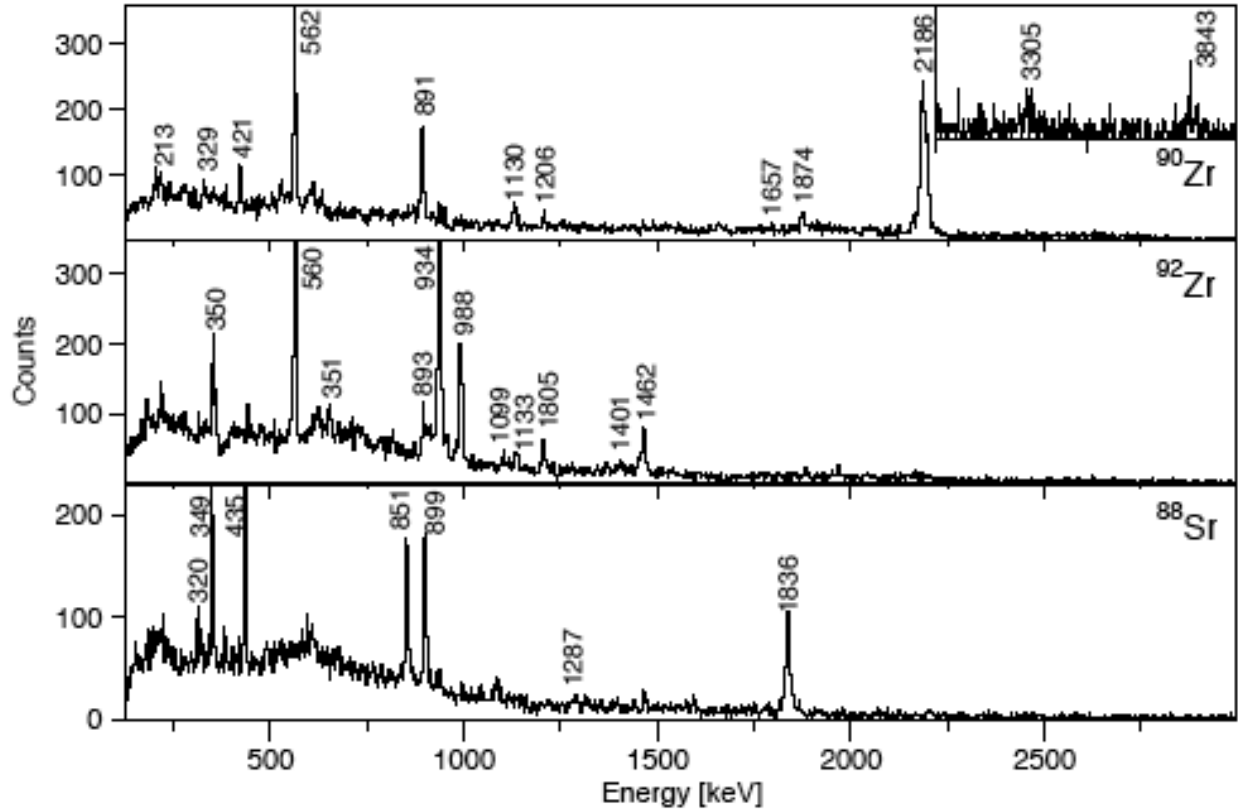
Figure 6.38: γ spectra for ^{90}Zr (top), ^{92}Zr (middle) and ^{88}Sr (bottom) isotopes. The inset shows the part of the ^{90}Zr spectrum with γ ray energies above 3 MeV [Ur06].

Regarding the ^{90}Zr, the pairing vibration 0^+ state is expected around 4 MeV. An illustration of the population of the levels of ^{90}Zr close to the pairing vibrational region, is shown in Fig. 6.39. In this isotope, 0^+ states at 4126 keV, 4424 keV and 5441 keV have been identified, although with an unknown decay pattern. We searched for their possible decays to 2^+ states (at 2186.3, 3308.8, 3842.2 keV) populated in our measurement. In these decays one would expect γ rays of 1940(3), 817(3), 284(3) keV (for the 0^+ state at 4126(3) keV); 2238(3), 1115(3) and 582(3) keV (in the case of the 0^+ state at 4424(3) keV), and 3255(5), 2132(5), 1599(5) keV (for the 0^+ state at 5441(5) keV). Those possible transitions are listed

108

in Table 6.15. Notice that 0^+ states at 0.0, 1760.7, 4126, 4424, 5441 MeV were populated with different strengths in (p, t) reactions; the 0^+ states at 5441, 4424 and 4124 keV were strongly populated (as seen in Fig. 6.41). Even if we observed a population of 2^+ states in this energy region where a phonon pairing -vibration state is expected, we did not observe assumed decays of the known 0^+ states to the lower lying 2^+ states.
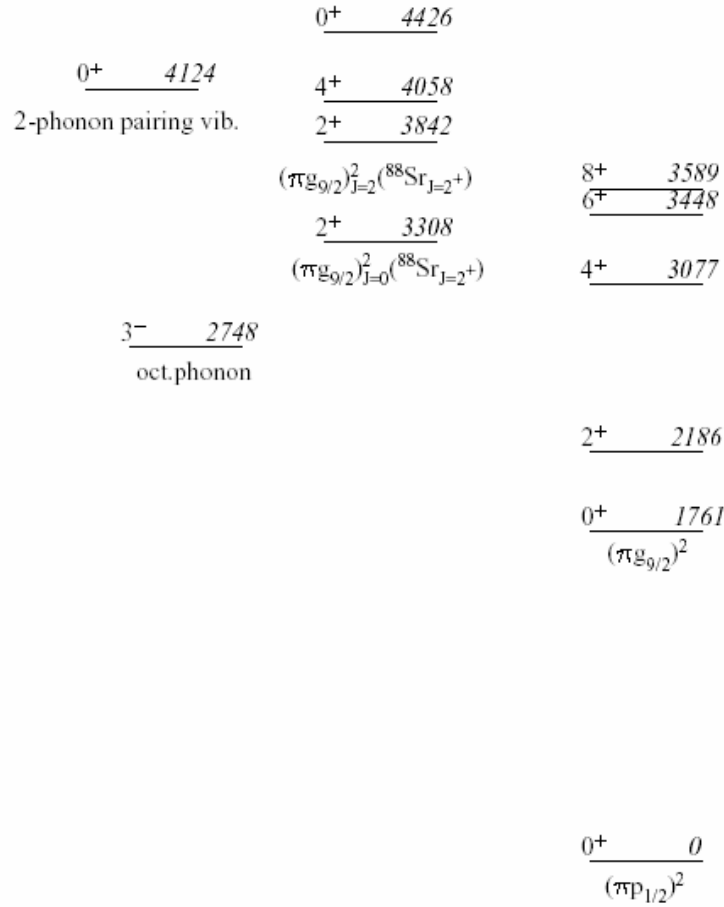
Figure 6.39: Illustration of the population of the levels close to the pairing vibrational region [Ur06].

In ^{92}Zr, 0^+ states at 2904.1, 3589, 3992 and 4283 keV were excited via ^{90}Zr$(t, p)^{92}$Zr reactions, while in the ^{94}Zr$(p, t)^{92}$Zr the state at 5.5 MeV was also populated. In addition to ^{90}Zr, we have searched for possible decays from 0^+ states to 2^+ states and they are listed in Table 6.15. Between these possible γ rays, the transition from the 0^+ state at $E_{\text{ex}} = 3992$
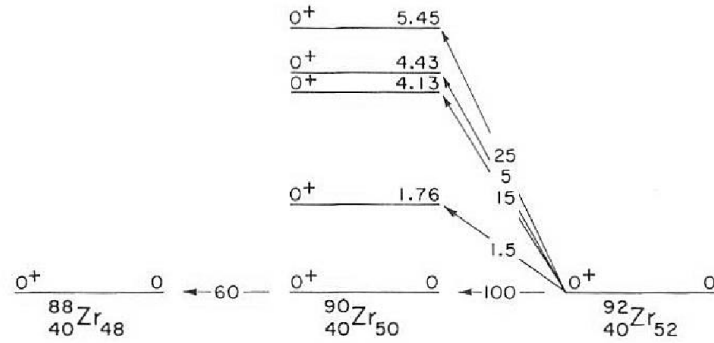
Figure 6.40: 0^+ states in ^{90}Zr observed in the (p,t) reactions (from ref. [RKL70]).

keV to the observed 2^+ state at $E_{\text{ex}} = 3057.4$ keV (denoted italics in Table 6.15) overlaps with the strongest transition in the ^{92}Zr isotope, the transition from the 2_1^+ state to the ground state.

We apply the same procedure to the ^{94}Zr isotope. Here, as the statistic of this channel is smaller when compared with the ^{90}Zr and ^{92}Zr, only the decay of the first 2^+ state ($E_{\text{ex}} = 918.8$ keV) has been observed. Possible decays from the higher lying 0^+ states ($E_{\text{ex}} = 1300.19(12)$ and $3776(7)$) to this 2^+ state have not been observed.

The reason that we couldn't identify the decay of the excited 0^+ states in Zr nuclei may partially lie in the fragmentation of strength of the assumed particle-vibration state over several 0^+ states, making the identification of particle-vibration states more complicated.

Table 6.14: Possible combinations of $0^+ \longrightarrow 2^+$ transitions in the ^{90}Zr: the first row lists 0^+ states, and the first column 2^+ states. The rest of the table contains possible γ energies from 0^+ to the 2^+ states (in keV)

$E(2^+)$ (keV) \ $E(0^+)$ (keV)	1760.7	4126	4424	5441
2186.7		1940(3)	2238(3)	33254(5)
3308.8		817(3)	1115(3)	2132(5)
3842.2		284(3)	582(3)	1599(5)
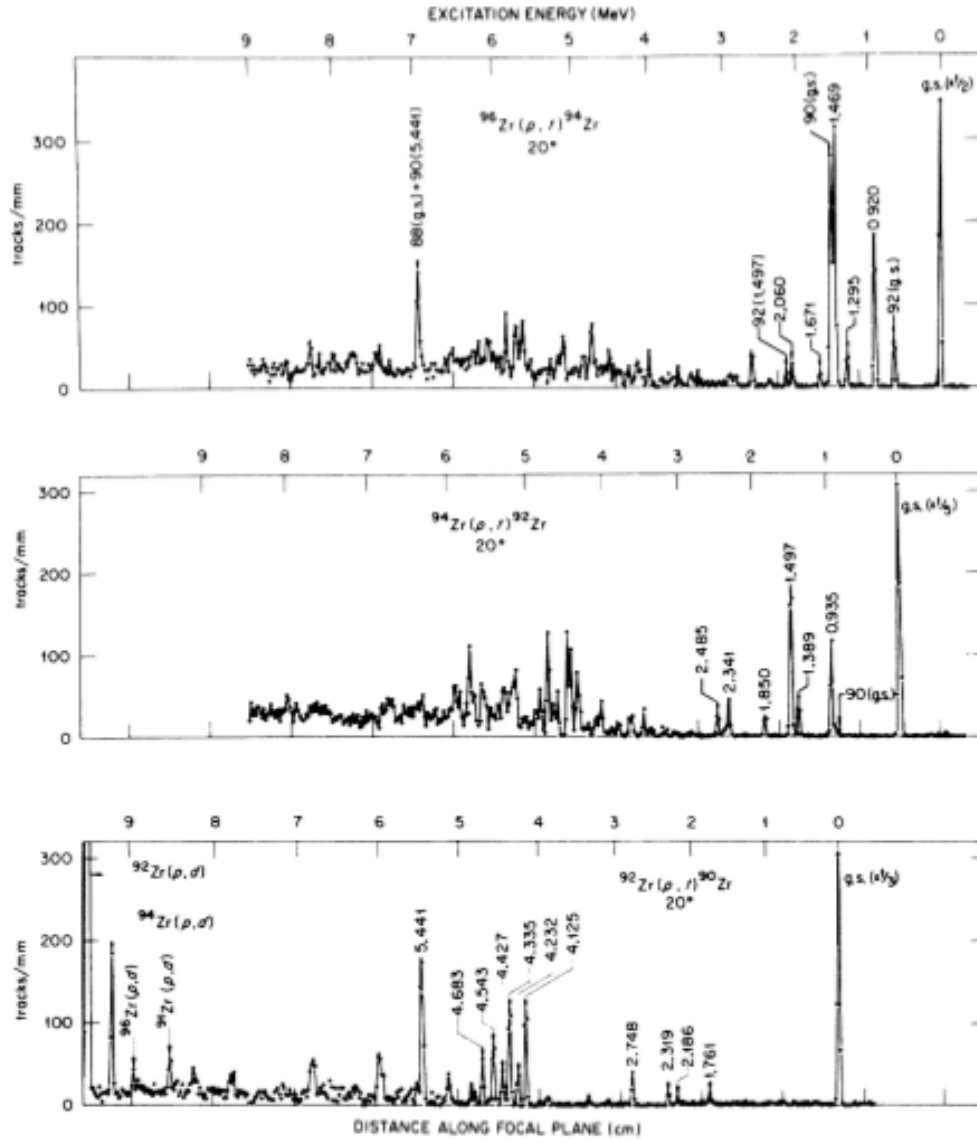
Figure 6.41: Energy spectra of tritons observed at a scattering angle of 20° from the interaction of 38-MeV protons with the zirconium isotopes: ^{90}Zr (bottom panel), ^{92}Zr (middle panel) and ^{94}Zr (top panel) [BAR71].
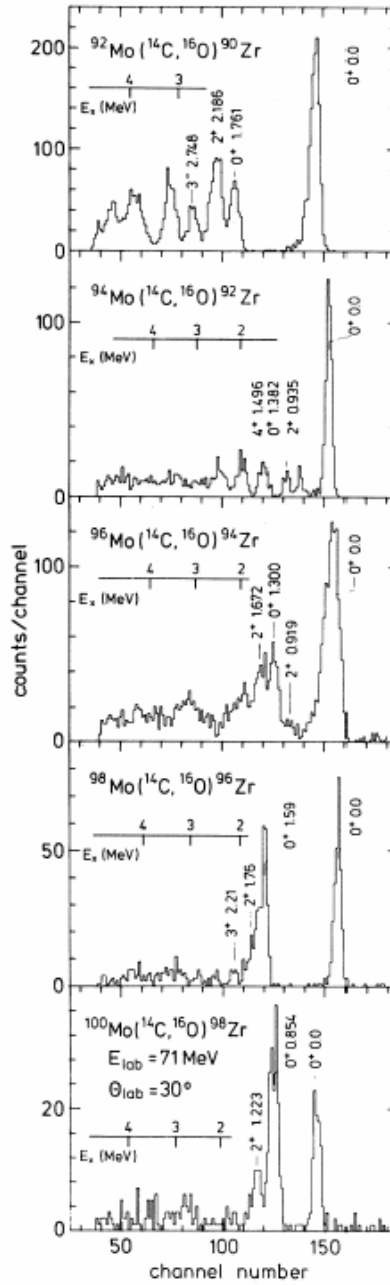
Figure 6.42: States of Zr isotopes populated in the (^{14}C,^{16}O) reactions (from Ref. [May82]).

Table 6.15: Possible combinations of $0^+ \longrightarrow 2^+$ transitions in the ^{92}Zr: the first row lists 0^+ states, and the first column 2^+ states. The rest of the table contains possible γ energies from 0^+ to the 2^+ states (in keV)

$E(2^+)$ (keV) \ $E(0^+)$ (keV)	2904.1	3589	3992	4283	5490
934.5	1970(18)	2655(10)	3058(10)	3349(10)	4556
2066.7	837(18)	1522(10)	1925(10)	2756(10)	3423
3057.4	532(10)	*935(10)*	1226(10)	2433	

Table 6.16: Possible combinations of $0^+ \longrightarrow 2^+$ transitions in the ^{94}Zr: the first row lists 0^+ states, and the first column 2^+ states. The rest of the table contains possible γ energies from 0^+ to the 2^+ states (in keV)

$E(2^+)$ (keV) \ $E(0^+)$ (keV)	1300.2	3776
918.8	381(12)	2857(7)
1671.4		2105(7)
2151.3		1325(7)
2366.12		*1410(7)*

6.3   γ-ray spectroscopy and structure of lead nuclei
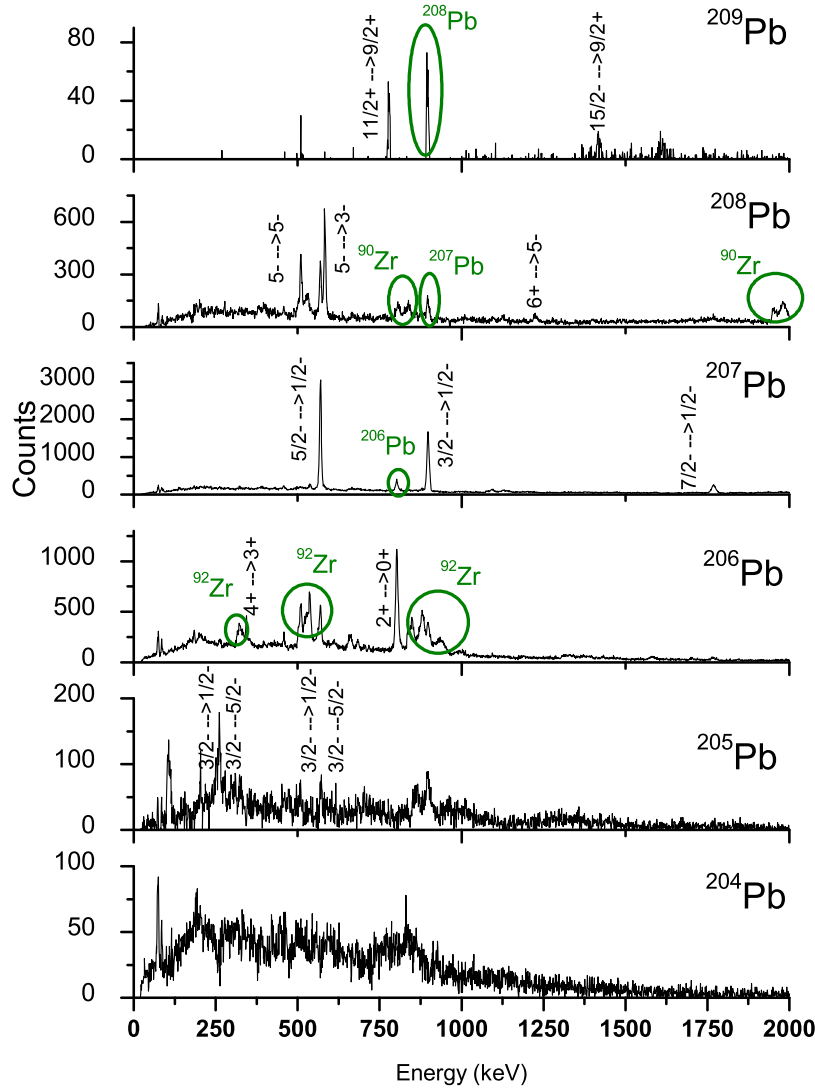
Figure 6.43: γ spectra of observed Pb isotopes. Presented spectra are obtained after cleaning described in Section 6.1. The strongest γ transitions are labeled with spin and parities on initial and final states as in [www4]. The area denoted green represent wrongly Doppler corrected γ rays from the light partner or evaporated γ rays from neighbouring Pb isotope.

Having analysed the observed spectra of Zr isotopes, the following sections will examine their binary partners, i.e. Pb isotopes. Figure 6.43 shows γ spectra of $^{204-209}$Pb isotopes

observed in our experiment. Spectra are cleaned beforehand in the way described in Section 6.1. The $-4n$ channel, i.e. ^{204}Pb is at the limit of the presently accumulated statistics and therefore it has not been discussed.

Here we point out that ^{208}Pb is a doubly magic nucleus, with a full proton $4\hbar\omega$ shell and a full neutron $5\hbar\omega$ shell (see Fig. 6.44). Lighter observed odd Pb isotopes (^{205,207}Pb) have one unpaired neutron hole in the $5\hbar\omega$ shell, and one observed heavier isotope (^{209}Pb) has one unpaired neutron in the $6\hbar\omega$ shell (see Fig. 6.44).
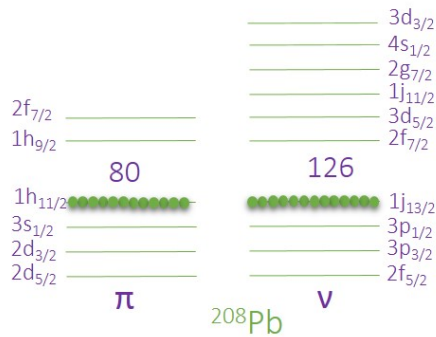
Figure 6.44: Schematic view of the proton and neutron orbitals of the ^{208}Pb, according to the classical shell model

As the ground states of ^{205,207}Pb are $5/2^-$ and $1/2^-$, respectively, it is expected that one unpaired neutron is in the $2f_{5/2}$ and $3p_{1/2}$, respectively. If one neutron from the same shell (or, more precise, from orbitals $1j_{13/2}$, $3p_{1/2}$, $3p_{3/2}$, $2f_{5/2}$, $2f_{7/2}$, $1g_{9/2}$) fills the hole in the "ground state orbital", this would result in a single-particle state of spin $13/2^+$, $1/2^-$, $3/2^-$, $5/2^-$, $7/2^-$ or $9/2^-$. On the other side, ^{209}Pb has one unpaired neutron in the $2g_{9/2}$ orbital, which causes its ground state to be $9/2^+$. If this neutron moves to a higher orbital of the same shell, possible single-particle states are $5/2^+$, $11/2^+$, $7/2^+$, $1/2^+$, $3/2^+$ or $15/2^-$.

6.3.1 ^{205}Pb

This isotope has a full proton $4\hbar\omega$ shell and 3 neutron holes in the $5\hbar\omega$ shell. Since ground state spin is $5/2^-$, we expect that one unpaired neutron is in the $2f_{5/2}$ orbital.

^{205}Pb has almost degenerate ground state (as can be seen in Fig. 6.45), with spins $J^\pi = 5/2^-$ and $J^\pi = 1/2^-$, which differ only by ~ 3 keV.

Spectrum of ^{205}Pb, with labeled recognized γ transitions is shown in Fig. 6.22, where it is seen that only a few γ rays have been observed, and they are listed in Table 6.17. There are also some yet unknown γ rays, which are listed in Table 6.18.

Table 6.17: γ transitions observed in the present work for the ^{205}Pb isotope. The first column contains energies of γ rays (E_γ) in keV, the second and third columns show energies (E_i), spins and parities (J_i^π) of initial states, while energies (E_f), spins and parities (J_f^π) of final states are listed in the fourth and fifth columns. In the last column, transition intensities after taking into account the Clara efficiency, are listed (normalized to the strongest transition).

E_γ (keV)	E_i (keV)	J_i^π	E_f (keV)	J_f^π	I_γ (%)
260.5	262.8	3/2-	2.3	1/2-	51.17
262.8	262.8	3/2-	0	5/2-	17.05
573.8	576.2	3/2-	2.3	1/2-	30.00
576.3	576.2	3/2-	0	5/2-	100.00

As Fig. 6.45 shows, three negative parity states are excited, and they deexcite through a transition to the ground state. Since, in the case of a light partner ^{93}Zr (see Section 6.1.5), we excited states of single-particle character, we suggest that excited states in ^{205}Pb are also single-particle states, due to a neutron hole in $3p_{1/2}$ or $2f_{5/2}$ orbitals.

One γ ray is missing $(E_\gamma = 313.4$ keV from $E_i = 576.2$ keV, $J_i^\pi = 3/2^-$ to $E_f = 262.8$ keV, $J_f^\pi = 3/2^-)$ due to its low decay branch $(I_\gamma = 5.5\%)$. Some low energy unknown γ rays have been detected, but due to a complex background caused by wrongly Doppler corrected γ rays of ^{93}Zr isotope, their attribution to the ^{205}Pb is not so certain.

Table 6.18: New γ rays observed in the present work for the ^{205}Pb isotope. The first column contains energies of γ rays (E_γ) in keV, and the second one their intensities after taking into account the Clara efficiency (normalized to the strongest transition, as in Table 6.17).

E_γ (keV)	I_γ (%)
102.5(2)*	32.97
106.9(3)*	39.22
202.9(1)*	32.95
250.9(5)*	81.12
257.2(4)*	43.49
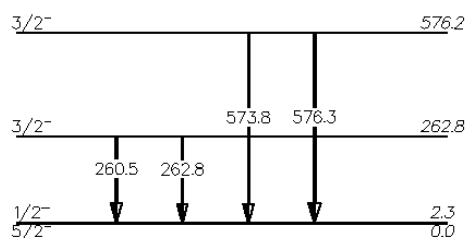
Figure 6.45: γ transitions observed in our measurement for ^{205}Pb. Relative γ ray intensities are indicated by widths of arrows. Energies, spins and parities of levels, their branching ratios and energies of transitions are as in Ref. [www4]. Only the first three excited levels have been observed.

6.3.2 ^{206}Pb

In Fig. 6.17, there are 3 parts of the ^{206}Pb spectrum (denoted green) where wrongly corrected strong γ rays from ^{92}Zr widen the area in the ^{206}Pb spectrum. As a consequence, some γ rays from ^{206}Pb are not clearly observed, namely $E_\gamma = 323$, 509, 568 and 848 keV. Also, $E_\gamma = 516.2$ keV ($E_i = 2200.2$ keV $J_i^\pi = 7^- \longrightarrow E_f = 1684.0$ keV $J_f^\pi = 4^+$) has not been observed in the spectrum (so it is denoted by the dashed line in Fig. 6.46) due to its long life ($T_{1/2} = 125$ μs), which is longer than the time needed for the ions to pass the Prisma spectrometer, so the coincidence between the fragment in the focal plane and its prompt γ ray cannot be established.

$E_\gamma = 497.1$ keV also has not been observed, because its peak has been lost in the widened area. As in previous cases, some γ rays are not seen because of their low intensity, and they are listed in Table 2 in the Appendix. Furthermore, there are some peaks in the spectrum, which are not known γ rays, but may also come from widening these parts of the spectrum. Those unknown γ rays are denoted by * in Table 6.19, where all the observed γ rays of ^{206}Pb are listed.

It is notable that $E_\gamma = 685.0$ keV (which is also denoted with * in Table 6.19) is a known transition, namely, from $E_i = 2149.0$ keV ($J_i^\pi = 2^+$) to $E_f = 1466.8$ keV ($J_f^\pi = 2^+$), and its tabulated intensity is 20%. Since we have not observed the other two γ rays with higher intensities from the same energy level ($E_\gamma = 808.6$, with $I_\gamma = 20\%$ and $E_\gamma = 1345.9$ keV with $I_\gamma = 100\%$), we did not include this level in the level scheme in Fig. 6.46.

In the ^{206}Pb spectrum, strongly excited states are $2^+, 3^+, 4^+$, but yrast 6^+ state is also present (see Fig. 6.46). In the positive parity band, all states up to $E_{\text{ex}} = 1704.5$ keV ($J^\pi = 1^+$) are excited, with the exception of $J^\pi = 0^+$ ($E_{\text{ex}} = 1166.4$ keV). In the negative parity band, all states up to ~ 3300 keV have been observed.

Table 6.19: γ transitions observed in the present work for the ^{206}Pb isotope. The first column contains energies of γ rays (E_γ) in keV, the second and third columns show energies (E_i), spins and parities (J_i^π) of initial states, while energies (E_f), spins and parities (J_f^π) of final states are listed in the fourth and fifth columns. In the last column, transition intensities after taking into account the Clara efficiency, are listed (normalized to the strongest transition).

| E_γ (keV)	E_i (keV)	J_i^π	E_f (keV)	J_f^π	I_γ (%)
184.0	2384.2	6-	2200.2	7-	3.80
260.5			^{205}Pb		
324.0(2)*					17.29
343.5	1684.0	4+	1340.5	3+	9.66
458.1	2658.3	9-	2200.2	7-	5.69
510.2(5)*					33.84
537.5	1340.5	3+	803.1	2+	37.64
569.7			^{207}Pb		
657.2	1997.7	4+	1340.5	3+	10.61
663.8	1466.8	2+	803.1	2+	8.93
685.0(2)*					8.74
803.1	803.1	2+	0	0+	100.00
850.4(6)*					12.89
881.0	1684.0	4+	803.1	2+	16.52
895.1	3279.2	5-	2348.2	6-	10.61
1433.5	2236.5		803.1	2+	5.61
1588.2	2391.3	6-	803.1	2+	1.76
1588.6	2929.1	4+	1340.5	3+	3.65
1576.4	3260.4	6+	1684.0	4+	1.35
1704.5	1704.5	1+	0	0+	1.99
1764.2	4000.7		2236.5		4.14
1844.5	2647.8	3-	803.1	2+	7.88
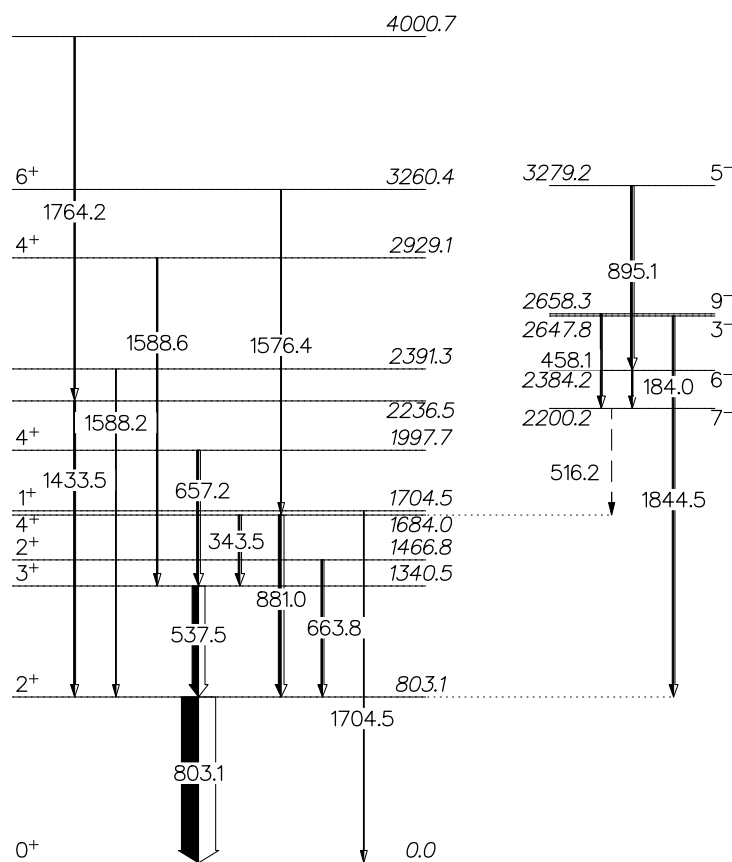
Figure 6.46: Positive (left) and negative (right) parity states observed in our measurement for ^{206}Pb. Relative γ ray intensities are indicated by widths of arrows. Energies, spins and parities of levels, their branching ratios and energies of transitions are as in [www4]. All excited states up to ~ 1700 keV in the positive parity band and up to ~ 3300 keV in the negative parity band have been observed, with the exception of 0^+ ($E_{\mathrm{ex}} = 1166.4$ keV).

6.3.3 ^{207}Pb

The γ spectrum of ^{207}Pb is shown in Fig. 6.12 (botom panel). The green area in the figure denote γ rays from ^{206}Pb (one neutron evaporated channel). There are some other γ rays from ^{206}Pb (which we also saw in the ^{206}Pb spectrum), and they are listed in Table 6.20, together with γ rays recognized as transitions in ^{207}Pb. One unknown (higher energy) γ ray, $E_\gamma = 1126.6$ keV remains unknown, for which a possible decay is still to be determined.

Although [www4] lists the $E_{ex} = 3414.2$ keV with spin 3/2, 5/2, 7/2, we believe that the spin of this state is $9/2^-$, as quoted in [RWB97], where three γ rays were observed via $(d, p\gamma)$ reactions to decay from $E_{ex} = 3414.2$: $E_\gamma = 2845$ keV ($I_\gamma = 100\%$), $E_\gamma = 972$ keV ($I_\gamma = 100\%$, which we have not observed possibly because of the strong $E_\gamma = 803.1$ keV in the ^{206}Pb, which also appears in the ^{207}Pb spectrum) and $E_\gamma = 751$ keV (I_γ undetermined).

Table 6.20: γ transitions observed in the present work for the ^{207}Pb isotope. The first column contains energies of γ rays (E_γ) in keV, the second and third columns show energies (E_i), spins and parities (J_i^π) of initial states, while energies (E_f), spins and parities (J_f^π) of final states are listed in the fourth and fifth columns. In the last column, transition intensities after taking into account the Clara efficiency, are listed (normalized to the strongest transition).

E_γ (keV)	E_i (keV)	J_i^π	E_f (keV)	J_f^π	I_γ (%)
458.1			^{206}Pb		
537.5			^{206}Pb		
569.7	569.7	5/2-	0.0	1/2-	98.35
803.1			^{206}Pb		
881.0			^{206}Pb		
897.8	897.7	3/2-	0	1/2-	100.00
1094.7	2727.9	9/2+	1633.4	13/2+	11.12
1126.6(11)*					6.94
1770.2	2339.9	7/2-	569.7	5/2-	28.20
2605.6	3175.7	9/2(+)	569.7	5/2-	3.12
2844.5	3414.2	9/2-	569.7	5/2-	2.06

In the negative parity band of ^{207}Pb (see Fig. 6.47), only the first three excited states have been observed, and with very high intensity (see Fig. 6.12). The state at $E_{\mathrm{ex}} = 3414.2$ keV does not have definite parity, and we drew it in the negative parity band, based on earlier discussion.

In the positive parity band of ^{207}Pb, $9/2_1^+$, $9/2_2^+$ and $13/2_1^+$ states are present (Fig. 6.47). Decay from $E_{\mathrm{ex}} = 1633.4$ keV, $J^\pi = 13/2^+$ (i.e. $E_\gamma = 1063.7$ keV) has not been observed because of its long life ($T_{1/2} = 0.806$ s), which is too long for the ions to pass the whole Prisma spectrometer so the coincidence between the fragment in the focal plane and its prompt γ ray cannot be established. In Table 2 in the Appendix other γ rays which have not been observed because of their low decay branches are listed.

All the excited states mentioned above can have a single-particle character. Since ^{207}Pb has one neutron hole in the $5\hbar\omega$ shell, single-particle states are determined by the position of that hole. That is, $5/2^-$, $3/2^-$, $7/2^-$ and $13/2^+$ can be understood as one neutron hole in the $2f_{5/2}$, $3p_{3/2}$, $2f_{7/2}$ or $1i_{13/2}$ orbital. Also, a $9/2^+$ state can be formed with the excitation of one neutron to the $2g_{9/2}$ orbital.
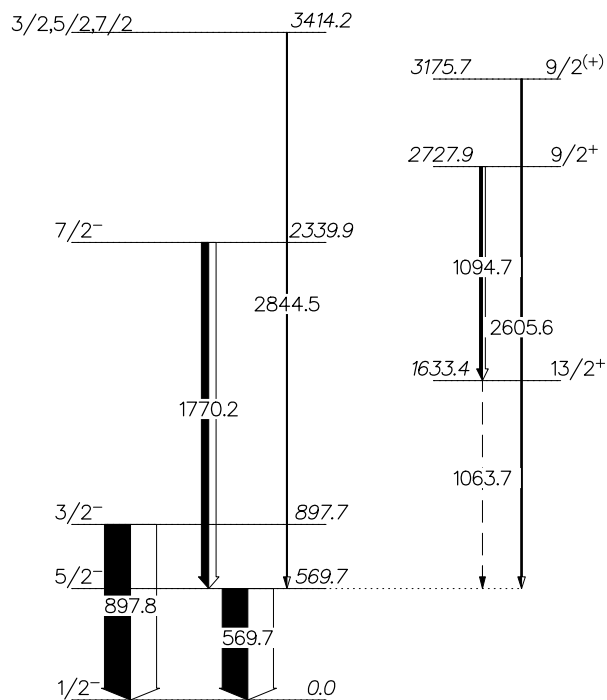
Figure 6.47: Positive (right) and negative (left) parity states observed in our measurement for ^{207}Pb. Relative γ ray intensities are indicated by widths of arrows. Energies, spins and parities of levels, their branching ratios and energies of transitions are as in [www4]. Only the first three negative parity states have been observed. The dashed line represents the γ ray that has not been observed because of its long life ($T_{1/2} = 0.806$ s - see text for explanation).

6.3.4 ^{208}Pb

Three areas marked green are present in the spectrum of ^{208}Pb (Fig. 6.9); the middle one denotes γ ray from ^{207}Pb (one neutron evaporated channel) and the other two (around 800 keV and 2000 keV) contain wrongly Doppler corrected γ rays from ^{90}Zr, since strong $E_\gamma = 890.6$ keV and $E_\gamma = 2186.2$ keV exist in ^{90}Zr. All the observed γ rays are listed in Table 6.21.

Strong γ rays in the spectrum of ^{208}Pb decay from negative parity states, and we excited the first four, as presented in Fig. 6.48. In the positive parity band, the first three positive parity states have been observed (up to $E_{\mathrm{ex}} = 4423.9$ keV), which are also a part of the yrast line. Suprisingly, the strongest transition in the positive parity band belongs to the decay of the non-yrast state 4_2^+ at $E_{\mathrm{ex}} = 5216.2$ keV.

There are again some γ rays not present in the spectrum because of their low decay branch, and they are listed in Table 2 in the Appendix, with the exception of $E_\gamma = 892.3$ keV ($E_i = 5216.2$ keV, $J_i^\pi = 4+ \longrightarrow E_f = 4323.9$ keV, $J_f^\pi = 4+$). The integration of this transition coincides with γ rays connected with the ^{207}Pb isotope (one neutron evaporated channel).

Table 6.21: γ transitions observed in the present work for the ^{208}Pb isotope. The first column contains energies of γ rays (E_γ) in keV, the second and third columns show energies (E_i), spins and parities (J_i^π) of initial states, while energies (E_f), spins and parities (J_f^π) of final states are listed in the fourth and fifth columns. In the last column, transition intensities after taking into account the Clara efficiency, are listed (normalized to the strongest transition).

E_γ (keV)	E_i (keV)	J_i^π	E_f (keV)	J_f^π	I_γ (%)
277.4	3475.1	4-	3197.7	5-	4.02
458.1			^{206}Pb		
510.7	3708.5	5-	3197.7	5-	48.81
569.7			^{207}Pb		
583.2	3197.7	5-	2614.5	3-	71.08
860.6	3475.1	4-	2614.5	3-	14.24
897.8			^{207}Pb		
1126.2	4323.9	4+	3197.7	5-	21.39
1125.9	4423.6	6+	3197.7	5-	26.22
2614.5	2614.5	3-	0	0+	100.00
2601.7	5216.2	4+	2614.5	3-	49.13
4085.5	4085.5	2+	0	0+	3.21
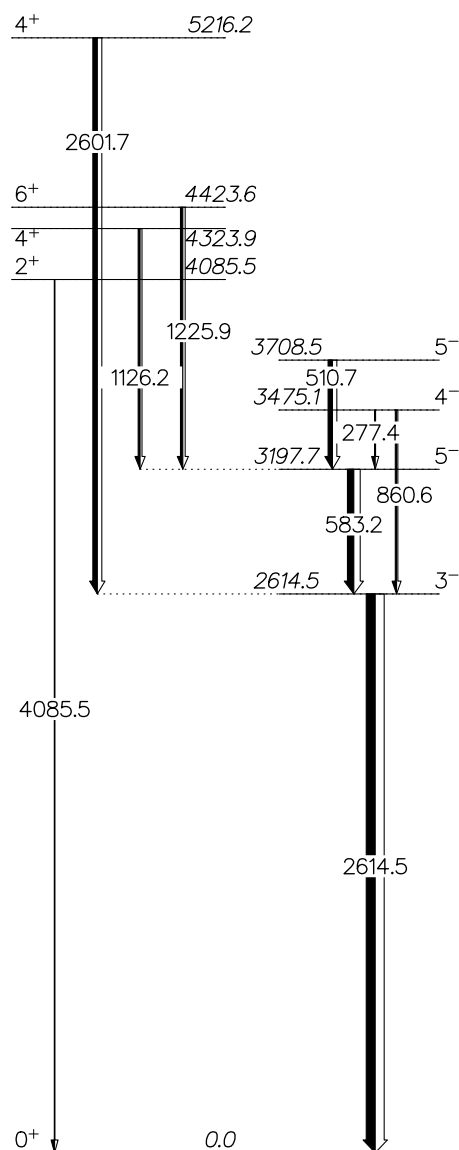
Figure 6.48: Positive (left) and negative (right) parity states observed in our measurement for ^{208}Pb. Relative γ ray intensities are indicated by widths of arrows. Energies, spins and parities of levels, their branching ratios and energies of transitions are as in [www4]. The lowest states, both in positive and negative parity bands have been observed, with the exception of 4_2^+ state at $E_{\mathrm{ex}} = 4423.6$ keV

6.3.5 ^{209}Pb

In the ^{209}Pb spectrum shown in Fig. 6.7 (rather weak channel), one observes two lowest γ transitions (from $J^\pi = 11/2^+$ and $15/2^-$), wich are shown in Fig. 6.49. $E_\gamma = 644.0$ keV (from $E_i = 1423$ keV, $J_i^\pi = 15/2^-$ to $E_f = 778.8$ keV, $J_i^\pi = 11/2^+$) has not been observed in the spectrum because of its low decay branch (tabulated $I_\gamma = 10\%$). $E_\gamma = 897.8$ keV belongs to ^{207}Pb, and $E_\gamma = 2601.7$ keV belongs to ^{208}Pb which is the effect of evaporation. Two new γ rays have been observed ($E_\gamma = 1606.6$ and 2223.3 keV), denoted by * in Table 6.22.

Table 6.22: γ transitions observed in the present work of the ^{209}Pb isotope. The first column contains energies of γ rays (E_γ) in keV, the second and third columns show energies (E_i), spins and parities (J_i^π) of initial states, while energies (E_f), spins and parities (J_f^π) of final states are listed in the fourth and fifth columns. In the last column, transition intensities after taking into account the Clara efficiency, are listed (normalized to the strongest transition).

E_γ (keV)	E_i (keV)	J_i^π	E_f (keV)	J_f^π (number)	I_γ (%)
777.8	778.8	1/2+	0	9/2+	23.53
897.8			^{207}Pb		
1423	1423	15/2-	0	9/2+	59.66
1606.6(7)*					70.18
2223.3(10)*					100.00
2601.7			^{208}Pb		
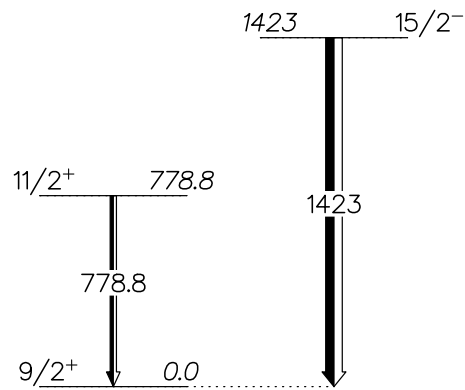
Figure 6.49: Positive (left) and negative (right) parity states observed in our measurement for ^{209}Pb. Relative γ ray intensities are indicated by widths of arrows. Energies, spins and parities of levels, their branching ratios and energies of transitions are as in [www4]. Only the first two excited levels have been observed.

6.4 General remarks about the Pb spectra

At this point, we would like to concentrate more on the effect of the evaporation. The present setup offers the possibility to quantitatively judge the effect of the evaporation, which can follow the transfer mechanism. The γ spectra of the Pb nuclei are constructed by exploiting the binary character of the studied reaction. By gating with Prisma on a specific Z and A of the light partner, the velocity vector of the undetected heavy partner can be evaluated and applied for Doppler correction of its corresponding γ rays. In those spectra, both, γ rays belonging to the primary binary partner, as well as the ones of the nuclei produced after evaporation takes place, are present. This is illustrated in Fig. 6.50, where we display γ spectra of Pb isotopes before the correction described in Section 6.1. These processes were also discussed in Ref. [Szi07], where it was concluded that for the $-2p + 2n$ channel (in the ^{40}Ca+^{96}Zr reaction), about 60% of the yield corresponds to true binary partner, while the rest was equally shared between isotopes corresponding to evaporation of one and two neutrons. For even weaker channels, such as the $4p$ channel, γ rays belonging to the primary binary partner have negligible yield. In the presented neutron transfer channels, most of the yield corresponds to true binary partner. This behaviour is closely connected with the observed TKEL. For the neutron pick-up channels, the major contribution in the TKEL is close to the optimum Q value ($Q_{opt} \sim 0$), but in the proton stripping channels larger TKEL are observed; thus the neutron evaporation has a stronger effect on the final mass partition.

Table 6.23 lists all the γ rays produced after evaporation that appear in certain Pb isotope. Figures 1.8 and 1.9 show mass and TKEL spectra obtained for neutron stripping and proton stripping channels [Cor13]. The evolution pattern as function of the number of transferred neutrons and protons is evident. With the increasing neutron number, TKEL increases, but the quasi-elastic peak remains visible in all neutron transfer channels. In proton pick-up channels, TKEL is more pronounced and has an almost similar (Gaussian) shape for channels $-3p$ and beyond. The effect of nucleon evaporation from the primary fragments is associated with large energy losses, and is visible via γ-partcile coincidences in spectra of Pb isotopes.

The dominant states populated in Pb isotopes, searching for single-particle states, will

Table 6.23: γ rays produced after evaporation that appear in certain Pb isotope. The first column lists observed Pb isotope, the second γ rays produced after evaporation takes place, and the third the nucleus produced after evaporation.

observed isotope	E_γ (keV)	evaporated channel
^{206}Pb	260.5	$-1n$ (^{205}Pb)
^{207}Pb	458.1	$-1n$ (^{206}Pb)
	537.5	$-1n$ (^{206}Pb)
	803.1	$-1n$ (^{206}Pb)
	881.0	$-1n$ (^{206}Pb)
^{208}Pb	458.1	$-2n$ (^{206}Pb)
	569.7	$-1n$ (^{207}Pb)
	897.7	$-1n$ (^{207}Pb)
^{209}Pb	897.8	$-2n$ (^{207}P9b
	2601.7	$-1n$ (^{208}Pb)

now be examined. Figures 6.51 and 6.52 show the strongest excited states of even and odd Pb isotopes, respectively. Since ^{208}Pb is a doubly magic nucleus, excitation energies of its levels are much higher than surrounding nuclei, so excitation energies up to ~ 5000 keV have been observed. In positive parity bands of both, ^{206}Pb and ^{208}Pb, yrast levels up to 6^+ are excited, although higher 2^+ and 4^+ states have been observed. In negative parity bands, strong γ rays from the de-excitation of the yrast 3^- and 5^- have been observed in both isotopes. In ^{206}Pb, 7^-, 6^- and 9^- states have been observed, while in ^{208}Pb, 4^- and the second 5^- states have also been observed.

In odd Pb isotopes, only a few lowest energy levels have been observed, except in ^{207}Pb, where we also excited two $9/2^+$ levels. For these low-lying levels we presume they have single-particle character, due to a neutron hole in $1i_{13/2}$, $3p_{1/2}$, $3p_{3/2}$, $2f_{5/2}$, $2f_{7/2}$, $1g_{9/2}$ orbital (for ^{205,207}Pb) or unpaired neutron in the $1i_{11/2}$ orbital for ^{209}Pb (see Fig. 6.44).

Figure 6.53 shows a comparison of excited levels of ^{90}Zr and its heavy binary partner ^{208}Pb, since we are dealing with semi-magic and magic nuclei. In both nuclei, we observed
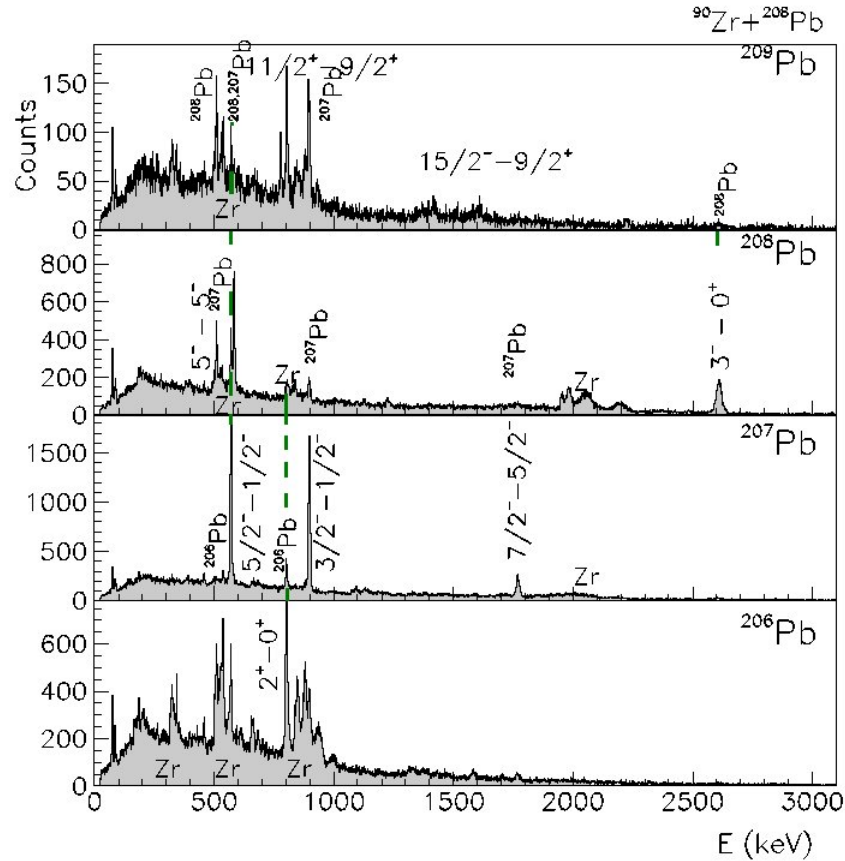
Figure 6.50: γ spectra of the observed Pb isotopes, before correction (explained in Section 6.1). The strongest γ transitions are labeled with spin and parities on initial and final states as in [www4].

yrast states in both positive and negative parity bands. In ^{90}Zr, we also observed the second and third 2^+ excited states and in ^{208}Pb, the second 4^+ and 5^- states. In both spectra, energy levels up to ≈ 5 MeV have been excited, which suggests that, after the reaction, both partners share approximately the same amount of energy.

There is one unknown γ ray in the ^{90}Zr with energy $E_\gamma = 1872$ keV, which, because of the similarity to ^{208}Pb we suggest it decays from the second 4^+ state with $E_{\mathrm{ex}} = 4062$ keV.

4⁺ 5216.2

6⁺ 4423.6
4⁺ 4323.9
2⁺ 4085.5

5⁻ 3708.5
4⁻ 3475.1

6⁺ 3260.4   5⁻ 3279.2

5⁻ 3197.7

4⁺ 2929.1

9⁻ 2658.3
3⁻ 2647.8

3⁻ 2614.5

6⁻ 2384.2
4⁺ 1997.7   7⁻ 2200.2

1⁺ 1704.5
4⁺ 1684.0
2⁺ 1466.8
3⁺ 1340.5

2⁺ 803.1

0⁺ 0.0   0⁺ 0.0
²⁰⁶Pb   ²⁰⁸Pb
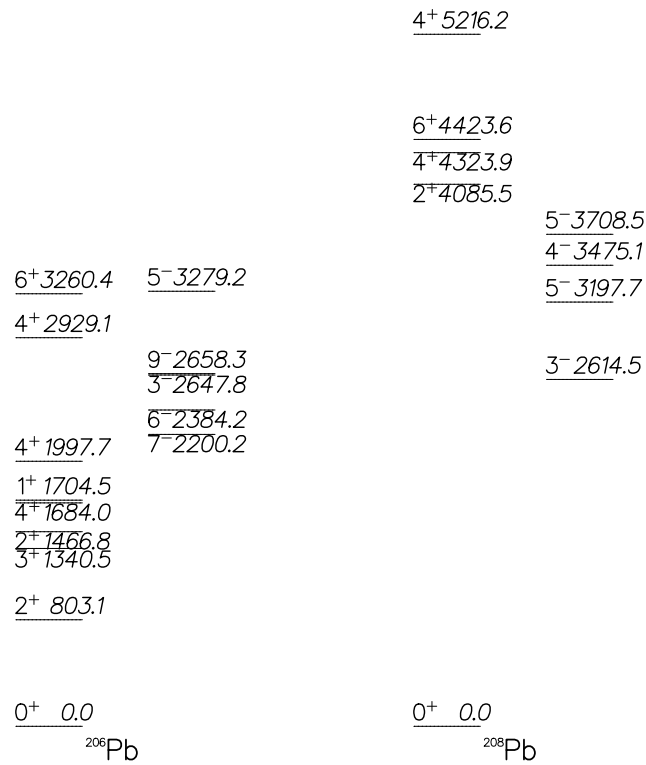
Figure 6.51: Simplified level schemes (only strongly excited states are plotted) of ²⁰⁶Pb (left) and ²⁰⁸Pb (right) isotopes. For each isotope positive (left) and negative (right) parity states are ploted separately.

9/2$^{(+)}$ 3175.7

9/2$^+$ 2727.9

7/2$^-$ 2339.9

13/2$^+$ 1633.4

15/2$^-$ 1423

3/2$^-$ 897.7

11/2$^+$ 778.8

3/2$^-$ 576.2

5/2$^-$ 569.7

3/2$^-$ 262.8

1/2$^-$ 2.3

1/2$^-$ 0.0

9/2$^+$ 0.0

5/2$^-$ 0.0
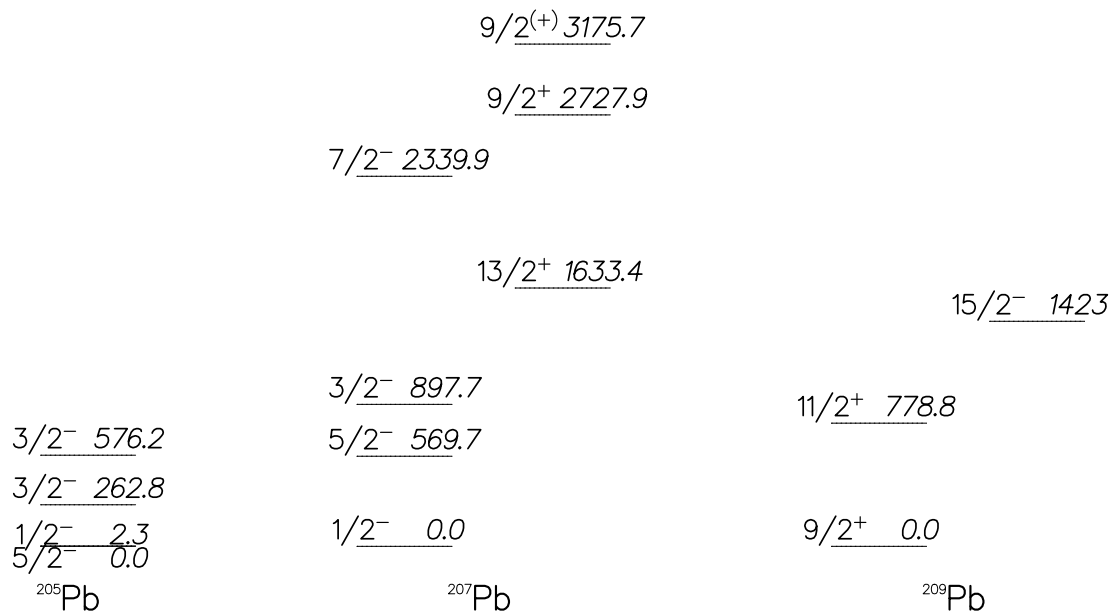
^{205}Pb

^{207}Pb

^{209}Pb

Figure 6.52: Simplified level schemes (only strongly excited states are plotted) of ^{205}Pb (left), ^{207}Pb (middle) and ^{209}Pb (right) isotopes. Positive and negative parities are plotted separately.

10⁺   5644.0

4⁺   5216.2

7⁻   4375.1

6⁺   4423.6
4⁺   4323.9
2⁺   4085.5

2⁺   3842.2

5⁻   3708.5

8⁺   3589.4
6⁺   3448.2
2⁺   3308.8

4⁻   3475.1

4⁺   3076.9

5⁻   3197.7

3⁻   2747.9
(4)⁻   2739.3

3⁻   2614.5

5⁻   2319.0

2⁺   2186.3

0⁺   0.0

⁹⁰Zr

0⁺   0.0
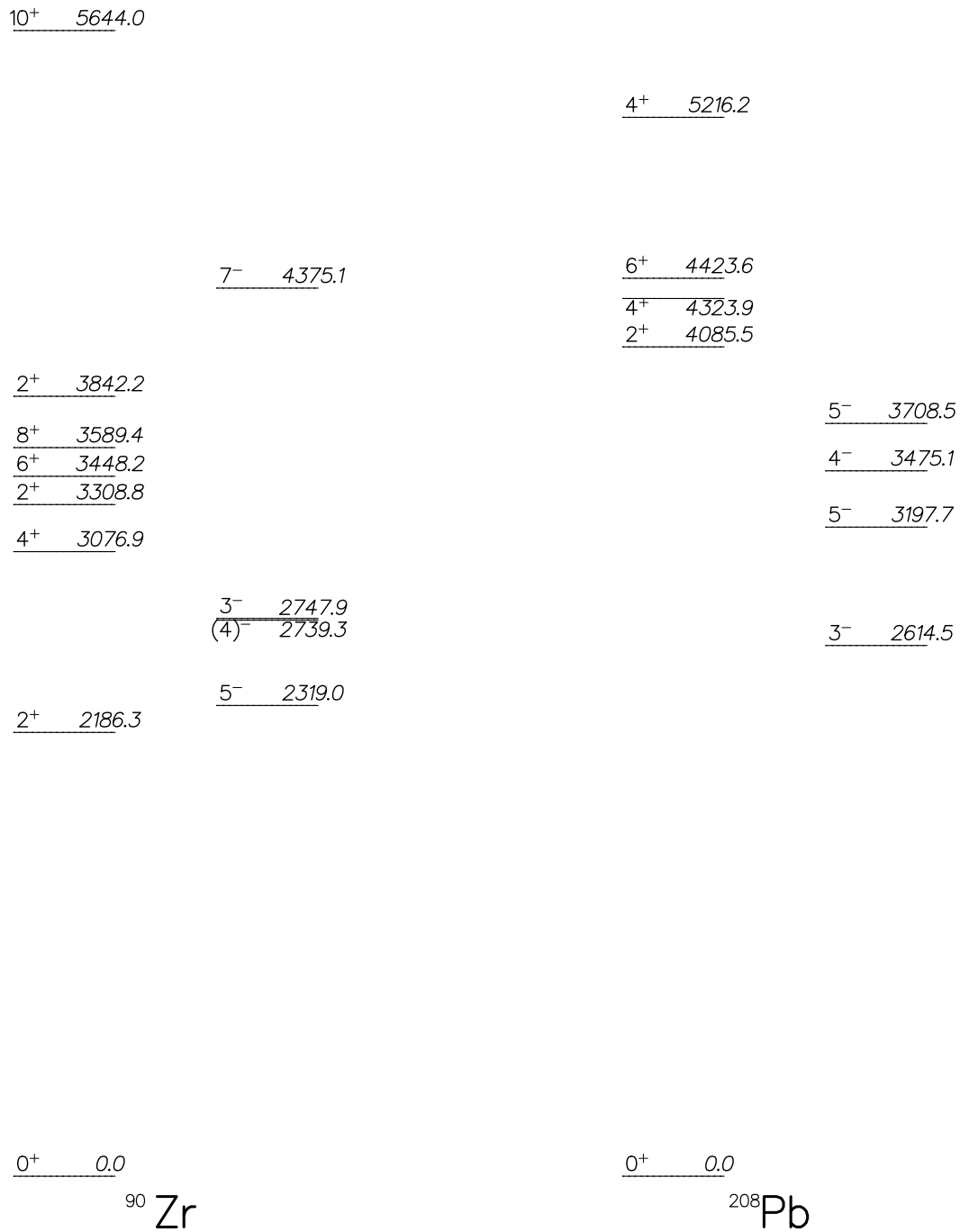
²⁰⁸Pb

Figure 6.53: Simplified level schemes of ⁹⁰Zr (left) and ²⁰⁸Pb (right) isotopes. Positive and negative parities are plotted separately.

6.5 Yttrium isotopes

Yttrium isotopes will be discussed in this chapter. The reaction ^{90}Zr+^{208}Pb excited yttrium isotopes with mass numbers $87 \leq A \leq 94$, that is, $(-1p - 2n)$ to $(-1p + 5n)$ channels. Yttrium nucleus has 39 protons, so it has one proton hole in the $2p_{1/2}$ orbital (see Fig. 6.54). It is shown that all the odd yttrium isotopes have ground state spin $1/2^-$, determined by this uncoupled proton.

Also, all the observed odd yttrium isotopes have a low-lying $9/2^+$ state, which can be a single-particle state with unpaired proton in the $1g_{9/2}$ orbital. A common feature of these states is that they all have a long lifetime (a few seconds) and decay mostly through isomeric transitions. Table 6.24 lists these states, together with their type of decay and lifetimes for all the observed yttrium isotopes.

Table 6.24: Isomeric states of observed yttrium isotopes. The first column lists the yttrium isotope of interest, the second and third columns show energies (E), spins and parities (J^π) of isomeric states, the fourth column lists the type of decay, together with the percentage of the decay, while the last column shows the lifetime of the state.

isotope	E_{ex} (keV)	J^π	type of decay	$T_{1/2}$
^{87}Y	380.8	9/2+	IT (98.43 %)	13.37 h
			ε (1.57 %)	
^{88}Y	392.9	1+	IT (100%)	0.301 ms
	674.6	8+	IT (100%)	13.98 ms
^{89}Y	909.0	9/2+	IT (100%)	15.663 s
^{90}Y	681.7	7+	(99.9982 %)	3.19 h
			β^- (0.0018 %)	
^{91}Y	555.6	9/2+	IT ($\approx$ 100%)	49.71 m
			β^- ($< 0.0018\%$)	
^{92}Y	$0.0 + X$	(J)		4.2 μs
^{93}Y	758.7	(9/2)+	IT (100%)	0.82 s
^{94}Y	1202.3	(5+)	γ	1.35 μs

With neutron numbers $48 \leq N \leq 55$, neutrons fill the $1g_{9/2}$ orbital for ^{87,88}Y and for $^{90-94}$Y, neutron $3\hbar\omega$ shell is closed, so neutrons fill the orbitals of the $4\hbar\omega$ shell (see Fig. 6.54).
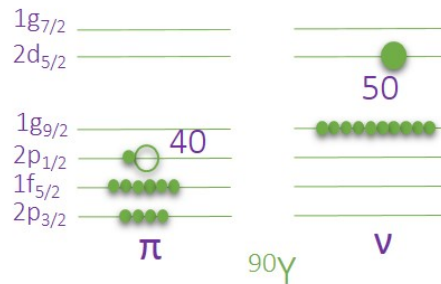
Figure 6.54: Schematic view of the proton and neutron orbitals of the ^{90}Y, according to the classical shell model

Analysis similar to zirconium isotopes will be conducted; all the γ spectra will be corrected through the procedure explained in Section 6.1, with subtracted spectra according to scaling factors listed in Table 6.25. In some γ spectra, γ rays from neighbouring nuclei appear, due to the "nonideal" charge separation (Q and Z), explained in Section 6.1.

Based on corrected γ spectra, γ rays will be recognized and level schemes for each isotope will be constructed. If any γ ray from plotted levels is missing from the level scheme, its absence is explained in the text. Most of the time, this absence is due to a low decay branch and the small number of expected events of the branch. All the missing γ rays are listed in Table 3 in the Appendix.

In several yttrium isotopes, yet unknown γ rays have been observed. When possible, their decays are suggested.

Table 6.25: Scaling factors and expressions used for correction of Y γ spectra. For example, corrected γ spectrum for ^{87}Y, with the name ^{87}Y$_{corr}$, has been obtained by subtraction of scaled ^{90}Y and ^{87}Sr spectra.

| corrected γ spectrum	mathematical expression used for the correction
^{87}Y$_{corr}$	^{87}Y-0.130*^{90}Y-0.100*^{87}Sr
^{88}Y$_{corr}$	^{88}Y-0.185*^{88}Sr
^{89}Y$_{corr}$	^{89}Y-0.215*^{89}Sr
^{90}Y$_{corr}$	^{90}Y-0.201*^{90}Sr
^{91}Y$_{corr}$	^{91}Y-0.146*^{90}Y
^{92}Y$_{corr}$	^{92}Y-0.212*^{92}Zr
^{93}Y$_{corr}$	^{93}Y-0.081*^{90}Y-0.071*^{93}Zr
^{94}Y$_{corr}$	^{94}Y-0.046*^{90}Y-0.055*^{92}Y

6.5.1 ^{87}Y
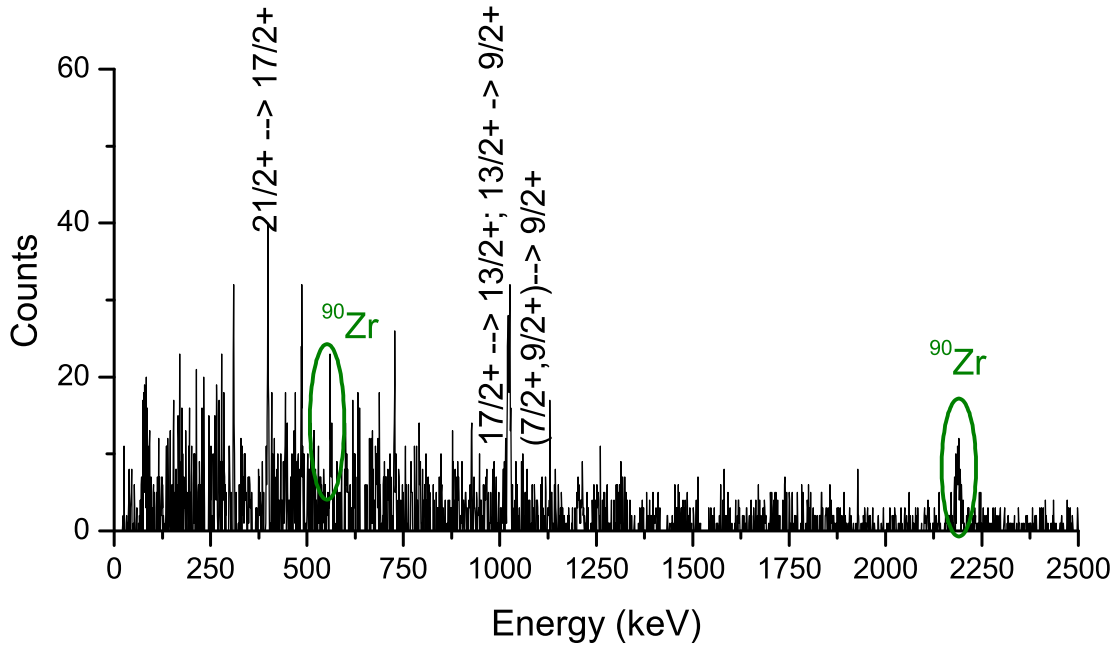
Figure 6.55: Doppler corrected γ spectrum of ^{87}Y. Spins and parities (as in [www4]) of initial and final states of the strongest transitions are tagged. Green areas denote $E_\gamma = 561.6$ and 2186.2 keV, which belong to ^{90}Zr.

Corrected spectrum of ^{87}Y is shown in Fig. 6.55, and recognized γ rays are listed in Table 6.26. Figure 6.56 shows high spin states that have been selectively observed in both, positive and negative parity bands. All the observed states above $15/2^-$ have so far been detected only with fusion-evaporation reactions, namely ^{85}Rb$(\alpha,\gamma 2n)$ ($E_{^{85}\text{Rb}} = 24.1 - 36.1$ MeV), ^{74}Ge$(^{18}$O$,\gamma 4np)$ ($E_{^{18}\text{O}} = 40 - 80$ MeV), ^{80}Se$(^{11}$B$,\gamma 4n)$ ($E_{^{11}\text{B}} = 45$ MeV) and ^{88}Sr$(p,\gamma 2n)$ ($E_p p = 22.8$ MeV).

$E_\gamma = 380.8$ keV from $E_{ex} = 380.8$ keV ($J^\pi = 9/2^+$) has not been observed in the spectrum because the level decays through isomeric transition, so this γ ray is drawn by a dashed line in Fig. 6.56. Also, $E_\gamma = 962.4$ keV from $E_i = 2366.9$ keV ($J_i = 15/2^-$) to $E_f = 1404.4$ keV ($J_i = 13/2^+$) has not been observed in the spectrum.

Table 6.26: γ transitions observed in the present work for the ^{87}Y isotope. The first column lists energies of γ rays (E_γ) in keV, the second and third columns show energies (E_i), spins and parities (J_i^π) of initial states, while energies (E_f), spins and parities (J_f^π) of final states are listed in the fourth and fifth columns. In the last column, transition intensities after taking into account the Clara efficiency, are listed (normalized to the strongest transition).

| E_γ (keV)	E_i (keV)	J_i^π	E_f (keV)	J_f^π (number)	I_γ (%)
309.1	2676.0	17/2-	2366.89	15/2-	35.44
399.1	2827.2	21/2+	2428.1	17/2+	62.77
486.4	4039.4	25/2+	3552.9	23/2+	42.56
725.8	3552.9	23/2+	2827.2	21/2+	21.97
726.4	3402.4	(19/2-)	2676.0	17/2-	39.05
1023.6	2428.1	17/2+	1404.4	13/2+	62.47
1024.0	1404.4	13/2+	380.8	9/2+	100.00
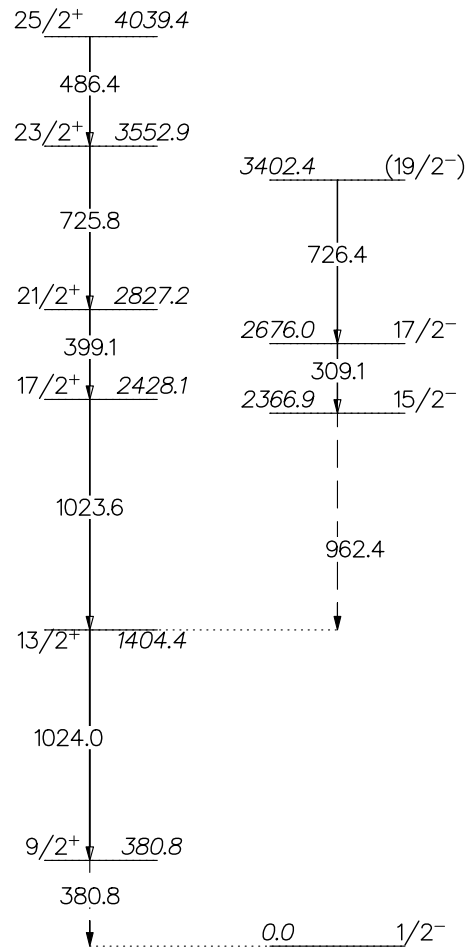
Figure 6.56: Experimental states observed in our measurement for ^{87}Y. Relative γ ray intensities are indicated by widths of arrows. Energies, spins and parities of levels, their branching ratios and energies of transitions are as in Ref. [www4]. In both, positive and negative parity bands, high spin levels have been selectively observed.
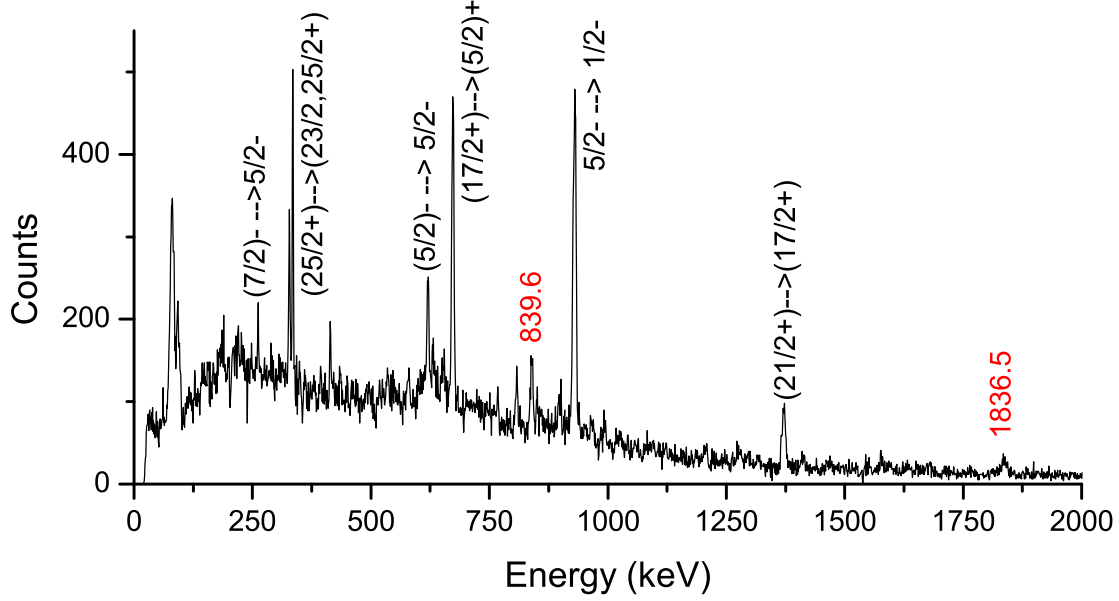
6.5.2 ^{88}Y
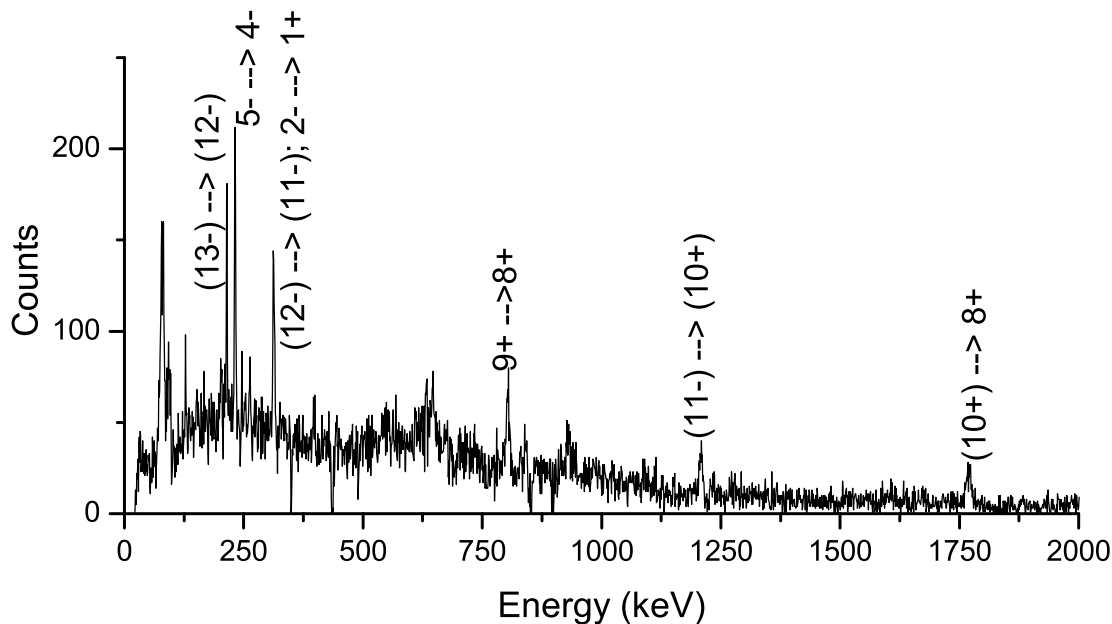
Figure 6.57: Doppler corrected γ spectrum of ^{88}Y. Spins and parities (as in [www4]) of initial and final states of the strongest transitions are tagged.

In Fig. 6.57, γ spectrum of ^{88}Y is shown, and recognized γ rays are listed in Table 6.27 and plotted in Fig. 6.58. In the positive parity band of ^{88}Y, states (10^+) (at $E_{ex} = 2443.9$ keV) and (9^+) (at $E_{ex} = 1476.9$ keV) have been strongly excited. In the negative parity band, the two lowest states have been excited, and then again high spin states (11^-), (12^-) and (13^-). These high spin states, together with 10^+ ($E_{ex} = 2443.9$ keV) have only been observed in fusion evaporation processes so far, namely ^{74}Ge(^{18}O,$\gamma 3np$) ($E_{^{18}O} = 40 - 80$ MeV), ^{76}Ge(^{18}O,$\gamma 5np$) ($E_{^{18}O} = 90$ MeV), ^{87}Rb($\alpha, \gamma 3n$) ($E_\alpha = 30 - 55$ MeV) and ^{85}Rb($\alpha, \gamma n$) ($E_\alpha = 11 - 14$ MeV).

It is notable that only $E_\gamma = 312.1$ keV from level $E_{ex} = 3964.2$ ($J^\pi = (12^-)$) has been observed, while the other known γ ray from the same level ($E_\gamma = 680.0$ keV) has not been observed. Intensities for both of these γ rays are unknown at the moment, thus we assume

that the observed $E_\gamma = 312.1$ keV has stronger intensity.

Two γ rays drawn by dashed lines ($E_\gamma = 392.2$ and $E_\gamma = 442.6$ keV) have not been observed because they decay through isomeric transitions. γ rays from plotted levels that have not been observed because of their low decay branches (which is in accordance with the expected number of events) are listed in Table 3 in the Appendix.

We have not observed $E_\gamma = 483.5$ keV from $E_{ex} = 715.1$ keV ($J^\pi = (6)^+$), which leads us to reconsider the $E_\gamma = 128.0$ keV from $E_i = 843.0$ keV ($J_i^\pi = (5)^+$) to $E_f = 715.1$ keV ($J_f^\pi = (6)^+$). It is possible that the $E_\gamma = 128.0$ keV does not belong to the abovementioned transition, but may decay from another excited level.

Table 6.27: γ transitions observed in the present work for the ^{88}Y isotope. The first column lists energies of γ rays (E_γ) in keV, the second and third columns show energies (E_i), spins and parities (J_i^π) of initial states, while energies (E_f), spins and parities (J_f^π) of final states are listed in the fourth and fifth columns. In the last column, transition intensities after taking into account the Clara efficiency, are listed (normalized to the strongest transition).

E_γ (keV)	E_i (keV)	J_i^π	E_f (keV)	J_f^π (number)	I_γ (%)
128.0	843.0	(5)+	715.1	(6)+	11.40
214.8	4178.2	(13-)	3964.2	(12-)	35.64
231.9	231.9	5-	0.0	4-	57.97
312.1	3964.2	(12-)	3652.1	(11-)	38.63
313.9	706.8	2-	392.9	1+	18.54
802.3	1476.9	9+	674.6	8+	90.01
1208.3	3652.1	(11-)	2443.9	(10+)	74.30
1769.3	2443.9	(10+)	674.6	8+	100.00

Since this nucleus has one neutron hole in the $N = 50$ shell and one proton hole in the subshell at $Z = 40$, its low-lying excitations are likely to be characterized by simple single-particle configurations that can be well described by the spherical-basis shell model. Figure 6.59 shows shell model calculations for the ^{88}Y taken from [Bun13]. The calculations were carried out in the valence space that covered the major shell from $Z, N = 28 - 50$, with a ^{56}Ni
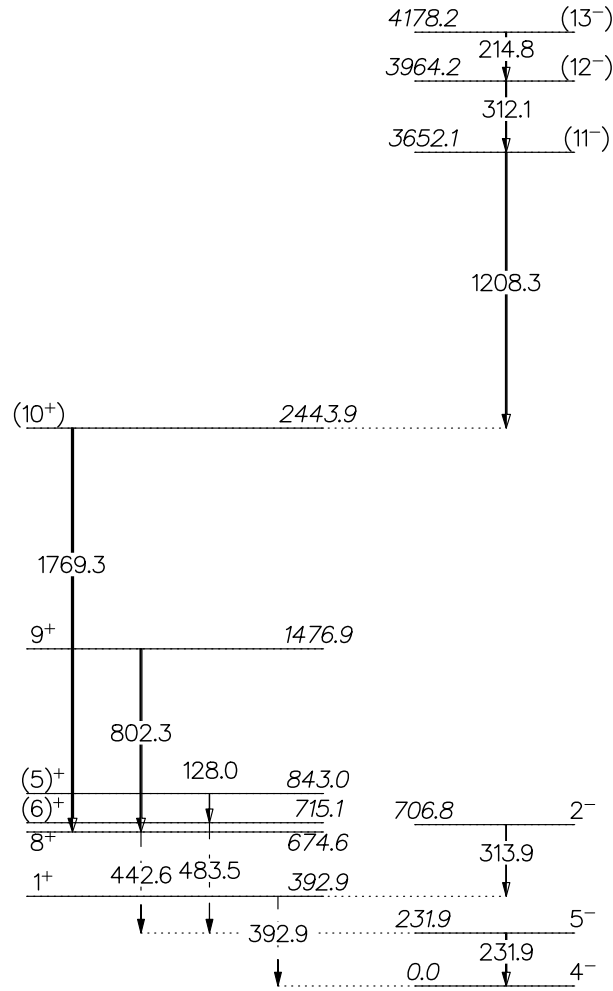
Figure 6.58: Experimental states observed in our measurement for ^{88}Y. Relative γ ray intensities are indicated by widths of arrows. Energies, spins and parities of levels, their branching ratios and energies of transitions are as in Ref. [www4]. The strongest γ rays decay from high spin states in both, positive and negative parity bands.

inert core. No subshell truncations were applied, allowing the valence particles to move freely between the $f_{5/2}$, $p_{3/2}$, $p_{1/2}$ and $g_{9/2}$ single-particle orbitals. According to these calculations, the wave functions of the 4^-, 5^-, 8^+ and 9^+ states observed in our measurement have more than 80% single-particle configuration.
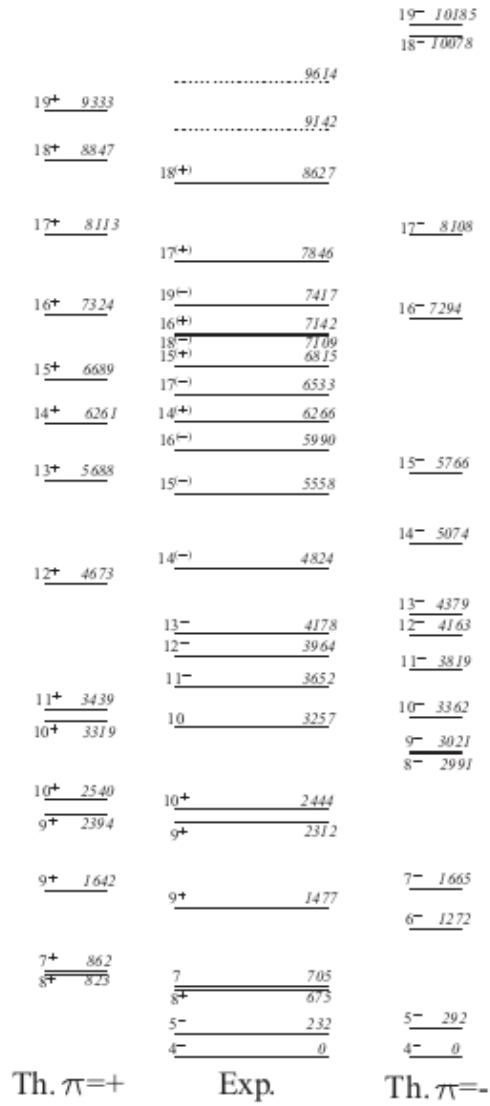
Figure 6.59: Experimental level scheme for ^{88}Y, alongside shell-model calculations, taken from [Bun13]. The calculations were carried out in the valence space that covered the major shell from $Z, N = 28 - 50$, with a ^{56}Ni inert core.

6.5.3 ^{89}Y
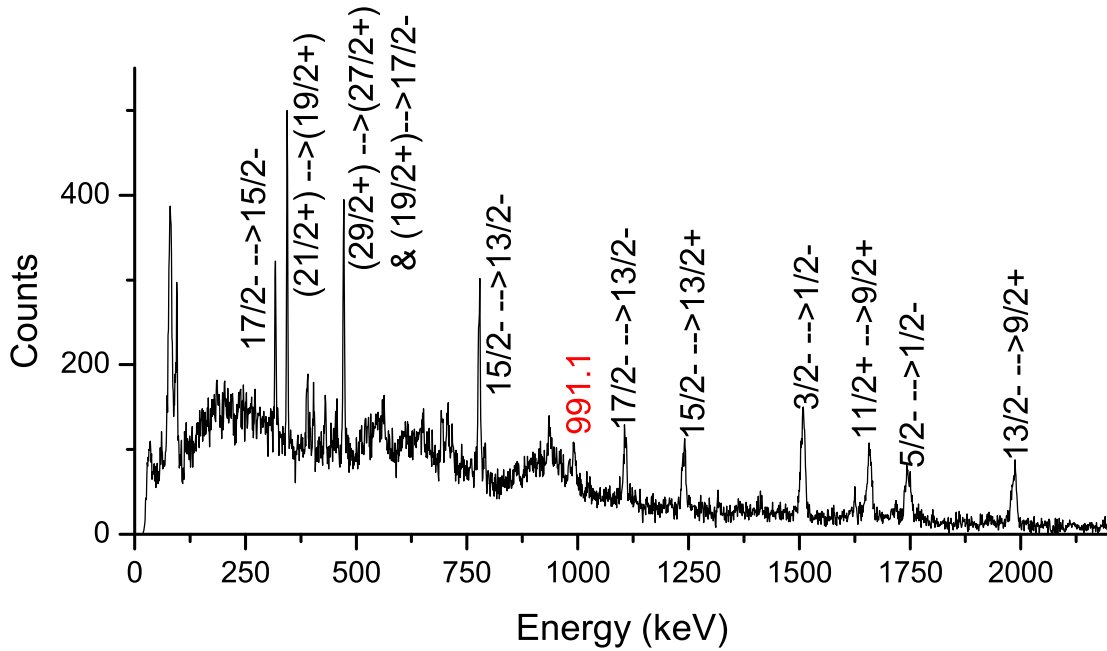
Figure 6.60: Doppler corrected γ spectrum of ^{89}Y. Spins and parities (as in [www4]) of initial and final states of strongest transitions are tagged. Energy (in keV) of a yet unknown γ ray (i.e. γ ray which could not be placed in the level scheme) is written in red.

Figure 6.60 shows γ spectrum of ^{89}Y, and Table 6.28 lists its observed γ rays. Figure 6.61 shows that, besides the first two lowest states in the negative parity band, high spin states have been selectively observed, and with energies up to ~ 8 MeV. Again, we notice that all the observed levels above ~ 4000 keV have been detected only in fusion-evaporation processes, namely ^{74}Ge(^{18}O,$\gamma 2np$), ^{76}Ge(^{18}O,$\gamma 4np$) ($E_{^{18}\text{O}} = 40 - 80$ MeV) and ^{87}Rb($\alpha,\gamma 2n$) ($E_\alpha = 27 - 36$ MeV).

Some γ rays from plotted levels from Fig. 6.61 have not been observed, which is expected because of their low decay branch, and they are listed in Table 3 in the Appendix. The state at $E_{\text{ex}} = 909.0$ keV, the lowest positive parity $9/2^+$ state, has a lifetime of $T_{1/2} = 16$ s, so $E_\gamma = 909.0$ keV from this level has not been observed. Also, $E_\gamma = 1232.6$ keV (from

$E_i = 7431.6$ keV, $J_i = (25/2^+)$ to $E_f = 6198.9$ keV, $J_f = (23/2^+)$) probably has not been observed because of its high energy, for which the detector efficiency decreases.

Table 6.28: γ transitions observed in the present work for the ^{89}Y isotope. The first column lists energies of γ rays (E_γ) in keV, the second and third columns show energies (E_i), spins and parities (J_i^π) of initial states, while energies (E_f), spins and parities (J_f^π) of final states are listed in the fourth and fifth columns. In the last column, transition intensities after taking into account the Clara efficiency, are listed (normalized to the strongest transition).

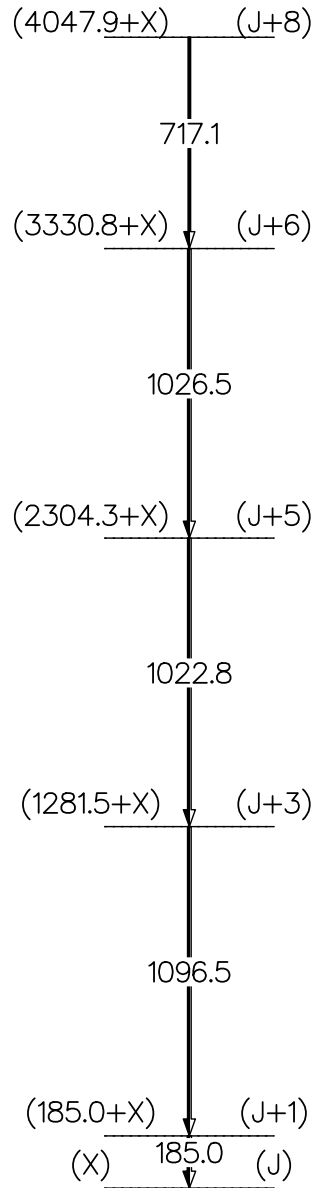| E_γ (keV)	E_i (keV)	J_i^π	E_f (keV)	J_f^π (number)	I_γ (%)
317.5	4449.8	17/2-	4132.2	15/2-	22.06
343.4	5263.9	(21/2+)	4920.5	(19/2+)	34.53
388.9	4838.6	19/2-	4449.8	17/2-	15.11
402.9	7834.6	(27/2+)	7431.6	(25/2+)	10.96
429.6	8264.2	(29/2+)	7834.6	(27/2+)	11.06
470.7	4920.5	(19/2+)	4449.8	17/2-	28.63
471.1	5309.8	(21/2-)	4838.6	19/2-	14.46
693.2	4825.4	17/2+	4132.2	15/2-	25.70
706.3	4838.6	19/2-	4132.2	15/2-	28.22
776.9	3343.4	13/2-	2566.6	11/2+	72.70
788.6	4132.2	15/2-	3343.4	13/2-	15.70
935.0	6198.9	(23/2+)	5263.9	(21/2+)	24.98
991.1(2)*					25.08
1106.5	4449.8	17/2-	3343.4	13/2-	55.86
1239.3	4132.2	15/2-	2893.0	13/2+	62.93
1507.4	1507.4	3/2-	0.0	1/2-	100.00
1620.8	2529.8	7/2+	909.0	9/2+	20.12
1657.5	2566.6	11/2+	909.0	9/2+	80.67
1744.7	1744.7	5/2-	0.0	1/2-	80.36
1984.1	2893.0	13/2+	909.0	9/2+	73.92
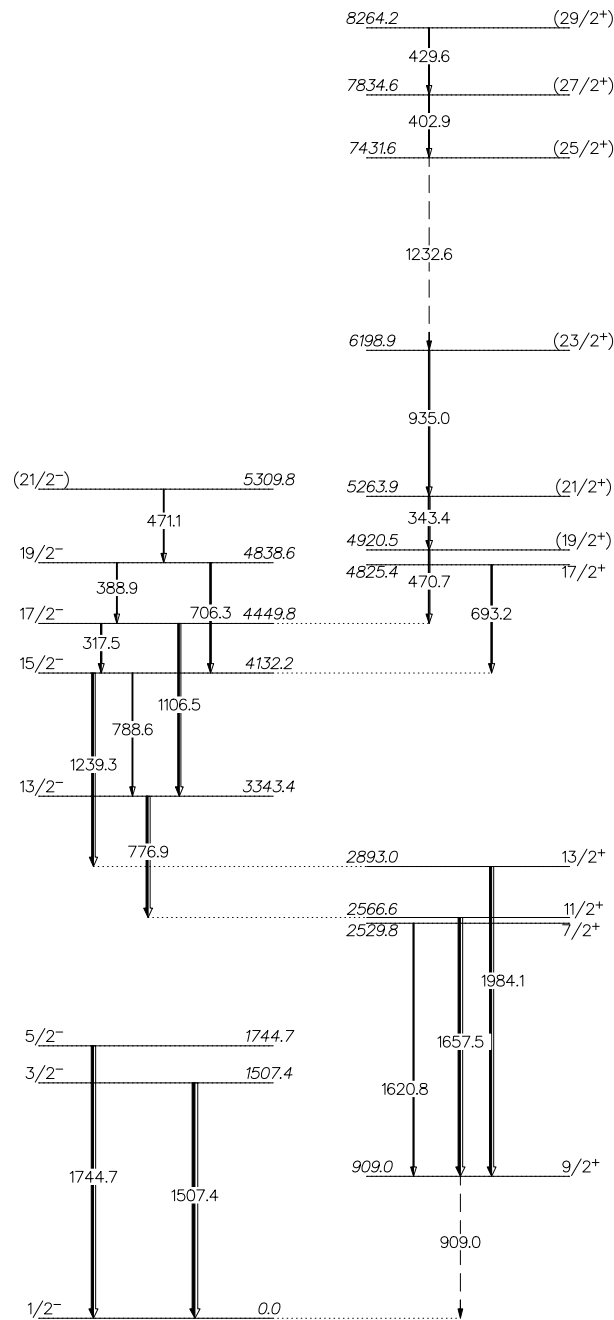
Figure 6.61: Experimental states observed in our measurement for ^{89}Y. Relative γ ray intensities are indicated by widths of arrows. Energies, spins and parities of levels, their branching ratios and energies of transitions are as in Ref. [www4]. Besides the first two excited states in the negative parity bands, high spin states have been selectively observed.
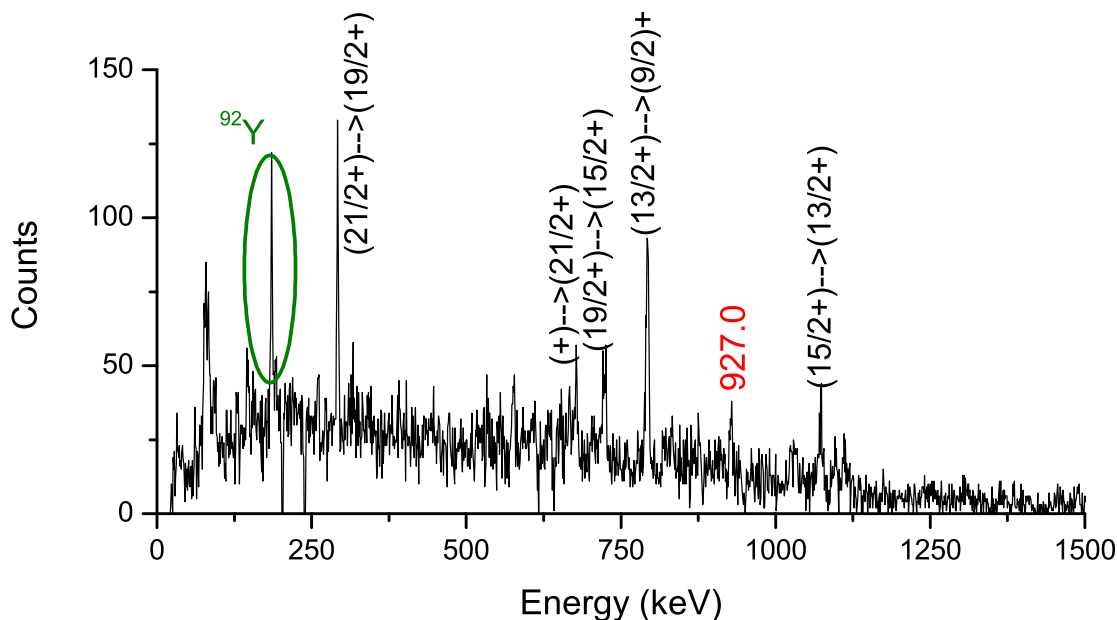
6.5.4 ^{90}Y
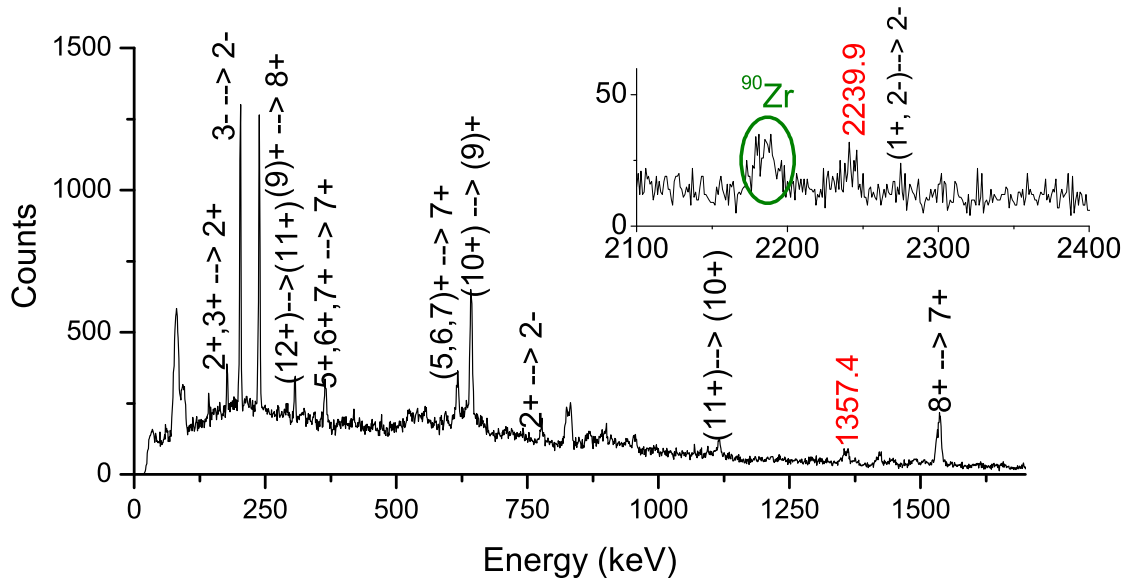
Figure 6.62: Doppler corrected γ spectrum of ^{90}Y. Spins and parities (as in [www4]) of initial and final states of the strongest transitions are tagged. Green area denotes $E_\gamma = 2186.2$ keV, which belongs to ^{90}Zr. Energies (in keV) of yet unknown γ rays (i.e. γ rays which could not be placed in the level scheme) are written in red.

Spectroscopic data concerning the ^{90}Y isotope come from different reactions. This nucleus was extensively studied in light-ion induced transfer reactions, using p, d, t, ^{3}He, and α as a probe, and by using heavier projectiles as ^{16}O, ^{12}C and ^{14}C. It has also been studied in fusion-evaporation reactions, Coulomb excitations, β^- decay etc. (see [www4] and references therein).

In the spectrum of ^{90}Y (see Figs. 6.62 and 6.63) all known excited levels up to $E_{ex} = 1189.7$ keV have been observed. All the observed γ rays are listed in Table 6.29. $E_\gamma = 2186.2$ keV (denoted green in Fig. 6.62), which appears in the spectrum of ^{90}Y, belongs to ^{90}Zr and it is one of the strongest γ rays among Zr isotopes. $E_\gamma = 479.2$ keV from $E_{ex} = 681.7$ keV has not been observed because its lifetime ($T_{1/2} = 3.19$ h) is too long for the prompt γ rays to be

observed (as explained earlier) and it primarily decays through isomeric transition, so it is denoted by a dashed line in Fig. 6.63. Some other γ rays from plotted levels have not been observed, which is expected because of their low decay branch, and they are listed in Table 3 in the Appendix.

Two γ rays are denoted by $*$ in Table 6.29. There are known transitions to which they could belong, but since we have not observed other strong γ rays that decay from same levels as those two rays, we left them out of the level scheme in Fig. 6.63 and suggest that they belong to another, yet unknown decay.

Again, high spin levels (above $J^\pi = 8^+$) observed with this experiment have previously been detected only in fusion-evaporation reactions: ^{74}Ge(^{18}O,γnp) and ^{76}Ge(^{18}O,$\gamma 3np$) ($E_{^{18}O} = 40 - 80$ MeV).

Table 6.29: γ transitions observed in the present work for the ^{90}Y isotope. The first column lists energies of γ rays (E_γ) in keV, the second and third columns show energies (E_i), spins and parities (J_i^π) of initial states, while energies (E_f), spins and parities (J_f^π) of final states are listed in the fourth and fifth columns. In the last column, transition intensities after taking into account the Clara efficiency, are listed (normalized to the strongest transition).

| E_γ (keV)	E_i (keV)	J_i^π	E_f (keV)	J_f^π (number)	I_γ (%)
142.5	1189.7		1046.9	5+,6+,7+	4.09
176.9	953.5	2+,3+	776.6	2+	9.28
202.5	202.5	3-	0.0	2-	46.17
236.2	1189.7		953.5	2+,3+	10.50
238.5	2455.3	(9)+	2216.8	8+	38.64
306.1	4518.8	(12+)	4212.7	(11+)	9.71
365.2	1046.9	5+,6+,7+	681.7	7+	17.60
616.1	1298.2	(5,6,7)+	681.7	7+	46.83
642.3	3097.6	(10+)	2455.3	(9)+	100.00
776.6	776.6	2+	0.0	2-	24.80
953.5	953.5	2+,3+	0.0	2-	25.88
1115.2	4212.7	(11+)	3097.6	(10+)	34.05
1357.4(9)*					25.91
1421.3	4518.8	(12+)	3097.6	(10+)	30.60
1534.6	2216.8	8+	681.7	7+	95.30
2239.9(7)*					19.46
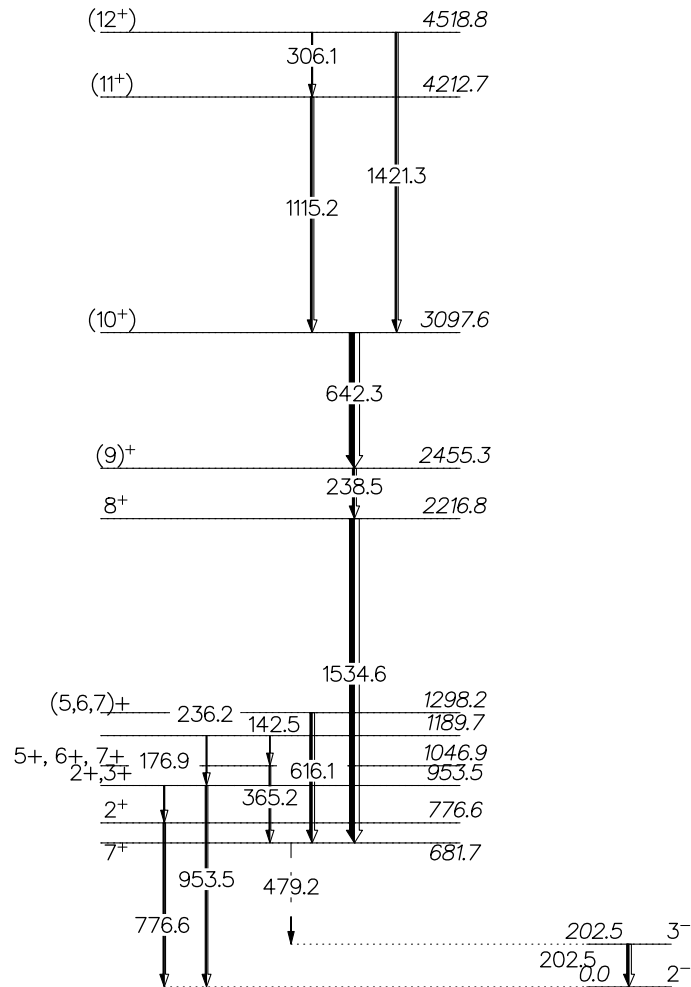
Figure 6.63: Experimental states observed in our measurement for ^{90}Y. Relative γ ray intensities are indicated by widths of arrows. Energies, spins and parities of levels, their branching ratios and energies of transitions are as in Ref. [www4]. All known energy levels up to $E_{\mathrm{ex}} = 1189.7$ keV have been observed. Above ~ 2000 keV, only high spin states have been selectively observed.

6.5.5 ^{91}Y

Figure 6.64: Doppler corrected γ spectrum of ^{91}Y. Spins and parities (as in [www4]) of initial and final states of the strongest transitions are tagged. Energies (in keV) of yet unknown γ rays (i.e. γ rays which could not be placed in the level scheme) are written in red.

Figure 6.64 shows γ spectrum of ^{91}Y, while Table 6.30 lists all the observed γ rays. Figs. 6.64 and 6.65 show that the strongest transition is from the first $5/2^-$ state ($E_{ex} = 925.7$ keV). In addition, most of the transfer flux is in the decay from high positive parity spin states. Some of the plotted levels do not have definite parities [www4], but they have been placed in the positive parity band because of succeeding cascades. All the observed energy levels in the positive parity band with energies above $E_{ex} = 1305.4$ keV have only been detected in fusion-evaporation processes so far: ^{12}C(^{82}Se, $\gamma 2np$) ($E_{^{12}C} = 38$ MeV), ^{173}Yb(^{24}Mg, $X\gamma$) ($E_{^{24}Mg} = 134.5$ MeV) and ^{176}Yb(^{23}Na, $X\gamma$) ($E_{^{23}Na} = 129$ MeV).

$E_\gamma = 555.6$ keV has not been observed because the level $E_{ex} = 555.6$ keV ($J^\pi = 9/2^+$) decays through isomeric transition, so this γ ray was plotted with a dashed line. Some other γ rays that haven't been observed due to their low decay branch are listed in Table 3 in

the Appendix. Also, there is one rather strong γ ray which we expected to observe, namely, $E_\gamma = 749.8$ keV ($E_i = 1305.4$ keV, $J_i^\pi = (5/2)^+$ to $E_f = 555.6$ keV, $J_i^\pi = 9/2^+$), but at this moment, we cannot explain its absence from the spectrum (also drawn by a dashed line). Two new γ rays have been observed and they are denoted by * in Table 6.30.

$E_\gamma = 619.2$ keV decays from $E_{ex} = 4147.0$ keV ($J^\pi = 23/2, 25/2^+$), but we leave the possibility that part of its decay flux belongs also to the transition from $E_i = 1545.9$ keV ($J_i^\pi = (5/2)^-$) to $E_f = 925.7$ keV ($J_i^\pi = 5/2^-$), as stated in Table 6.30. Since we have not observed similar transitions, i.e. transitions from second $5/2_2^-$ state, in other yttrium isotopes, we believe that this possibility is rather weak.

The state at $E_{ex} = 4808.5$ keV does not have definite parity. Based on similarity with ^{89}Y, where γ cascade starts at spin $(29/2^+)$ and decays through $(27/2^+) \longrightarrow (25/2^+) \longrightarrow (23/2^+) \longrightarrow (21/2^+) \longrightarrow (19/2^+)$ etc., we suggest that the state $E_{ex} = 4808.5$ keV in ^{91}Y has spin state $27/2^+$. Also, we believe that state at $E_{ex} = 4147.0$ keV, for which tabulated spin (from [www4]) is $(23/2, 25/2^+)$, has spin $23/2^+$, and then decays to $E_{ex} = 3527.7$ with spin $(21/2^+)$.

Table 6.30: γ transitions observed in the present work for the ^{91}Y isotope. The first column lists energies of γ rays (E_γ) in keV, the second and third columns show energies (E_i), spins and parities (J_i^π) of initial states, while energies (E_f), spins and parities (J_f^π) of final states are listed in the fourth and fifth columns. In the last column, transition intensities after taking into account the Clara efficiency, are listed (normalized to the strongest transition).

E_γ (keV)	E_i (keV)	J_i^π	E_f (keV)	J_f^π (number)	I_γ (%)
261.2	1186.9	(7/2)-	925.7	5/2-	10.38
327.4	4808.5		4481.2	(25/2+)	19.13
334.2	4481.2	(25/2+)	4147.0	(23/2, 25/2+)	24.78
413.8	4147.0	(23/2, 25/2+)	3733.2	(19/2, 21/2)	9.80
619.2	4147.0	(23/2, 25/2+)	3527.7	(21/2+)	34.73
620.1	1545.9	(5/2)-	925.7	5/2-	
631.3	1186.9	(7/2)-	555.6	9/2+	20.65
672.0	2157.1	(17/2+)	1305.4	(5/2)+	42.65
806.2	3568.1	(19/2, 21/2)	2761.9	(15/2, 17/2)	15.24
839.6(3)*					27.10
925.8	925.7	5/2-	0.0	1/2-	100.00
929.5	1485.1	(13/2+)	555.6	9/2+	26.44
1276.8	2761.9	(15/2, 17/2)	1485.1	(13/2+)	20.54
1370.6	3527.7	(21/2+)	2157.1	(17/2+)	28.75
1576.3	3733.2	(19/2, 21/2)	2157.1	(17/2+)	10.51
1836.5(6)*					13.72
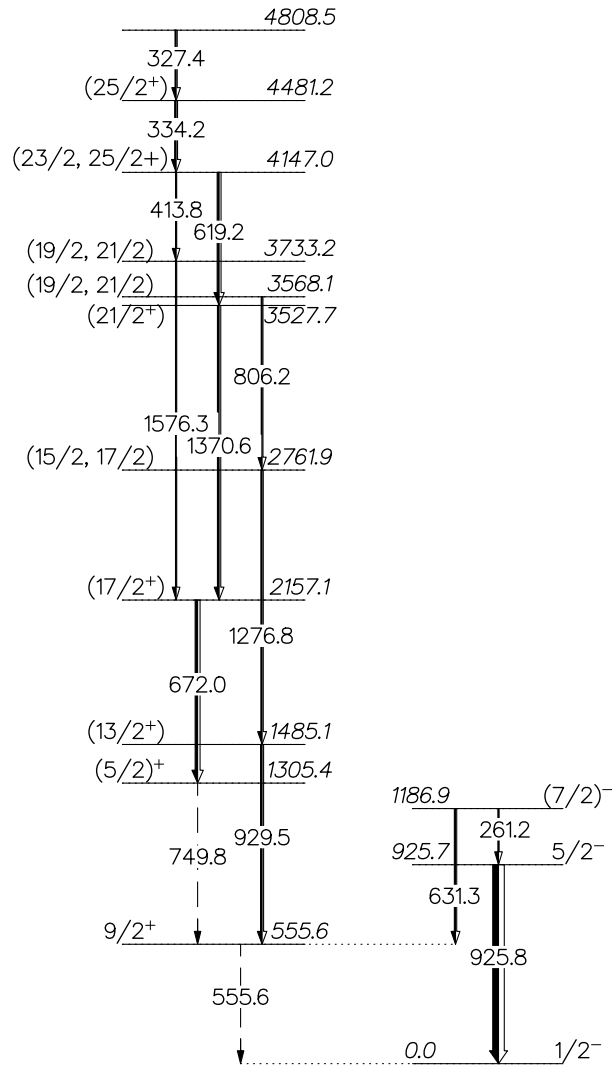
Figure 6.65: Experimental states observed in our measurement for ^{91}Y. Relative γ ray intensities are indicated by widths of arrows. Energies, spins and parities of levels, their branching ratios and energies of transitions are as in Ref. [www4]. Strongest γ rays decay from high positive parity spin states.

6.5.6 ^{92}**Y**
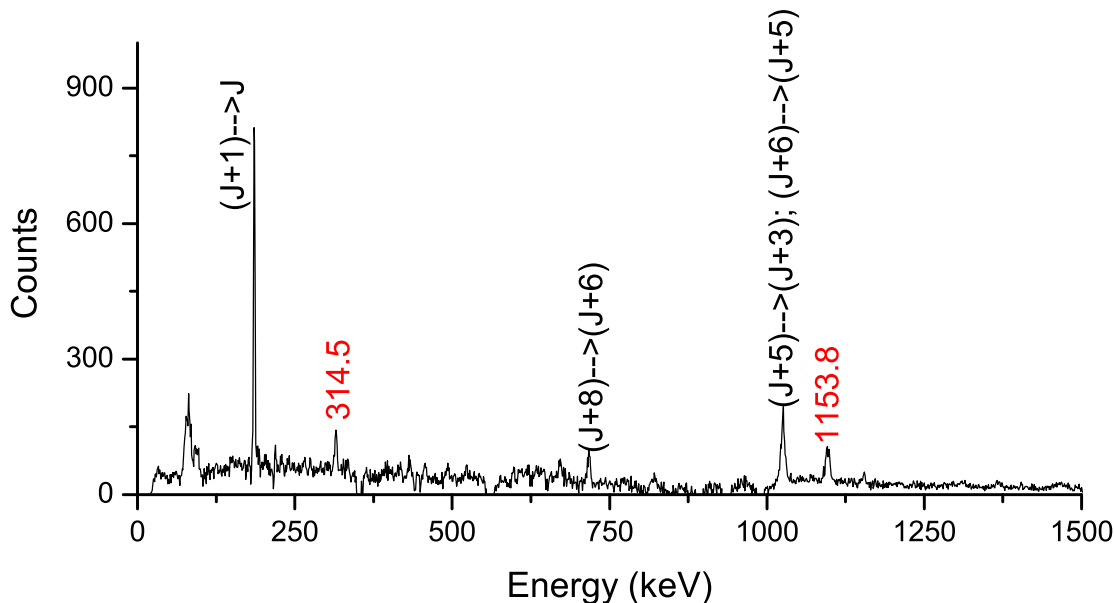
Figure 6.66: Doppler corrected γ spectrum of ^{92}Y. Spins and parities (as in [www4]) of initial and final states of the strongest transitions are tagged. Energies (in keV) of yet unknown γ rays (i.e. γ rays which could not be placed in the level scheme) are written in red.

There are a few strong γ rays in the spectrum of ^{92}Y (Fig. 6.66), and they belong to transitions listed in Table 6.31. Clearly, from Table 6.31 and Fig. 6.67, only relative energies and spins of energy levels from which these γ rays decay are known at this time. From the level scheme, we see that the observed γ rays form a cascade that ends at the isomer state with energy $E_{ex} = 0.0 + X$ keV, which is a pattern similar to what we observed with other yttrium and zirconium isotopes, where we noticed strong excitation of yrast spin states. That is why we expect that spins of the excited levels of ^{92}Y belong to the yrast line. It is noticeable that all the observed levels were detected only in fusion-evaporation reactions so far; ^{238}U(^{82}Se, $X\gamma$) ($E_{^{82}\text{Se}} = 505$ MeV) and ^{208}Pb(^{90}Zr, $X\gamma$) ($E_{^{90}\text{Zr}} = 590$ MeV).

Two unknown γ rays have been observed, and they are denoted by * in Table 6.31. $E_\gamma = 314.5$ keV could be a γ ray that decays from $E_i = 310(10)$ keV ($J_i^\pi = 2^-, 3^-, 4^-$) to

the ground state ($J_f^\pi = 2^-$), based on energy difference between energy levels.

Table 6.31: γ transitions observed in the present work for the ^{92}Y isotope. The first column lists energies of γ rays (E_γ) in keV, the second and third columns show energies (E_i), spins and parities (J_i^π) of initial states, while energies (E_f), spins and parities (J_f^π) of final states are listed in the fourth and fifth columns. In the last column, transition intensities after taking into account the Clara efficiency, are listed (normalized to the strongest transition).

E_γ (keV)	E_i (keV)	J_i^π	E_f (keV)	J_f^π (number)	I_γ (%)
185.0	185.0+X	(J+1)	X	J	100.00
314.5(1)*					34.64
717.1	4047.9+X	J+8	3308.8+X	J+6	60.15
1022.8	2304.3+X	J+5	1281.5+X	J+3	84.80
1026.5	3330.8+X	J+6	2304.3+X	J+5	83.90
1096.5	1281.5+X	J+3	185.0+X	J+1	85.72
1153.8(7)*					29.97

(4047.9+X)   (J+8)

717.1

(3330.8+X)   (J+6)

1026.5

(2304.3+X)   (J+5)

1022.8

(1281.5+X)   (J+3)

1096.5

(185.0+X)   (J+1)
(X)   185.0   (J)

Figure 6.67: Experimental states observed in our measurement for ^{92}Y. Relative γ ray intensities are indicated by widths of arrows. Energies, spins and parities of levels, their branching ratios and energies of transitions are as in Ref. [www4]. Only relative energies and spins of plotted energy levels are known at this time. All the observed γ rays form a cascade.

6.5.7 ^{93}Y

Figure 6.68: Doppler corrected γ spectrum of ^{93}Y. Spins and parities (as in [www4]) of initial and final states of the strongest transitions are tagged. Energy (in keV) of a yet unknown γ ray (i.e. γ ray which could not be placed in the level scheme) is written in red. $E_\gamma = 185.0$ keV (green area in the spectrum) belongs to ^{92}Y.

The ^{93}Y nucleus was not so extensively studied. The majority of data come from transfer reactions, induced with (very) light ions (p, d, ^{3}He and α), which will be discussed in more details later on. Recently, ^{93}Y has also been produced as fission fragment following fusion reactions ^{31}P+^{176}Yb, ^{24}Mg+^{173}Yb, ^{36}S+^{162}Dy [Pan05, Fot02].

In the spectrum of ^{93}Y (Fig. 6.68), only four γ rays have been assigned to known transitions and they are listed in Table 6.32 and shown in Fig. 6.23. Figure 6.69 shows that all the observed γ rays form a cascade, similar to ^{91}Y, and also, that the excited levels belong to the yrast line. Again, we encounter the situation that all the observed states have previously been observed only in fusion-evaporation reaction, namely, ^{238}U(^{82}Se, $X\gamma$) with $E_{^{82}\text{Se}} = 505$

MeV. $E_\gamma = 168.5$ keV is represented by dashed line in Fig. 6.23 because level $E_{\text{ex}} = 758.7$ keV decays through isomeric transition, thus it has not been observed in the experiment. Also, the state at $E_{\text{ex}} = 590.2$ keV has not been directly excited, so $E_\gamma = 590.2$ keV has not been observed. One new γ ray has been observed and it is denoted by * in Table 6.32.

Table 6.32: γ transitions observed in the present work for the ^{93}Y isotope. The first column lists energies of γ rays (E_γ) in keV, the second and third columns show energies (E_i), spins and parities (J_i^π) of initial states, while energies (E_f), spins and parities (J_f^π) of final states are listed in the fourth and fifth columns. In the last column, transition intensities after taking into account the Clara efficiency, are listed (normalized to the strongest transition).

| E_γ (keV)	E_i (keV)	J_i^π	E_f (keV)	J_f^π (number)	I_γ (%)
291.4	3636.8	(21/2+)	3345.4	(19/2+)	33.11
677.2	3414.0	(+)	3636.8	(21/2+)	25.69
722.6	3345.4	(19/2+)	2622.8	(15/2+)	59.52
791.7	1550.4	(13/2+)	758.7	(9/2)+	100.00
927.0(3)*					35.54
1072.4	2622.8	(15/2+)	1550.4	(13/2+)	83.86
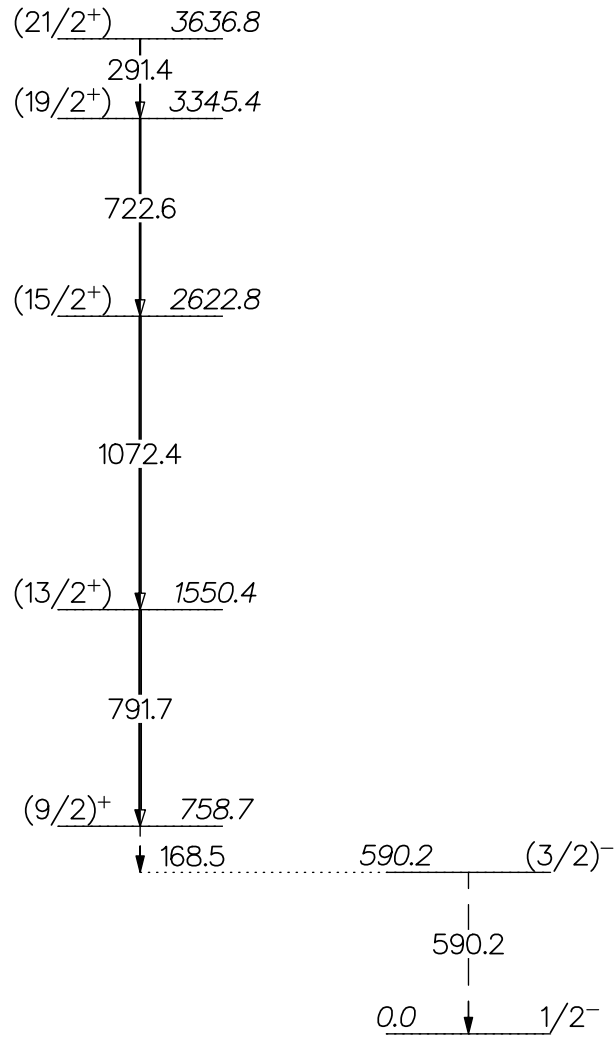
Figure 6.69: Experimental states observed in our measurement for ^{93}Y. Relative γ ray intensities are indicated by widths of arrows. Energies, spins and parities of levels, their branching ratios and energies of transitions are as in Ref. [www4]. High spin levels in the positive parity band have been selectively observed.

6.5.8 ^{94}Y
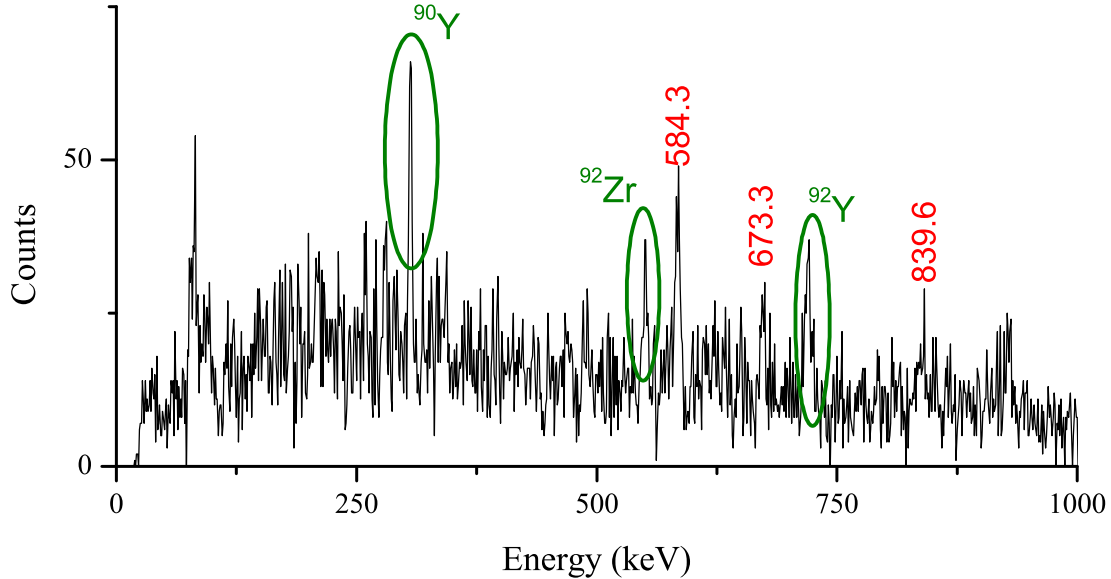
Figure 6.70: Doppler corrected γ spectrum of ^{94}Y. Energies (in keV) of yet unknown γ rays (i.e. γ rays which could not be placed in the level scheme) are written in red. Green areas in the spectrum denote γ rays that belong to other elements, as marked.

High spin states of ^{94}Zr have been studied in fusion-fission reactions [Pan05, Fot02]. Beside β-decay and Coulomb excitations, most of the data are from the n, p, d, t, ^{3}He and α scattering experiments (see [www4] and references therein). Limited information is available from transfer reactions: ^{92}Zr(t,p) [Fly74], ^{96}Zr(p,t) [BAR71], ^{98}Mo$(d,^6$Li) [SJP79], ^{94}Mo$(^6$Li,^{8}B) [TGB82], and ^{94}Mo$(^{14}$C,^{16}O) [May82].

Figure 6.70 shows ^{94}Y γ spectrum and Table 6.33 lists observed γ rays. We noticed that several γ rays belong to stronger transfer channels with the same Z (^{90}Y and ^{92}Y) or the same A (^{94}Zr). They are listed in Table 6.33 and denoted in Fig. 6.70. Besides these γ rays, we also observed yet unknown γ rays, which are denoted by * in Table 6.34.

Based on the observed spectra of ^{90}Y and ^{92}Y, it can be concluded that the strongest γ rays form a cascade, therefore, a level scheme drawn in Fig. 6.69 is proposed. The sequence

Table 6.33: γ transitions observed in the present work for the ^{94}Y isotope. The first column lists energies of γ rays (E_γ) in keV, and the second column lists transition intensities after taking into account the Clara efficiency (normalized to the strongest transition).

E_γ (keV)	I_γ (%)
306.1	^{90}Y
550.9	^{94}Zr
584.3(2)*	76.56
673.3(2)*	55.76
717.1	^{92}Y
839.6(5)*	100.00

of proposed energy levels and associated γ rays is determined by intensities of observed γ rays. Proposed transitions are listed in Table 6.34.

Table 6.34: Suggested γ transitions for the observed γ rays in the present experiment for the ^{94}Y isotope. The first column lists energies of γ rays (E_γ) in keV, the second and third columns show energies (E_i) initial states and final states, respectively, and in the last column, transition intensities after taking into account the Clara efficiency, are listed (normalized to the strongest transition).

E_γ (keV)	E_i (keV)	E_f (keV)	I_γ (%)
584.3(2)*	$X + 1423.9$	$X + 839.6$	76.56
673.3(2)*	$X + 2097.2$	$X + 1423.9$	55.76
839.6(5)*	$X + 839.6$	X	100.00
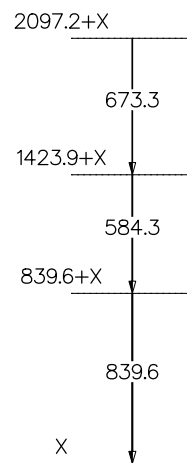
Figure 6.71: Suggested states and γ transitions for ^{94}Y. Relative γ ray intensities are indicated by widths of arrows.

6.6 General remarks about the Y spectra

As with zirconium isotopes, we would like to compare level schemes of odd and even yttrium isotopes. Figures 6.72 and 6.73 show strongly excited states of even and odd yttrium isotopes, respectively.

In schemes of even isotopes, high spin states have been excited. In the spectum of ^{90}Y, positive parity yrast states up to (12^+) have been observed, but in the negative parity band, only the first excited level is present. This may be explained in following way: if we compare spectra of all mentioned yttrium isotopes, we notice that high spin states have been selectively observed. In ^{90}Y, only low negative parity spin states are known at this time, making it possible for some of the observed γ rays to belong to a decay from a still unknown state of high spin and negative parity.

This selection of high spin states is also visible in the scheme of ^{92}Y, although only relative energies and spins of energy levels from which these γ rays decay are known at this time.

As noted in Section 6.7, one proton hole in the $2p_{1/2}$ orbital causes ground state spin of odd yttrium isotopes to be $1/2^-$. Single particle proton states we expect to encounter in odd Y isotopes are $5/2^-$, $3/2^-$ and $7/2^-$ caused by proton hole in the $1f_{5/2}$, $2p_{3/2}$ or $1f_{7/2}$ orbital, some of which we have observed in our experiment.

In level schemes of odd yttrium isotopes, again, we encounter selectivity of high spin levels (even up to $(29/2^+)$ in ^{89}Y) with high excitation energies. In the case of ^{91}Y and ^{93}Y, only the first few negative parity states have been observed. The reason may be that, for these isotopes, the decay of higher spin states, which we expect to observe (based on similarity with neighbouring isotopes), is still unknown, thus we cannot include them in our level scheme at this time.
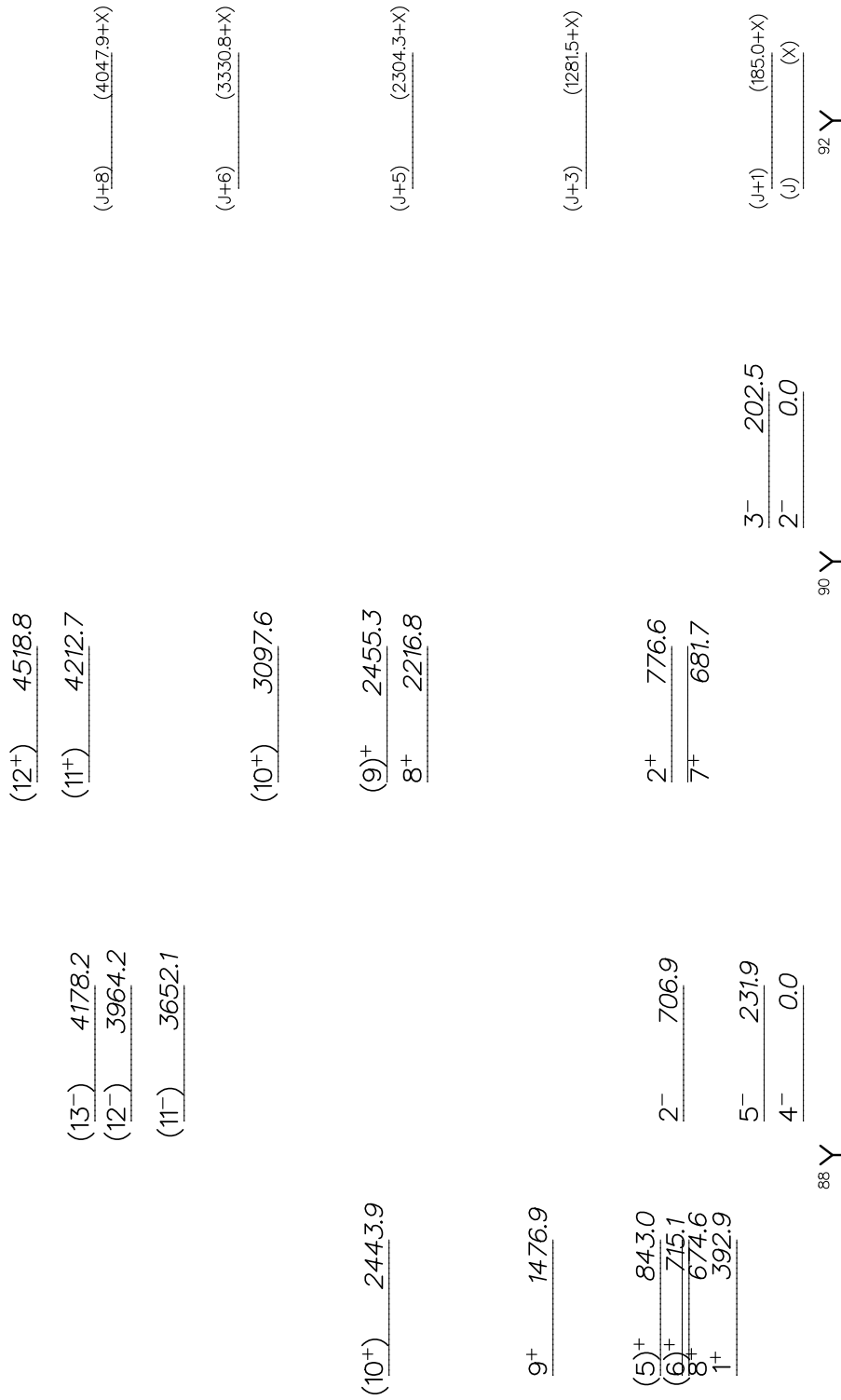
Figure 6.72: Simplified level schemes (only strongly excited states are plotted) of ^{88}Y (left), ^{90}Y (middle) and ^{92}Y (right) isotopes. For ^{88,90}Y, positive (left) and negative (right) parity states are plotted separately.
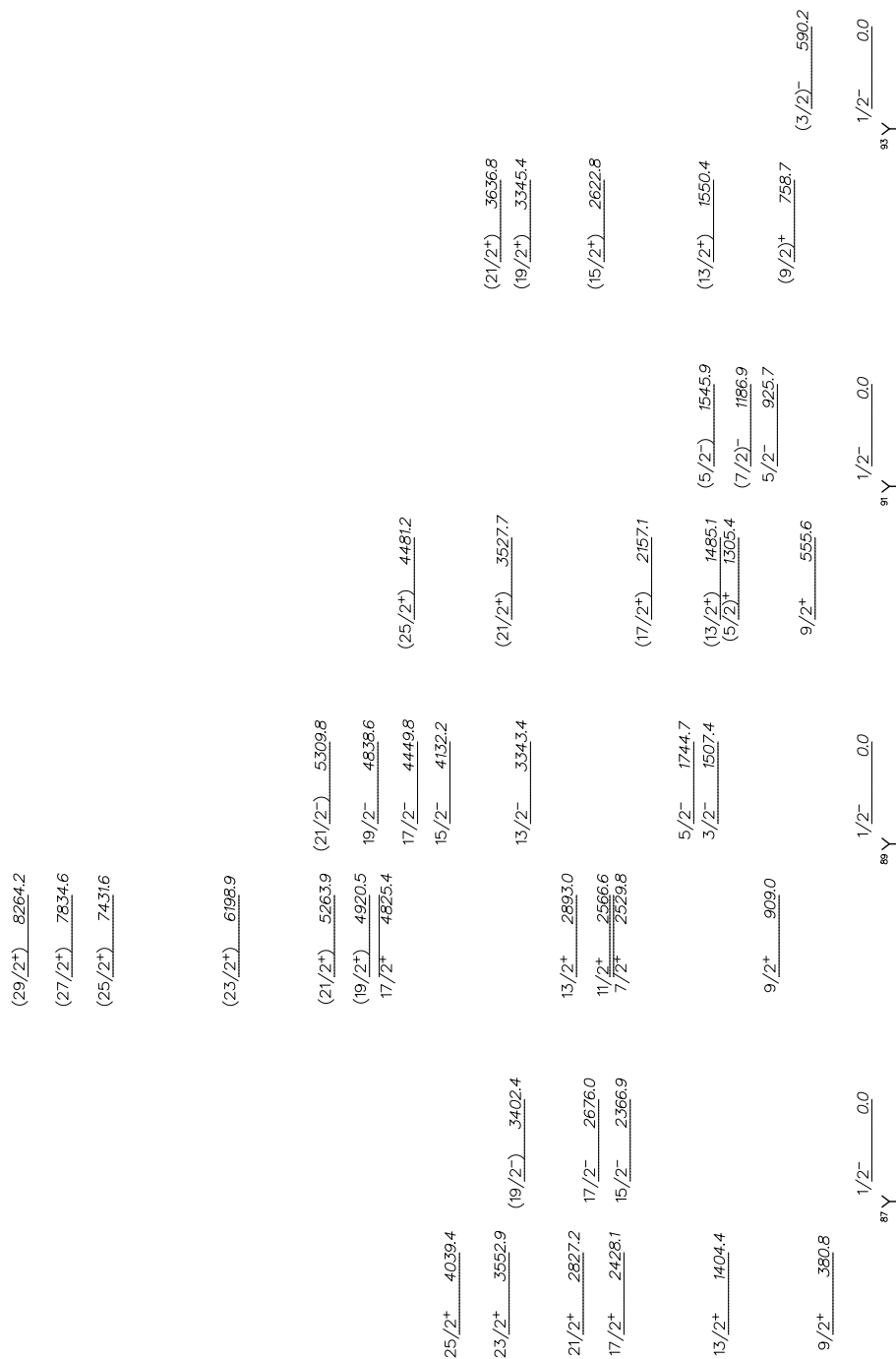
Figure 6.73: Simplified level schemes (only strongly excited states are plotted) of ^{87}Y (first from the left), ^{89}Y (second from the left), ^{91}Y (third from the left) and ^{93}Y (right) isotopes. For each isotope positive (left) and negative (right) parity states are plotted separately.

6.7 Strontium isotopes

In this chapter, we will discuss strontium isotopes observed in the experiment, namely isotopes with a mass number $85 < A < 91$, or, more precisely, from the $-2p-3n$ to the $-2p+3n$ channel.

According to the classical shell model, in strontium isotopes, 20 protons fill the $2\hbar\omega$ shell, while the rest of 18 protons occupy $1f_{7/2}$, $2p_{3/2}$ and $1f_{5/2}$ orbitals (8, 4 and 6 protons in each orbital, respectively). Figure 6.74 shows schematic evolution of the shells as a function of the filling of the proton $1d_{5/2}$, $1f_{7/2}$ and $1g_{9/2}$ orbits. Strontium isotopes of interest (i.e. isotopes with a mass number $85 \leq A \leq 91$) have filled $3\hbar\omega$ neutron subshell (with 40 neutrons), while the rest of the neutrons fill the $1g_{9/2}$ orbital for $85 < A < 88$, and orbitals of the $4\hbar\omega$ shell for $89 \leq A \leq 91$ (see Fig. 6.75). In the classical shell model picture, we expect ^{85}Sr and ^{87}Sr to have ground state $9/2^+$ due to the odd number of neutron holes in the $1g_{9/2}$ orbital. Regarding ^{89}Sr and ^{91}Sr, because of unpaired neutrons in the $2d_{5/2}$, the ground state spin is $5/2^+$. Therefore, it is reasonable to assume that the unpaired neutron defines the ground state of an isotope.

Nonetheless, it is worth mentioning that in heavier systems, single-particle orbitals can migrate with changing neutron-excess, which can affect locations of shell closures in exotic nuclei [Sha12]. Fig. 6.76 shows the ordering of single-particle levels in three nuclei, with a single particle or hole sampling the shell from 50 to 82.

Also, as will be seen in following sections, strongly excited states in odd Sr isotopes are those related to neutron degrees of freedom, which is similar to what we already encountered with odd Zr isotopes. This is why we expect the reaction, besides single particle states, to excite states of particle-vibration character. In even Sr isotopes, high spin states are excited, with emphasis on yrast positive parity states.

Similar to Zr and Y isotopes, some γ rays that do not belong to the observed Sr isotope of interest were found, which is caused by nonideal Z and A resolution. To clean spectra of Sr isotopes from these γ rays, we perform the procedure explained in Section 6.1, i.e. we scale the spectrum to which these "intruder" γ rays actually belong and subtract it from the Sr spectrum in which they occur. Used spectra and applied scaling factors are listed in
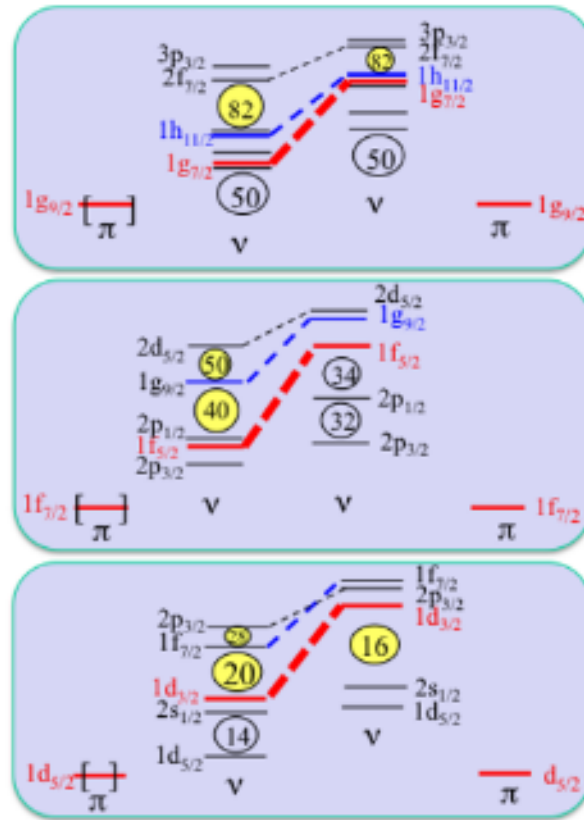
Figure 6.74: Schematic evolution of the shells as a function of the filling of the proton (from bottom to top panels) $1d_{5/2}$, $1f_{7/2}$ and $1g_{9/2}$ orbits. The thickness of the dashed lines connecting the neutron levels scales with the intensity of the proton-neutron interaction into play.
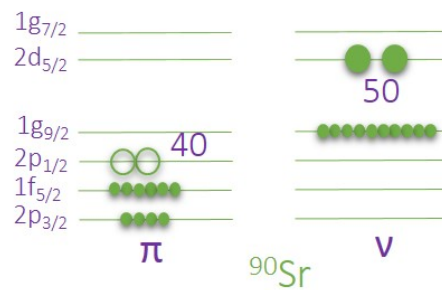
Figure 6.75: Schematic view of the proton and neutron orbitals of the ^{90}Sr
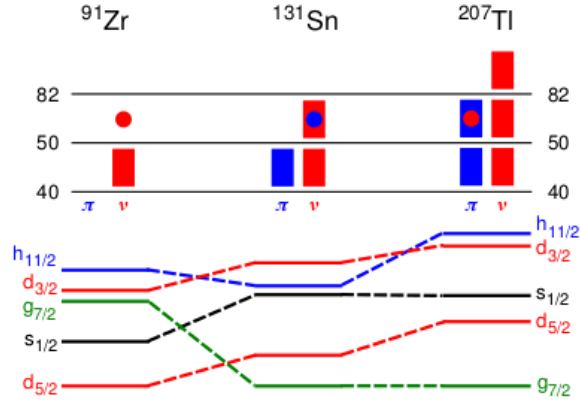
Figure 6.76: Illustration of core dependence on single-particle levels, taken from [Sha12].

Table 6.35. In this chapter, only γ spectra corrected this way will be considered. Based on γ spectra shown in this chapter, level schemes of Sr isotopes are constructed and presented.

Table 6.35: Scaling factors and expressions used for correction of Sr γ spectra. For example, corrected γ spectrum for ^{85}Sr, with the name ^{85}Sr$_{corr}$, has been obtained by subtraction of scaled ^{88}Sr and ^{85}Rb spectra.

corrected γ spectrum	mathematical expression used for the correction
^{85}Sr$_{corr}$	^{85}Sr-0.050*^{88}Sr-0.150*^{85}Rb
^{86}Sr$_{corr}$	^{86}Sr-0.250*^{86}Rb
^{87}Sr$_{corr}$	^{87}Sr-0.240*^{87}Rb
^{88}Sr$_{corr}$	left uncorrected
^{89}Sr$_{corr}$	^{89}Sr-0.150*^{88}Sr
^{90}Sr$_{corr}$	^{90}Sr-0.200*^{90}Y
^{91}Sr$_{corr}$	^{91}Sr-0.100*^{91}Y-0.200*^{90}Sr

Again, in some cases, we observed only γ transitions of the strongest decay branches decaying from certain excited levels, while weaker decay branches have not been observed, according to an expected (small) number of counts. These γ rays are listed separately in Table 4 in the Appendix, together with their intensities (I_γ). Also, if any γ rays are missing in the cascades, their absence is explained in the text.
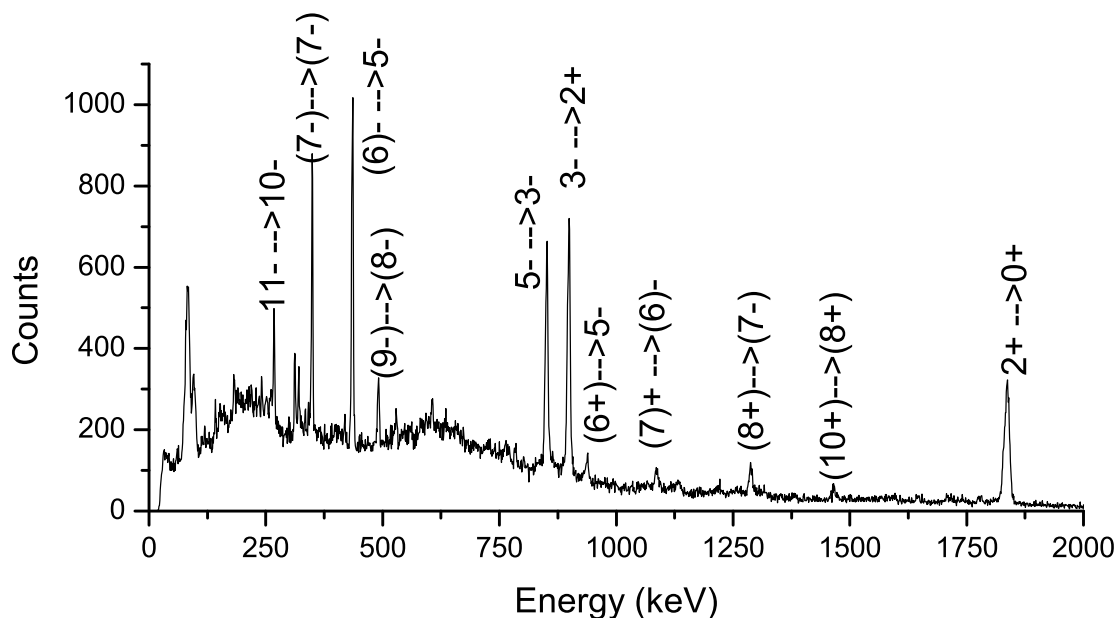
6.7.1 ^{85}Sr
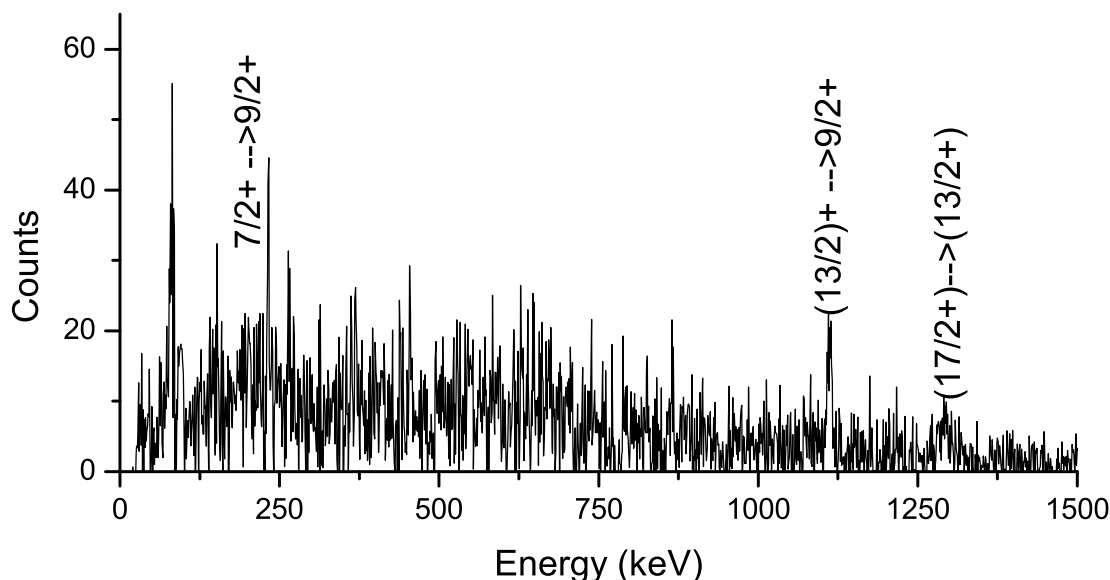
Figure 6.77: Doppler corrected γ spectrum of ^{85}Sr. Spins and parities (as in [www4]) of initial and final states of the strongest transitions are tagged.

Figure 6.77 displays the Doppler corrected γ spectrum of ^{85}Sr, together with the identification of the strongest γ rays. These transitions are listed in Table 6.36 and plotted in Fig. 6.78. The most visible feature of the ^{85}Sr spectrum is the excitation of states of a rather high spin.

Since neutron degrees of freedom are important in the selection of excited states (as in odd Zr isotopes), we expect, besides the strong population of states of single-particle character, to encounter states of particle-vibration character in odd Sr isotopes. In ^{85}Sr, such coupling is expected to appear for the $(13/2)^+$ state. This spin $(13/2)^+$ could be constructed by coupling of the ground state ($J^\pi = 9/2^+$) to a 2^+ vibration quanta in the stretched configuration. Such states could have similar characteristics (energy and strength of the electromagnetic transitions) as the 2^+ state of a neighbouring nucleus. We recognize that the state $J^\pi = (13/2)^+$ ($E_{\mathrm{ex}} = 1111.3$) in ^{85}Sr fulfils these requirements, as will be discussed

in Section 6.8. This state has also been excited in the (p, t) reaction.

To demonstrate the possibility of multinucleon transfer reactions to excite high spin states, we note that the high spin state state $17/2^+$ ($E_{\mathrm{ex}} = 2400.3$ keV) has been so far observed only in fusion-evaporation reaction ($^{82}\mathrm{Kr}(\alpha, \gamma)n$, $E_\alpha = 14-21$ MeV and $^{84}\mathrm{Kr}(\alpha, \gamma)3n$, $E = 35-45$ MeV).

Table 6.36: Strongest γ transitions observed in the present work for the $^{85}\mathrm{Sr}$ isotope. The first column lists energies of γ rays (E_γ) in keV, the second and third columns show energies (E_i), spins and parities (J_i^π) of initial states, while energies (E_f), spins and parities (J_f^π) of final states are listed in the fourth and fifth columns. In the last column, transition intensities after taking into account the Clara efficiency, are listed (normalized to the strongest transition).

E_γ (keV)	E_i (keV)	J_i^π	E_f (keV)	J_f^π (number)	I_γ (%)
231.7	231.7	7/2+	0.0	9/2+	32.22
1111.4	1111.3	(13/2)+	0.0	9/2+	100.00
1288.9	2400.3	(17/2)+	1111.3	(13/2+)	81.45
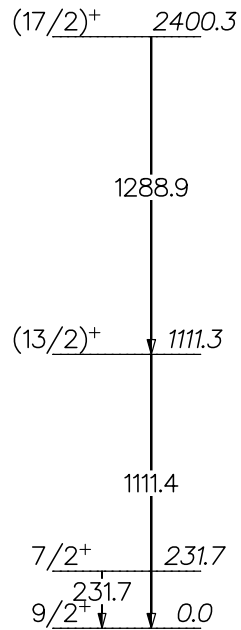
Figure 6.78: Experimental states observed in our measurement for ^{85}Sr. Relative γ ray intensities are indicated by widths of arrows. Energies, spins and parities of levels, their branching ratios and energies of transitions are as in Ref. [www4]. Only positive parity states have been observed, with rather high spins.
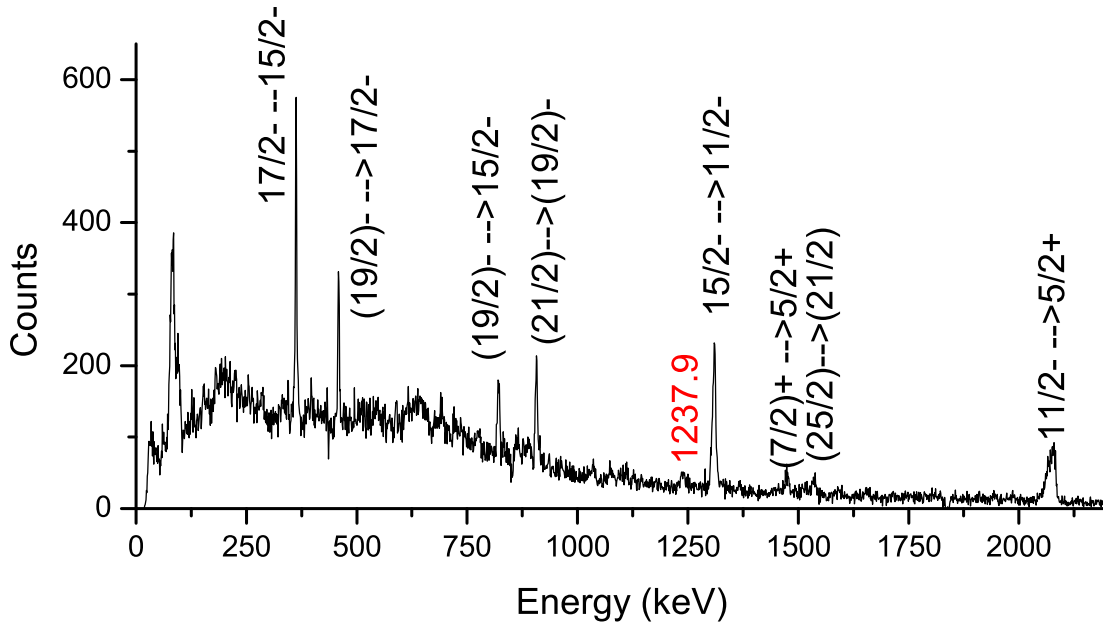
6.7.2 ^{86}Sr
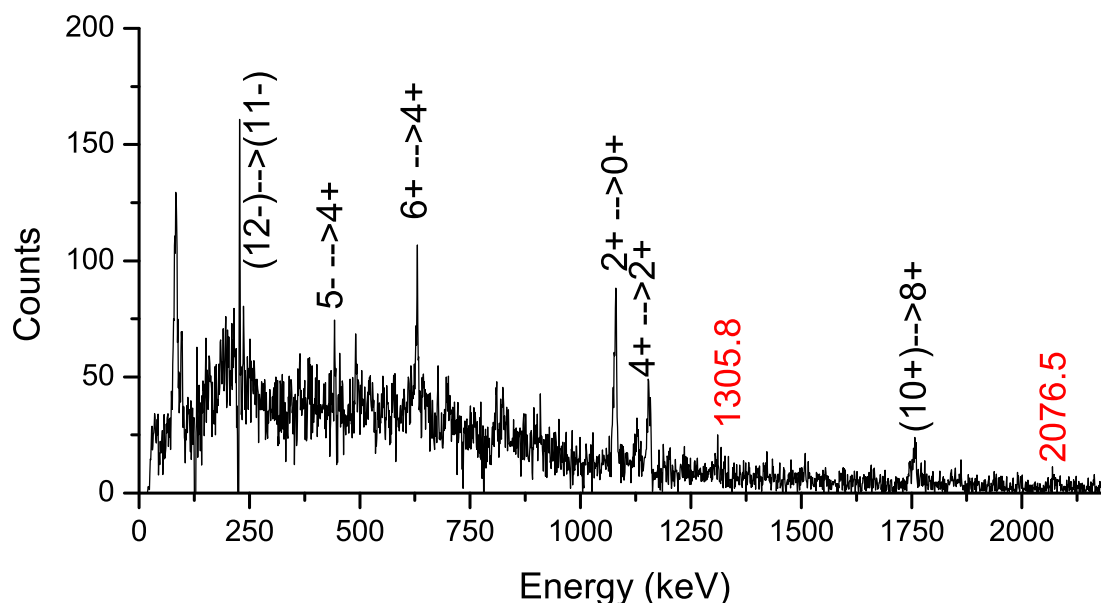
Figure 6.79: Doppler corrected γ spectrum of ^{86}Sr. Spins and parities (as in [www4]) of initial and final states of strongest transitions are tagged. Energies (in keV) of yet unknown γ rays (i.e. γ rays which could not be placed in the level scheme) are written in red.

Figure 6.79 shows γ spectrum of ^{86}Sr and Table 6.37 lists γ rays observed in the spectrum. Figure 6.80 shows that in the positive parity band, yrast states up to (10^+) are excited, while in the negative parity band, the first 3^- and 5^- states have been observed, and then again high spin states (11^-) and (12^-) at relatively high energy (~ 6 MeV). These, relatively high negative spin states $((11^-)$ and $(12^-))$ have previously been, up to now, only observed in fusion-evaporation reactions; ^{84}Kr(^{3}He,n) ($E_{^3\text{He}} = 25.4$ MeV) and ^{74}Ge(^{18}O,$\gamma 2n$) ($E_{^{18}\text{O}} = 40 - 80$ MeV).

This situation seems to happen in all Sr isotopes which can be, besides in the transfer of nucleons, produced in the neutron evaporation reactions. ^{88}Sr being the strongest channel, all Sr isotopes with $A < 88$ may receive considerable contributions from the evaporation processes. Several measured cases have proven that for massive proton transfer channels,

the yield drifts toward lower masses, indicating that evaporation processes influence the final isotopic distributions (see for example Ref. [Szi05]). Thus, it is possible that the character of populated states reflects these two mechanisms, direct transfer, and transfer followed by the neutron evaporations.

Some γ rays from plotted levels have not been observed in the experiment because of their low decay branch and they are listed in Table 4 in the Appendix. $E_\gamma = 777.4$ keV, which belongs to decay from $E_i = 1854.2$ keV ($J^\pi = 2_2^+$) to $E_f = 1076.7$ keV ($J^\pi = 2_1^+$) and $E_\gamma = 809.4$ keV ($E_i = 3482.2$ keV ($J^\pi = 6_2^+$) to $E_f = 2672.8$ keV ($J^\pi = 5^-$)) were not clearly separated in the cleaned and corrected γ spectrum of ^{86}Sr (because there are γ rays with similar energies in the spectrum of ^{86}Rb) and are thus plotted as dashed lines in Fig. 6.80. $E_\gamma = 98.7$ keV ($E_i = 2955.7$ keV ($J^\pi = 8^+$) to $E_f = 2857.0$ keV ($J^\pi = 6^+$)) has also been plotted as a dashed line, because the γ ray absorber used during the experiment interfered with its observation (due to low energy). Two unknown γ rays have been observed ($E_\gamma = 1305.8$ and 2076.5 keV), and they are listed in Table 6.37 (denoted by *).

Table 6.37: γ transitions observed in the present work for the ^{86}Sr isotope. The first column lists energies of γ rays (E_γ) in keV, the second and third columns show energies (E_i), spins and parities (J_i^π) of initial states, while energies (E_f), spins and parities (J_f^π) of final states are listed in the fourth and fifth columns. In the last column, transition intensities after taking into account the Clara efficiency, are listed (normalized to the strongest transition).

| E_γ (keV)	E_i (keV)	J_i^π	E_f (keV)	J_f^π (number)	I_γ (%)
226.7	6061.1	(12-)	5834.5	(11-)	16.09
443.1	2672.8	5-	2229.7	4+	19.93
490.8	3973.0		3482.2	6+	26.08
627.2	2857.0	6+	2229.7	4+	48.52
627.5	2481.9	3-	1854.2	2+	9.37
1076.6	1076.7	2+	0.0	0+	100.00
1125.5	5834.5	(11-)	4708.9	(10+)	33.02
1153.0	2229.7	4+	1076.7	2+	63.39
1305.8(3)*					33.65
1753.1	4708.9	(10+)	2955.7	8+	53.34
2076.5(12)*					18.61
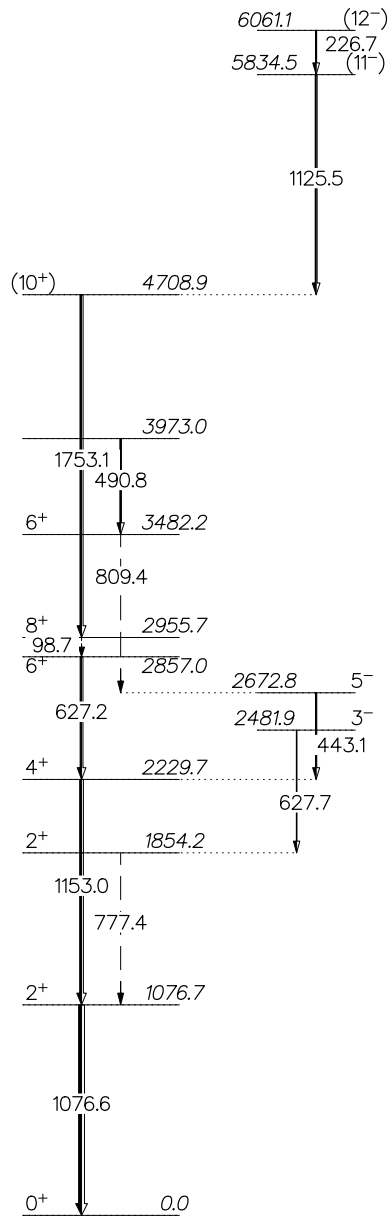
Figure 6.80: Experimental positive (left) and negative (right) parity states observed in our measurement for ^{86}Sr. Relative γ ray intensities are indicated by widths of arrows. Energies, spins and parities of levels, their branching ratios and energies of transitions are as in Ref. [www4]. The strongest excited levels are 2^+ and 4^+, but yrast states up to (10^+) have been observed. In the negative parity band, the first 5^- and 3^- states have been observed, together with high spin states (11^-) and (12^-).
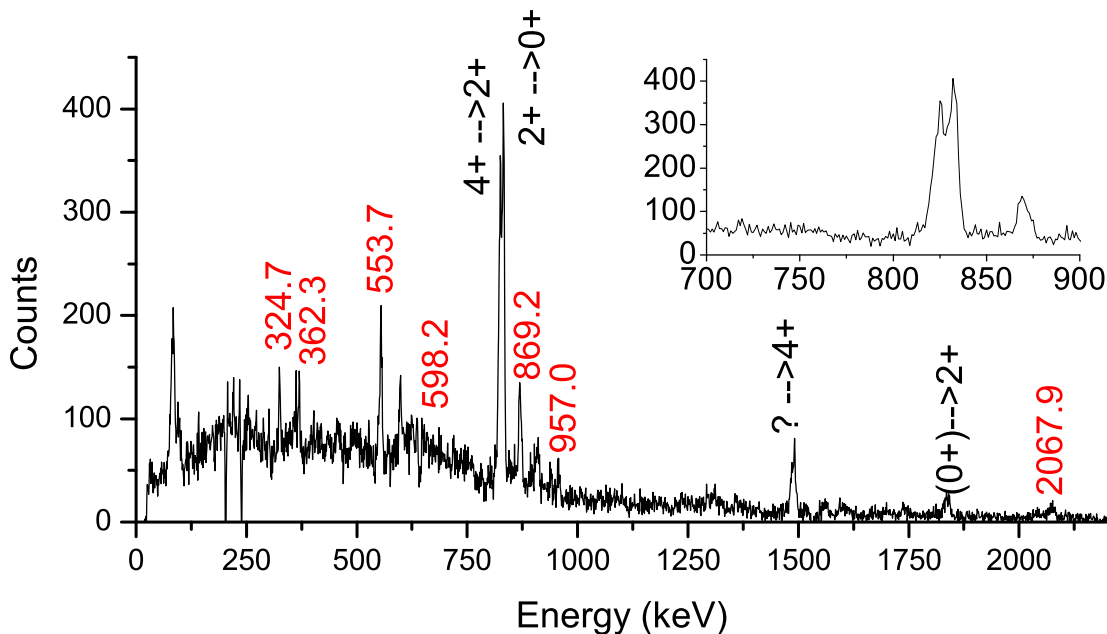
6.7.3 ^{87}Sr
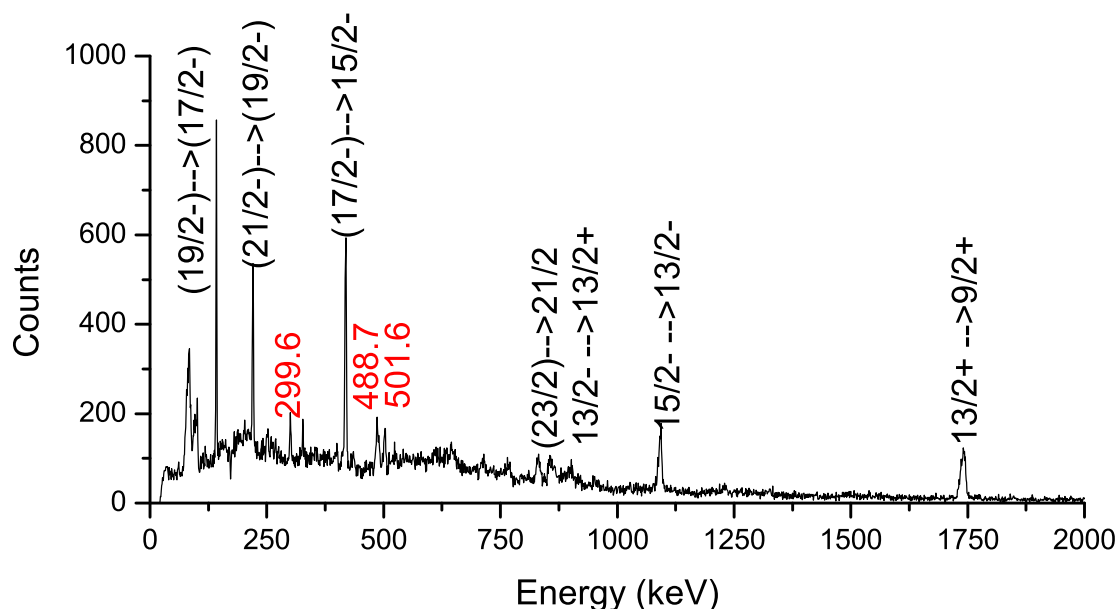
Figure 6.81: Doppler corrected γ spectrum of ^{87}Sr. Spins and parities (as in [www4]) of initial and final states of the strongest transitions are tagged. Energies (in keV) of yet unknown γ rays (i.e. γ rays which could not be placed in the level scheme) are written in red.

Figure 6.81 shows that in the spectrum of ^{87}Sr, high spin states are strongly excited. All observed γ rays are listed in Table 6.38 and observed energy levels are plotted in Fig. 6.82. Only one positive parity state is exited ($E_{\mathrm{ex}} = 1740.0$ keV, $J^\pi = 13/2^+$). The reason may be that higher lying positive parity states decay through transitions with energies near or above 2000 keV, for which the efficiency of the Clara γ array decreases.

Decays of these high lying negative parity states are finally going through the $13/2^+$ state. When all feedings are subtracted from the the $13/2^+$ state, direct population of this $13/2^+$ turns out to be 27%. Since neutron degrees of freedom are important in the selection of excited states, we can assume that the $13/2^+$ could arise from the coupling of a 2^+ vibration quanta of ^{88}Sr to the ground state spin $9/2^+$ (defined with the unpaired neutron in the $1g_{9/2}$ orbital), in the stretched configuration. This possibility will be discussed in more detail in

Section 6.8.

In the negative parity band, besides the first two states, which have been relatively weakly excited, only high spin states have been selectively observed up to 23/2 at ~ 4.5 MeV. Note that the γ ray with energy $E_\gamma = 388.5$ keV is drawn by a dashed line in Fig. 6.82 due to its isomeric transition.

Table 6.38: γ transitions observed in the present work for the ^{87}Sr isotope. The first column lists energies of γ rays (E_γ) in keV, the second and third columns show energies (E_i), spins and parities (J_i^π) of initial states, while energies (E_f), spins and parities (J_f^π) of final states are listed in the fourth and fifth columns. In the last column, transition intensities after taking into account the Clara efficiency, are listed (normalized to the strongest transition).

E_γ (keV)	E_i (keV)	J_i^π	E_f (keV)	J_f^π	I_γ (%)
141.5	3390.9	(19/2-)	3249.4	(17/2-)	19.32
220.0	3610.9	(21/2)	3390.9	(19/2-)	18.56
299.6(1)*					8.91
327.1	3718.0	(15/2) TO (23/2)	3390.9	(19/2-)	7.91
418.2	3249.4	(17/2)-	2831.2	15/2-	36.35
484.8	873.4	3/2-	388.5	1/2-	8.99
488.7(8)*					7.73
501.6(2)*					13.44
829.4	4440.4	(23/2)	3610.9	(21/2)	20.96
855.9	2596.0	13/2-	1740.0	13/2+	23.30
1091.3	2831.2	15/2-	1740.0	13/2+	49.58
1739.8	1740.0	13/2+	0.0	9/2+	100.00

In addition, three yet unknown γ rays, denoted by (*) in Table 6.38 have been observed. Their energies ($300-500$ keV) are in the energy range ($220-830$ keV) of the observed transitions between negative parity spin states from the excited levels with energies $2.5-4.5$ MeV. As in our fragment-γ coincident measurement no additional information for these γ rays are available, we search for the possible matching of the energy difference between known

energy levels, as listed in Table 6.39.

In all cases, these unknown γ rays correspond to decays of negative parity states of unknown spins to levels already recognized and excited in our level scheme.

Table 6.39: Possible assignments of new γ rays of ^{87}Sr, based on the energy difference between initial and final levels. The first column contains energies of newly observed γ rays (E_γ) in keV, the second and third columns show energies (E_i), spins and parities (J_i^π) of suggested initial states, while energies (E_f), spins and parities (J_f^π) of belonging final states are listed in the fourth and fifth columns. In the last column, transition intensities after taking into account the Clara efficiency, are listed (normalized to the strongest transition, as in Table 6.38).

E_γ (keV)	E_i (keV)	J_i^π	E_f (keV)	J_f^π	I_γ (number)
299.6(1)	2893(8)		2596.0(5)	13/2-	8.91
	3551(8)		3249.4(5)	17/2-	
448.7(8)	3792.38(17)		3249.4(5)	(17/2-)	7.73
501.6(2)	3894(8)		3390.9(6)	(19/2-)	13.44
	4943.3(4)		4440.4(10)	(23/2)	
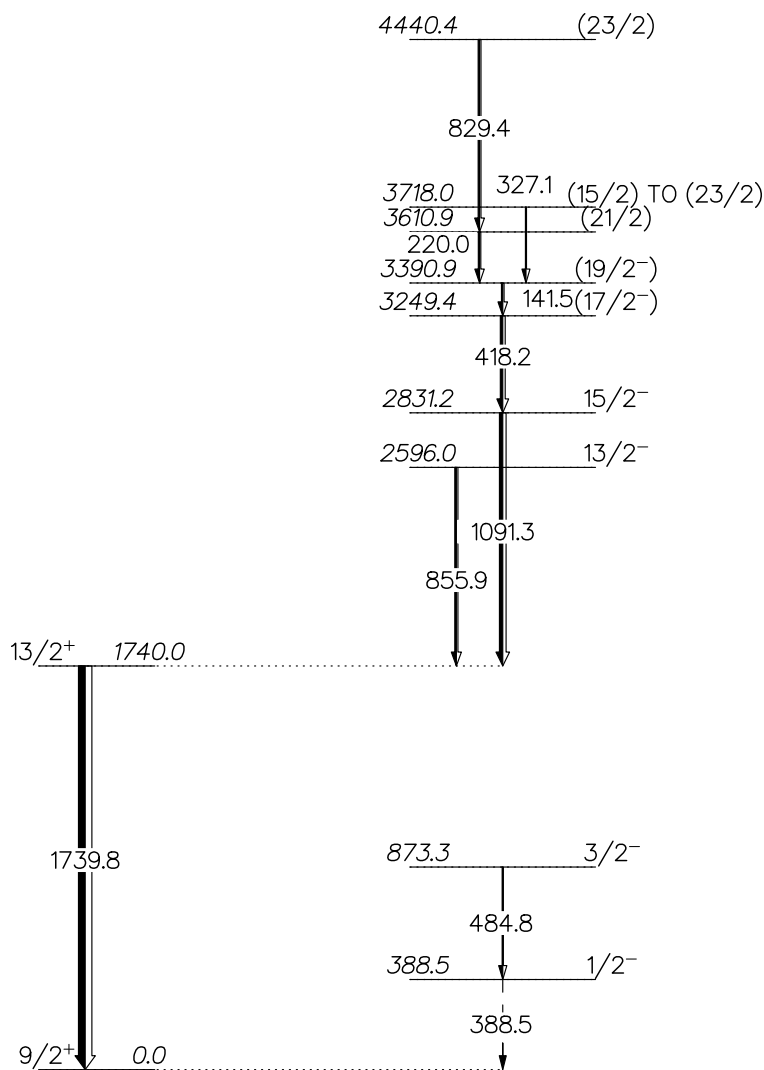
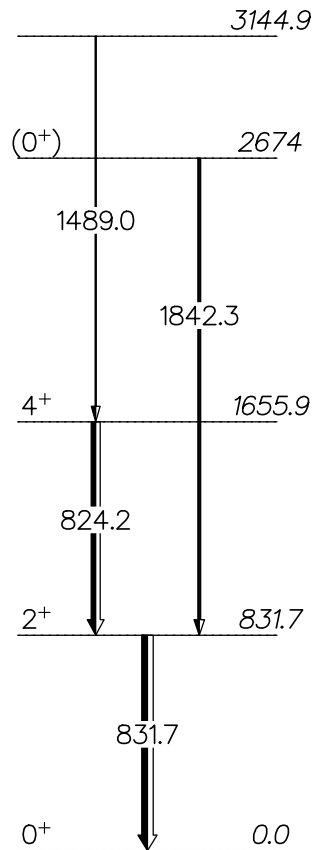Figure 6.82: Experimental positive (left) and negative (right) parity states observed in our measurement for ^{87}Sr. Relative γ ray intensities are indicated by widths of arrows. Energies, spins and parities of levels, their branching ratios and energies of transitions are as in Ref. [www4]. Only one positive parity state is excited. In the negative parity band, except for the first two excited states, only high spin states have been selectively observed.
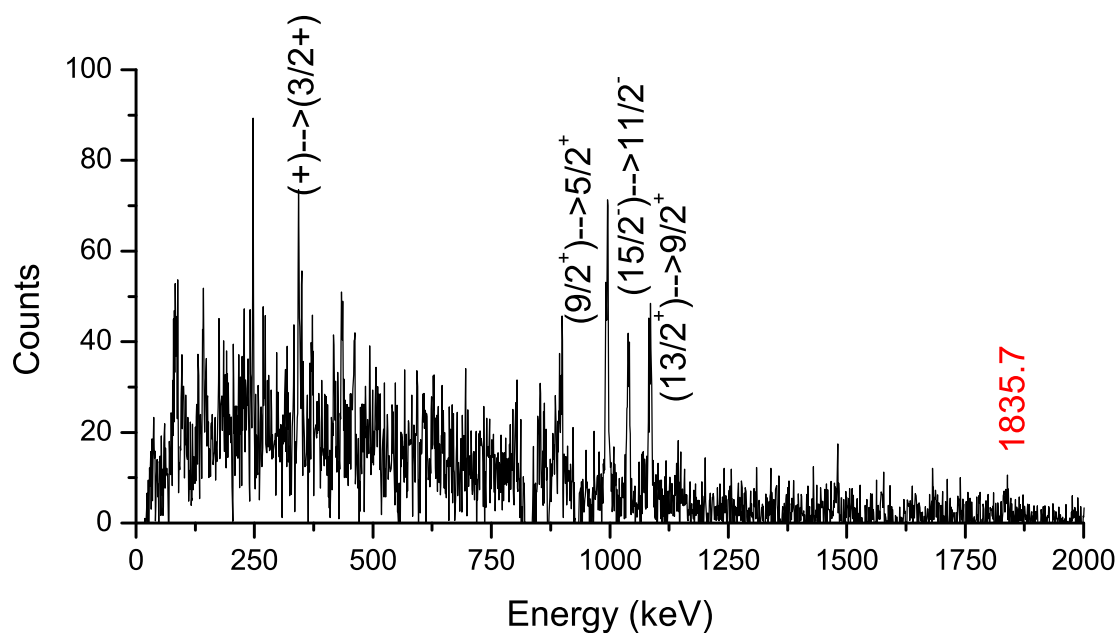
6.7.4 ^{88}Sr

Figure 6.83: Doppler corrected γ spectrum of ^{88}Sr. Spins and parities (as in [www4]) of initial and final states of the strongest transitions are tagged.

Figures 6.83 and 6.84 show that strongly excited states in ^{88}Sr are 2^+, 3^- and 5^-. In the higher energy part of the scheme ($E > 5$ MeV, see Fig. 6.84), most of the excited energy levels do not have definite parity [www4]. Nevertheless, γ rays form a cascade which starts at $E_{\text{ex}} \sim 7.5 - 8$ MeV and spin ($J \sim 10 - 11$). In Fig. 6.84 these cascades are separated in two bands for the sake of clarity.

When comparing the levels excited in the ^{86}Sr and ^{88}Sr isotopes, yrast states up to $J \sim 10$ have been observed. In this comparison it is notable that ^{88}Sr has the $4\hbar\omega$ neutron sub-shell closed, and consequently its excitation energies are higher than in ^{86}Sr, especially for the low-lying states. Notably, in both cases, high spin states have been previously observed only in fusion-evaporation reactions. In the case of ^{88}Sr, these are ^{80}Se(^{11}B,$\gamma 2np$) ($E_{\text{B}} = 45$ MeV), ^{176}Yb(^{28}Si,Fγ) ($E_{\text{Si}} = 145$ MeV) and ^{173}Yb(^{24}Mg,Fγ) ($E_{\text{Mg}} = 134.5$ MeV) reactions.

Some γ rays from plotted levels have not been observed in the spectrum due to their low decay branch (tabulated $I_\gamma < 23\%$) and they are listed in Table 4 in the Appendix. For the state at $E_{\text{ex}} = 6235.5$ keV, $J = (7)$, the proposed decay is via 3 γ rays: 1132.1 ($I_\gamma = 88\%$), 1713.9($I_\gamma = 100\%$), and 1867.4($I_\gamma = 94\%$), of which we see only the $E_\gamma = 1132.1$ keV.

Table 6.40: γ transitions observed in the present work for the ^{88}Sr isotope. The first column lists energies of γ rays (E_γ) in keV, the second and third columns show energies (E_i), spins and parities (J_i^π) of initial states, while energies (E_f), spins and parities (J_f^π) of final states are listed in the fourth and fifth columns. In the last column, transition intensities after taking into account the Clara efficiency, are listed (normalized to the strongest transition).

E_γ (keV)	E_i (keV)	J_i^π	E_f (keV)	J_f^π	I_γ (%)
267.1	5370.5		5103.3	(7)	5.63
266.9	7908.8	(11)	7641.9	(10)	3.58
311.3	7641.9	(10)	7330.6	(9)	7.45
319.6	4687.4	(7)	4367.9	(7-)	6.38
348.3	4367.9	(7-)	4019.6	(6)-	22.89
434.9	4019.6	(6)-	3584.8	5-	35.99
489.9	7330.6	(9)	6840.6	(8)	9.82
605.1	6840.6	(8)	6235.5	(7)	7.65
850.6	3584.8	5-	2734.1	3-	70.30
898.0	2734.1	3-	1836.1	2+	83.71
936.6	4521.4	(4+)	3584.8	5-	10.06
1083.6	5103.3	(7)	4019.6	(6)-	11.72
1132.1	6235.5	(7)	5103.3	(7)	8.84
1287.4	5655.3	(8)	4367.9	(7-)	16.52
1464.0	7119.2	(10)	5655.3	(8)	14.50
1706.6	4440.8		2734.1	3-	7.85
1717.7	4452.0	(4)+	2734.1	3-	6.43
1778.9	7434.2	(10)	5655.3	(8)	9.01
1836.1	1836.1	2+	0.0	0+	100.00
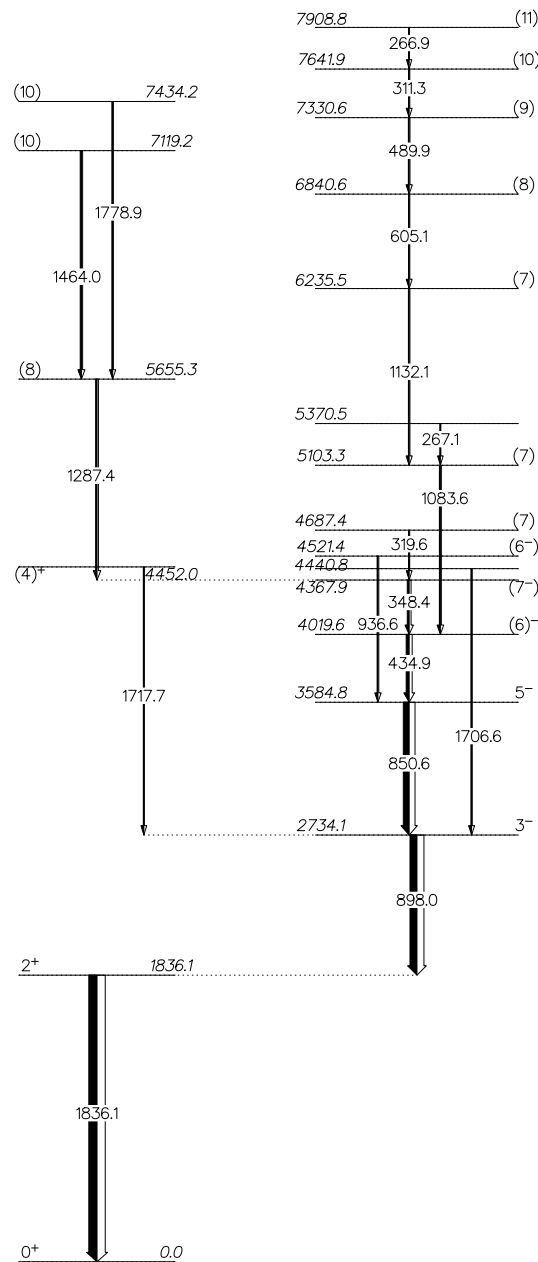
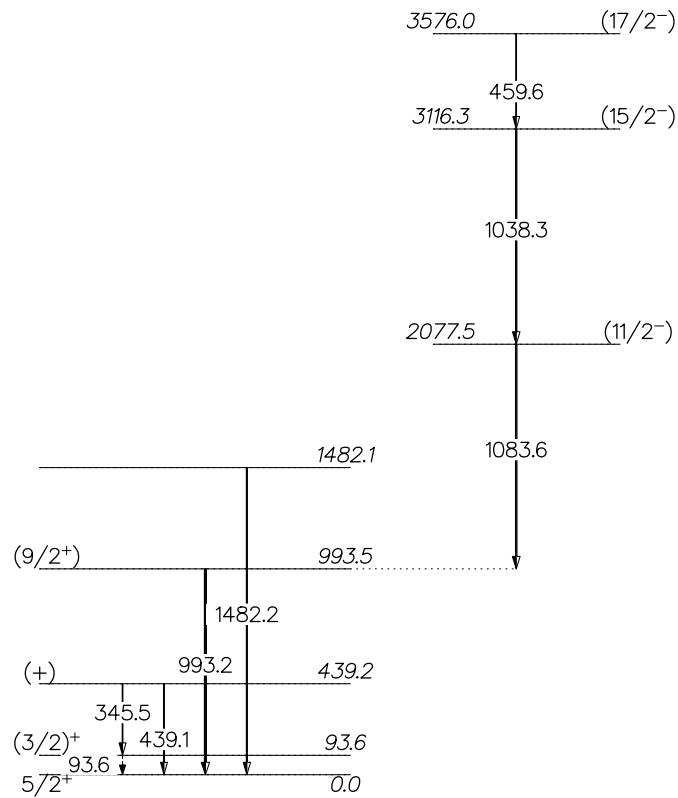Figure 6.84: Experimental positive (left) and negative (right) parity states observed in our measurement for ^{88}Sr. Relative γ ray intensities are indicated by widths of arrows. Energies, spins and parities of levels, their branching ratios and energies of transitions are as in Ref. [www4]. The strongest excited levels are 2^+, 3^- and 5^-, but yrast states up to (11) in have been observed.

6.7.5 ^{89}Sr

Figure 6.85: Doppler corrected γ spectrum of ^{89}Sr. Spins and parities (as in [www4]) of initial and final states of the strongest transitions are tagged. Energy (in keV) of yet unknown γ ray (i.e. γ ray which could not be placed in the level scheme) is written in red.

In the positive parity band of ^{89}Sr, only the first two excited levels have been observed ($J^\pi = 1/2^+$ and $J^\pi = (7/2)^+$) (see Figs. 6.85 and 6.86), which are also the two lowest states, and they can be explained as single-particle states with one unpaired neutron in $3s_{1/2}$ or $1g_{7/2}$ orbital.

Taking into account available orbitals, the following states are expected: $1/2^+$, $7/2^+$, $5/2^+$, $3/2^+$ and $11/2^-$, arising from unpaired neutrons in the $3s_{1/2}$, $1g_{7/2}$, $2d_{5/2}$, $2d_{3/2}$ or $1h_{11/2}$ orbitals. Concerning low-energy positive parity states ($E < 1.5$ MeV), we observed only the population of the two lowest energy states, ($J^\pi = 1/2^+$ and $J^\pi = (7/2)^+$) (see Fig. 6.85 and 6.86).

However, taking into account the coupling of the 2^+ vibration quanta with the $5/2^+$

ground state, the $9/2^+$ state, as its stretched configuration, is expected. This state, $9/2_1^+$ (at $E_{\text{ex}} = 2061.5$ keV) decays with the $E_\gamma = 2061.6$ keV, which overlaps with a wide peak centered at 2079 keV and recognized as the decay from the $11/2^-$ state. The γ spectrum of the ^{89}Sr is characterized by strong excitation of negative parity high spin states. High spin states (up to $(19/2)^-$) and $(21/2)$, $(25/2)$ with undefined parity, have been selectively observed. Taking into account this selectivity, and following their decay to the $(19/2)^-$ state, we can conclude that the states $(21/2)$ and $(25/2)$ belong to the negative parity band.

Table 6.41: γ transitions observed in the present work for the ^{89}Sr isotope. The first column lists energies of γ rays (E_γ) in keV, the second and third columns show energies (E_i), spins and parities (J_i^π) of initial states, while energies (E_f), spins and parities (J_f^π) of final states are listed in the fourth and fifth columns. In the last column, transition intensities after taking into account the Clara efficiency, are listed (normalized to the strongest transition).

E_γ (keV)	E_i (keV)	J_i^π	E_f (keV)	J_f^π	I_γ (%)
362.4	3750.7	17/2-	3388.1	15/2-	39.92
458.4	4208.8	(19/2)-	3750.7	17/2-	27.16
820.4	4208.8	(19/2)-	3388.1	15/2-	34.89
906.0	5115.1	(21/2)	4208.8	(19/2)-	44.47
1032.0	1032.0	1/2+	0.0	5/2+	14.24
1237.9(5)*					21.82
1309.3	3388.1	15/2-	2079.0	11/2-	98.98
1473.3	1473.4	(7/2)+	0.0	5/2+	25.42
1534.7	6649.9	(25/2)	5115.1	(21/2)	20.61
2079.4	2079.0	11/2-	0.0	5/2+	100.00

One new γ ray has been observed, $E_\gamma = 1237.9$ keV (denoted by * in Table 6.41). Based on energy difference between known states, this γ ray could be attributed to one of the following transitions: $E_i = 4626(10)$ keV (J_i^π unknown) $\longrightarrow E_f = 3388.1(7)$ keV ($J_f^\pi = 15/2^-$) or $E_i = 5442(10)$ keV (J_i^π unknown) $\longrightarrow E_f = 4208.8(10)$ keV ($J_f^\pi = (19/2)^-$). Both of these starting levels of unknown spin and parity have been observed only in the (p, d)

reaction, with limited angular momentum transfer. Observing rather high spin states, we prefer to attribute this γ ray to yet unknown high spin negative parity state in the energy region above 5 MeV. This is also in agreement with its intensity, which is very close to the intensity of the 1534.7 keV line.
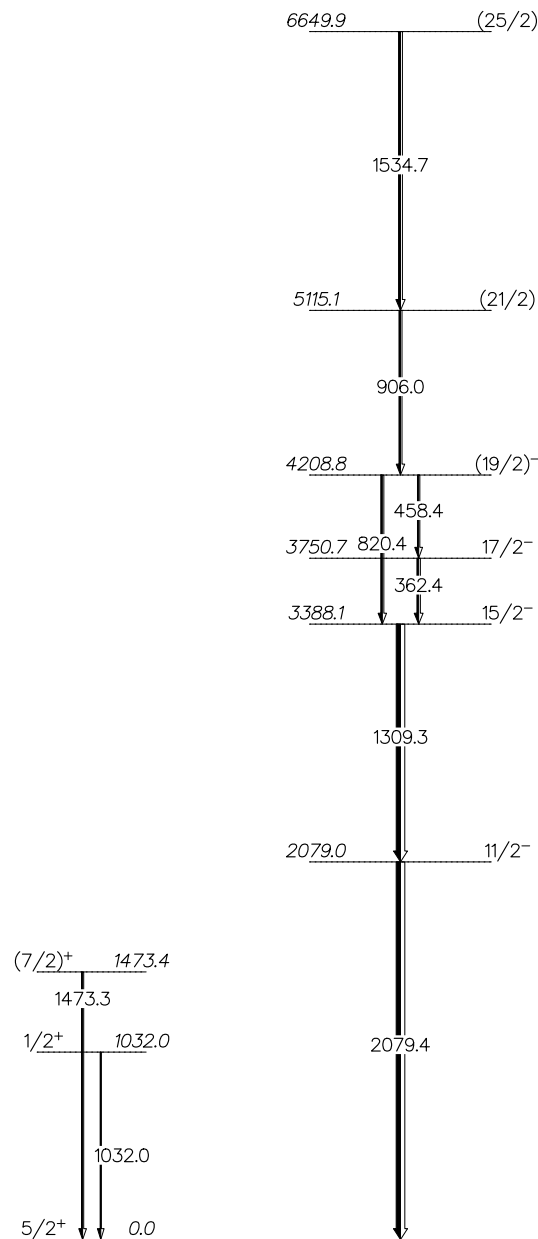
Figure 6.86: Experimental positive (left) and negative (right) parity states observed in our measurement for ^{89}Sr. Relative γ ray intensities are indicated by widths of arrows. Energies, spins and parities of levels, their branching ratios and energies of transitions are as in Ref. [www4]. Negative parity states have been strongly excited and rather high spin states (up to (19/2)-) have been selectively observed. There are also higher spin states ((21/2), (23/2)) with undefined parity, but we put them in the negative parity band because of the succeeding γ cascade.

6.7.6 ^{90}Sr

Figure 6.87: Doppler corrected γ spectrum of ^{90}Sr. Spins and parities (as in [www4]) of initial and final states of strongest transitions are tagged. The expanded part of the spectrum around 800 keV is here to show double peak structure.

Knowledge about the excited states of ^{90}Sr is very scarce. The ^{90}Sr nucleus has been studied mainly via β decay [TWA81] and (t, p) [FHS76] measurements. From the decay of known ^{90}Sr states, four γ rays in the ^{90}Sr were recognized (see Figs. 6.87 and 6.88). They are listed in Table 6.42. The strongest γ rays decay from the first 2^+ ($E_{\mathrm{ex}} = 831.7$ keV) and 4^+ ($E_{\mathrm{ex}} = 1655.9$ keV) states (see double peak structure in the inlet of Fig. 6.87).

In addition, we recognized the decay from the second (0^+) state at 2674 keV ($E_\gamma = 1842.3$ keV), which was populated in the (t, p) reaction. This is the only one of the observed isotopes for which we excited the second 0^+ state. Such strong excitation of the second 0^+ state has been observed in the (t, p) reaction ([FHS76]), where it is explained by the fact that for transfers $N = 50 \longrightarrow N = 52$, orbitals $2d_{3/2}$ and $3s_{1/2}$ contribute to transfer amplitudes

with similar magnitudes, so this large part of the cross section to the 0^+ state may occur from pairing interactions dominated by the $d_{3/2}$ orbit and at the same time for an excited state transition dominated by the $s_{1/2}$ orbit, which can have a large cross section. This phenomenon becomes more pronounced as we progress towards heavier isotopes.

We attributed the γ ray $E_\gamma = 1489.0$ keV to the decay of the state at 3144.9 keV. For a nearby (or in fact same) state at 3146(10) keV, populated in the (t,p) reaction, the suggested spin (from the comparison with the DWBA calculation) was (5-). We would like to underline that the negative parity band was strongly excited in the ^{88}Sr nuclei, in particular 5- state.

Table 6.42: γ transitions recognized in the present work for the ^{90}Sr isotope. The first column lists energies of γ rays (E_γ) in keV, the second and third columns show energies (E_i), spins and parities (J_i^π) of initial states, while energies (E_f), spins and parities (J_f^π) of final states are listed in the fourth and fifth columns. In the last column, transition intensities after taking into account the Clara efficiency, are listed (normalized to the strongest transition, i.e. $2^+ \longrightarrow 0^+$).

E_γ (keV)	E_i (keV)	J_i^π	E_f (keV)	J_f^π	I_γ (%)
824.2	1655.9	4+	831.7	2+	78.64
831.7	831.7	2+	0.0	0+	100.00
1489.0	3144.9		1655.9	4+	9.34
1842.3	2674	(0+)	831.7	2+	24.22

Most of the γ rays attributed to the ^{90}Sr nucleus are yet unknown. They are listed in Table 6.43. It is important that the spectrum plotted in Fig. 6.87 has been derived after the cleaning procedure (as explained in section 6.1). In this procedure we subtracted scaled (factor 0.2) spectra of ^{90}Y. Looking at the spectra of ^{90}Y, only three γ lines from Table 6.43 are "close" in the energy to the recognized γ of ^{90}Y: 142.5 keV (with about 4% of intensity), 365.2 keV (18%), and 953.5 keV (26%). We are confident that strongest γ rays in Table 6.43 (with intensities $> 15\%$) belong to the ^{90}Sr nucleus.

Comparing the states populated in the ^{88}Sr and ^{90}Sr nuclei, it is observed that we excited the states up to spin $\sim$10 in ^{88}Sr. Thus, we expect that unrecognized γ transitions listed

Table 6.43: γ transitions observed in the present work for the ^{90}Sr isotope, which weren't recognized as known transitions. The first column lists energies of γ rays (E_γ) in keV, the second and third columns show energies (E_i), spins and parities (J_i^π) of initial states, while energies (E_f), spins and parities (J_f^π) of final states are listed in the fourth and fifth columns. In the last column, transition intensities after taking into account the Clara efficiency, are listed (normalized to the strongest transition, i.e. $2^+ \longrightarrow 0^+$).

E_γ (keV)	I_γ (%)
141.9(1)*	2.30
324.7(1)*	9.39
362.3(3)*	5.83
368.5(1)*	7.78
553.7(2)*	35.81
598.2(2)*	23.07
869.2(4)*	39.47
939.2(6)*	9.13
957.0(3)*	12.44
2067.9(5)*	18.95

in Table 6.43 belong to decays of high spin states in ^{90}Sr. Such states would not be easily excited by the (t, p) and β decay reactions, contrary to the presented heavy-ion induced transfer reactions. The attribution of these new γ rays also agrees with their observed intensities. In ^{88}Sr, intensities of γ rays from decays of higher spin states ($J \sim 7$ or 8) are about 20% of the decay of the 2_1^+ state. Looking at Table 6.43, we notice that the majority of the new γ rays are in this category, with intensities of about 20 to 30% of the strongest 2_1^+ to the ground state transition. In order to construct the level scheme, additional studies which assume the $\gamma - \gamma$ coincidences are needed.

Figure 6.88: Excited states observed in our measurement for ^{90}Sr. Relative γ ray intensities are indicated by widths of arrows. Energies, spins and parities of levels, their branching ratios and energies of transitions are as in Ref. [www4]. Only four γ rays from the spectrum could be placed in the level scheme, and the strongest γ rays decay from the first 2^+ and 4^+ excited states.

6.7.7 ^{91}Sr

Figure 6.89: Doppler corrected γ spectrum of ^{91}Sr. Spins and parities (as in [www4]) of initial and final states of strongest transitions are tagged. Energy (in keV) of yet an unknown γ ray (i.e. γ ray which could not be placed in the level scheme) is written in red.

Small statistics of collected data (around $\sim$ 29000) in this channel left only a few distinguishable γ rays (Figs. 6.89 and 6.90). The strongest transitions have been attributed to decays of the $(9/2^+)$, $(11/2^-)$ and $(15/2^-)$ states.

Similarly as for the ^{89}Sr, strong excitation of the high spin states has been observed. They are known in these nuclei via fusion-evaporation studies, namely ^{173}Yb$(^{24}$Mg, $\gamma Xn)$ $(E_{^{24}\text{Mg}} = 134.5$ MeV$)$ and ^{159}Tb$(^{36}$S,$F\gamma)$ $(E_{^{36}\text{S}} = 165$ MeV$)$. Looking at states populated in the ^{159}Tb$(^{36}$S,$F\gamma)$ reaction, we can conclude that up to the excitation energy of 3.6 MeV we populated all of them (with the exception of the second $15/2^-$ state) with similar intensities. Similar conclusions follows from the comparison with states populated in the ^{173}Yb$(^{24}$Mg,$Fxn\gamma)$ reactions.

In addition to these higher spin states, we have observed all known low lying energy levels up to the $9/2^+$ state ($E_{\mathrm{ex}} = 993.5$ keV). $E_\gamma = 93.6$ keV was drawn in Fig. 6.90 by a dashed line because it has not been observed in the experiment due to its too low energy to be recognized with Clara γ array. γ rays with weak decay branches that have not been observed in the spectrum are listed in Table 4 in the Appendix.

Two of the observed γ rays, $E_\gamma = 142.5$ keV and $E_\gamma = 892.9$ keV, have been attributed to ^{90}Y (where they have been observed as rather strong transitions). We attributed γ ray $E_\gamma = 1835.7$ keV (denoted by * in Table 6.44) to ^{91}Sr.

It is interesting to discuss in more detail the $(9/2^+)$ state ($E_{\mathrm{ex}} = 993.5$ keV). This state could be of a single particle character due to a neutron hole in the $1g_{9/2}$ orbital or it could be of a particle-vibration character, if a 2^+ vibration quanta couples to the ground state spin $5/2^+$ in the stretched configuration. Further explanation will be given in Section 6.8. Similarly, the state at 2077.5 keV ($J^\pi = 11/2^-$) has been suggested to arise from a coupling to the 3^- state.

Table 6.44: γ transitions observed in the present work for the ^{91}Sr isotope. The first column lists energies of γ rays (E_γ) in keV, the second and third columns show energies (E_i), spins and parities (J_i^π) of initial states, while energies (E_f), spins and parities (J_f^π) of final states are listed in the fourth and fifth columns. In the last column, transition intensities after taking into account the Clara efficiency, are listed (normalized to the strongest transition).

E_γ (keV)	E_i (keV)	J_i^π	E_f (keV)	J_f^π	I_γ (%)
345.5	439.2	(+)	93.6	(3/2+)	32.67
459.5	3576.0	(17/2-)	3116.3	(15/2-)	24.34
993.2	993.5	(9/2+)	0.0	5/2+	100.00
1038.3	3116.3	(15/2-)	2077.5	(11/2-)	61.57
1083.6	2077.5	(11/2-)	993.5	(9/2+)	72.71
1482.2	1482.1		0.0	5/2+	50.62
1835.7(11)*					42.44

Figure 6.90: Experimental positive (left) and negative (right) parity states observed in our measurement for ^{91}Sr. Relative γ ray intensities are indicated by widths of arrows. Energies, spins and parities of levels, their branching ratios and energies of transitions are as in Ref. [www4]. The first three positive parity and the first two negative parity states have been observed.

6.8   General remarks about Sr spectra
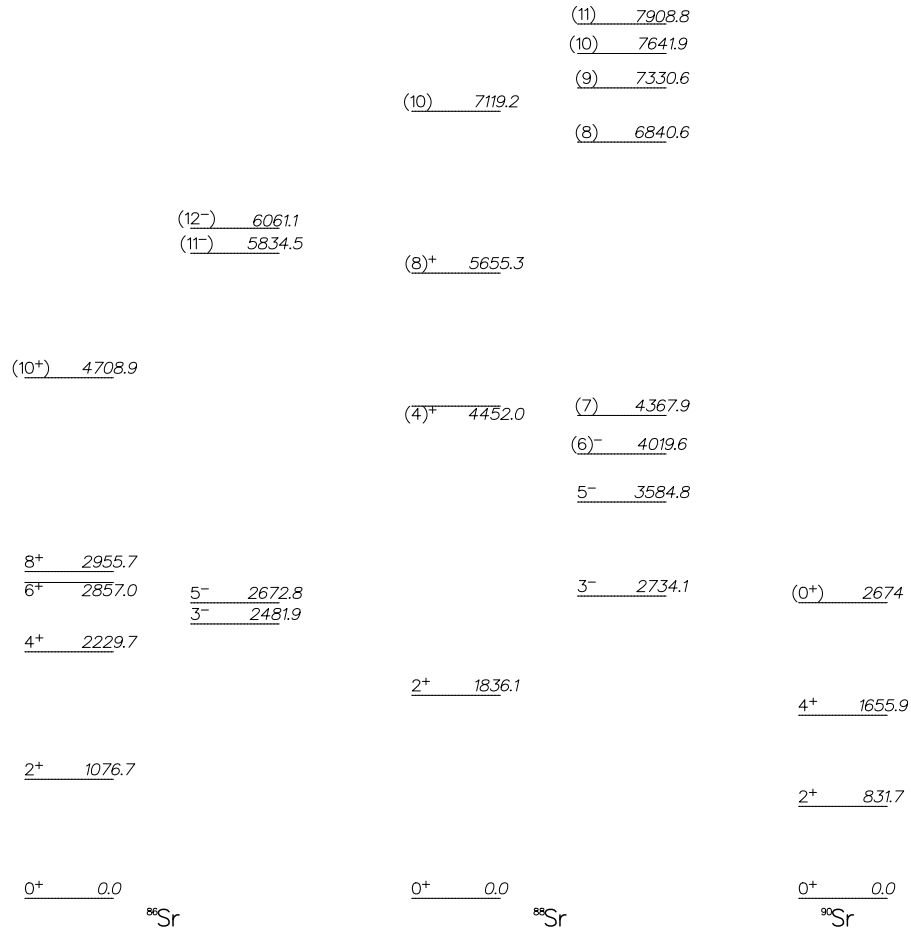
Figure 6.91: Simplified level schemes (only strongly excited states are plotted) of ^{86}Sr (left), ^{88}Sr (middle) and ^{90}Sr (right) isotopes. For each isotope positive (left) and negative (right) parity states are plotted separately.

Figures 6.91 and 6.92 show the strongest excited energy levels in even and odd Sr isotopes, respectively. In the strongest reaction channels, namely $^{86-89}$Sr, high energy levels have been observed, nearly up to 8000 keV (in ^{88}Sr), with rather high spins. The strongest excited states in even Sr isotopes are first 2^+ and 4^+ states, but yrast states up to (10^+) are also present. Unlike Zr isotopes, negative parity states are also strongly excited, with spins up to $(11)^-$ in ^{88}Sr. The exception is ^{90}Sr, which has been, until now, examined only through β^- and (t,p) reactions. These reactions are not likely to populate high spin states, which we expect to excite through MNT reactions because of the large transfer of angular momenta.

197
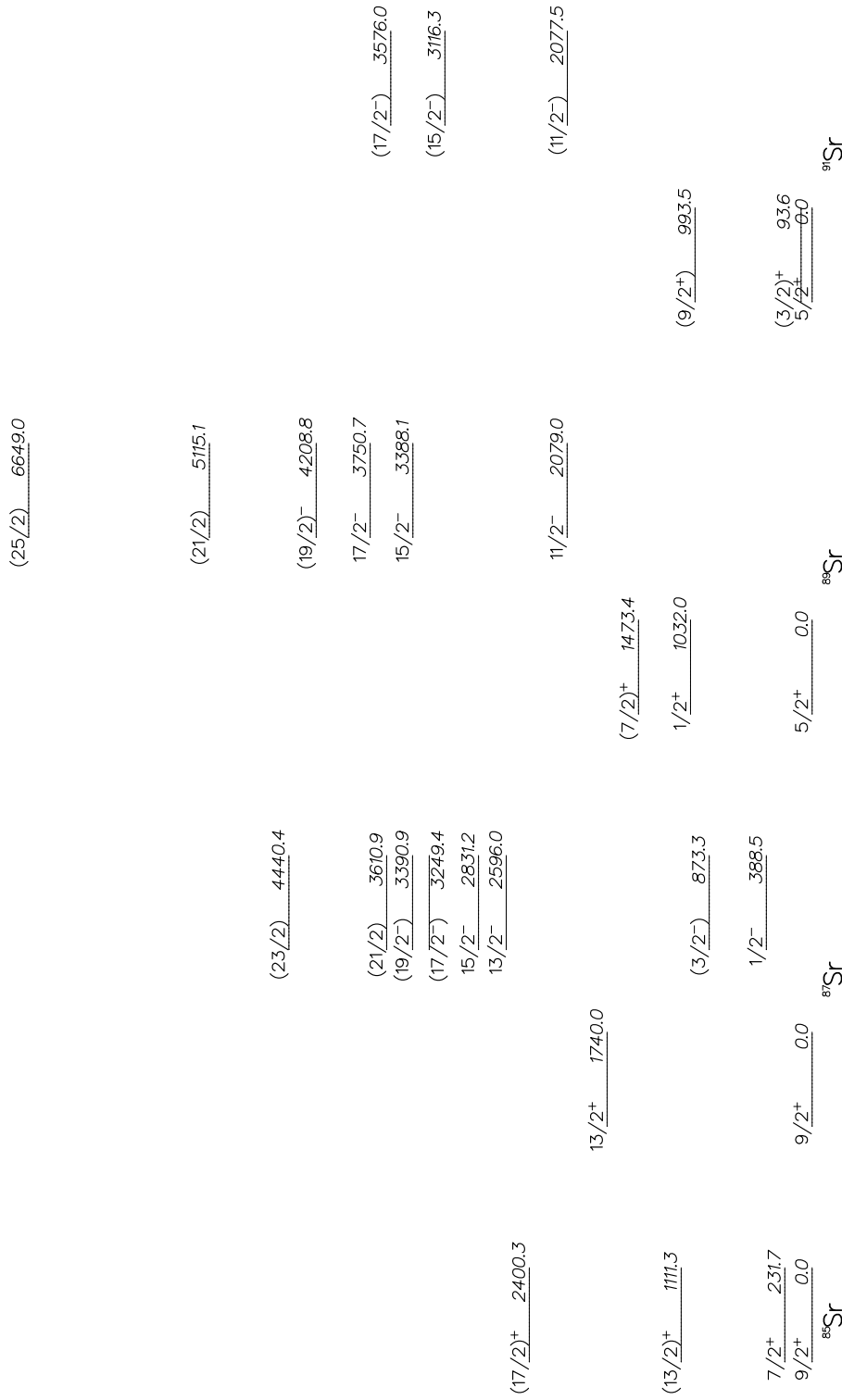
Figure 6.92: Simplified level schemes (only strongly excited states are plotted) of ^{85}Sr (first from the left), ^{87}Sr (second from the left), ^{89}Sr (third from the left) and ^{91}Sr (right) isotopes. For each isotope positive (left) and negative (right) parity states are plotted separately.

Due to low statistics of ^{85}Sr spectrum, only the first few excited levels have been observed. In level schemes of ^{87}Sr, ^{89}Sr and ^{91}Sr, rather high spin states have been observed in negative parity bands. In level schemes of ^{87}Sr and ^{89}Sr, there are high spin states with undefined parities ($J^\pi = (21/2)$ and $(23/2)$ in ^{87}Sr and $J^\pi = (21/2)$ and $(25/2)$ in ^{89}Sr), which we plotted in negative parity bands because of following cascades of γ rays. Again, as in even Sr isotopes, high spin states have only been observed so far in fusion-evaporation reactions.

Thirty-eight protons in Sr leave the proton $2p_{1/2}$ orbital of the $3\hbar\omega$ unoccupied. However, neutron $3\hbar\omega$ subshell is closed in observed Sr isotopes, and, going from ^{85}Sr to ^{91}Sr, neutrons fill the $1g_{9/2}$, and then the $2d_{5/2}$ orbital (see Fig. 6.75).

As concluded earlier, the unpaired neutron in odd Sr isotopes determines the ground state spin and parity, so unpaired neutrons in the $1g_{9/2}$ orbital cause the ^{85}Sr and ^{87}Sr ground state spin to be $9/2^+$, and unpaired neutrons in the $2d_{5/2}$ cause the ground state spin of ^{89}Sr and ^{91}Sr to be $5/2^+$.

Since neutron degrees of freedom are shown to have significant influence in the selection of excited states in Zr isotopes, it is interesting to consider possible single particle states in Sr isotopes. In the case of the ^{85}Sr and ^{87}Sr, in the classical shell model picture, states $1/2^-$, $5/2^-$, $3/2^-$ and $7/2^-$ are expected, if this unpaired neutron is in the $1p_{1/2}$, $1f_{5/2}$, $2p_{3/2}$ or $1f_{7/2}$ orbitals. For ^{89}Sr and ^{91}Sr, states of single-particle character, $7/2^+$, $3/2^+$, $1/2^+$ and $11/2^+$, are expected from the unpaired neutron in the $1g_{7/2}$, $2d_{3/2}$, $3s_{1/2}$ or $1h_{11/2}$ orbital. Figure 6.92 shows that spins could really originate from the single-particle configuration.

In Section 6.2 we examined the structure of excited states of odd Zr isotopes and concluded that most of the strongly excited states of odd Zr isotopes can be described as single particle states or as coupling of ground state spin to a vibration quanta. In order to examine whether a similar particle-vibration coupling occurs in odd Sr isotopes, Figs. 6.93 and. 6.94, which show energies of first 2^+ and 3^- states in even Sr isotopes, respectively, are presented, as well as energies of states in odd Sr isotopes whose spin can be obtained by coupling of the ground state spin to a 2^+ or 3^- vibration quanta in the stretched configuration. The ground state spin of ^{85,87}Sr is $9/2^+$, and of ^{89,91}Sr is $5/2^+$, so coupling to a 2^+ vibration quanta in the stretched configuration would result in spin $13/2^+$ for ^{85,87}Sr and $9/2^+$ for ^{89,91}Sr, as listed in Table 6.45. Coupling the ground state spin to a 3^- quanta would result in spin $15/2^-$ for

^{85,87}Sr and $11/2^-$ for ^{89,91}Sr. Data presented for ^{89,92}Sr in Figure 6.93 are taken from [www4].

Table 6.45: Expected states of possible couplings of the ground state (second column) in Sr isotopes (first column) to a 2^+ (third column) and 3^- (fourth column) vibration quanta, considering the stretched configuration only.

isotope	$J^\pi_{g.s.}$	$J^\pi_{g.s.} \otimes 2^+$	$J^\pi_{g.s.} \otimes 3^-$
^{85,87}Sr	$9/2^+$	$13/2^+$	$15/2^-$
^{89,91}Sr	$5/2^+$	$9/2^+$	$11/2^-$
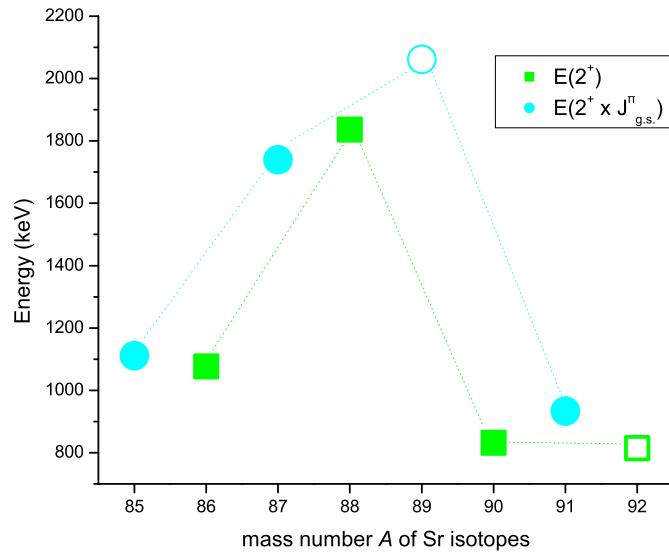
Figure 6.93: Energies of first 2^+ states (green squares) in even Sr isotopes, together with energies of $13/2^+_1$ states in ^{85,87}Sr and $9/2^+$ in ^{89,91}Sr (blue circles). Full circles and squares denote observed energy levels, while empty ones denote data from [www4]. Dashed lines are here only to guide the eyes.

Analogous with Zr isotopes, some neighbouring Sr isotopes have similar energies of plotted states. Indeed, this comparison is even more pronounced than in Zr isotopes, especially for the coupling of the ground state to a 3^- vibration quanta. Namely, energies of $13/2^+$ states in ^{85,87}Sr are similar to energies of 2^+ states of ^{86,88}Sr, respectively, and $9/2^+$ state of ^{91}Sr

has similar energy to 2^+ state of ^{90}Sr. Figure 6.94 shows that the situation repeats with 3^- states in ^{88,90,92}Sr and $15/2^-$ and $11/2^-$ in ^{87,89,91}Sr, respectively, which is in favour with the assumption of the particle-vibrational character of these states.
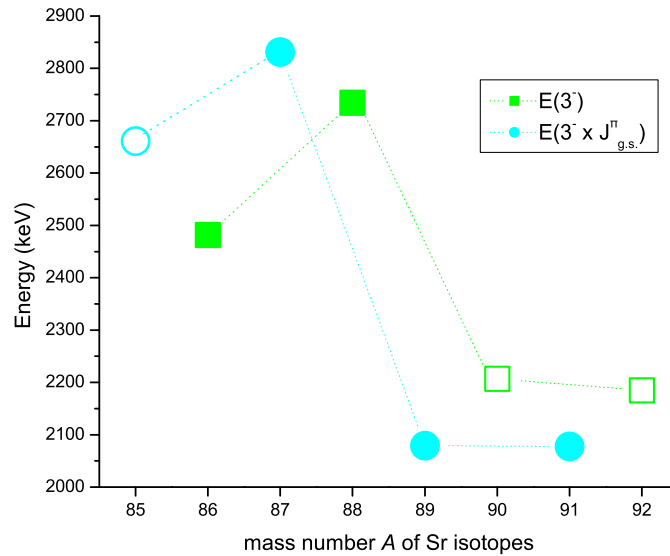
Figure 6.94: Energies of first 3^- states in even Sr isotopes (green squares), and energies of first $15/2_1^-$ in ^{87}Sr and first $11/2_1^-$ in ^{89}Sr (blue circles). Full circles and squares denote observed energy levels, while empty ones denote data from [www4]. Dashed lines are here only to guide the eyes.

Chapter 7

Conclusion

Multinucleon transfer reactions have been studied in the ^{90}Zr+^{208}Pb system close to the Coulomb barrier energy with the Prisma + Clara set-up, at the *Laboratori Nazionali di Legnaro-INFN* accelerator center.

In the ^{90}Zr+^{208}Pb multinucleon transfer experiment, nuclei with $Z = 30 - 40$ and $A = 60 - 94$ were populated. In this thesis, we mainly focused on the spectra of the Zr (together with their heavy partner, Pb), Y and Sr isotopic chains. We put the main focus on Zr isotopes $^{89-94}$Zr, which are the strongest reaction channels. ^{90}Zr is a semi-magic nucleus with a closed neutron $3\hbar\omega$ shell. In odd Zr and Sr ($-2p$ channel) nuclei, the unpaired neutron determines the ground state of the isotope, which is $9/2^+$ in ^{89}Zr and ^{85,87}Sr (due to a neutron hole in the $1g_{9/2}$ orbital) and $5/2^+$ in ^{91,93}Zr and ^{89,91}Sr (due to uncoupled neutron in the $2d_{5/2}$ orbital). It is expected that the active single particle orbitals in the observed Zr and Sr isotopes originate from the unpaired neutron in $2p_{1/2}$, $1f_{5/2}$ or $2p_{3/2}$ orbitals. In ^{89}Zr and ^{85,87}Sr, this would result in $1/2^-$, $5/2^-$ and $3/2^-$ single particle states. In the case of ^{91,93}Zr and ^{89,91}Sr unpaired neutron in $1g_7/2$, $2d_{5/2}$, $2d_{3/2}$, $3s_{1/2}$ or $1h_{11/2}$ would provide the $7/2^+$, $5/2^+$, $3/2^+$, $1/2^+$ or $11/2^+$ states. In the presented level schemes (see Chapter 6), those spin states dominate the low-lying energy part of spectra in the observed and discussed odd Zr and Sr isotopes. The strongest populated channels, mainly the $^{89-94}$Zr isotopes, were studied in more detail.

The nature of assumed single-particle states of isotopes ^{91}Zr and ^{93}Zr is discussed by comparing the population of these states obtained in our measurement to those obtained

in different (p,d) measurements (see Figs. 6.14, 6.26), where the reaction is more likely to excite single-particle states. The comparison showed similar population strengths for $1/2^+$ ($E_{\text{ex}} = 1204.8$ keV) and $3/2^+$ ($E_{\text{ex}} = 2042.4$ keV) states of ^{91}Zr, as well as $1/2^+$ ($E_{\text{ex}} = 947.1$ keV) and $3/2^+, 5/2^+$ ($E_{\text{ex}} = 1425.5$ keV) states of ^{93}Zr, indicating single-particle character of these states.

We also compared our results to the shell model calculations described in [SNL09] and [DBI11] (see Figs. 6.16 and 6.27), where a shell model study of Zr isotopes was performed in an extended ([SNL09]) or full ([DBI11]) shell model space ($1f_{5/2}$, $2p_{1/2}$, $2p_{3/2}$, $1g_{9/2}$) for protons and ($2d_{5/2}$, $3s_{1/2}$, $2d_{3/2}$, $1g_{7/2}$, $1h_{11/2}$) for neutrons. These comparisons support our assumption of the single-particle character of the low lying states.

Special attention was devoted to the study of the states of the phonon-fermion nature, as this degree of freedom proved to be an important ingredient in the reaction models. In the study of the underlying structure of the strongly excited states we investigated the possibility of the coupling of the ground state of the odd Zr and Sr nuclei to the 2^+ or 3^- vibration quanta in the stretched configuration (see Tables 6.10 and 6.45). This stretched configuration is favored by the transfer mechanisms as the transfer probability has its maximum at the largest angular momentum transfer [BW00]. The results, presented in Figs. 6.36, 6.37, 6.93 and 6.94, show that in most of the studied isotopes, the decay modes and the energies of the 2^+ and 3^- states in even isotopes have similar decay modes and energies as the expected particle-vibration states in the odd nuclei. The similarity in energies of the first 2^+ (and 3^-) states in even isotopes and of the states states that could correspond to coupling of 2^+ (i.e. $13/2^+$ in ^{85,87}Sr and $9/2^+$ in ^{91}Sr) and 3^- phonon (i.e. $15/2^-$ and $11/2^-$ in ^{87,89,91}Sr) to the ground state in the stretched configuration is even more pronounced in Sr than in Zr isotopes.

Of special interest were states $9/2_1^+$, $9/2_2^+$, $11/2_1^-$ and $11/2_2^-$ in ^{91}Zr, as those states can have, both, the single-particle, as well as the particle-vibration character. To further investigate the character of these states, we considered decay patterns and associated decay strengths of states of interest (i.e. 2^+ and 3^- states in even isotopes, and expected particle-vibrational states in odd isotopes). Also, we compared our result to theoretical models from [BHK76] and [SNL09]. Our conclusions about the importance of the particle-vibration

coupling were partially obscured because the structure of some states of interest display a rather mixed configuration [BHK76, SNL09].

In our experiment, we were searching for excitation of the 0^+ states that were recognized as pairing vibration states, and that were strongly excited in the (t, p) reactions [BW00]. At the level of the accumulated statistic we could not undoubtedly confirm the excitation of those states.

In all the observed nuclei (with the exception of the weaker reaction channels, such as ^{89}Zr, ^{85}Sr or ^{94}Y), it is clear that most of the excited states belong to the yrast states, i.e. the states which have the highest spin for the given energy. In some isotopes, high spin states were selectively observed (up to 16^+ in ^{92}Zr or $29/2^+$ in ^{89}Y), showing that the multinucleon transfer reactions with heavy ions are a good tool to excite high spin and energy states.

Through study of the Pb isotopes (the heavy binary partner of Zr), the effect of evaporation, which strongly affect the primary yields, has been discussed. The isotopes produced after the evaporation of one or two neutrons were recognized through their γ rays, while their relative strengths allow to quantitatively estimate the effect of the evaporation for the first time in such a heavy system. In the observed neutron transfer channels ($^{205-209}$Pb), most of the yield corresponds to true binary partner.

A thorough examination of the γ spectra revealed that new γ transitions have been identified (which were not previously reported in the National Nuclear Data Center at Brookehaven National Laboratory-http://www.nndc.bnl.gov), and uniquely attributed to the specific isotope. In addition, for the Zr isotopes, the γ spectra obtained in the previous ^{40}Ca+^{96}Zr [Szi07] measurement were used. When possible, decay patterns for these rays have been suggested and the level schemes have been updated based mainly on systematics with neighbouring nuclei. For these new γ transitions we proposed that some of them decay from high spin states (in the higher energy part of the spectrum) and some of them arise from states that might have single particle origin or may originate from the particle-vibration coupling. These γ rays are listed in Table 5 in the Appendix.

Presented results, in general, contribute significantly to the understanding of the selectivity of the multinucleon transfer reaction mechanism in the selection of the states of specific structure. In particular, the strong excitation of the states connected with the coupling of

single-particle degrees of freedom to nuclear vibration quanta was observed. It is difficult to disentangle the effect of the fermion-boson coupling from energy systematics only, therefore further understanding of these important degrees of freedom in this mass and charge region requires additional measurements of other relevant properties, such as the strength of electromagnetic transitions.

Appendix

Table 1: γ rays of Zr isotopes not observed in the spectrum because of their low intensity. The first column represents energies (E_γ) of γ rays, second and third columns list energies (E_i) and spins and parities (J_i^π) of initial levels, fourth and fifth columns show energies (E_f) and spins and parities (J_f^π) of final states, while the last column shows tabulated intensities (I_γ) of γ transitions. All the data are as in [www4].

E_γ (keV)	E_i (keV)	J_i^π	E_f (keV)	J_f^π	I_γ (%)
		^{89}Zr			
587.8	587.8	1/2-	0.0	9/2+	100
356.4	1451.2	5/2-	1094.9	3/2-	56
565.0	2724.1	17/2+	2159.0	(17/2-)	0.19
573.9	2724.1	17/2+	2150.6	(15/2-)	0.6
68.79	2995.3	21/2+	2926.5	(19/2-)	0.9
460.1	4737.6	25/2+	4277.7	(25/2+)	1.2
1160.7	4737.6	25/2+	3576.8	(23/2)+	10.7
		^{90}Zr			
425.5	2186.3	2+	1760.7	0+	0.027
132.7	2319.0	5-	2186.3	2+	5.04
429.0	2747.9	3-	2319.0	5-	<4
2747.8	2747.9	3-	0.0	0+	4.1
337.5	3076.9	4+	2739.3	(4)-	1.4
758.0	3076.9	4+	2319.0	5-	2.22

236.5	3308.8	2+	3076.9	4+	
371.3	3448.2	6+	3076.9	4+	1.95
1270.4	3589.4	8+	2319.0	5-	1.94

			⁹¹Zr		

38.7	2170.2	(11/2)-	2131.5	(9/2)+	2.5
28.0	2287.8	(15/2)-	2259.9	(13/2)-	100
60.3	2320.5	(11/2)-	2259.9	(13/2)-	
289.8	3146.9	(17/2)+	2857.1	(13/2)+	13.3
2574	5471.3		3167.3	(21/2+)	
305	5613.1		5308.2		
901	5613.1		4712.1		
20.4	3167.3	(21/2+)	3146.9	(17/2)+	7
879.4	3167.3	(21/2+)	2287.8	(15/2)-	100

			⁹²Zr		

219.2	2066.7	2+	1847.3	2+	0.79
571.4	2066.7	2+	1495.5	4+	0.66
272.9	2339.7	3-	3066.7	2+	0.17
492.5	2339.7	3-	1847.3	2+	10.4
844.2	2339.7	3-	1495.5	4+	26.3
2339.9	2339.7	3-	0.0	0+	0.30
902.9	2398.4	4+	1495.5	4+	100.00
1928.7	2863.4	4+	934.5	2+	28
717.9	2057.4	2+	2339.7	3-	31.5
1674.9	2057.4	2+	1382.8	0+	6.7
2123.0	2057.4	2+	934.5	2+	39.1
3057.2	2057.4	2+	0.0	0+	8.2
366.6	3275.9	(2+,3)	2909.5	2+,3+	8.9
877.5	3275.9	(2+,3)	22398.3	4+	24.4
2341.0	3275.9	(2+,3)	934.5	2+	48

		^{93}Zr			
680.2	947.1	1/2+	266.8	3/2+	31.4
1158.5	1425.3	3/2+, 5/2+	266.8	3/2+	12.3
1203.3	1470.1	(1/2+, 3/2+, 5/2+)	266.8	3/2+	100
		^{94}Zr			
537.2	3142.4	(6+)	2605.0	5-	17.9
588.0	2057.6	3-	1469.6	4+	2.8
860.0	2329.9	4+	1469.6	4+	< 3
537.2	3142.4	(6+)	2605.0	5-	17.9
1672.9	3142.4	(6+)	1469.6	4+	3.8

Table 2: γ rays of Pb isotopes not observed in the spectrum because of their low intensity. The first column represents energies (E_γ) of γ rays, second and third columns list energies (E_i) and spins and parities (J_i^π) of initial levels, fourth and fifth columns show energies (E_f) and spins and parities (J_f^π) of final states, while the last column shows tabulated intensities (I_γ) of γ transitions. All the data are as in [www4].

E_γ (keV)	E_i (keV)	J_i^π	E_f (keV)	J_f^π	I_γ (%)
		^{205}Pb			
313.4	576.2	3/2-	262.8	3/2-	5.5
		^{206}Pb			
126.4	1466.8	2+	1340.5	3+	3.8
1466.8	1466.8	2+	0.0	0+	30.4
313.7	1997.7	4+	1684.0	4+	21.0
657.7	1997.7	4+	803.1	2+	14.5
202.4	2200.2	7-	1997.7	4+	0.1
516.2	2200.2	7-	1684.0	4+	100.0

35.0	3279.2	5-	3244.2	4-	0.1
262.7	3279.2	5-	3016.4	5-	19.3
339.9	3279.2	5-	2939.6	6-	
452.8	3279.2	5-	2826.3	(4)-	1.0
497.1	3279.2	5-	97.8	2782.17	97.8
1281.8	3279.2	5-	1997.7	4+	0.4
1595.3	3279.2	5-	1684.0	4+	32.0
2476.7	3279.2	5-	803.1	2+	0.1
964.2	2647.8	3-	803.1	2+	6.4

^{207}Pb					
328.1	897.7	3/2-	569.7	5/2-	0.5
1422.2	2339.9	7/2-	897.7	3/2-	1.9
388.2	2727.9	9/2+	2339.9	7/2-	19.5
2158.2	2727.9	9/2+	569.7	5/2-	2.4
447.8	3175.7	9/2(+)	2727.9	9/2+	44.0
835.7	3175.7	9/2(+)	2339.9	7/2-	62.0
1542.3	3175.7	9/2(+)	1633.4	13/2+	91.0

^{208}Pb					
233.3	3708.5	5-	3475.1	4-	1.6
1094.0	3708.5	5-	2614.5	3-	1.8
1471.5	4085.5	2+	2614.5	3-	0.5
362.8	4323.9	4+	3961.8	5-	14.8
848.9	4323.9	4+	3475.1	4-	2.4
1709.6	4323.9	4+	2614.5	3-	0.5
4324.3	4323.9	4+	0	0+	0.3
715.2	4423.3	6+	3708.5	5-	8.6
892.3	5216.2	4+	4323.9	4+	31.0

^{209}Pb					
644.0	1423	15/2-	0.0	9/2+	10

Table 3: γ rays of Y isotopes not observed in the spectrum because of their low intensity. The first column represents energies (E_γ) of γ rays, second and third columns list energies (E_i) and spins and parities (J_i^π) of initial levels, fourth and fifth columns show energies (E_f) and spins and parities (J_f^π) of final states, while the last column shows tabulated intensities (I_γ) of γ transitions. All the data are as in [www4].

E_γ (keV)	E_i (keV)	J_i^π	E_f (keV)	J_f^π	I_γ (%)
			^{87}Y		
380.8	380.8	9/2+	0.0	1/2-	100.0
962.4	2366.9	15/2-	1404.4	13/2+	100.0
27.2	2676.0	17/2-	2648.9	(15/2-)	
247.9	2676.0	17/2-	2428.1	17/2+	20
440.9	3402.4	(19/2-)	2961.4	17/2-	51
			^{88}Y		
392.9	392.9	1+	0.0	4+	100.0
442.6	674.6	8+	231.9	5-	100.0
483.5	715.1	(6)+	231.9	5-	100.0
706.3	706.8	2-	0.0	4-	8
611.0	843.0	(5)+	231.9	5-	39
842.5	843.0	(5)+	0.0	4-	41
131.4	2443.9	(10+)	2312.2	(9+)	2.8
967.6	2443.9	(10+)	1476.9	9+	9
395.6	3652.1	(11-)	3256.5	(10-)	31.9
680.0	3964.2	(12-)	3284.1	(11+)	
			^{89}Y		
909.0	909.0	9/2+	0.0	1/2-	100.0
326.5	2893.0	13/2+	2566.6	11/22	1.4
3247.5	3247.6	(3/2, 5/2)	0.0	1/2-	7.4
450.5	3343.4	13/2-	2893.0	13/2+	6.2

570.5	4825.4	17/2+	4254.4	(15/2+)	11
1931.9	4825.4	17/2+	2893.0	13/2+	14
95.1	4920.5	(19/2+)	4825.4	17/2+	38
425.6	5236.9	(21/2+)	4838.6	19/2-	1.6
860.1	5309.8	(21/2-)	4449.8	17/2-	5.3
1360.3	6198.9	(23/2+)	4838.6	19/2-	
172.1	7431.6	(25/2+)	7259.5	(23/2+)	34
757.1	7431.6	(25/2+)	6674.4	(23/2+)	42
1232.6	7431.6	(25/2+)	6198.9	(23/2+)	100.0
244.6	7834.6	(27/2+)	7590.0	(25/2+)	58
650.9	7834.6	(27/2+)	7183.7	(25/2+)	100.00
832.9	8264.2	(29/2+)	7431.6	(25/2+)	< 15
		^{90}Y			
479.2	681.7	7+	202.5	3-	100.0
681.8	681.7	7+	0.0	2-	0.4
574.1	776.6	2+	202.5	3-	26
176.9	953.5	2+,3+	776.6	2+	61
751.3	953.5	2+,3+	202.5	3-	6.9
250.8	1298.2	(5, 6, 7) +	1046.9	5+, 6+, 7+	5.0
718.0	2133.5	(1, 2-)	1416.6	3-, (2)-	6.3
762.4	2133.5	(1, 2-)	1371.1	1-	91
921.7	2133.5	(1, 2-)	1211.6	0-	6.9
2133.3	2133.5	(1, 2-)	0.0	2-	21
1032.6	2244.3	(1+, 2-)	1211.6	0-	16
1290.8	2244.3	(1+, 2-)	953.5	2+, 3+	14
1467.6	2244.3	(1+, 2-)	776.6	2+	48
		^{91}Y			
555.6	555.6	9/2+	0.0	1/2-	100.0
272.6	925.7	5/2-	653.0	3/2-	6.8
533.9	1186.9	(7/2)-	653.0	3/2-	13.9

118.5	1305.4	(5/2)+	1186.9	(7/2)-	0.311
379.9	1305.4	(5/2)+	925.7	5/2-	0.622
652.3	1305.4	(5/2)+	653.0	3/2-	12.6
749.8	1305.4	(5/2)+	555.6	9/2+	100.0
1305.3	1305.4	(5/2)+	0.0	1/2-	0.071
359.1	1545.9	(5/2)-	1186.9	(7/2)-	2.8
892.9	1545.9	(5/2)-	653.0	3/2-	4.0
359.1	1545.9	(5/2)-	1186.9	(7/2)-	2.83
892.9	1545.9	(5/2)-	653.0	3/2-	3.96
1545.9	1545.9	(5/2)-	0.0	1/2-	3.8
1410.8	3568.1	(19/2,21/2)	2157.1	(17/2+)	98
570.3	3733.2	(19/2,21/2)	3162.9	(15/2,17/2)	88
413.8	4147.0	(23/2,25/2+)	3733.2	(19/2,21/2)	44
578.6	4147.0	(23/2,25/2+)	3568.1	(19/2,21/2)	30
953.5	4481.2	(25/2+)	3527.7	(21/2+)	10.9
		^{93}Y			
590.2	590.2	(3/2)-	0.0	1/2-	100.0
168.5	758.7	(9/2)+	590.2	(3/2)-	100.0

Table 4: γ rays of Sr isotopes not observed in the spectrum because of their low intensity. The first column represents energies (E_γ) of γ rays, second and third columns list energies (E_i) and spins and parities (J_i^π) of initial levels, fourth and fifth columns show energies (E_f) and spins and parities (J_f^π) of final states, while the last column shows tabulated intensities (I_γ) of γ transitions. All the data are as in [www4].

E_γ (keV)	E_i (keV)	J_i^π	E_f (keV)	J_f^π	I_γ (%)
		^{86}Sr			

777.4	1854.2	2+	1076.7	2+	100
1854.4	1854.2	2+	0.0	0+	76.5
252.1	2481.9	3-	2229.7	4+	1.14
1404.8	2481.9	3-	1076.7	2+	0.56
2482.1	2481.9	3-	0.0	0+	0.354
190.8	2672.8	5-	2481.9	3-	6.2
98.7	2955.7	8+	2857.0	6+	100
809.4	3482.2	6+	2672.8	5-	100
469.24	3968.9	3-,4,5-	3499.9	(3,4,5)-	55
783.6	3698.9	3-,4,5-	3185.2	(3)-	48
971.4	3698.9	3-,4,5-	2997.4	3-	50

	^{87}Sr				
388.5	388.5	1/2-	0.0	9/2+	100
235.2	2381.2	15/2-	2596.0	13/2-	6.7

	^{88}Sr				
2734.1	2734.1	3-	0.0	0+	0.77
782.9	4367.9	(7-)	3584.8	5-	11.8
867.1	4452.0	(4)+	3584.8	5-	7.5
2615.9	4452.0	(4)+	1836.1	2+	1.31
581.8	5103.3	(7)	4521.4	(6)-	18.0
1713.9	6235.5	(7)	4521.4	(6)-	100.0
1867.4	6235.5	(7)	4367.9	(7-)	94.0
1470.1	6840.6	(8)	5370.5		23.0
2153.4	6840.6	(8)	4687.4	(7)	30
2473.3	6840.6	(8)	4367.9	(7-)	11.2
1902.9	7330.6	(9)	5427.5	(8)	13.3
522.7	7641.9	(10)	7119.2	(10)	10.9

	^{89}Sr				
536.5	4208.8	(19/2)-	3672.1	(15/2-)	5.1

			^{91}Sr		
93.6	93.6	(3/2)+	0.0	5/2+	100.0
1388.1	1482.1		93.6	(3/2)+	15.1
271.4	3576.0	(17/2-)	3304.4	(15/2-)	21

Table 5: Possible new transitions for yet unknown γ rays of the observed isotopes, based on the energy difference of known energy levels. The first column lists energies of γ rays (E_γ) in keV, the second and third columns show energies (E_i), spins and parities (J_i^π) of suggested initial states, while energies (E_f), spins and parities (J_f^π) of suggested final states are listed in the fourth and fifth columns.

isotope	E_γ (keV)	E_i (keV)	J_i^π	E_f (keV)	J_f^π
^{90}Zr	1872(1)	4062(5)	4^+	2186.3(15)	2^-
		4946(6)	4^+	3076.9(15)	4^+
^{93}Zr	1081.6(7)	2025.0(10)	9/2-, 11/2-	947.1(8)	1/2+
	1605(1)	1598.0(5)	7/2+, 9/2+	0.0	5/2+
	1472(1)	1735		266.8(5)	3/2+
		2638(10)	7/2+, 9/2+	1168.6(20)	1/2+
^{92}Y	314.5(0.1)	310(10)	2^-, 3^-, 4^-	0.0	2^+
^{94}Y	584.3(0.2)*	$X + 1423.9$		$X + 839.6$	
	673.3(0.2)*	$X + 2097.2$		$X + 1423.9$	
	839.6(0.5)*	$X + 839.6$		X	
^{87}Sr	299.6(0.1)	2893(8)		2596.0(5)	13/2-
		3551(8)		3249(5)	17/2-
	448.7(0.8)	3792.3(17)		3249.4(5)	(17/2-)
	501.6(0.2)	3894(8)		3390.9(6)	(19/2-)
		4943(4)		4440.0(10)	(23/2)
^{89}Sr	1273.9(0.5)	4626(10)		3388.1(7)	$15/2^-$
		5442(10)		4208.8(10)	$(19/2)^-$

List of Figures

List of Tables

Bibliography

[BAR71] J. B. Ball, R. L. Auble, and P. G. Roos.: *Study of the Zirconium Isotopes with the (p,t) Reaction*, Physical Review C, Volume 4, 196, 1971

[Beg05] S. Beghini et.al.: *The Focal Plane Detector for the magnetic spectrometer Prisma*, Nuclear Instruments and Methods in Physics Research Section A: Accelerators, Spectrometers, Detectors and Associated Equipment, Volume 551, Issues 2-3, Pages 364-374, 2005

[BH70] C. R. Bingham, M. L. Halbert: *Neutron Shell Structure in ^{91}Zr and ^{92}Zr by (d,p) and $(\alpha, {}^{3}He)$ Reactions*, Physical Review C, Volume 2, Number 6, 2297-2309, 1970

[BF73] C. R. Bingham, G.T: Fabian: *Neutron Shell Structure in ^{93}Zr, ^{95}Zr and ^{97}Zr by (d,p) and $(\alpha, {}^{3}He)$ Reactions*, Physical Review C, Volume 7, Issue 4, 1509-1518, 1973

[BHK76] H. P. Blok, L. Hulstman, E. J. Kaptein, J. Blok: *Investigation of ^{91}Zr by high resolution (d,p) and (p,d) reactions*, Nuclear Physics A273, 142-171, 1976

[BM69] A. Bohr and B. Mottelson: *Nuclear Structure, edited by W. A. Benjamin*, Inc., New York, Volume 1, 1969

[Bro73] R.A. Broglia, et al.: *Advances in Nuclear Physics, edited by M. Baranger and E. Vogt*, Plenum, New York, Volume 6, p. 287, 1973

[BW00] R.A. Broglia, A. Winther: *Heavy ion reactions; The elementary prosesses, parts I and II*, Westview press, Boulder, 2000

[Bro06] R. BRODA: *Spectroscopic studies with the use of deep-inelastic heavy-ion reactions*, Journal of Physics G: Nuclear and Particle Physics, Volume 32, Number 6, R151 2006

[Bun13] M. BUNCE ET AL.: *High-spin study of the shell model nucleus $^{88}Y_{49}$*, Physical Review C, Volume 87, 044337, 2013

[CMN05] E. CAURIER, G. MARTÍNEZ-PINEDO, F. NOWACKI, A. POVES, A. P. ZUKER: *The Shell Model as Unified View of Nuclear Structure*, Reviews of Modern Physics, Volume 77, 427-488, 2005

[Cor99] L. CORRADI ET AL.: *Multinucleon transfer processes in $^{64}Ni+^{238}U$*, Physical Review C Volume 59, 261, 1999

[CPS09] L. CORRADI, G. POLLAROLO, S. SZILNER *Multinucleon transfer processes in heavy-ion reactions*, Journal of physics G: Nuclear and particle physics 36, 113101, 2009

[Cor09] L. CORRADI ET.AL. *Heavy ion transfer reactions studied with Prisma + Clara*, Acta physica polonica B, Vol. 40, No. 3, 2009

[Cor13] L. CORRADI ET.AL. *Multinucleon transfer reactions : present status and perspectives*, Nuclear Instruments and Methods in Physics Research. Section B: Beam Interactions with Materials and Atoms, Vol. 317, Part B; 743-751, 2013

[DPW94] C. H. DASSO, G. POLLAROLO, A. WINTHER *Systematics of isotope production with radioactive beams*, Physical Review Letters, Volume 73, Number 14, 1994

[DBI11] S. S. DIMITROVA, D. BIANCO, N. LO IUDICE, F. ANDREOZZI, A. PORRINO *Shell-Model Calculations for ^{91}Zr*, Nuclear Theory, Volume 30, 100, 2011

[Dra96] G. D. DRACOULIS *Trends in nuclear structure with heavy ions*, Nuclear instruments and methods in physics research A 382, 1-19, 1996

[Elh08] E. ELHAMI ET AL.: *Experimental study of the low-lying structure of ^{94}Zr with the $(n, n\gamma)$ reaction*, Physical Review C, Volume 78, 064303, 2008

[FBA68] E. R. Flynn, A. G. Blair, D. D. Armstrong: *Inelastic Scattering of 20 MeV Tritons from ^{90}Zr*, Physical Review C, Volume 170, Issue 4, 1142-1156, 1968

[Fly74] E. R. Flynn et al.: *The (t,p) reaction to the low-lying levels of the zirconium isotopes*, Nuclear Physics A218, 285-306, 1974

[FHS76] E. R. Flynn, O. Hansen, J. D. Sherman, N. Stein and J. W. Sunierj: *The $^{88}Sr(t,p)^{90}Sr$ reaction at 20 MeV and the systematics of pairing excitations near $N = 50$*, Nuclear Physics A, Volume 264, Issue 2, 253267, 1976

[For87] G. Fortuna et.al.: *The Alpi project at Legnaro National Laboratory*, Proceedings of the third workshop on RF superconductivity, Argonne National Laboratory, Illinois, USA, 1987

[Fot02] N. Fotiades et al.: *High-spin excitations in $^{92,93,94,95}Zr$*, Physical Review C, Volume 65, 044303, 2002

[Gad04] A. Gadea et al.: *Coupling a CLOVER detector array withthe Prisma magnetic spectrometer. Investigation of moderately neutron-richnuclei populated by multinucleon transfer and deep inelastic collisions*, The European Physical Journal A 20, 193197, 2004

[Gar03] P. E. Garrett et al.: *Nuclear structure of the closed subshell nucleus ^{90}Zr studied with the $(n,n\gamma)$ reaction*, Physical Review C, Volume 68, 024312, 2003

[Got07] A. Gottardo: *Study of neutron-rich nuclei with the Clara-Prisma setup and first tests of the ancillary detector Dante*, Tesi per il conseguimento della laurea specialistica in fisica, 2007

[Hod82] P. E. Hodgson *Heavy ion reactions*, Contemporary Physics, Vol. 23. No. 5, 495-512, 1982

[IMB75] S. S. Ipson, K. C. McLean, W. Booth, J. G. B. Haigh: *Experimental and shell-model studies of the reactions $^{91}Zr(p,d)^{92}Zr$ and $^{90}Zr(t,d)^{92}Zr$*, Nuclear Physics A253, 189-215, 1975

[Lat04] A. Latina *Study of Heavy-Ion Reactions with the Magnetic Spectrometer Prisma: On-line and Off-line Data Analysis*, Dottorato di ricerca in fisica, Torino University, 2004

[LDV03] I. Y. Lee, M. A. Deleplanque, K. Vetter: *Developments in largeγ-ray detector arrays*, Reports on progress in physics 66, 1095-1144, 2003

[Lun07] S. Lunardi et al.: *Spectroscopy of neutron-rich Fe isotopes populated in the ^{64}Ni + 238U reaction*, Physical Review C, Volume 76, Issue 3, 034303, 2007

[May82] W. Mayer et al.: *Strong population of excited 0^+ states in even Zr isotopes observed with the (^{14}C, ^{16}O) reaction*, Physical Review C, Volume 26, 500, 1982

[Mar09] N. Marginean et.al. *Evolution of deformation in the neutron-rich krypton isotopes: The ^{96}Kr nucleus*, Physical Review C 80, 021301 (R), 2009

[Mer06] A. Meroni *Ricostruzione delle triettorie e analisi dati con Prisma*, Universita degli Studi di Padova, 2006

[Mij12] T. Mijatović et al.: *Nuclear Structure and Dynamics*, AIP Conference Proceedings, Volume 1491, 346, 2012

[Mon97] G. Montagnoli et.al. *Multinucleon transfer reactions of $^{40}Ca+^{90,96}Zr$*, Journal of Physics G: Nuclear and Particle Physics, Volume 23, Number 10, 14311437, 1997

[Mon00] G. Montagnoli et.al. *The time-of-flight spectrometer for heavy ions PISOLO*, Nuclear instruments and methods in physics research A 454, 306-314, 2000

[Mon05] G.Montagnoli et.al.: *The large-area micro-channel plate entrance detector of the heavy-ion magnetic spectrometer Prisma*, Nuclear Instruments and Methods in Physics Research Section A, Volume 547, Issue 2-3, p. 455-463., 2005.

[Mon09] D. Montanari: *Reaction dynamics of neutron rich nuclei in Ca isotopes with heavy ions andγ spectroscopy*, Dottorato di ricerca in fisica, astrofisica e fisica applicata, 2009

[Mon11] D. Montanari et al.: *Response function of the magnetic spectrometer Prisma*, The European Physical Journal A, Volume 47, 4, 2011

[MLG12] D. Montanari, S. Leoni, A. Gadea, G. Pollarolo: *γ spectroscopy of calcium nuclei around doubly magic ^{48}Ca using heavy-ion transfer reactions*, Physical Review C Volume 85, 044301, 2012

[Pan05] D. Pantelica et al.: *High-spin states in $^{92-96}Zr$ nuclei*, Physiocal Review C, Volume 72, 024304, 2005

[PBV10] G. Potel, F. Barranco, E. Vigezzi, and R. A. Broglia: *Evidence for Phonon Mediated Pairing Interaction in the Halo of the Nucleus ^{11}Li*, Physical Review Letters, Volume 105, 172502, 2010

[PIB13] G. Potel, A. Idini, F. Barranco, E. Vigezzi, R. A. Broglia: *Cooper pair transfer in nuclei*, Reports on Progress in Physics, Volume 76, Number 10, 106301, 2013

[Pul08] S. Pullanhiotan *Characterization of a large acceptance spectrometer and its application to spectroscopy of exotic nuclei*, Doctoral thesis, 2008

[RWB97] E. Radermarcher, M. Wilhelm, P. von Brentano, R. V. Jolos: *The γ-decay of single-particle states in ^{205}Pb and ^{207}Pb using an Euroball Cluster detector*, Nuclear Physics A, Volume 620, Issue 2, 151170, 1997

[RKL70] R. C. Ragaini, J. D. Knight, and W. T. Leland: *Levels of ^{88}Sr from the $^{86}Sr(t,p)^{88}Sr$ Reaction*, Physical Review C, Volume 2, 1020, 1970

[Rec12] F. Recchia et al.: *Spectroscopy of odd-mass cobalt isotopes toward the N=40 subshell closure and shell-model description of spherical and deformed states*, Physical Review C, Volume 85, Issue 6, 064305, 2012

[Reh91] K. E. Rehm *Quasi-elastic heavy-ion collisions*, Annu. Rev. Nucl. Part. Sci. 41: 429-68, 1991.

[Reh88] K. E. Rehm et al.: *Transition from quasi-elastic to deep-inelastic reactions in the $^{48}Ti+^{208}Pb$ system*, Physical Review C, Volume 37, Number 6, 2629-2646, 1988

[SJP79] A. Saha, G. D. Jones, L. W. Put, R. H. Siemssen: *Unusually strong excitation of the 1.59 MeV 0^+ state in the $^{100}Mo(d,^6Li)^{96}Zr$* , Physics Letters B, Volume 82, Issue 2, 208-211, 1979

[SL13] G. Scamps, D. Lacroix: *Effect of pairing on one- and two-nucleon transfer below the Coulomb barrier: A time-dependent microscopic description*, Physical Review C, Volume 87, 014605, 2013

[SY13] K. Sekizawa, K Yabana: *Time-dependent Hartree-Fock calculations for multinucleon transfer processes in $^{40,48}Ca+^{124}Sn$, $^{40}Ca+^{208}Pb$, and $^{58}Ni+^{208}Pb$ reactions*, Physical Review C, Volume 88, 014614, 2013

[Sha12] K. D. Sharp: *Trends in single-particle energies in $N = 51$ nuclei*, PhD. thesis, The University of Manchester, 2012.

[Sha13] K. D. Sharp et al.: *Neutron single-particle strength outside the $N = 50$ core*, Physical Review C, Volume 87, 014312, 2013

[SIM82] R. Shima, F. Ishihara, T. Mikumo: *Empirical formula for the average equilibrium charge-state of heavy ions behind various foils* Nuclear Instruments and Methods in Physics Research, Volume 200, Issues 23, 605608, 1982

[SNL09] K. Sieja, F. Nowacki, K. Langanke, G. Martínez-Pinedo: *Shell model description of zirconium isotopes*, Physical Review C, Volume 79, Issue 6, 064310, 2009

[Sim10] C. Simenel: *Particle Transfer Reactions with the Time-Dependent Hartree-Fock Theory Using a Particle Number Projection Technique*, Physical Review Letters, Volume 105, 192701, 2010

[SSS92] J. Sinatkas, L. D. Skouras, D. Strottman and J. D. Vergados: *Shell-model calculations in the $A = 80 - 100$ mass region: II. A study of the $N = 49, 48$*

nuclei, Journal of Physics G: Nuclear and Particle Physics, Volume 18, Number 8, 181401, 1992

[Sor14] O. Sorlin: *Shell evolutions and nuclear forces*, EPJ Web of Conferences, 66, 01016, 2014

[Ste02] A. M. Stefanini et.al.: *The heavy-ion magnetic spectrometer PRISMA*, Nuclear Physics A 701, 217c-221c, 2002

[Ste06] A. M. Stefanini et.al.: *Fusion of $^{48}Ca+^{90,96}Zr$ above and below Coulom barrier*, Physical Review C, Volume 73, Issue 3, 0,3606, 2006

[Szi05] S. Szilner et al.: *Multinucleon transfer processes in $^{40}Ca+^{208}Pb$*, Physical Review C, Volume 71, Issue 4, 044610, 2005

[Szi07] S. Szilner et al.: *Multinucleon transfer reactions in closed-shell nuclei*, Physical Review C, Volume 76, Issue 2, 024604, 2007

[Szi11] S. Szilner et al.: *Interplay between single-particle and collective excitations in argon isotopes populated by transfer reactions*, Physical Review C, Volume 84, Issue 1, 014325, 2011

[TWA81] W. L. Talbert, F. K. Wohn, L. J. Alquist, C. l. Duke: *Decay of $^{90}Rb^g$ and $^{90}Rb^m$*, Physical Review C, Volume 23, 1726, 1981

[Tho08] N. J. Thompson: *Gamma-Ray Spectroscopy and Shell Model Description of High Spin States in β-Stable $^{91,92}Zr$*, Ph.D. thesis, University of Surrey, 2008

[TGB82] R. S. Tickle, W. S. Gray, , R. D. Bent: *Two-proton pickup in the zirconium region using the (^6Li, ^8B) reaction*, Nuclear Physics A, Volume 376, Issue 2, Pages 309-324, 1982

[Ur06] C. A. Ur et al.: *Nuclear spectroscopy study of the isotopes populated via multinucleon transfer in the $^{90}Zr+^{208}Pb$ reaction*, AIP Conference Proceedings, Volume 853, 43-48, 2006

[Val09] J. J. VALIENTE-DOBON ET AL.: *Lifetime Measurements of the Neutron-Rich N =
30 Isotones ^{50}Ca and ^{51}Sc: Orbital Dependence of Effective Charges in the fp Shell*,
Physical Review Letters, Volume 102, 242502, 2009

[Win94] A. WINTHER: *Grazing reactions in collisions between heavy nuclei*, Nuclear Physics
A, Volume 572, 191, 1994

[Win95] A. WINTHER: *Dissipation, polarization and fluctuation in grazing heavy-ion colli-
sions and the boundary to the chaotic regime*, Nuclear Physics A, Volume 594, 203,
1995

[ZG08] V. ZAGREBAEV, W. GREINER: *Production of New Heavy Isotopes in Low-Energy
Multinucleon Transfer Reactions*, Physical Review Letters, Volume 101, 122701, 2008

[Zis73] M. S. ZISMAN ET AL.: *Heavy-Ion-Induced Single-Nucleon Transfer Reactions in the
Zr-Mo Region*, Physical Review C, Volume 8, Number 6, 1886-1891, 1973

[www1] `http://www.atomki.hu/atomki/PoAtomki/`

[www2] `http://www.e18.physik.tu-muenchen.de/research/bl/q3d.html`

[www3] `http://www.lnl.infn.it/accelerators/accelerators.html`

[www4] National   Nuclear   Data   Center,   Brookehaven   National   Laboratory
[http://www.nndc.bnl.gov] and Nuclear Data Sheets therein

[www5] `htpp:/www.to.infn.it/nanni/GRAZING`

Curriculum vitae

Maja Varga Pajtler was born on 19th of April 1984 in Osijek. She finished primary and secondary school in Osijek. In 2007 she was granted a BSc degree in mathematics and physics from the Department of Mathematics, University of Osijek. In 2008 she started PhD study in the field of Nuclear Physics at the Faculty of science, University of Zagreb.

From July 2007 she is employed as an assistant at the Department of Physics, University of Osijek. She is an active participant in the popularization of science through various project, such as Festival znanosti or Zimska škola fizike, which take place at the University of Osijek. In 2010, she participated at the 41st International Physics Olympiad in Zagreb as an evaluator.

She is a member of the Croatian Physical Society and the Croatian Radiation Protection Association.